IL
NUOVO CIMENTO
ORGANO DELLA SOCIETÀ ITALIANA DI FISICA
SOTTO GLI AUSPICI DEL CONSIGLIO NAZIONALE DELLE RICERCHE
E DEL COMITATO NAZIONALE PER L'ENERGIA NUCLEARE

VOL. XXII, N. 6 *Serie decima* 16 Dicembre 1961

Angular Correlations in $K^- + p \to \Lambda^0 + \pi^+ + \pi^-$.

B. SAKITA (*)

Department of Physics, University of Wisconsin - Madison, Wis.

(ricevuto il 10 Febbraio 1961)

Summary. — The angular correlations in $K^- + p \to \Lambda^0 + \pi^+ + \pi^-$ process are investigated in terms of the Λ-π resonance (Y*) isobar model. Two regions of the incident K-meson energy are considered: one is the region which gives separated bands in the Dalitz plot; the other gives overlapped bands. If the produced Y* is polarized for the separated case, it is shown that the forward-backward and outward-inward decay asymmetries of the Λ^0 give useful information to determine the spin and parity of the Y*. For the overlapped case, it is shown that there is up-down asymmetry of Λ-decay with respect to the plane containing Λ^0, π^+ and π^- in the center of mass system, and this asymmetry gives useful information to determine the parity of Y*.

1. – It has been reported [1] that the pion-hyperon resonant state (Y*) has been observed in the reaction $K^- + p \to \Lambda^0 + \pi^+ + \pi^-$, by measuring the energies of both π-mesons in the center of mass system. In this note we discuss the possibility to determine the spin s, and the parity η [2] of the Y* from the angular correlation in the ensuing Λ-decay.

(*) Work supported in part by the University of Wisconsin Research Committee with funds granted by the Winsconsin Alumni Research Foundation and in part by the U. S. Atomic Energy Commission under Contract No. AT(11-1)-30.

(1) M. ALSTON, L. W. ALVAREZ, P. EBERHARD, M. L. GOOD, W. GRAZIANO, H. K. TICHO and S. G. WOJCICKI: *Phys. Rev. Lett.*, **5**, 520 (1960).

(2) In this note the parity of strange particles refers always to the Λ^0 hyperon.

We will confine our attention to the reaction

$$K^- + p \to \Lambda^0 + \pi^+ + \pi^- ,$$

though a part of discussion in this note may apply to processes such as $\pi + p \to \Lambda^0 + K + \pi$, etc. Experiments reported can be well understood in terms of the isobar model, that is, the successive production and decay of the isobar Y^*:

(I) $$K^- + p \to Y^{*-} + \pi^+ \to \Lambda^0 + \pi^- + \pi^+$$

(II) $$\to Y^{*+} + \pi^- \to \Lambda^0 + \pi^+ + \pi^- .$$

Experimentally, mechanisms (I) and (II) are shown by the appearance of the corresponding two bands in the Dalitz plot. Those two bands separate or overlap, depending upon the incident K-meson energies ([3]) (Fig. 1). For the

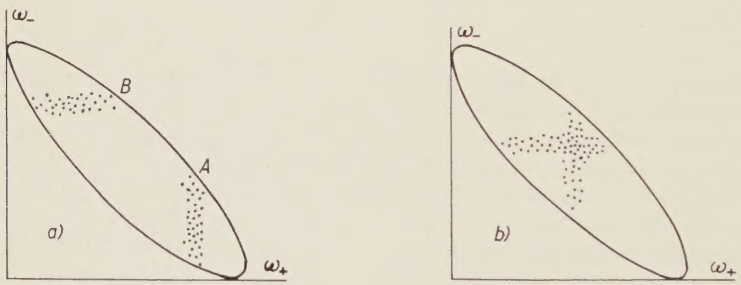

Fig. 1. – Dalitz plot for $K^- + p \to \Lambda^0 + \pi^+ + \pi^-$. *a*) Separated case. *b*) Overlapped case.

well separated case (Fig. 1*a*) the events in band *A* can be explained by mechanism (I) and correspondingly band *B* by mechanism (II). For the overlapping case (Fig. 1*b*) on the other hand, the mutual interference of the amplitudes due to both mechanisms (I) and (II) might become important ([4]) because the width of the resonance is broad enough to give a wide overlapping region. In this case, therefore, we expect that both the angular correlation of decay products of the Λ^0 and the energy distribution of the π-meson are quite different from that in the separated case. We shall show that as a characteristic

([3]) The overlapping band shown in Fig. 1*b*) is actually observed in the Berkeley experiment. M. FERRO-LUZZI: private communication.

([4]) Regarding the energy distribution of π mesons in the reaction $\pi + p \to \pi + \pi + n$, BERGIA *et al.* stressed the importance of this kind of interference; S. BERGIA, F. BONSIGNORI and A. STANGHELLINI: *Nuovo Cimento*, **16**, 1073 (1960).

of this interference in the overlapping case there is an up-down asymmetry of the Λ-decay with respect to the plane containing Λ^0, π^+ and π^- in the center of mass system, even after averaging over the incident K-meson direction.

2. – We first consider the well separated case (5). Events in this case can be understood as two-step reactions:

(i) $$K^- + p \to Y^* + \pi$$

(ii) $$Y^* \to \Lambda^0 + \pi .$$

Reaction (i) with an unpolarized incident target can be specified by the statistical tensor of Y^*, $R_{q,K}$, which, of course, depends on the production angle of Y^* (6). It is known (7) that the statistical tensor $R_{q,K}$ has the following properties:

(1) $$R^*_{q,K} = (-)^K R_{q,-K}$$

(2) $$R_{q,K} = 0 \qquad \text{for } K = \text{odd}$$

when the co-ordinate axes are chosen such that the z-axis is normal to the production plane (specified by $\hat{n}$) and the x-axis is along the direction of Y^* (see Fig. 2). Eq. (1) is the statement of the hermiticity of the density matrix of Y^*, while eq. (2) is the statement of parity conservation in the production process of Y^*.

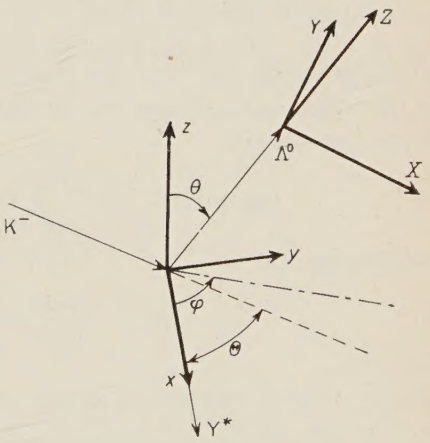

Fig. 2. – Co-ordinate systems (x, y, z) and (X, Y, Z). z, Z and X are in same plane. Z is the direction of Λ^0 in the rest system of Y^*.

Let us consider the decay of Y^* in its rest system. We assume that the spin of Y^* is s while the spin of the Λ^0 is $\frac{1}{2}$. If we specify the initial Y^* state by the z component of the Y^* spin, γ, while the final Λ-π state is specified by

(5) While this work was being carried out the author had a chance to see a paper by R. GATTO and H. P. STAPP, who consder the problem in this section for $s = \frac{1}{2}$ and $\frac{3}{2}$. The author wishes to thank Professor GOOD for drawing his attention to that paper. This problem was also studied by R. H. CAPPS (preprint).

(6) The highest rank of this statistical tensor $R_{q,K}$ depends on the spin of Y^*: $q_{\max} = 2s$. U. FANO and G. RACAH: *Irreducible Tensors* (New York, 1958).

(7) M. JACOB and G. C. WICK: *Ann. Phys.*, **7**, 404 (1959).

the direction of Λ^0 (the polar angle of which is θ, φ) and the helicity λ of Λ^0 in the rest system of the Y* (see Fig. 2), then the decay matrix element [8] is proportional to

$$M_{\lambda\gamma} \sim \exp[i\gamma\varphi]\, \mathrm{d}^s_{\gamma\lambda}(\theta)\varepsilon^{\frac{1}{2}-\lambda}\,, \tag{3}$$

where ε is related to η (the parity of Y*) by

$$\varepsilon = (-)^{s+\frac{1}{2}}\eta\,. \tag{4}$$

We define the new co-ordinate system (X, Y, Z) in which the Z axis is along the direction of Λ^0 in the rest system of Y*. The X axis is in the plane containing the direction Λ^0 and the normal to the production plane $\hat{n}$ (see Fig. 2).

The density matrix of Λ^0 in the new co-ordinate system is given by

$$\varrho_{\lambda\lambda'} \sim \sum_{\gamma\gamma' qK} M_{\lambda\gamma} M^*_{\lambda'\gamma'}(-)^{s-\gamma} C(ssq;\ \gamma - \gamma')\,\delta_{K,\gamma-\gamma'} R_{q,K}\,.$$

Substituting eq. (3) into the above equation and using the product formula of the d-functions [7] and the unitarity relation of the Clebsch-Gordon coefficients, we obtain

$$\varrho_{\lambda\lambda'} \sim (-)^{s-\lambda'}\varepsilon^{1+\lambda+\lambda'} \sum_{l,K=\text{even}} C(ssl;\ \lambda - \lambda')\, R_{l,K}\, d^l_{K,\lambda-\lambda'}(\theta)\, e^{iK\varphi}\,. \tag{5}$$

Writing eq. (5) as

$$\varrho_{\lambda\lambda'} \sim (-)^{s-\frac{1}{2}}[\xi_0(\theta,\varphi) + \boldsymbol{\xi}(\theta,\varphi)\cdot\boldsymbol{\sigma}]_{\lambda\lambda'}\,, \tag{6}$$

then [9]

$$\left.\begin{aligned}
\xi_0 &= \sum_{\substack{l=\text{even}\\K=\text{even}}} C(ssl;\ \tfrac{1}{2}\ -\tfrac{1}{2})\, d^l_{K,0}(\theta)\ \mathrm{Re}[R_{l,K}e^{iK\varphi}],\\
\xi_x &= -\varepsilon \sum_{\substack{l=\text{odd}\\K=\text{even}}} C(ssl;\ \tfrac{1}{2}\ \tfrac{1}{2})\, d^l_{K,1}(\theta)\ \mathrm{Re}[R_{l,K}e^{iK\varphi}]\,,\\
\xi_y &= -\varepsilon \sum_{\substack{l=\text{odd}\\K=\text{even}}} C(ssl;\ \tfrac{1}{2}\ \tfrac{1}{2})\, d^l_{K,0}(\theta)\ \mathrm{Im}[R_{l,K}e^{iK\varphi}],\\
\xi_z &= \sum_{\substack{l=\text{odd}\\K=\text{even}}} C(ssl;\ \tfrac{1}{2}\ -\tfrac{1}{2})\, d^l_{K,0}(\theta)\ \mathrm{Re}[R_{l,K}e^{iK\varphi}],
\end{aligned}\right\} \tag{7}$$

where Re[ ] means the real part of [ ] while Im means the imaginary part. The density matrix of Λ^0 in its rest system is the same as (5) and (6) because

[8] M. Jacob: *Nuovo Cimento*, **9**, 826 (1958).

[9] From eq. (1) $R_{q,0}$ is real, while $R_{q,k}$ for $K \neq 0$ and $K \neq$ odd is, in general, complex.

the rest system of the Λ^0 can be reached from the rest system of the Y^* by a Lorentz transformation along the Z axis so that the z-component of the Λ^0 spin is invariant.

The decay of Λ^0 is characterized by a matrix Q_Λ ([10]) when the polarization of the final proton is averaged out, and serves as an analyzer for Λ^0-polarization:

$$Q_\Lambda = 1 + \alpha \boldsymbol{\sigma} \cdot \hat{p} \,, \tag{8}$$

where α is the asymmetry parameter of Λ-decay and $\hat{p}$ is the unit vector in the direction of the outgoing π^- in the rest system of the Λ^0. Therefore the correlation function of the π^- produced by decay of the Λ^0, is in the rest frame of the Λ^0,

$$\mathrm{Tr}\,(\varrho Q_\Lambda) \sim \xi_0 + \alpha \boldsymbol{\xi} \cdot \hat{p} \,, \tag{9}$$

where ξ_0, $\boldsymbol{\xi}$ are given by eq. (7). We define forward and backward by the direction of positive Z and of negative Z for a given θ, φ and Θ (production angle of Y^*), outward and inward by positive X and negative X, and right and left by positive Y and negative Y (see Fig. 2).

$$\left\{ \begin{array}{l} \dfrac{N_{\mathrm{for}} - N_{\mathrm{back}}}{N_{\mathrm{tot}}} = \dfrac{\alpha \xi_z}{2\xi_0} \,, \\ \dfrac{N_{\mathrm{right}} - N_{\mathrm{left}}}{N_{\mathrm{tot}}} = \dfrac{\alpha \xi_y}{2\xi_0} \,, \\ \dfrac{N_{\mathrm{out}} - N_{\mathrm{in}}}{N_{\mathrm{tot}}} = \dfrac{\alpha \xi_x}{2\xi_0} \,, \end{array} \right. \tag{10}$$

where, *e.g.* N_{for} is the number of events in which the decay pion is emitted forward in the Λ^0 rest frame. Note that N_{for} is a function of θ, φ and Θ (the production angle of Y^*). Note also that $\xi_y = 0$ for $s = \frac{1}{2}$ so that there is no right-left asymmetry when the Y^* spin is $\frac{1}{2}$.

In order to determine the spin and parity, however, it seems enough to consider the results after integration over φ. Then we obtain

$$\left\{ \begin{array}{l} \overline{\xi}_0(\theta) = \displaystyle\sum_{l=\mathrm{even}} C(ssl;\, \tfrac{1}{2}\ -\tfrac{1}{2}) R_{l,0} P_l(\cos\theta) \,, \\ \overline{\xi}_x(\theta) = -\varepsilon \displaystyle\sum_{l=\mathrm{even}} C(ssl;\, \tfrac{1}{2}\ \tfrac{1}{2}) R_{l,0} \frac{\sin\theta}{\sqrt{l(l+1)}} P_l'(\cos\theta) \,, \\ \overline{\xi}_y(\theta) = 0 \,, \\ \overline{\xi}_z(\theta) = \displaystyle\sum_{l=\mathrm{odd}} C(ssl;\, \tfrac{1}{2}\ -\tfrac{1}{2}) R_{l,0} P_l(\cos\theta) \,, \end{array} \right. \tag{11}$$

([10]) See for example L. MICHEL and H. ROUHANINEJAD: University of Wisconsin, preprint.

where the bar means the average over the angle φ and $P'(x) = (\mathrm{d}/\mathrm{d}x)\,P(x)$. We define r by

$$r = \frac{\mathcal{N}_{\mathrm{out}} - \mathcal{N}_{\mathrm{in}}}{\mathcal{N}_{\mathrm{for}} - \mathcal{N}_{\mathrm{back}}}, \tag{12}$$

where, *e.g.*.., $\mathcal{N}_{\mathrm{for}}(\theta, \Theta) = \int \mathrm{d}\varphi\, N_{\mathrm{for}}(\theta, \varphi, \Theta)$. From (9) and (11)

$$r = (\bar{\xi}_x/\bar{\xi}_0) = -\varepsilon \frac{\sum_{l=\mathrm{odd}} C(ssl;\, \tfrac{1}{2}\ \tfrac{1}{2})\, R_{l,0}\, (\sin\theta/\sqrt{l(l+1)})\, P_l'(\cos\theta)}{\sum_{l=\mathrm{odd}} C(ssl;\, \tfrac{1}{2}\ -\tfrac{1}{2})\, R_{l,0}\, P_l(\cos\theta)}. \tag{13}$$

For $s = \frac{1}{2}$ and $s = \frac{3}{2}$, r is given by

$$\begin{cases} r(s=\tfrac{1}{2}) = -\varepsilon \dfrac{1}{\sqrt{2}} \operatorname{tg}\theta\,, \\ r(s=\tfrac{1}{2}) = -\varepsilon \dfrac{1}{\sqrt{2}} \operatorname{tg}\theta \left[\dfrac{1 - (\lambda/4)(10\cos\theta - 3)}{1 - (3/2\sqrt{2})\,\lambda(5\cos\theta - 3)}\right], \end{cases} \tag{14}$$

where λ is a parameter $(R_{3,0}/R_{1,0})$ which depends on the production angle Θ.

Needless to say, the method in this section works only in the case that the Y* is polarized in its production process.

3. – We consider next the overlapped case. As we mentioned before, it is important in this case to take into account the interference effects of mechanisms (I) and (II).

Denote the energy (momentum) of Λ^0, π^+, π^- in the center of mass system by E_Λ $(\boldsymbol{p}_\Lambda)$, ω_+ $(\boldsymbol{p}_{\pi^+})$ and ω_- $(\boldsymbol{p}_{\pi^-})$ and the helicities of the proton (incident), Y* (intermediate and final) by μ, γ and λ. According to the isobar model [4] the matrix element is given by

$$\begin{cases} T = T_{\mathrm{I}} + T_{\mathrm{II}}\,, \\ T_{\mathrm{I}} \sim \sum_{\gamma} \langle \boldsymbol{p}_\Lambda, \boldsymbol{p}_{\pi^-};\, \lambda | T |\, Y^{*-};\, -\boldsymbol{p}_{\pi^+};\, \gamma \rangle \langle \boldsymbol{p}_{\pi^+};\, \gamma | T | \boldsymbol{k};\, \mu \rangle F(\omega_+)\,, \end{cases} \tag{15}$$

where $F(\omega)$ has the form:

$$F(\omega) = \frac{1}{\omega - \omega_0 + i\Gamma(\omega)}. \tag{16}$$

ω_0 is the resonance energy which is related to the mass of the isobar (M^*)

and the total energy of the system (E) by

$$\omega_0 = \frac{E^2 + \mu^2 - M^{*2}}{2E}, \qquad (E = E_\Lambda + \omega_+ + \omega_-),$$

while Γ is its width which might depend on ω. T_{II}, the matrix element due to the mechanism (II), can be obtained from (15) by interchanging — and +. In eq. (15), $\langle \boldsymbol{p}_{\pi^+}; \gamma | T | \boldsymbol{k}; \mu \rangle$ and $\langle \boldsymbol{p}_\Lambda, \boldsymbol{p}_{\pi^-}; \lambda | T | Y^{*-}; -\boldsymbol{p}_{\pi^+}; \gamma \rangle$ are the matrix elements of processes i) and ii) in the two-step reaction. In the spirit of the isobar model, we treat them as matrix elements between stable states.

According to JACOB and WICK [7],

$$\langle \boldsymbol{p}_{\pi^-}; \gamma | T | \boldsymbol{k}; \mu \rangle = \sum_J A^{(+)J}_{\gamma\mu} \mathscr{D}^*_{\mu\gamma}(-\varphi_+, \theta_+, -\alpha_+) , \tag{17}$$

where θ_+, φ_+ are the polar angles of the direction of π^+ $\hat{p}_{\pi^+}$ in the center of mass system when the direction of the incident K-meson $\hat{k}$ is taken as the z axis, and α_+ is the angle of rotation around $\hat{p}_{\pi^+}$ which carries the plane containing $\hat{k}$ and $\hat{p}_{\pi^+}$ into the plane containing $\hat{p}_{\pi^+}$ and $\hat{p}_{\pi^-}$ (see Fig. 3). $A^{(+)J}_{\gamma\gamma}$ is the factor depending only on the total energy. From parity conservation in the reaction, we see that

$$A^{(+)J}_{-\gamma-\mu} = \varkappa A^{(+)J}_{\gamma\mu} , \tag{18}$$

$$\varkappa = \eta\eta_K(-)^{\frac{1}{2}-s} , \tag{19}$$

where η and η_K are the parities of the Y* and the K-meson, respectively. The decay matrix element of the Y* is given by (3) in which we set $\varphi = 0$ since α^+ is defined such that the Y axis of the new co-ordinate system (X, Y, Z) which can be reached by this rotation $\{\varphi_+, \theta_+, \alpha_+\}$ from the old co-ordinate system is perpendicular to the production plane (see Fig. 3). Since λ in eq. (3) is the helicity of the Λ^0 in the center of mass system of Λ^0-π^-, while λ in eq. (15) is the helicity of Λ^0 in the center of mass system of Λ^0-π^--π^+, we must transform from the center of mass system of Λ^0-π^- to the center of mass system of Λ^0-π^--π^+ by a Lorentz transformation along $\boldsymbol{p}_{\pi^+}$ in order to obtain the

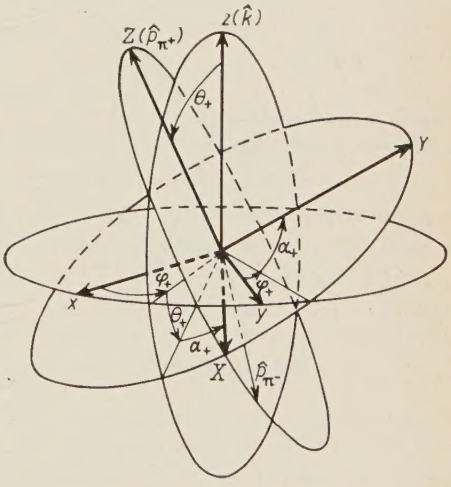

Fig. 3. – Angles θ_+, φ_+ and α_+. $\hat{k}$: direction of incident K meson in the c.m. system; $\hat{p}_{\pi^+}$: direction of π^+ in the c.m. system; $\hat{p}_{\pi^-}$: direction of π^- in the c.m. system.

decay matrix element of Y* in eq. (15). This transformation affects the helicity of Λ^0 and can be described by a single rotation around the Y axis ([11]).

$$(20)\quad \langle \boldsymbol{p}_\Lambda, \boldsymbol{p}_{\pi^-};\ \lambda|T|Y^{*-};\ -\boldsymbol{p}_{\pi^+};\ \gamma\rangle = \sum_{\lambda'} \langle \boldsymbol{p}_\Lambda;\ \lambda|\mathscr{L}_{\beta_+}|\boldsymbol{p};\ \lambda'\rangle\langle \boldsymbol{p}_+;\ \lambda'|T|Y^{*-};\ \gamma\rangle \sim$$

$$\sim \varepsilon^{\frac{1}{2}-\gamma'} d^s_{\gamma\lambda'}(\Omega_+) d^{\frac{1}{2}}_{\lambda'\frac{1}{2}}(K_+)\,,$$

where $\mathscr{L}_{\beta_+}$ denotes the Lorentz transformation operator which transforms the Λ^0-π^+-π^- center of mass system into the Λ^0-π^+-π^- center of mass system, $\boldsymbol{p}_+$ is the momentum of Λ^0 in the Λ^0-π^- center of mass system, and Ω_+ and K_+ are the angles from $-\hat{p}_{\pi^+}$ to $\hat{p}_+$, and from $\hat{p}_+$ to $\hat{p}_\Lambda$, respectively (see Fig. 4). We obtain

$$(21)\qquad T_{\mathrm{I}} \sim \sum_{J\gamma\lambda'} A^{(+)J}_{\gamma\mu} \mathscr{D}^{J*}_{\mu\gamma}(-\varphi_+,\ \theta_+,\ -\alpha_+) d^s_{\gamma\lambda'}(\Omega_+) d^{\frac{1}{2}}_{\lambda'\frac{1}{2}}(K_+) \varepsilon^{\frac{1}{2}-\lambda'}(F\omega_+)\,.$$

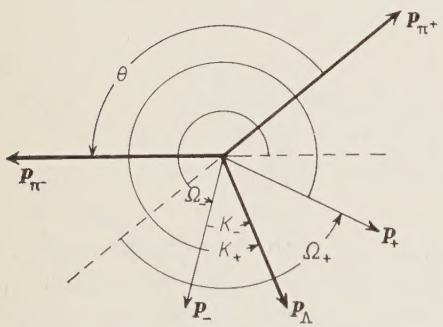

Fig. 4. – The angles θ, $\Omega_\pm$ and $K_\pm$ on the plane containing Λ^0, π^+ and π^- in the c.m. system.

Note that Ω_+ and K_+ depend only on ω_+, ω_- and the total energy of the system E. If we change $+$ to $-$, we obtain T_{II}.

The density matrix of Λ^0 in the center of mass system of the unpolarized proton target is given by

$$(22)\quad \varrho = \sum_\mu (T_{\mathrm{I}} T^*_{\mathrm{I}} + T_{\mathrm{II}} T^*_{\mathrm{II}} + T_{\mathrm{I}} T^*_{\mathrm{II}} + T_{\mathrm{II}} T^*_{\mathrm{I}})\,.$$

In order to demonstrate the up and down asymmetry of Λ-decay with respect to the plane containing Λ^0-π^+-π^- in the center of mass system, we consider the case in which we averaged over the direction of the incident K-meson.

We integrate ϱ over θ_+ and α_+. Using

$$\mathscr{D}^{*J}_{\mu\gamma}(-\varphi_-,\ \theta_-,\ -\alpha_-) = \sum_{\gamma'} \mathscr{D}^{*J}_{\mu\gamma'}(-\varphi_+,\ \theta_+,\ -\alpha_+) \mathscr{D}^{*J}_{\gamma'\gamma}(0,\ \theta,\ 0)\,,$$

([11]) This rotation angle, K_+ in this case, is the sum of the angle of the rotation of Λ^0 direction and spin direction due to the Lorentz transformation. The latter is a purely relativistic effect so that we might be able to neglect it in a good approximation. For this spin rotation, see H. P. Stapp: *Phys. Rev.*, **103**, 625 (1956).

where θ is the angle between π^+ and π^-, we obtain

$$\varrho_{\lambda\lambda'} = \delta_{\lambda\lambda'} \sum_{\substack{l=\text{even} \\ \gamma=\text{even}}} C(ssl;\tfrac{1}{2}\ \tfrac{1}{2})C(ssl;\ \gamma\ -\gamma)(-)^{\gamma-\frac{1}{2}} \cdot \tag{23}$$

$$\cdot[P_l(\Omega_+)\sum_J \mathscr{A}^{++J}_{\gamma\gamma}|F(\omega_+)|^2 + P_l(\Omega_-)\sum_J \mathscr{A}^{--J}_{\gamma\gamma}|F(\omega_-)|^2] +$$

$$+ \sum_{J\gamma\gamma'}\{(\tau^J_{\lambda\lambda';\gamma\gamma'} + \tau^J_{\lambda'\lambda;\gamma'\gamma})\ \mathrm{Re}[\mathscr{A}^{+-J}_{\gamma\gamma'}F(\omega_+)F^*(\omega_-)] +$$

$$+ i(\tau_{\lambda\lambda';\gamma\gamma'} - \tau^J_{\lambda'\lambda;\gamma'\gamma})\ \mathrm{Im}[\mathscr{A}^{+-}_{\gamma\gamma'}F(\omega_+)F^*(\omega_-)]\}\ ,$$

where

$$\mathscr{A}^{\pm\pm J}_{\gamma\gamma'} = \sum_\mu A^{(\pm)J}_{\gamma\mu}A^{(\pm)J*}_{\gamma'\mu}\left(\frac{1}{2J+1}\right), \tag{24}$$

and

$$\tau^J_{\lambda\lambda';\gamma\gamma'} = \sum_{\lambda''\lambda'''} \varepsilon^{1+\lambda''+\lambda'''} d^{\frac{1}{2}}_{\lambda\lambda''}(-K_+)d^s_{\lambda''\gamma}(-\Omega_+)d^J_{\gamma\gamma'}(\theta)d^s_{\gamma'\lambda'''}(\Omega_-)d^{\frac{1}{2}}_{\lambda'''\lambda'}(K_-)\ . \tag{25}$$

By the definition of τ, eq. (25), and the properties of the d-functions, we obtain

$$\tau^J_{-\lambda-\lambda';-\gamma-\gamma'} = (-)^{\lambda-\lambda'}\tau_{\lambda\lambda';\gamma\gamma'}\ . \tag{26}$$

Therefore

$$\varrho_{\lambda\lambda'} = (-)^{\lambda-\lambda'}\varrho_{-\lambda-\lambda'}\ . \tag{27}$$

Since there is no a priori reason that the off diagonal elements of ϱ must vanish eq. (27) shows that there is, in general, an asymmetry along the Y direction (normal to the plane containing Λ^0-π^+-π^-). In order to see this asymmetry much more explicitly, let us assume that the S state is dominant in the final state of the reaction (i); that is $K^- + p \to Y^* + \pi$. Then, $J = s$ and $\mathscr{A}^{\pm\pm s}_{\gamma\gamma'}$ does not depend on γ and γ' so that we obtain

$$\varrho_{\lambda\lambda'}(S\text{ dominant}) \sim \delta_{\lambda\lambda'}(-)^{s-\frac{1}{2}}\sqrt{s+\tfrac{1}{2}}[\mathscr{A}^{++}|F(\omega_+)|^2 + \mathscr{A}^{--}|F(\omega_-)|^2] + \tag{28}$$

$$+ (\tau^s_{\lambda\lambda'} + \tau^s_{\lambda'\lambda})\ \mathrm{Re}[\mathscr{A}^{+-}F(\omega_+)F^*(\omega_-)] + i(\tau^s_{\lambda\lambda'} - \tau^s_{\lambda'\lambda})\ \mathrm{Im}[\mathscr{A}^{+-}F(\omega_+)F^*(\omega_-)]\ ,$$

where

$$\tau^s_{\lambda\lambda'} = \sum_{\lambda''\lambda'''} \varepsilon^{1+\lambda''+\lambda'''} d^{\frac{1}{2}}_{\lambda\lambda''}(-K_+)d^s_{\lambda''\lambda'''}(\theta+\Omega_--\Omega_+)d^{\frac{1}{2}}_{\lambda'''\lambda'}(K_-)\ . \tag{29}$$

Now writing

$$\varrho \sim \zeta_0 + \boldsymbol{\zeta}\cdot\boldsymbol{\sigma}\ , \tag{30}$$

$$\begin{cases} \zeta_0 = (-)^{s-\frac{1}{2}}\sqrt{s+\tfrac{1}{2}}[\mathscr{A}^{++}|F(\omega_+)|^2 + \mathscr{A}^{--}|F(\omega_-)|^2] + \\ \qquad\qquad + 2\tau_{++}\ \mathrm{Re}[\mathscr{A}^{+-}F(\omega_+)F^*(\omega_-)]\ , \\ \zeta_x = \zeta_z = 0\ , \\ \zeta_y = -2\tau_{+-}\ \mathrm{Im}[\mathscr{A}^{+-}F(\omega_+)F^*(\omega_-)]\ . \end{cases} \tag{31}$$

Using eq. (29), we obtain

$$(32)\quad \begin{cases} \tau_{++} = \dfrac{1}{l+1}\left[\left(P'_{l+1}(\cos\hat{\vartheta}) - P(\cos\hat{\vartheta})\right)\cos^2\hat{\vartheta} + \right. \\ \qquad\qquad \left. + \varepsilon\left(P'_{l+1}(\cos\hat{\vartheta}) + P'_{l}(\cos\hat{\vartheta})\right)\sin^2\hat{\vartheta}\right], \\ \tau_{+-} = \dfrac{\sin\hat{\vartheta}}{2(l+1)}\left[(1+\varepsilon)P'_{l}(\cos\hat{\vartheta}) - (1-\varepsilon)P'_{l+1}(\cos\hat{\vartheta})\right], \end{cases}$$

where $\hat{\vartheta}$ is the angle between $\hat{p}_+$ and $\hat{p}_-$, that is, the angle between the direction of the Λ^0 in the Λ^0-π^+ center of mass system and the direction of the Λ^0 in the Λ^0-π^- center of mass system, and $l = s - \frac{1}{2}$.

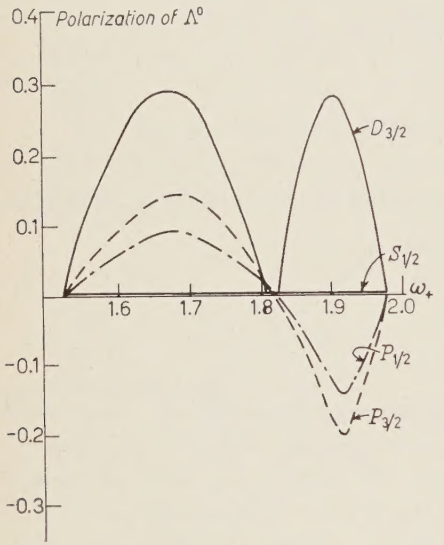

Fig. 5. – Polarization of the Λ^0 as a function of ω_+, when $\omega_- = \omega_0 = 1.82\,\mu$, $\Gamma/2 \sim$ ~ 20 MeV and $\mathscr{A}^{++} = \mathscr{A}^{+-} = \mathscr{A}^{--}$ are chosen.

From eqs. (30), (31), we can see that the polarization of Λ^0 is proportional to τ_{+-}, whose explicit form is given in eq. (22). From eq. (32) we can also see that for a given l (*i.e.* for a given s), whether τ_{+-} is an even or odd function of $\cos\hat{\vartheta}$ depends on ε which is related to the parity of Y* by eq. (4). This allows a determination of the parity of the Y* in case the Y*π is dominantly produced in the S state [12].

The results are illustrated in Fig. 5, which shows the polarization of the Λ^0 as a function of energy of the π^+, when the π^- energy is fixed at the resonance energy. We assume in this plot that $\mathscr{A}^{++} = \mathscr{A}^{+-} = \mathscr{A}^{--}$ and $E = 11.8\,\mu$ (corresponding K^- laboratorium momentum $= 680$ MeV/c) $\omega_- = \omega_0 = 1.82\mu$, $1.52\mu < \omega_+ < 1.98\mu$ and $\Gamma/2 \sim 20$ MeV where μ is the π-meson mass.

* * *

The author would like to express his thanks to Professor R. G. Sachs for stimulating him into the study of this problem. He his greateful to Professor

[12] For higher Y* spin, it is unlikely that Y* will be produced in the S state because the energy required in this reaction is rather small. In this case we have to go back to eq. (23) from which it is hard to see whether we can obtain the meaningful information about Y*.

M. L. GOOD for suggestions and comments on this work. He also wishes to thank Dr. L. E. EVANS for his comments and reading of the manuscript.

RIASSUNTO (*)

Si studiano, in funzione del modello isobarico (Y*) della risonanza Λ-π, le correlazioni angolari nel processo $K^- + p \to \Lambda^0 + \pi^+ + \pi^-$. Si prendono in considerazione due zone dell'energia del mesone K incidente: una zona dà bande separate nel diagramma di Dalitz; l'altra dà bande sovrapposte. Se, nel caso con separazione delle bande, l'Y* prodotto è polarizzato, si mostra che le asimmetrie antero-posteriore ed interna-esterna del decadimento del Λ^0 danno informazioni utili per determinare lo spin e la parità dell'Y*. Nel caso con sovrapposizione, si mostra che si ha una asimmetria alto-basso del decadimento Λ rispetto al piano contenente il Λ^0, ed i π^+ e π^- nel sistema del centro di massa, e questa asimmetria dà informazioni utili per determinare la parità dell'Y*.

(*) *Traduzione a cura della Redazione.*

A Theory of Hyperfragments.

II. – Mesic Decay of Hyperfragments (*).

S. Iwao (**)

Department of Physics and Astronomy, University of Rochester - Rochester, N. Y.

(ricevuto il 15 Marzo 1961)

Summary. — Mesic decay of hyperfragments is discussed systematically on the basis of our previous model for hyperfragments. The general formalism for the two-body and three-body mesic decay is developed. The polarization-direction correlation and the angular correlation for the two-body and the three-body decays are discussed together with the decay probability. The formalism is developed so as to include the isotopic spin selection rule ($\Delta I = \frac{1}{2}$ and $\frac{3}{2}$) for the mesic decays. The theory developed here is applied especially for the low mass number hyperfragments where we found that the branching ratios of the two-body and the three-body mesic decays of ${}^3\mathrm{H}_\Lambda$ and ${}^4\mathrm{H}_\Lambda$, $({}^3\mathrm{H}_\Lambda \to {}^3\mathrm{He} + \pi^-)/({}^3\mathrm{H}_\Lambda \to \mathrm{D} + \mathrm{p} + \pi^-)$ and $({}^4\mathrm{H}_\Lambda \to {}^4\mathrm{He} + \pi^-)/({}^4\mathrm{H}_\Lambda \to {}^3\mathrm{H} + \mathrm{p} + \pi^-)$, can be used for the determination of the spins of both hyperfragments. The fraction of the p-wave decay rate for the free Λ decay obtained from the ${}^5\mathrm{He}_\Lambda \to {}^4\mathrm{He} + \mathrm{p} + \pi^-$ where the decay proceeds through two resonant states ($p_{\frac{3}{2}}$ and $p_{\frac{1}{2}}$) is given by $p^2/(s^2 + p^2) \approx .4$ which gives spin zero of ${}^4\mathrm{H}_\Lambda$ in connection with the Dalitz and Liu plot and hence odd parity for the kaon. The decay rate of the charged and the neutral mode is always 2/1 if, and only if, the condition obtained by Okubo, Marshak and Sudarshan is satisfied. Finally we show that the final state interaction for the two-body mesic decay can be described by the pion and residual nucleus scattering phase shifts by making use of the invariance of the total S-matrix of the decay processes under the Wigner (weak) time reversal.

(*) Supported in part by the U.S. Atomic Energy Commission.

(**) Now at the Department of Physics, Syracuse University, Syracuse, New York.

1. – Introduction.

We had, in earlier papers ([1,2]) investigated the properties of hyperfragments in relation to the binding energies of the Λ-hyperon and it was pointed out that the experimental binding energies of the Λ-hyperon for p-shell hypernuclei can be explained by both antiparallel and parallel spins. The main results of our previous papers are the evidence for the preference for the antiparallel spin couplings for s-shell hypernuclei and hence the odd kaon parity ([1,2]). The internal consistency of our model and method were discussed in succeeding reports ([3,4]). The method applied for the ordinary nuclei shows that the qualitative features (*e.g.* the ground state spins and the total binding energies) are in agreement with the experiments but a precise fit, (*e.g.* for the detailed level structure) cannot be obtained. It can be improved by making use of the intermediate coupling wave function for nucleons obtained from the current shell model calculations and couple the Λ wave function to it. This is rather satisfactory because the Λ-hyperon is loosely bound (with a strength of about 1/2.5 of that of $\mathcal{N}$-$\mathcal{N}$ forces) to the individual nucleons (compare the parameters given in papers cited above). But this is a rather complicated procedure and misses the essential point of the problem. The precise calculation should be undertaken after arriving at the essential results. Therefore in this paper we will continue to confine ourselves to the extreme j-j scheme and study the main features of the mesic decays of hyperfragments. Among several investigations of this problem Dalitz and Liu ([5]) have calculated the ratio of two-body mesic decays to all decay modes making use of their variational wave functions for $A = 3$ and 4 hyperfragments although they assumed the isotopic spin selection rule $\Delta I = \frac{1}{2}$ for Λ-decay. The mesic decay of p-shell hyperfragments has been investigated by Lawson and Rotenberg ([6]) but it is confined to two-body decays alone. The purpose of this paper is to derive a theory for the mesic decay of hyperfragments and to determine the properties of hyperfragments as well as the nature of the decay interactions.

It is rather hard to determine the absolute lifetime of the bound Λ-particle experimentally because it is hard to discriminate between hyperfragment decays in flight and decays at rest (for low energy production) and hence the ambiguity

([1]) S. Iwao and E. C. G. Sudarshan: *Phys. Rev. Lett.*, **4**, 140 (1960).
([2]) S. Iwao: *Nuovo Cimento*, **17**, 491 (1960).
([3]) E. C. G. Sudarshan and S. Iwao: *Proc. Ind. Acad. Sci.*, **52**, 27 (1960).
([4]) S. Iwao, F. B. Wang and S. Morin: *U. S. Atomic Energy Commission Document* NYO-9536 (1961).
([5]) R. H. Dalitz and L. Liu: *Phys. Rev.*, **116**, 1312 (1959).
([6]) R. D. Lawson and M. Rotenberg: *Nuovo Cimento*, **17**, 449 (1960).

arises from the measurement of the track length (*). The decays occur through π-mesic and non-mesic channels with several decay modes. The former is identified more easily than the latter because the maximum charge state and the suitable energy release make easier the identification. We want to investigate the spin states of parent hyperfragments, s-wave and p-wave admixture ratio of the free Λ-decay, the isotopic spin selection rule, $\Delta I = \frac{1}{2}$ and $\frac{3}{2}$ including the phase difference of both amplitudes (we do not confine ourselves to the $\Delta I = \frac{1}{2}$ rule) and so on.

The experimental information for the decay processes is rather poor at present except for a few hyperfragments; we summarize the possible topics for the theoretical investigations in the following:

1) Two-body mesic decay: decay branching ratio to the various residual states of the nucleus, branching ratio of π^--mesic and π^0-mesic decay, polarization-direction correlation of the produced hyperfragment and the decay pion.

2) Three-body mesic decay: angular correlation of the successive emission of the pion and the nucleon if the decay occurs through the intermediate state with a definite angular momentum, parity and isotopic spin (decay through a compound state of the nucleus).

3) Branching ratio of the two-body and the three-body mesic decays.

In order to correlate the experimental information with our method of analysis we will develop a formalism in Section 2. In Section 3 we will derive a numerical table suitable for the treatment of the two-body mesic decay branching probabilities for various residual states for configurations with both parallel and antiparallel spins of the parent hyperfragments. General comments for each mesic decay are given. It is pointed out that in some cases the observation of the decay modes will uniquely determine the spin of the hyperfragment. In Section 4 we will discuss the isotopic spin selection rule from the two-body mesic decay. The poor experimental statistics of the neutral decay mode gives us no definite information. In Section 5 we study three-body mesic decays but restrict ourselves to the $A = 3$, 4 and 5 hyperfragments and give a convenient table for the applications. In Section 6 we compare the calculated two-body and the three-body mesic decay branching ratios of $A = 3$ and 4 with experiment. The proton decay mode of the $A = 5$ hyperfragment through two intermediate states $p_{\frac{1}{2}}$ and $p_{\frac{3}{2}}$ is compared with experiment. Conclusions about the spin of s-shell hyperfragments and the fraction of the p-wave probability of the free Λ-decay are derived from the

(*) It was pointed out by Professors Harth and Leitner that the measurement of the absolute lifetime by a bubble chamber (private communication) has an ambiguity of about a factor of three.

comparison given in this section. In all these discussions we always consider the branching ratio; hence only the kinematical parameters are significant quantities in our treatment. In the last section we derive a relation which takes into account the final state interaction of the pion in the two-body mesic decay making use of the weak time reversal invariance for the S-matrix (Section 7). In Appendix I we will summarize the calculation of the phase volume of the three-body mesic decay including the matrix elements. In Appendix II we point out that the parameters derived from s-shell hyperfragment and p-shell hyperfragment binding energies favor the antiparallel coupling of spins for p-shell hyperfragments provided that there is no anomalously strong spin-orbit coupling of N-Λ forces. A brief communication on the principal results of this part of our investigation has already been published ([7]).

2. – Formalism.

Spin $\frac{1}{2}$ of the Λ-hyperon, parity non-conservation in Λ-decay ([8]) and the possible isotopic spin changes $\Delta I = \frac{1}{2}$ and $\frac{3}{2}$ for the decays into strongly interacting particles ([9]) (we will consider both possibilities without referring to the usual $\Delta I = \frac{1}{2}$ rule ([10])) lead to the following form of operator for the decay of the Λ-particle:

$$(1) \qquad H = \{a_{\frac{1}{2}s} D^{(\frac{1}{2})} + a_{\frac{3}{2}s} D^{(\frac{3}{2})}\} - i\{a_{\frac{1}{2}p} D^{(\frac{1}{2})} + a_{\frac{3}{2}p} D^{(\frac{3}{2})}\} \boldsymbol{\sigma} \cdot \boldsymbol{\nabla} / p_\Lambda = \\ = \sum_{\Delta I, \Delta J} a_{\Delta I, \Delta J} D^{(\Delta I)} \boldsymbol{\sigma}^{(\nabla J)} \cdot (-i \boldsymbol{\nabla} / p_\Lambda)^{(\Delta J)},$$

where $a_{\Delta I, \Delta J}$, $D^{(\Delta I)}$, $\boldsymbol{\sigma}$, $\boldsymbol{\nabla}$ and p_Λ are the relative amplitudes of ΔI, ΔJ-contribution, the operator in isotopic spin space, Pauli spin matrix, gradient operator for the pion wave function and the magnitude of the relative momentum of the pion in free Λ-decay at rest, respectively. From the conservation of angular momentum $\Delta J = 0$ and 1. (We put p_Λ in the expression for the p-wave contribution so as to give give the same dimensionality for both channels.)

The outgoing pion wave relative to the residual nucleus depends on the orbital state of the nucleon in the residual nucleus. For this reason it will be

([7]) S. Iwao and E. G. G. Sudarshan: *Mesic Decay of Hyperfragments*, Proceedings of the Tenth Annual High Energy Conference at Rochester (New York, 1960), p. 607.

([8]) T. D. Lee and C. N. Yang: *Phys. Rev.*, **109**, 1755 (1958).

([9]) S. Okubo, R. E. Marshak and E. C. G. Sudarshan: *Phys. Rev.*, **113**, 944 (1959).

([10]) M. Kawaguchi and K. Nishijima: *Prog. Theor. Phys.*, **15**, 180 (1956); C. Iso and M. Kawaguchi: *Prog. Theor. Phys.*, **16**, 177 (1956); M. S. Swami and B. M. Udgaonkar: *Nuovo Cimento*, **14**, 836 (1959).

convenient to introduce new names « direct term » and « derivative term » corresponding terms of s-wave and p-wave pion in the *free* Λ-decay.

In order to evaluate the expectation value of eq. (1) we will rewrite it in the tensor operator form. It is given by

$$(2)\quad H = -\{a_{\frac{1}{2}s}\sqrt{\tfrac{3}{2}}[t^{(1)}XD^{(\frac{1}{2})}]^{(\frac{1}{2})}_{\frac{1}{2}} + a_{\frac{1}{2}s}\sqrt{\tfrac{1}{6}}[t^{(1)}XD^{(\frac{1}{2})}]^{(\frac{1}{2})}_{\frac{1}{2}}\}\sum_{l,m}[l]i^l j_l(kr)C^{(l)}_m(\boldsymbol{r})D(l,\,m0;\,\boldsymbol{k}) -$$

$$-\{a_{\frac{1}{2}s}\sqrt{\tfrac{2}{3}}[t^{(1)}XD^{(\frac{1}{2})}]^{(\frac{1}{2})}_{\frac{1}{2}} - a_{\frac{3}{2}p}\sqrt{\tfrac{1}{6}}[t^{(1)}XD^{(\frac{1}{2})}]^{(\frac{1}{2})}_{\frac{1}{2}}\}j(k/p_\Lambda)\sum_{l}[l]\sum_{\lambda,m+q}[l\lambda]^{\frac{1}{2}}C^{l1\lambda}_{000}i^l j_l(kr)[C^{(l)}X\sigma^{(1)}]^{(\lambda)}_{m+q}\cdot$$

$$\cdot D(\lambda,\,m+q\,0;\,\boldsymbol{k})\,,$$

where $t^{(1)}$, $j_l(kr)$ and C^{abc}_{def} are the isotopic spin wave function of the pion field, the spherical Bessel function of order l and a Clebsch-Gordan coefficient respectively.

$$C^{(l)}_m(\boldsymbol{r}) = \left(4\pi/[l]^{\frac{1}{2}}\right)Y^{(l)}_m(\boldsymbol{r})$$

and

$$D(l,\,m0;\,\boldsymbol{k}) = \left(4\pi/[l]^{\frac{1}{2}}\right)Y^{(l)*}_m(\boldsymbol{k})\,.$$

The former relation is convenient for calculating the matrix element in coordinate space and the latter relation is convenient for the angular correlation problem and the related probability ([11]). We can obtain the corresponding expression for the neutral pion and neutron decay by replacing $\sqrt{\frac{2}{3}}$ and $\sqrt{\frac{1}{6}}$ in front of the isotopic spin operator by $\sqrt{\frac{1}{3}}$ and $-\sqrt{\frac{1}{3}}$ respectively and the magnetic quantum number $\frac{1}{2}$ for the isotopic spin operator by $-\frac{1}{2}$.

Wave functions for the initial and final states Ψ_i and Ψ_f are given in terms of French diagrams by

(3)

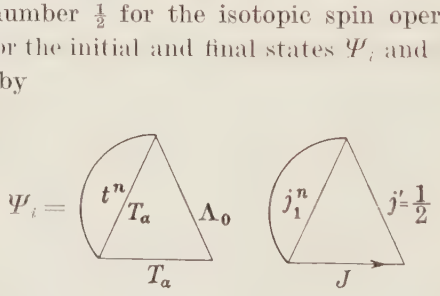

and

(4)

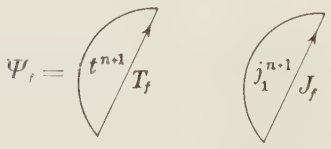

([11]) L. C. Biedenharn and M. E. Rose: *Rev. Mod. Phys.*, **25**, 729 (1953).

for the rearrangement of the decay nucleon in the j_1-shell which is not occupied by nucleons of the original hyperfragment; and by

(5) $\Psi_f =$ 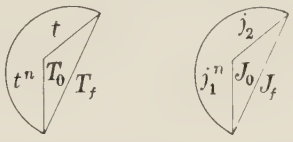

for the case where there is rearrangement of the decay nucleon in the j_2-shell (which is a different shell from the shell occupied by the nucleons in the hyperfragment). The curly brackets on the French diagram show that nucleons in it are totally antisymmetrized. The decay operator is not isoscalar so we have to introduce the wave function in the isotopic spin space (compare the notation in paper I). Equations (4) and (5) are rewritten in convenient forms by making use of the coefficient of fractional parentage (c.f.p.)

(6) $$\Psi_f = \sum_{T_x, J_x} \langle T_f J_f | T_x J_x \tfrac{1}{2} j_1 \rangle$$ 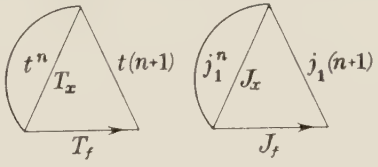

and

(7) $$\Psi_f = 1/\sqrt{n+1}$$ 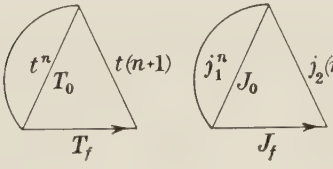

$$- \sqrt{n/(n+1)} \sum_{\substack{T_1, T_2 \\ J_1, J_2}} (-)^{J_1+J_f-J_0-J_2} U(j_1 J_1 J_f j_2;\, J_0 J_2) \cdot$$

$$\cdot \langle T_0 J_0 | T_1 J_1 \tfrac{1}{2} j_1 \rangle$$ 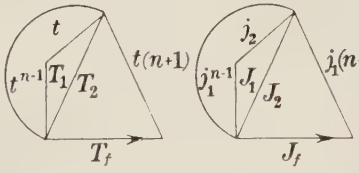

,

where the c.f.p. is given in charge-space-spin states. The coefficient U is related to the Racah coefficient by

(8) $$U(abcd;\, ef) = [ef] W(abcd;\, ef) ,$$

where $[ef] = (2e+1)(2f+1)$. It is clear that the second term of (7) does not

contribute to the matrix element for two-body mesic decay because the n-th nucleon has a different configuration from that of the hyperfragment. As mentioned before the s-shell hyperfragment takes the same expression in both L-S and j-j schemes.

We obtain the complete matrix element in the form

$$\langle f|H|i\rangle = \sqrt{n+1}\, C^{T_\alpha \frac{1}{2} T_f}_{m_{T_\alpha} \frac{1}{2} m_{T_f}} / \sqrt{2} \sum_l i^l \langle R_p | j_l(kr) | R_\Lambda \rangle \cdot$$

$$\cdot (-)^{\frac{1}{2}-J}[J]^{\frac{1}{2}} \delta_{l,l} T_f J_f | T_\alpha J_\alpha \tfrac{1}{2} j_1 \rangle (-)^{J_\alpha} \Big[-s\, W(\tfrac{1}{2} j_1 J J_f; l J_\alpha) \sum_m C^{J \; l \; J_f}_{m_J m m_{J_f}} D(l, m0; \boldsymbol{k}) +$$

$$+ \sqrt{6}[l_1|p \sum_\lambda W(\tfrac{1}{2} J j_1 J_f; J_\alpha \lambda)\, W(l\lambda \tfrac{1}{2} \tfrac{1}{2}; l j_1) C^{l 1 \lambda}_{0\,0\,0} \sum_{m+q} C^{J \; \lambda \; J_f}_{m_J m\, -q\, m_{J_f}} D(\lambda, m-q\, 0; \boldsymbol{k}) \Big] ,$$

where R_p and R_Λ are the radial wave function of the bound proton and the Λ-hyperon, respectively,

$$s = \sqrt{\tfrac{2}{3}} a_{\frac{1}{2}s} + \sqrt{\tfrac{1}{6}} a_{\frac{3}{2}s} , \tag{10}$$

$$p = (k/p_\Lambda)(\sqrt{\tfrac{2}{3}} a_{\frac{1}{2}p} + \sqrt{\tfrac{1}{6}} a_{\frac{3}{2}p}) . \tag{11}$$

Here a contains the reduced matrix element for the isotopic spin operator. The corresponding quantities for the neutral pion and the neutron decay will be defined by s' and p' respectively. The factor $\sqrt{n+1}$ in the front of the right-hand side of (9) comes from the indistinguishability of the nucleons in the final state in the j_1-shell. The matrix element for the neutral mesic decay is obtained replacing s, p by s', p' and the magnetic quantum number for the Clebsch-Gordan coefficient $\frac{1}{2}$ by $-\frac{1}{2}$ as we discussed for the derivation of the operator under eq. (2). The decay into final state (7) is obtained replacing $(n+1)$ by 1 for both mesic decays. Other kinematical factors should also be changed into the corresponding quantities, for instance, j_1 into j_2, etc.

2·1. *Two-body mesic decay.*

a) Polarization-direction correlation. Before calculating the decay probability we wish to talk about the polarization-direction correlation which is possible only if the hyperfragment produced has a non-zero spin and a definite polarization. The kaon absorption in flight by the nucleus and the consequent production of hyperfragment and pion can produce such a state. The polarized hyperfragment decay gives an asymmetry for the momentum distribution of the decay pion. This will become one of the independent tests for the determination of the spin of $^4\mathrm{He}_\Lambda$ from its decay in $\mathrm{K}^- + {}^4\mathrm{He} \rightarrow$

$\to {}^4\mathrm{He}_\Lambda + \pi^-$ experiment ([12]) and hence the relative parity of the kaon. Although the above experiment was done for the kaon absorption at rest up to the present. Most of the hyperfragments are observed in nuclear plates and hence an associated emission of many nucleons makes ambiguous the polarization of the hyperfragment. The state of the polarization is specified by the magnetic quantum number m_J of the angular momentum J of the hyperfragment. Thus in the completely polarized state only a definite value of m_J is allowed. The absolue square of (9) with no summation with respect to m_J gives the probability of the correlation. The example discussed above will be shown explicitly at the end of Section 3.

b) Decay probability. In computing the total mesic decay probability we will first « rotate » the matrix element (9) in the momentum space so that the argument of the third component of the D-function changes from zero to M and then we will take the average over the initial spin for the absolute square of the matrix element and sum over the magnetic quantum number of the hyperfragment. (No summation should be taken for m_J in the correlation problem discussed in *a*) above.) Making use of the nature of the D-function and the Clebsch-Gordan coefficient the correlation function, $E(m_{J_f}, m'_{J_f})$, defined by

$$E(m_{J_f}, m'_{J_f}) = 1/[J] \sum_{m_J} |\langle f|H|i \quad ^2 \tag{12}$$

reduces to a simpler form. The decay probability is obtained by integrating over the momentum $\boldsymbol{k}$ multiplying the δ-function of the conservation of energy to the correlation function defined above, (12), summed over the magnetic quantum number of the residual nuclear states in the non-relativistic limit:

$$w_{fi} = \int \mathrm{d}\boldsymbol{k}\, \delta(E_i - E_f) \sum_{m_{J_f},\, m'_{J_f}} E(m_{J_f}, m'_{J_f}) \,. \tag{13}$$

The result of the calculation is given by

$$\begin{aligned} w_{fi} = {} & (n+1)[J_f](C^{T\ \frac{1}{2}\ T_f}_{m_T\ \frac{1}{2}\ m_{T_f}})^2 \langle R_p|j_{l_1}(kr)|R_\Lambda\rangle^2 2\pi\mu k \cdot \\ & \cdot \Big[|s|^2 [j_1]^{\frac{1}{2}} \langle T_f J_f | T_\lambda J_\alpha \tfrac{1}{2}\, j_1\rangle W(\tfrac{1}{2}\, j_1 J J_f;\, l_1 J_\lambda)^{\ 2} + \\ & + 6\ p|^2 \sum_\lambda [\lambda](C^{l_1 1 \lambda}_{0\ 0\ 0})^2 |[j_1 l_1]^{\frac{1}{2}} \langle T_f J_f | T_\alpha J_\alpha \tfrac{1}{2}\, j_1\rangle W(\tfrac{1}{2}\, J j_1 J_f;\, J_\lambda \lambda) W(l_1 \lambda_1 \tfrac{1}{2}\, \tfrac{1}{2};\, l j_1)^{\ 2} \Big] , \end{aligned} \tag{14}$$

([12]) The Helium Bubble Chamber Collaboration Group: *Proceedings of the Tenth Annual High Energy Conference at Rochester* (New York, 1960), p. 419, presented by G. Puppi.

where μ and k are the pion mass and relative momentum of the pion and the residual nucleus. We made an approximation that the pion mass is small compared to that of the residual nucleus. In the exact non-relativistic approach we have to use the reduced mass $M\mu/(M-\mu)$ instead of μ (where M is the mass of the residual nucleus).

2·2. *Three-body mesic decay through « compound nucleus ».*

i) Angular correlation. In most of the three-body mesic decays the pion will be emitted without appreciable final state interaction because of the small phase shifts of the low energy pion-nucleon interaction. On the other hand the nucleon will have a strong final state interaction with the residual nucleus because of the existence of the various compound states of the nucleus. This confines the spin and the parity of the outgoing nucleon and the residual nucleus. It will provide means for the investigation of the unknown nature of hyperfragments and the structure of the decay interaction of the Λ-hyperon. Therefore we will first formulate the case in which the outgoing nucleon decays through the compound state. The lifetime of the resonance state is of the order of the nuclear lifetime so we will expect the disturbance in the intermediate state of the problem to be very little ([13]). The (differential) probability for this channel will be given by the product of two correlation functions by taking the complex conjugate for one of them and summing over the magnetic quantum numbers in the intermediate state, one of the correlation functions being for the pion emission and the other for the nucleon emission. The first one is given by (12) replacing the isotopic spin T_f, and the spin J_f by their intermediate values T_I and J_I. Of course all other quantities appearing in the final state should be taken the same as the intermediate ones. In order to obtain the second one we expand the nucleon wave function in plane waves:

$$(15)\qquad \Psi(\boldsymbol{r}) \quad u(\boldsymbol{p})\exp[i\boldsymbol{p}\cdot\boldsymbol{r}] \quad u(\boldsymbol{p})\sum_{L,M}(4\pi[L])^{\frac{1}{2}}i^L j_L(pr)\,Y_{LM}(\boldsymbol{r})\,D(L,M0;\boldsymbol{p}) -$$

$$= \sum_{L,M}(4\pi[L])^{\frac{1}{2}}i^L j_L(pr)\sum_{\substack{j\\ M+m_s}} C^{L\,\frac{1}{2}\,j}_{M\,m_s}\;\begin{array}{c} L \quad\quad \frac{1}{2} \\ j \end{array}\; D(L,M0;\boldsymbol{p})\,,$$

where $u(p)$ is the Pauli spinor. The correlation function, $E^{(2)}(m_{J_T}, m'_{J_T})$, is

([13]) For the electromagnetic disturbance, see the discussion given by Biedenharn and Rose, reference ([11]).

given by

$$(16)\qquad E^{(2)}(m_{J_I}, m'_{J_I}) = (-)^{N-m_{J_I}-J_f}(C^{T_I\ \frac{1}{2}\ T_f}_{m_{T_I}\ m_{T_f}})^2 4\pi[L]\cdot$$

$$\cdot\ \langle R_p\,|\,j_L(pr)\rangle^2 \sum_{\substack{J_f\\ M_J+M+m_s}} C^{J\alpha\ \ j_1}_{M_{J_\alpha}M+m_s\ J_f} C^{J\alpha\ \ j'_1\ \ J_f}_{M_{J_\alpha}M+m_s} \sum_{\substack{j\\ M+m_s}} C^{L\,\frac{1}{2}\,j_1}_{M\,m_s} C^{L'\ \frac{1}{2}\ j'_1}_{M\ m_s}.$$

$$\cdot\, C^{L\ \ L'\ \nu}_{-N\ N'} C^{J_I\ \ J'_I\ \nu}_{m_{J_I}\,m'_{J_I}} W(J_I J_I L L'; \nu J_f)\, D(\nu,\ m'_{J_I} - m_{J_I},\ N' - N;\ \mathscr{R}_2)\,,$$

where we have chosen a general co-ordinate system in momentum space. Making use of the orthogonality of the Clebsch-Gordan coefficients and the relation for the product of D-functions we have the double correlation function, W, in the following form

$$(17)\qquad W = \sum_{m_{J_I}; m_{J_I}} E^{(1)}(m_{J_I}, m'_{J_I}) E^{(2)*}(m_{J_I}, m'_{J_I}) =$$

$$= (n+1)(C^{T\ \frac{1}{2}\ T_I}_{m_T\ \frac{1}{2}})^2 (C^{T_I\ \frac{1}{2}\ T_f}_{m_{TI}\ \frac{1}{2}})^2 / 2 \langle R_p\,|\,j_{l'}(kr)\,|\,R_\Lambda\rangle^* \langle R_p\,|\,j_{l_1}(kr)\,|\,R_\Lambda\rangle\cdot$$

$$\cdot \langle R_p\,|\,j_{L'}(pr)\ ^*\cdot\ R_p\,|\,j_{L'}(pr)\rangle (-)^{J-m_{J_I}+J_I-m'_{J_I}} [j_1 j'_1 l_1 l'_1]\cdot$$

$$\cdot 4\pi[LL']^{\frac{1}{2}} \sum_{\substack{J_f\\ M_J+M+m_s}} C^{J\ \ j_1\ \ J_f}_{m_J\ M+m_s} C^{J\ \ j'_1\ \ J_f}_{m_J\ M+m_s} \sum_{M+m_s} C^{L\ \frac{1}{2}\ j_1}_{m\ m_s} C^{L'\ \frac{1}{2}\ j'_1}_{M\ m_s}.$$

$$\cdot \langle T_I J_I\,|\,T_\alpha J_\alpha\, \tfrac{1}{2}\, j_1\rangle \langle T_I J_I]\,|\,T_\alpha J_\alpha\, \tfrac{1}{2}\, j_1\rangle [\,|\,s\,|^2 W(\tfrac{1}{2} j_1 J J_I;\ l_1 J_\alpha)\cdot$$

$$\cdot W(\tfrac{1}{2} j'_1 J J_I;\ l'_1 J_\alpha)(-)^n C^{l_1\ \ l'_1\ \ \nu}_{-n\ \tau_1+n} W(J_I J_I l_1 l'_1;\ \nu J) -$$

$$- \sqrt{6}[l'_1]\, s^* p\, W(\tfrac{1}{2} j_1 J J_I;\ l_1 J_\alpha)\, W(\tfrac{1}{2} J j_1 J_I;\ J_\alpha \lambda')\, W(l'_1 \lambda' \tfrac{1}{2}\,\tfrac{1}{2};\ l_1 9 j_1)\cdot$$

$$\cdot C^{l'_1 1 \lambda'}_{0\ 0\ 0} (-)^n C^{l_1\ \ \lambda'\ \ \nu}_{-1\ \tau_1+n} W(J_I J_I l_1 \lambda;'\ \nu J)\cdot$$

$$- \sqrt{6}[l_1] p^* s\, W(\tfrac{1}{2} J j_1 J_I;\ J_\alpha \lambda)\, W(l_1 \lambda \tfrac{1}{2}\,\tfrac{1}{2};\ l j_1)\, W(\tfrac{1}{2} j_1 J J_I;\ l'_1 J_\alpha)\cdot$$

$$\cdot C^{l_1 1 \lambda}_{0\ 0\ 0} (-)^n C^{l_1\ \ \lambda\ \ \nu}_{-n\ \tau_1+n} W(J_I J_I \lambda l'_1;\ \nu J) +$$

$$+ 6[l_1 l'_1]^{\frac{1}{2}} |\,p\,|^2 W(\tfrac{1}{2} J j_1 J_I;\ J_\alpha \lambda)\, W(\tfrac{1}{2} J j'_1 J_I;\ J_\alpha \lambda')\, W(l_1 \lambda \tfrac{1}{2}\,\tfrac{1}{2};\ 1 j_1)\cdot$$

$$\cdot W(l'_1 \lambda' \tfrac{1}{2}\,\tfrac{1}{2};\ 1 j'_1) C^{l_1 1 \lambda}_{0\ 0\ 0} C^{l'_1 1 \lambda'}_{0\ 0\ 0} [\lambda \lambda'] (-)^n C^{\lambda\ \ \lambda'\ \ \nu}_{-n\ \tau_1+n} W(J_I J_I \lambda \lambda';\ \nu J)]\cdot$$

$$\cdot (-)^N C^{L\ \ L'\ \ \nu}_{-N\ \tau_2+n} W(J_I J_I L L';\ \nu J_f)\, D(\nu,\ \tau_2 \tau_1;\ \mathscr{R}_2^{-1} \mathscr{R}_1)\,,$$

where the D-function is the function of the relative angle between pion and nucleon momenta in the general co-ordinate system. The knowledge of the direction-direction correlation of momentum distribution of pion and nucleon is ob-

tained by putting $\tau_1 = \tau_2 = 0$. As seen from (17) the correlation is completely determined by the angular momentum if the decay occurs through the pure intermediate state. The multiplication factor arising from the radial dependence is unimportant for the correlation.

ii) Decay probability. The three-body mesic decay probability, w_{fi}, is obtained by integrating the correlation function (17) (keeping $\tau_1 = \tau_2 = 0$) over the momentums of the pion $\boldsymbol{k}$ and the nucleon $\boldsymbol{p}$ multiplying the δ-function for the conservation of the total energy,

$$w_{fi} = \int \mathrm{d}\boldsymbol{k} \int \mathrm{d}\boldsymbol{p}\, \delta(E_i - E_f)\, W\,, \tag{18}$$

where a multiplicative constant such as a weight factor with respect to spin is neglected. Fixing the direction of the proton momentum as a reference system the argument of the Legendre polynomial P (arising from the D-function in (17)) is exactly the angle between $\boldsymbol{k}$ and $\boldsymbol{p}$ in the new system. Then the integration for the angle of $\boldsymbol{p}$ will give 4π and the total integration reduces to the integral for the relative angle and the magnitude of k and p. Rewriting the δ-function in a suitable form we obtain w_{fi} in the form

$$w_{fi} = 2(2\pi)^2 M \int p\, \mathrm{d}p \int k\, \mathrm{d}k\, \mathrm{d}(\cos\beta) \cdot \tag{19}$$

$$\cdot \delta(\cos\beta + (M+m)p/2mk + (M+\mu)/k2\mu p - ME/pk)\, W\,,$$

where μ, m and M are masses of the pion, nucleon and residual nucleus respectively. This integration can be done analytically if we specify the rank ν of the Legendre polynomial (see Appendix I).

2·3. *Three-body mesic decay without compound nucleus formation.* – The p-shell nuclei have so many levels that the outgoing nucleon will have final state interaction corresponding to each level of the compound state. Even if there is no appreciable level structure the ground state can contribute to the final state interaction. In some of the decay processes the outgoing nucleon has a proper energy and no appreciable final state interaction appears, for instance, for s-shell hyperfragment decay. In order to treat this type of problem we will develop here formulae for the three-body mesic decay without final state interactions. The decay Hamiltonian is given by (2) and the outgoing nucleon is described by (15). The wave function for the final state with the angular momentum J is given by the decoupling of the nucleon wave function with the angular momentum J_ν. Thus the Clebsch-Gordan coefficients give the possible weights of admixtures. The matrix element for the process

is given by

$$\langle f|H|i\rangle = \sum (C^{T\ \frac{1}{2}\ T}_{m_T\,\frac{1}{2}\,m_{T_f}})^2/\sqrt{2}\sum_l i^{2l}\sqrt{4\pi}\cdot \tag{20}$$

$$\cdot\ j_l(pr)\,|j_l(kr)\rangle R_\Lambda\rangle(-)^{\frac{1}{2}-J}\sum_j [Jj]^{\frac{1}{2}}[l](-)^{J_\alpha}\,C^{J_\alpha\ j\ J_f}_{MJ_\alpha\ M+m_s\ m}C^{l\ \frac{1}{2}\ j}_{M\ m_s}\cdot$$

$$\cdot[-s\,W(\tfrac{1}{2}jJJ_f;\,lJ_\alpha)\sum_m C^{J\ l\ J_f}_{m_J\,m}D(l,\,m0;\,\boldsymbol{k})\,D(l,\,M0;\,\boldsymbol{p})-$$

$$-\sqrt{6}[l]p\sum_{\lambda,\,m+q} W(\tfrac{1}{2}Jj J_f;\,J_\alpha\lambda)\,W(l\lambda\tfrac{1}{2}\tfrac{1}{2};\,lj)\,C^{l\,1\,\lambda}_{0\,0}[\lambda]\cdot$$

$$\cdot C^{J\ \lambda\ J_f}_{m_J\,m+q}D(\lambda,\,m+q,\,0;\,\boldsymbol{k})\,D(l,\,M0;\,\boldsymbol{p})]\,,$$

where the first sum on the right is over the possible value of the isotopic spin for the residual nucleus and the outgoing nucleon. The summation over the angular momentum state is not given explicitly. In order to calculate the decay probability we have to take the absolute square of eq. (20) sum over the final magnetic quantum numbers and average over the initial spin. We do not give an explicit form of it here but numerical values for the s-shell hyperfragment are tabulated in a later section (See Table IV).

3. – Two-body mesic decay; applications.

In this section we want to apply to the two-body mesic decay processes the theory developed in the preceding section.

3·1. *Decay probability.* – As seen in Section 2 all the mesic decays are described by the absolute square of the radial matrix element with numerical coefficients arising from the number of nucleons, the spin of the residual nucleus, the weight factor from the charge space, $2\pi\mu k$ and the amplitude multiplied by the kinematical factors (see eq. (14)). The amplitudes s and p contain the reduced matrix elements in charge space. These are for the charged mesic decay amplitudes. For the neutral mesic decay we have to change numerical factors of the amplitudes as we discussed in Section 2. We will first tabulate the kinematical coefficients and discuss for individual hyperfragments.

Assuming the same s-wave and p-wave rate in the decay interaction we can discuss about the decay branching ratio using Table I. We will give an example how to use the Table and analyse the more interesting examples. Let us take the $^{10}\mathrm{Be}_\Lambda$ negative mesic decay which leads to $^{10}\mathrm{B}+\pi^-$. The hole-hole configuration of the $p_{\frac{3}{2}}$-shell and all four states belonging to this configuration are stable; hence the branching ratios to spin 0, 1, 2 and 3 are interesting. They are obtained to be 2:4:20:21 and 90:140:360:189 for the antiparallel

TABLE I. – *Two-body mesic decay probabilities.*

Decay scheme	J	J_f	Coefficients of Radial term	Direct term	Derivative term
$^3H_\Lambda \to \pi^- + {}^3He$	1/2	1/2	6	1/4	1/12
	3/2	1/2	6	0	1/3
$^3H_\Lambda \to \pi^0 + {}^3H$	1/2	1/2	6	1/4	1/12
	3/2	1/2	6	0	1/3
$^4H_\Lambda \to \pi^- + {}^4He$	0	0	2	1	0
	1	0	2	0	1
$^4He_\Lambda \to \pi^0 + {}^4He$	0	0	2	1	0
	1	0	2	0	1
$^6He_\Lambda \to \pi^- + {}^6Li$	1	0	1	1/3	0
	1	1	3	5/18	1/6
	1	2	5	1/6	1/2
	1	3	7	0	1
	2	0	1	0	1
	2	1	3	1/30	9/10
	2	2	5	1/10	7/10
	2	3	7	1/5	2/5
$^7He_\Lambda \to \pi^- + {}^7Li$	1/2	3/2	4	$5^5/24$	25/24
$^7Li_\Lambda \to \pi^- + {}^7Be$	1/2	1/2	6	$2^5/9$	0
	1/2	3/2	12	1/24	3/40
	3/2	1/2	6	1/72	3/16
	3/2	3/2	12	1/18	3/20
$^8Li_\Lambda \to \pi^0 + {}^8Li$	1	2	20	1/30	1/10
	2	2	20	1/50	7/50
$^9Li_\Lambda \to \pi^- + {}^9Be$	3/2	3/2	40/3	1/5	1/5
	5/2	3/2	40/3	1/30	1/10
$^9Be_\Lambda \to \pi^0 + {}^9Be$	1/2	3/2	20	5/24	25/24
$^{10}Be_\Lambda \to \pi^- + {}^{10}B$	1	0	6	1/3	0
	1	1	9	5/18	1/6
	1	2	30	1/6	1/2
	1	3	21	0	1
	2	0	6	0	1
	2	1	9	1/30	9/10
	2	2	30	1/10	7/10
	2	3	21	1/5	2/5

TABLE I (*continued*).

Decah scheme	J	J_f	Coefficients of		
			Radial term	Direct term	Derivative term
$^{10}Be_\Lambda \rightarrow \pi^0 + {}^{10}Be$	1	0	6	1/3	0
	1	2	30	1/6	1/2
	2	0	6	0	1
	2	2	30	1/10	7/10
$^{10}B_\Lambda \rightarrow \pi^- + {}^{10}C$	1	0	6	1/3	0
	2	0	6	0	1
$^{11}Be_\Lambda \rightarrow \pi^- + {}^{11}B$	1/2	3/2	56/3	1/2	5/2
	1/2	1/2	4/3	1/14	5/14
$^{11}B_\Lambda \rightarrow \pi^- + {}^{11}C$	5/2	3/2	28	1/6	1/4
	5/2	1/2	—	0	0
	7/2	3/2	—	0	0
	7/2	3/2	—	0	0
$^{11}B_\Lambda \rightarrow \pi^0 + {}^{11}B$	5/2	3/2	28	1/5	1/14
	5/2	1/2	—	0	0
	7/2	3/2	—	0	0
	7/2	1/2	—	0	0
$^{11}C_\Lambda \rightarrow \pi^0 + {}^{11}C$	1/2	3/2	56/3	1/2	5/2
	1/2	1/2	4/3	1/14	5/14
$^{12}B_\Lambda \rightarrow \pi^- + {}^{12}C$	1	0	4	1/3	0
	1	2	5/2	1/3	0
	2	0	4	0	1
	2	2	5/2	1/10	1/5
$^{12}B_\Lambda \rightarrow \pi^0 + {}^{12}B$	1	1	3/2	1/18	1/3
	1	2	5/2	1/6	0
	2	1	3/2	1/6	0
	2	2	5/2	1/10	0
$^{13}C_\Lambda \rightarrow \pi^- + {}^{13}N$	1/2	1/2	2	1/2	1/2
	1/2	1/2 (p)	2	1/2	1/2
	1/2	1/2 (s)	2	1/2	3/2
$^{14}C_\Lambda \rightarrow \pi^- + {}^{14}N$	0	1		1/3	0
	0	0	—	0	0
	1	1	6	2/9	1/2
	1	0	4	1/3	0

TABLE I (*continued*).

Decay scheme	J	J_f	Coefficients of Radial term	Direct term	Derivative term
$^{11}N_\Lambda \rightarrow \pi^0 + {}^{11}N$	0	1	6	1/3	0
	0	0	4	0	0
	1	1	6	2/9	1/2
	1	0	4	1/3	0
$^{15}N_\Lambda \rightarrow \pi^- + {}^{15}O$	1/2	1/2 (p)	6	1/18	1/2
	1/2	5/2 (d)	6	7/30	3/4
	1/2	1/2 (s)	2	1/2	1/6
	1/2	3/2 (d)	4	1/10	1/2
	3/2	1/2 (p)	6	2/5	0
	3/2	5/2 (d)	6	2/15	1/3
	3/2	1/2 (s)	2	0	2/3
	3/2	3/2 (d)	4	1/5	1/5
$^{16}N_\Lambda \rightarrow \pi^- + {}^{16}O$	0	0	2	0	1
	1	0	2	1/3	0
$^{16}N_\Lambda \rightarrow \pi^0 + {}^{16}N$	0	0 (s)	1	1	0
	0	1 (s)	3	0	1/3
	0	2 (d)	5	3/5	0
	0	3 (d)	7	0	6/7
	1	0 (s)	1	0	1
	1	1 (s)	3	1/3	2/3
	2	2 (d)	5	2/15	2/3
	1	3 (d)	7	1/3	8/21
$^{16}O_\Lambda \rightarrow \pi^0 + {}^{16}O$	0	0	2	0	1
	0	0	0	1/3	0
$^{17}O_\Lambda \rightarrow \pi^- + {}^{17}F$	1/2	5/2 (d)	6	1/2	7/2
	1/2	1/2 (s)	2	1/2	3/2
$^{17}O_\Lambda \rightarrow \pi^0 + {}^{17}O$	1/2	5/2 (d)	6	1/2	7/2
	1/2	1/2 (s)	2	1/2	3/2

Notations s, p and d in the bracket after J_f show the configuration of the decay nucleons which are different from the original configuration of the nucleons.

spin and parallel spin of $^{10}Be_\Lambda$ respectively. These ratios are not sufficiently sensitive so it is better to find out more crucial examples. One sees from Table I that the $^{11}B_\Lambda$ decay into the negative and the neutral two-body decay modes are allowed only for spin $\frac{5}{2}$. Thus the observation of the two-body decay mode uniquely determines the antiparallel-favoured spin for $p_{\frac{1}{2}}$-shell hyperfragments. Another less definite example is the two-body decay mode of $^{11}B_\Lambda$ where the decay into the $J_r = 0$ state is forbidden for the anti-parallel favoured spin configuration. This will be used for the determination of the relative preference for parallel and antiparallel-spin configuration for $p_{\frac{1}{2}}$-shell hyperfragments.

3·2. *Polarization and direction correlation.* – The case of the cascade decay

$$K^- + {}^4He \to {}^4He_\Lambda + \pi^- \tag{21}$$

$$\searrow \; {}^4He + \pi^0 \tag{22}$$

may be examined. The correlation will be obtained only for $J=1$ for $^4He_\Lambda$. Assuming a complete polarized state for ^4He, $J=1$, $m_J=1$ leads to the correlation, $W(\theta)$:

$$W(\theta) = (1/6)\,|p|^2 \sin^2\theta\,. \tag{23}$$

The distribution of the pion momentum with respect to the direction of the polarization of $^4He_\Lambda$ is symmetric with respect to the decay plane. There is no up-down asymmetry hence the correlation probability, X, is defined by

$$X \equiv \alpha = \int_{\pi/4}^{\frac{3}{4}\pi} W(\theta)\,\sin\theta\,\mathrm{d}\theta \Big/ \int_0^{\pi} W(\theta)\,\sin\theta\,\mathrm{d}\theta = \frac{\sqrt{2}}{2} \tag{24}$$

The value αP_1 is compared with the experimental value where P_1 is the polarization with magnetic quantum number 1.

4. – Isotopic spin selection rule.

In this section we will consider the isotopic spin selection rule. This can be done from the decay branching ratio of the negative and the neutral pion modes. Unfortunately we do not have enough data for this purpose so we will confine ourselves to the theoretical investigation and show how to apply our ideas to the problem. The negative and neutral decay rate takes the

simple form

$$w(\pi^-)/w(\pi^0) = (a|s|^2 + b|p|^2)/(a|s'|^2 + b|p'|^2) , \tag{25}$$

where a and b are numbers which are tabulated in Table II.

TABLE II. – *Branching ratio for the negative and neutral mesic decay.*

Hyperfragment	J	J_f	a	b
$^3H_\Lambda$	1/2	1/2	1	1/3
	3/2	1/2	0	1
$^7Li_\Lambda$	1/2	1/2	1	0
	1/2	3/2	1/3	3/5
	3/2	1/2	1/9	3/2
	3/2	3/2	1/9	3/10
$^{10}Be_\Lambda$	1	0	1	0
	1	2	1	3
	2	0	0	1
	2	2	1	7
$^{10}B_\Lambda$	1	0	1	0
	2	0	0	1
$^{11}B_\Lambda$	3/2	3/2	7	3
$^{13}C_\Lambda$	1/2	1/2	1	1

As stated earlier the parameters which we are using are related to those for free Λ-decay of OKUBO *et al.* (9) by

$$\begin{cases} a_{\frac{1}{2}s} = A_1\langle\tfrac{1}{2}\|[t^{(1)}XD^{(\frac{1}{2})}]^{(\frac{1}{2})}\|0\rangle , \\ a_{\frac{3}{2}s} = A_3\langle\tfrac{1}{2}\|[t^{(1)}XD^{(\frac{3}{2})}]^{(\frac{1}{2})}\|0\rangle , \\ a_{\frac{1}{2}p} = B_1\langle\tfrac{1}{2}\|[t^{(1)}XD^{(\frac{1}{2})}]^{(\frac{1}{2})}\|0\rangle , \\ a_{\frac{3}{2}p} = B_3\langle\tfrac{1}{2}\|[t^{(1)}XD^{(\frac{3}{2})}]^{(\frac{1}{2})}\|0\rangle . \end{cases} \tag{26.a}$$

The reality of A, B and the π^-, π^0 branching ratio of the free Λ-decay, 2/1 give

$$A_3 = \sqrt{2}\,A_1 , \qquad B_3 = \sqrt{2}\,B_1 . \tag{26.b}$$

If we write the reduced matrix element in the form

$$\sqrt{2}\langle\tfrac{1}{2}\|[t^{(1)}XD^{(\frac{1}{2})}]^{(\frac{1}{2})}\|0\rangle = \langle\tfrac{1}{2}\|[t^{(1)}XD^{(\frac{3}{2})}]^{(\frac{1}{2})}\|0\rangle , \tag{26.c}$$

we see that conditions (26) give the ratio 2/1 for all the cases of Table II. One may consider also the decay branching ratios of the same hyperfragment to the different residual state for π^- and π^0 decay which is not always 2/1 even if we confine to the $\Delta I = \frac{1}{2}$ o $\frac{3}{2}$ rules. But the ratio does not change in the case with the simultaneous contribution of the $\Delta I = \frac{1}{2}$ and $\frac{3}{2}$ rules.

5. – Three-body mesic decay (numerical).

5·1. *Nucleon through definite states in decay. Directional correlation.* – It is well known that the directional correlation is a good technique to determine the spin of the nuclear states. We will consider the pion and proton directional correlation for assignments of the various possible spins of hyperfragments. Now we are considering the decay through the definite spin (parity) of the nucleus so that the single j_1 and l_1 ($l_1 = L = l$) contribute as the intermediate state of the proton and residual nucleus interaction. Assuming the angle θ between the directions of the pion and the proton we have the correlation function in the form

$$W(\theta) = a\langle j_l(pr)\,|\,R_p\rangle^2\langle R_p\,|\,j_l(kr)\,|\,R_\Lambda\rangle^2[b\,|\,s\,|^2\{c\,D(0,\,00;\,\mathscr{R}) + d\,D(2,\,00;\,\mathscr{R})\} + \\ + e\,|\,p\,|^2\{f\,D(0,\,00;\,\mathscr{R}) + g\,D(2,\,00;\,\mathscr{R})\}]\,, \tag{27}$$

where $D(k,\,00;\,\mathscr{R}) = P_k(\cos\theta)$ and $\mathscr{R}$ is the short notation for $\mathscr{R}_2^{-1}\mathscr{R}_1$ (see (17)). The cross term between the direct and derivative terms vanishes for the cases in which we are interested. The coefficients a, b, ..., g are numbers given by

$$a = ((n+1)/2((C^{T\alpha\ \frac{1}{2}\ T_I}_{m_{T_\alpha}\ \frac{1}{2}\ m_{T_I}} C^{T_I\ \frac{1}{2}\ T_f}_{m_{T_I}\ \frac{1}{2}\ m_{T_f}})^2[jl]4\pi[L]\,, \tag{28.a}$$

$$b = W(\tfrac{1}{2}jJJ_I;\,lJ_\alpha)\,W(\tfrac{1}{2}jJ\,J_I;\,lJ_\alpha)\,, \tag{28.b}$$

$$c = \sum_{J_f}[J_f]/2\,(-)^n C^{l\ l\ 0}_{-n\ n}\,W(J_I J_I ll;\,0J)(-)^N C^{l\ l\ 0}_{-N\ N}\,W(J_I J_I ll;\,0J_f)\,, \tag{28.c}$$

$$d = \sum_{J_f}[J_f]/2\,(-)^n C^{l\ l\ 0}_{-n\ n}\,W(J_I J_I ll;\,2J)(-)^N C^{l\ l\ 0}_{-N\ N}\,W(J_I J_I ll;\,2J_f)\,, \tag{28.d}$$

$$e = W(\tfrac{1}{2}Jj J_I;\,J_\alpha\lambda)\,W(\tfrac{1}{2}Jj J_I;\,J_\alpha\lambda')\,W(l\lambda\tfrac{1}{2}\tfrac{1}{2};\,lj)\,W(l\lambda'\tfrac{1}{2}\tfrac{1}{2};\,lj)\cdot \\ \cdot C^{l\,1\,\lambda}_{0\,0\,0}\,C^{l\,1\,\lambda'}_{0\,0\,0}[\lambda\lambda']\,, \tag{28.e}$$

$$f = \sum_{J_f}[J_f]/2\,(-)^n C^{\lambda\,\lambda'\,0}_{-n\ n}\,W(J_I J_I\lambda\lambda';\,0J)(-)^N C^{l\ l\ 2}_{-N\ N}\,W(J_I J_I ll;\,0J_f)\,, \tag{28.f}$$

$$g = \sum_{J_f}[J_f]/2\,(-)^n C^{\lambda\,\lambda'\,2}_{-n\ n}\,W(J_I J_I\lambda\lambda';\,2J)(-)^N C^{l\ l\ 2}_{N\ N}\,W(J_I J_I ll;\,2J_f)\,. \tag{28.g}$$

The classification of the coefficients given here is convenient for the cal-

culation. We will calculate these values for the various intermediate spins J_I for the decay of the three hyperfragments with $A = 3$, 4 and 5. The three-body mesic decay of $^3H_\Lambda$ is given by

(29) $$^3H_\Lambda \to D + p + \pi^- .$$

TABLE III. – *Three-body mesic decay-nucleon through definite state in decay.*

J	J_I	J_f	State of p	a	b	c	d	e	f	g
					$^3H_\Lambda \to D + p + \pi^-$					
1/2	1/2	1/2, 3/2	$s_{1/2}$	6	1/42	1	0	3/46	1	0
3/2	1/2	1/2, 3/2	$s_{1/2}$	6	0	0	0	1/2	1	0
1/2	1/2	1/2, 3/2	$p_{3/2}$	24	1/9	1/6	0	0	0	0
1/2	3/2	1/2, 3/2	$p_{3/2}$	24	5/72	1/15	4/45	5/8	3/120	13/300
1/2	1/2	1/2, 3/2	$p_{1/2}$	12	1/36	1/6	0	1/8	3/6	0
1/2	3/2	1/2, 3/2	$p_{1/2}$	12	1/9	1/12	13/180	0	0	0
3/2	1/2	1/2, 3/2	$p_{3/2}$	24	1/144	1/12	0	24/144	1/20	0
3/2	3/2	1/2, 3/2	$p_{3/2}$	24	1/36	1/6	16/225	5/4	$1/80\sqrt{15}$	0
3/2	5/2	3/2, 5/2	$p_{3/2}$	24	1/256	5/52	4/135	35/48	1/18	38/2205
3/2	1/2	1/2, 3/2	$p_{1/2}$	12	1/9	1/6	0	0	0	0
3/2	3/2	1/2, 3/2	$p_{1/2}$	12	5/72	$1/6\sqrt{2}$	0	5/24	$1/4\sqrt{3}$	0
					$^4H_\Lambda \to {}^3H + p + \pi^-$					
0	0	0	$s_{1/2}$	4	1/2	1	0	0	0	0
0	0	1, 2	$p_{3/2}$	9	1/6	4/27	2/27	0	0	0
0	2	1, 2	$p_{3/2}$	9	0	0	0	5/2	4/75	4/75
0	0	0, 1	$p_{1/2}$	9/2	0	0	0	1/2	2/3	0
0	1	0, 1	$p_{1/2}$	9/2	1	2/27	2/27	0	0	0
1	1	1, 2	$p_{3/2}$	9	1/36	4/27	1/27	25/12	4/45	$1/9\sqrt{105}$
1	2	1, 2	$p_{3/2}$	9	1/12	4/45	28/45	5/4	$4/25\sqrt{15}$	1/150
1	0	0, 1	$p_{1/2}$	9/2	1/6	2/9	0	0	0	0
1	1	0, 1	$p_{1/2}$	9/2	1/9	2/27	5/108	25/12	2/45	1/12
					$^5He_\Lambda \to {}^4He + p + \pi^-$					
1/2	3/2	1/2, 3/2	$p_{3/2}$	72π	1/8	1/12	1/12	25/8	1/20	1/20
1/2	1/2	1/2, 3/2	$p_{1/2}$	36π	1/4	1/5	0	3/4	1/2	0

The bound state of D+p, ^{3}He, is $^2S_{\frac{1}{2}}$ which gives rather strong effect because it is a strongly bound state. Other intermediate states can only be possible for the p-wave nucleon. In computing the table (see Table III) we neglected d-wave nucleons. The decays of $^4H_\Lambda$ and $^4He_\Lambda$ are given respectively by

(30) $$^4H_\Lambda \to {}^3H + p + \pi^-$$

and

$$^4\mathrm{He}_\Lambda \to {}^3\mathrm{He} + \mathrm{p} + \pi^- . \tag{31}$$

In these decays we have also considered up to p-wave protons.

The decay of $^5\mathrm{He}_\Lambda$ is given by

$$^5\mathrm{He}_\Lambda \to {}^4\mathrm{He} + \mathrm{p} + \pi \ . \tag{32}$$

This is a typical hyperfragment decay with strong final state interaction of the nucleon and the residual nucleus through the $p_{\frac{3}{2}}$ and $p_{\frac{1}{2}}$ channels. The spin of ^{4}He is zero so the proton state is equivalent to the total J_f. We tabulate all the cases discussed above in Table III.

5·2. *Nucleon with no definite state.* – In this case we consider only s-wave protons because the decay proton from s-state Λ stays in s-state without having interaction. The correlation function for $^3\mathrm{H}_\Lambda$, $^4\mathrm{H}_\Lambda$ and $^4\mathrm{He}_\Lambda$ decays are given by

$$W(\theta) = a' \ j_0(pr) \ j_0(kr) \ R_\Lambda^{\,2}\{ |s|^2\{b' D(0, 00; \mathscr{R}) + c' D(2, 00; \mathscr{R})\}_j - \tag{33}$$

$$- 2 (k/p_\Lambda) \ \mathrm{Re}\,(s^* p) d' D(1, 00; \mathscr{R}) + (k^2/p_\Lambda^2) |p|^2\{e' D(0, 00; \mathscr{R}) + f' D(2, 00; \mathscr{R})\}] .$$

The results of the calculation are given in Table IV.

TABLE IV. – *There-body mesic decay-nucleon with no definite state.*

J_i	J_f	a'	b'	c'	d'	e'	f'
			$^3\mathrm{H}_\Lambda \to \mathrm{D} + \mathrm{p} + \pi^-$				
1/2	1/2, 3/2	2	1/42	0	— 1/83	1/24	1/44
3/2	1/2, 3/2	2	0	0	0	7/32	1/28
			$^4\mathrm{H}_\Lambda \to {}^3\mathrm{H} + \mathrm{p} + \pi^-$				
0	0, 1	1/2	1/2	0	0	0	0
1	0, 1	1/2	0	0	0	11/54	1/27

It is seen from the table that there is an asymmetry for the pion and proton angular correlation for the spin $J = \frac{1}{2}$ state decay of $^3\mathrm{H}_\Lambda$ but no such term for the $J = \frac{3}{2}$ state. For $^4\mathrm{H}_\Lambda$ decay the $J = 1$ state contains a P_2 term about one fifth of the P_0 term but no P_2 term for the $J = 0$ state.

6. – Mesic decay of $A = 3$, 4 and 5 hyperfragments and their spins.

For the mesic decay of hyperfragments with low mass number there are comparatively adequate data in contrast to the case of high mass numbers; so we will in this Section confine ourselves to hypernuclei of mass number 3, 4 and 5 and discuss them rather in detail. The important data is the ratio between the two-body and three-body mesic decays $A = 3$ and 4 and the three-body mesic decay rate of $^5\mathrm{He}_\Lambda$ through the unstable ground state and the first excited state of $^5\mathrm{He}$. Assuming no final state interaction for the former we can determine whether for $^3\mathrm{H}_\Lambda$ and $^4\mathrm{H}_\Lambda$ the parallel or antiparallel spin coupling is favoured. From the latter we can determine the mixing rate of s- and p-wave for Λ-decay. We will start from the $^4\mathrm{H}_\Lambda$ decay. For $J = 1$ the p-wave pion and the s-wave nucleon contribute. Thus the numerical constants arising from the arbitrary normalization in our formalism for the relative two-body and three-body decay rates are determined from the decay of $^4\mathrm{H}_\Lambda$ both for the parallel and antiparallel spins of the $^4\mathrm{H}_\Lambda$-decay. This simple result arises only if the outgoing nucleon is in s-state both for $^3\mathrm{H}_\Lambda$ and $^4\mathrm{H}_\Lambda$ decays. We will arbitrarily introduce the constants C_1 and C_2 for $^4\mathrm{H}_\Lambda$-decays by

$$w(^4\mathrm{H}_\Lambda \to {}^4\mathrm{He} + \pi^-) = 4\pi k C_1 |s|^2 \qquad \text{for } J = 0, \tag{34.a}$$

$$= 4\pi k C_1 1.29 (p_\Lambda^2/k^2) |p|^2 \qquad \text{for } J = 1, \tag{34b}$$

and

$$w(^3\mathrm{H}_\Lambda \to {}^3\mathrm{H} + \mathrm{p} + \pi^-) = 4\pi p_\Lambda C_2 0.17 |s|^2 \qquad \text{for } J = 0, \tag{35.a}$$

$$= 4\pi p_\Lambda C_2 (p^2/k^2) |p|^2 \qquad \text{for } J = 1, \tag{35b}$$

where $k/p_\Lambda \approx 1.32$. We can determine the ratio C_1/C_2 comparing with the experimental rate [14] of

$$\frac{w(^4\mathrm{H}_\Lambda \to {}^4\mathrm{He} + \pi^-)}{w(^4\mathrm{H}_\Lambda \to {}^3\mathrm{H} + \mathrm{p} + \pi^-)} = 28/6 .$$

This values fixes $C_1/C_2 \approx \frac{3}{5}$ and $\frac{1}{3}$ for $J = 0$ and 1 respectively. Using the same definition of C_1 and C_2 we have,

$$w(^3\mathrm{H}_\Lambda \to {}^3\mathrm{He} + \pi^-) = 12\pi k C_1 [0.25 |s|^2 + 0.11 (p_\Lambda^2/k^2) |p|^2] \qquad \text{for } J = \tfrac{1}{2}, \tag{36.a}$$

$$= 12\pi k C_1 0.33 (p_\Lambda^2/k^2) |p|^2 \qquad \text{for } J = \tfrac{3}{2}. \tag{36.b}$$

[14] R. G. Ammar, R. Levi-Setti, W. E. Slater, S. Limentani, P. E. Schlein and P. H. Steinberg: preprint.

$$(37.a) \quad w(^3\mathrm{H} \to \mathrm{D} + \mathrm{p} + \pi^-) = 16 p C_2 [0.13\,|s|^2 + 0.014 (p_\Lambda/k) \mathrm{Re}\,(s^* p) + + 0.05 (p_\Lambda^2/k^2)\,|p|^2] \qquad \text{for } J = \tfrac{1}{2},$$

$$(37.b) \quad = 16\pi p_\Lambda C_2\, 0.27 (p_\Lambda^2/k^2)\,|p|^2 \qquad \text{for } J = \tfrac{3}{2}.$$

It must be remarked that the asymmetry term with respect to pion-nucleon correlation does not vanish even for the total decay probability; we obtain from (36) and (37) the relations

$$\frac{w(^3\mathrm{H}_\Lambda \to {}^3\mathrm{He} + \pi^-)}{w(^3\mathrm{H} \to \mathrm{D} + \mathrm{p} + \pi^-)} \approx \frac{(11 + 4.6x^2) C_1}{6.5 + 0.7\ \mathrm{Re}\,(x) + 2.5x^2) C_2} \qquad \text{for } J = \tfrac{1}{2} \quad (38.a)$$

$$\approx \frac{C_1}{C_2} \qquad \text{for } J = \tfrac{3}{2} \quad (38.b)$$

where $x = (p_\Lambda/k) p/s$. If we use C_1/C_2 obtained from the $^4\mathrm{H}_\Lambda$ decay we have for (38.*a*) and (38.*b*) respectively ≈ 1 and $\frac{1}{3}$. Experimental data for (38) is $\frac{4}{8} = .5$ ([14]) thus we cannot draw a definite conclusion from this investigation but the ratios 1 and $\frac{1}{3}$ are big enough for a final decision (compare also our previous report ([7])).

The decay rate of $^5\mathrm{He}_\Lambda \to {}^4\mathrm{He} + \mathrm{p} + \pi^-$ through the ground state $p_{\frac{3}{2}}$ and the first excited state $p_{\frac{1}{2}}$ of ^{5}He is given by

$$(39) \qquad w/w^* \approx (17 + 55x^2)/(20 - 6x^2),$$

where w and w^* are the relative probabilities of the three-body mesic decay through the ground and the first excited states respectively. The experimental rate of (39) is $\approx 54/18 = 3/1$ ([15]) which gives $x^2(k^2/p_\Lambda^2) \approx .6$ and $p^2(p_\Lambda^2/k^2)/(p^2 p_\Lambda^2/k^2 + s^2) \approx .4$. This is consistent with the value obtained from the free Λ-decay, $0.2 \div 0.8$ ([5]). If we accept the value 0.4 Dalitz and Liu's calculation for the ratio of two-body decays to all the mesic decays for $^4\mathrm{H}_\Lambda$ definitely gives the spin 0 of the $^4\mathrm{H}_\Lambda$ and hence spin zero for $^4\mathrm{He}_\Lambda$ by the charge independence of N-Λ forces. Thus we are again led to the conclusion that the kaon parity is odd from the observed

$$(40) \qquad \mathrm{K}^- + {}^4\mathrm{He} \to {}^4\mathrm{He}_\Lambda + \pi^-$$

reaction ([12]).

([15]) R. Ammar, R. Levi-Setti, W. E. Slater, S. Limentani, P. E. Schlein and P. H. Steimberg: *Nuovo Cimento*, **13**, 1156 (1959).

7. – Final state interaction in two-body mesic decay.

Assuming weak time reversal invariance ([16]) for the decay of the hyperon ([17]) we can express the matrix element of the reaction matrix of the hyperfragment decay in terms of the absolute value of the matrix element times an appropriate phase factor from the pion-nucleus scattering ([18]). Expanding the amplitude corresponding to the two-body mesic decay in partial waves (as we did in our formulation) we can write the partial amplitude in the form

$$\pm |R_T(J, L)| \exp i\,\delta_T(J, L)\,, \tag{41}$$

where $|R_T(J, L)|$ is the absolute value of the partial amplitude, $\delta_T(J, L)$ is the pion-nucleus scattering phase shift, T, J and L are the total isotopic spin in the final state, total angular momentum and the relative orbit of the pion and the residual nucleus.

It is especially interesting to see the effect on the isotopic spin selection rule. As an example let us take the ${}^3\mathrm{H}_\Lambda$-decay: we have the following relation for ${}^3\mathrm{H}_\Lambda$-decay (Table II) and (26):

$$\begin{matrix} w({}^3\mathrm{H}_\Lambda \to {}^3\mathrm{He} + \pi^-) \\ w({}^3\mathrm{H}_\Lambda \to {}^3\mathrm{H} \ + \pi^0) \end{matrix} = \begin{matrix} 6\ e^{i\delta_1'} + 2e^{i\delta_3'}|^2 + 2y^2 |e^{i\delta_{11}'} + 2\ e^{i\delta_{31}'}|^2 \\ 3\,|e^{i\delta_1'} - 4e^{i\delta_3'}|^2 + \ \ y^2\ e^{i\delta_{11}'} - 4\ e^{i\delta_{31}'}|^2 \end{matrix}, \tag{42}$$

where δ_1', δ_3', δ_{11}', δ_{31}' are the pion-^{3}He scattering s-wave, p-wave phase shifts in isotopic spin $\frac{1}{2}$, $\frac{3}{2}$ respectively and $y = |B_1/A_1|$. We have no available data for the pion-nucleus phase shift at about 40 MeV. If we assume that it is about equal to the mass number of the residual nucleus times the pion-single nucleon phase sift ([19]) we obtain an appreciable effect on the ratio (42). Using the experimental values of the pion-nucleon phase shifts ([19]) $\delta_1 \approx 8°$, $\delta_3 \approx -4°$, $\delta_{11} \approx 0°$ and $\delta_{31} \approx 0°$ the ratio of the s-wave contribution changes from 2:1 to 5:4 which is an appreciable change. Thus we conclude that the pion-nucleus scattering phase shifts at about 40 MeV are very important for the determination of the isotopic spin selection rule from the two-body mesic decay of hyperfragments.

([16]) P. T. Matthews: *The relativistic quantum theory of elementary particle interactions (lectures notes)*, (University of Rochester, 1957).

([17]) R. E. Marshak: *Science*, **132**, 269 (1960).

([18]) K. M. Watson: *Phys. Rev.*, **95**, 228 (1954); M. Kawaguchi and S. Minami: *Prog. Theor. Phys.*, **12**, 789 (1954); M. Kawaguchi and K. Nishijima: *Prog. Theor. Phys.*, **15**, 180 (1956).

([19]) G. Puppi: *Annual International Conference on High Energy Physics at CERN* (1958).

* * *

The author expresses his cordial thanks to Professor E. C. G. SUDARSHAN for his critical comments and discussions in the course of this work and regarding the final version of the paper. The author also expresses his thanks to Professor R. E. MARSHAK for suggesting the investigation in this field. He has benefitted from discussions with Mr. S. HATSUKADE and for his check of a part of his calculation of Appendix I.

APPENDIX I

Integrals for the three-body mesic decay probabilities.

The integrals appearing in the three-body mesic decay probabilities are given by

$$(A.1)\quad A = \int \mathrm{d}\boldsymbol{Q}\,\mathrm{d}\boldsymbol{p}\,\mathrm{d}\boldsymbol{k}\,\delta(\boldsymbol{Q}+\boldsymbol{p}+\boldsymbol{k})\,\delta(E - Q^2/2m_1 - p^2/2m_2 - k^2/2m_3)\,F(p, k, \cos\theta),$$

where $\boldsymbol{Q}$, $\boldsymbol{p}$, $\boldsymbol{k}$ and m_1, m_2, m_3 are momenta and masses of the residual nucleus, the proton and the pion respectively. θ is an angle between the momentum of the proton and the pion. The scalar function $(Fp, k, \cos\theta)$ takes 1, k^2p^2, $k^2p^2\cos\theta$, $k\cos\theta$, $k^3p^2\cos\theta$ k^2, k^4p^2, $k^2\cos\theta$ and $k^4p^2\cos^2\theta$ for the cases in which we are interested. They come out from the spherical wave expansion of the pion wave function. The argument of the Bessel functions appearing in the expansion is small so that we may take the lowest terms in an expansion with respect to their argument. After performing an integration with respect to $\boldsymbol{Q}$ we obtain

$$(A.2)\quad A = 2(2\pi)^2 m_1 \int p\,\mathrm{d}p\,k\,\mathrm{d}k\,\mathrm{d}(\cos\theta)\cdot$$
$$\cdot\,\delta(\cos\theta - m_1E/pk + (m_1+m_2)p/2m_2k + (m_1+m_3)k/2m_3p)\,F(p, k, \cos\theta)\,.$$

The upper and the lower limit of the integral will be determined by the δ-function given by (1). To find out the limit of p and k in eq. (2) we proceed as follows

$$(A.3)\quad p^2/m_2 + k^2/m_3 + (\boldsymbol{p}+\boldsymbol{k})^2/m_1 = 2E\,,$$

$$(A.4)\quad k^2(1/m_1+1/m_3) + 2kp\cos\theta/m_1 + p^2(1/m_1+1/m_2) - 2E = 0\,.$$

Hence

$$(A.5)\quad k = \frac{-p\cos\theta/m_1 \pm \sqrt{p^2\cos^2\theta/m_1^2 - (1/m_3+1/m_1)\{(1/m_1+1/m_2)p^2 - 2E\}}}{1/m_1+1/m_3} =$$
$$= \frac{-p\cos\theta \pm \sqrt{2(1+m_1/m_3)Em_1 + p^2(\cos^2\theta - (1+m_1/m_2)(1+m_1/m_3))}}{1+m_1/m_3}\,.$$

Since k is always real,

$$p^2\{(1+m_1/m_2)(1+m_1/m_3)-\cos^2\theta\}\leqslant 2m_1E(1+m_1/m_3)$$

or

$$p\leqslant\sqrt{2m_1E(1+m_1/m_3)}/\{(1+m_1/m_2)(1+m_1/m_3)-\cos^2\theta\}\,. \tag{A.6}$$

To find the maximum value of k for a fixed value of p we vary $\cos\theta$ in (4) or (5) and maximize k if the value $\cos\theta$ so obtained is inside the range $-1\leqslant\cos\theta\leqslant 1$ otherwise it is on the boundary $\cos\theta=\pm 1$. Differentiating (5) with respect to $\cos\theta$ for fixed p we get $\partial k/\partial(\cos\theta)$ to zero for extreme we find either $p=0$; or,

$$\sqrt{2m_1E(1+m_1/m_3)}+p^2\{\cos^2\theta-(1+m_1/m_2)(1+m_1/m_3)\}=p\cos\theta$$

or

$$p^2=2m_1E/(1+m_1/m_2)=2m_1m_2E/(m_1+m_2)$$

and arbitrary $\cos\theta$. But for this value of p^2

$$k=(-p\cos\theta\pm p\cos\theta)/(1+m_1/m_3)=0 \qquad \text{since } k\geqslant 0.$$

Hence an extremum is for $k=0$ or $p=0$ and arbitrary $\cos\theta$. In all other cases we have to choose the arbitrary values $\cos\theta=\pm 1$. Thus

$$k_{\min}\leqslant k\leqslant k_{\max}$$

with

$$k_{\substack{\min\\\max}}=\frac{\mp p+\sqrt{2m_1E(1+m_1/m_3)-p^2\{(1+m_1/m_2)(1+m_1/m_3)-1\}}}{1+m_1/m_3} \tag{A.7}$$

and

$$0\leqslant p\leqslant\sqrt{2m_1E(1+m_1/m_3)}/\{(1+m_1/m_2)(1+m_1/m_3)-1\} \tag{A.8}$$

Making use of these values we obtain the integral A in the form:

$F=1$:

$$A_1=2(2\pi)^2m_1\big(m_3/(m_1+m_3)\big)^2I_1\,. \tag{A.9}$$

$F=k^2p^2$:

$$A_2=(4\pi)^2m_1\big(m_3/(m_1+m_3)\big)^4\left|2m_1(m_1+m_3)EI_2/m_3-\frac{m_1(m_1+m_2+m_3)-m_2m_3}{m_2m_3}I_3\right|. \tag{A.10}$$

$F = k^2p^2\cos^2\theta$:

$$A_3 \equiv 2(2\pi)^2 m_1\big(m_3/(m_1+m_3)\big)^2\Big[\tfrac{4}{3}m_1m_3EI_2/(m_1+m_3) + \\ + (m_1+m_2)m_3(1-\beta)/m_2(m_1+m_3) + \tfrac{1}{6}\big(m_3/(m_1+m_3)\big)^2(3-10\beta+3\beta^2)I_3\Big]\,. \tag{A.11}$$

$F = k\cos^2\theta$:

$$A_4 \equiv 2(2\mathrm{p})^2 m_1\big(m_3/(m_1+m_3)\big)^2\,\frac{m_1m_2 - m_1m_3 - 2m_2m_3}{m_2m_3}\,J_2\,. \tag{A.12}$$

$F = k^3p^2\cos\theta$:

$$A_5 \equiv 2(2\pi)^2 m_1\big(m_3/(m_1+m_3)\big)^4\cdot \\ \cdot\Big[\frac{\alpha}{m_2(m_1+m_3)}\big\{m_2m_3(3\beta-7) - (m_1+m_2)(m_1+m_3)\big\}J_3 + \\ + \big\{(\beta-1)(m_1+m_2)/m_2 - \tfrac{1}{3}\big(m_3/(m_1+m_3)\big)(3-10\beta+3\beta^2)\big\}J_4\Big]\,. \tag{A.13}$$

$F = k^2$:

$$A_6 \equiv (4\pi)^2 m_1\big(m_3/(m_1+m_3)\big)^4\cdot \\ \cdot\Big[2(m_1+m_3)m_1EI_1/m_3 - \frac{m_1(m_1+m_2+m_3) - m_2m_3}{m_2m_3}\,I_2\Big]\,. \tag{A.14}$$

$F = k^4p^2$:

$$A_7 \equiv \big(2(2\pi)^2/3\big)\,m_1\big(m_3/(m_1+m_3)\big)^6\cdot \\ \cdot\big[(6-20\beta+6\beta^2)I_4 + \alpha(20-12\beta)I_3 + 6\beta^2I_2\big]\,. \tag{A.15}$$

$F = k^2\cos^2\theta$:

$$A_8 \equiv \frac{4(2\pi)^2}{3}\,m_1\big(m_3/(m_1+m_3)\big)^3\cdot \\ \cdot\Big[2m_1EI_1 + \frac{m_3}{(m_1+m_3)}\Big\{3 - \frac{m_1(m_1+m_2+m_3)}{m_2m_3}\Big\}\,I_2\Big]\,. \tag{A.16}$$

$F = k^4p^2\cos^2\theta$:

$$A_9 \equiv 2(2\pi)^2 m_1\big(m_3/(m_1+m_3)\big)^4\Big[\frac{17}{3}\,m_1^2E^2I_2 - \frac{2}{3}\,m_1m_3\,\frac{E(16-7\beta)I_3}{(m_1+m_3)} + \\ + \frac{2}{3}\big(m_3/(m_1+m_3)\big)^2(3-8\beta+\beta^2)\,I_4\Big]\,, \tag{A.17}$$

where I_n and J_n are defined by

$$I_n = \int_0^{p_{\max}} x^{2n}\,\mathrm{d}x\,\sqrt{\alpha-\beta x^2} \qquad n = 0,\ 1,\ 2,\ \ldots \tag{A.18}$$

and

$$J_n = \int_0^{p_{\max}} x^{2n-1}\,\mathrm{d}x\,\sqrt{\alpha - \beta x^2} \qquad n = 1, 2, \ldots, \tag{A.19}$$

where α and β are given by

$$\alpha = 2m_1(m_1 + m_3)E/m_3 \quad \text{and} \quad \beta = m_1(m_1 + m_2 + m_3)/m_2 m_3 .$$

These integrals become simple if we use the fact that the pion mass is small compared to the mass of the hyperfragment. They are given by

$$I_0 \approx 2\,\left((A-1)/A\right)^{\frac{1}{2}}\left((m_N + m_\pi)/m_\pi\right)^{\frac{1}{2}} m_N E\,\left\{\left(1/A\,(A-1)\right)^{\frac{1}{2}}(m_\pi/m_N)^{\frac{1}{2}}\,\tfrac{1}{2} + \pi/2\,\right\},$$

$$I_1 \approx 2^2\left((A-1)/A\right)^{\frac{3}{2}}\left((m_N + m_\pi)/m_\pi\right)^{\frac{1}{2}} m_N^2 E^2\,\left\{\left(1/A\,(A-1)\right)^{\frac{1}{2}}(m_\pi/m_N)^{\frac{1}{2}}\,\tfrac{1}{12} - \pi/12\right\},$$

$$I_2 \approx 2^2\left((A-1)/A\right)^{\frac{5}{2}}\left((m_N + m_\pi)/m_\pi\right)^{\frac{1}{2}} m_N^3 E^3\,\left\{\left(1/A\,(A-1)\right)^{\frac{1}{2}}(m_\pi/m_N)^{\frac{1}{2}}\,\tfrac{1}{12} - \pi/24\right\},$$

$$I_3 \approx 2^3\left((A-1)/A\right)^{\frac{7}{2}}\left((m_N + m_\pi)/m_\pi\right)^{\frac{1}{2}} m_N^4 E^4\,\left\{\left(1/A\,(A-1)\right)^{\frac{1}{2}}(m_\pi/m_N)^{\frac{1}{2}}\,\tfrac{1}{13} - \pi/30\right\},$$

$$I_4 \approx 2^4\left((A-1)/A\right)^{\frac{9}{2}}\left((m_N + m_\pi)/m_\pi\right)^{\frac{1}{2}} m_N^5 E^5\,\left\{\left(1/A\,(A-1)\right)^{\frac{1}{2}}(m_\pi/m_N)^{\frac{1}{2}}\,\tfrac{1}{26} - \pi/33\right\},$$

where A is the mass number of the hyperfragment.

$$J_1 \approx (1/3)(\alpha/\beta)\alpha^{\frac{1}{2}},$$

$$J_2 \approx (2/15)(\alpha/\beta)^2\alpha^{\frac{1}{2}},$$

$$J_3 \approx (8/105)(\alpha/\beta)^3\alpha^{\frac{1}{2}},$$

$$J_4 \approx (16/315)(\alpha/\beta)^4\alpha^{\frac{1}{2}}.$$

Appendix II

Spin of $p_{\frac{3}{2}}$-shell hyperfragments.

In the previous paper ([1-3]) we pointed out that the *binding energies* of the $p_{\frac{3}{2}}$-shell hyperfragments are explained equally well by the parameters derived for both antiparallel and parallel-favoured spins. We want to point out here that from a comparison of the parameters of s-shell and p-shell hyperfragments with no extremely strong spin-orbit interaction can give the antiparallel-favoured spins for $p_{\frac{3}{2}}$-shell hyperfragments. As is well known the effective nucleon-nucleon forces in the nucleus give very small expectation value of the tensor interaction which is effectively almost zero ([20]). If we accept this concept for the effective N-Λ forces we can determine the parameter for the spin-

([20]) J. P. Elliott and A. M. Lane: *Handb. d. Phys.*, Vol. **39** (Berlin, 1957).

orbit interaction of N-Λ forces from the relation derived before. The actual potential is defined in the form

$$V_{N\Lambda} = (1 + a\sigma_N \cdot \sigma_\Lambda + bS_{N\Lambda} + c\boldsymbol{L}\cdot\boldsymbol{S})V(r)\,, \tag{A.20}$$

where $a \approx -.24$. Using the relations (38) and (39) in paper I and $b \approx 0$ we have $c \approx -.22$ and 3.8 for the antiparallel and parallel spin respectively. Thus for a not too strong spin-orbit force we have the antiparallel spins of the $p_{\frac{3}{2}}$-shell hyperfragments.

RIASSUNTO (*)

Sulla base del nostro precedente modello per gli iperframmenti si discute sistematicamente il loro decadimento mesico. Si sviluppa il formalismo generale per il decadimento mesico a due corpi e a tre corpi. Si discutono la correlazione polarizzazione-direzione e la correlazione angolare per i decadimenti a due ed a tre corpi, assieme alle probabilità di decadimento. Si sviluppa il formalismo in modo da includere la regola di selezione dello spin isotopico ($\Delta I = \frac{1}{2}$ e $\frac{3}{2}$) per i decadimenti mesici. La teoria qui sviluppata è applicata specialmente agli iperframmenti con piccolo numero di massa, in cui si trova che il rapporto di branching dei decadimenti mesici a due ed a tre corpi del ${}^3\mathrm{H}_\Lambda$ e ${}^4\mathrm{H}_\Lambda$, $({}^3\mathrm{H}_\Lambda \to {}^3\mathrm{He} + \pi^+)/({}^3\mathrm{H}_\Lambda \to \mathrm{D} + \mathrm{p} + \pi^+)$ e $({}^4\mathrm{H}_\Lambda \to {}^4\mathrm{He} + \pi^+)/({}^4\mathrm{H}_\Lambda \to {}^3\mathrm{H} + \mathrm{p} + \pi^+)$ può essere usato per la determinazione dello spin di entrambi gli iperframmenti. La frazione della porzione di decadimento in onda p per il decadimento Λ libero, ottenuto da $\mathrm{He}_\Lambda \to \mathrm{He} + \mathrm{p} + \pi$, in cui il decadimento passa per due stati risonanti ($p_{\frac{3}{2}}$ e $p_{\frac{1}{2}}$), è data da $p^2/(s^2 + p^2) \approx .4$ che dà lo spin nullo del ${}^4\mathrm{H}_\Lambda$ in connessione al diagramma di Dalitz e Liu e quindi parità dispari per il kaone. Il rapporto di decadimento del modo con carica e di quello neutro è sempre 2/1 se e soltanto se è soddisfatta la condizione ottenuta da Okubo, Marshak e Sudarshan. Finalmente mostriamo che l'interazione nello stato finale per il decadimento mesico a due corpi può essere descritto dallo spostamento di fase dello scattering del pione e del nucleo residuo facendo uso dell'invarianza della matrice S totale dei processi di decadimento nella inversione (debole) del tempo di Wigner.

(*) *Traduzione a cura della Redazione.*

Interactions of 1.15 GeV/c K^- Mesons in Emulsion - III.

C. M. Garelli, A. Marzari Chiesa, G. Rinaudo and M. Vigone

Istituto di Fisica dell'Università - Torino
Istituto Nazionale di Fisica Nucleare - Sezione di Torino

(ricevuto il 20 Maggio 1961)

Summary. — In the previous two parts of this work we have found some results about the emission of charged Σ hyperons from K interactions. Here we consider the experimental energy distribution of these Σ, and we try to explain it taking into account the processes inside the nucleus.

1. – In previous works [1,2] we studied the emission of charged Σ-hyperons in the interaction of K^--mesons of 1.15 GeV/c with emulsion nuclei. We found that, after taking into account scanning loss corrections, the percentage of emitted charged Σ-hyperons is 16.4 %. The energy distribution of the charged hyperons in the laboratory system is given in Fig. 1, where the dashed line represents the observed spectrum and the full line the spectrum obtained taking into account the corrections.

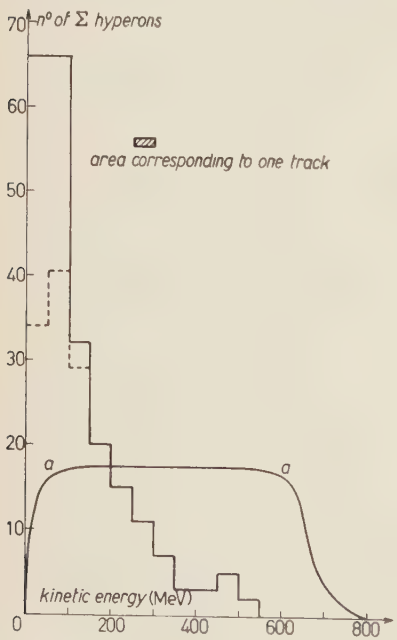

Fig. 1.

This energy spectrum is very different from the curve one expects if the hyperons were produced in the reaction

(1) $K^- + N \to \Sigma + \pi$.

(1) C. M. Garelli, B. Quassiati and M. Vigone: *Nuovo Cimento*, **17**, 786 (1960).

(2) A. Marzari Chiesa, B. Quassiati and G. Rinaudo: *Nuovo Cimento*, **19** 1171 (1961).

with an isotropic angular distribution in the centre of mass system (curve *a* of Fig. 1). In the present paper we make a rough analysis of the possible processes arising from K^- interactions with emulsion nuclei in order to see if this discrepancy can be explained.

2. – First of all we must take into account that at 1.15 GeV/c the cross-section for the reaction:

$$K^- + \mathcal{N} \to \Sigma + \pi + \pi \tag{2}$$

is not negligible. This is shown both from the results of ALVAREZ [3] and GOOD [4] and from observations in nuclear emulsion made in our own laboratory [1,2]. In fact, analysing the stars in which two pions are emitted, we concluded that reaction (2) occurs in about 30% of the cases. Recent experiments [4] gave evidence for an isobar Y^* that decays in the mode $Y^* \to \Lambda^0 + \pi$ but nothing has been said yet on the decay mode $Y^* \to \Sigma + \pi$ (*). If this mode of decay occurred frequently, one would observe a peak in the Q value distribution calculated for the stars from which both Σ and π emerge. Such an effect was not observed in our 74 stars. This result, however, is not very significant owing to secondary processes in nuclear matter. For this reason we simply calculated the energy distribution of the Σ produced in reaction (2) with phase space considerations, neglecting the contribution via the isobar production. The results are indicated in Fig. 2 (curve *b*). As one can see, the disagreement between calculated and experimental spectra is still important.

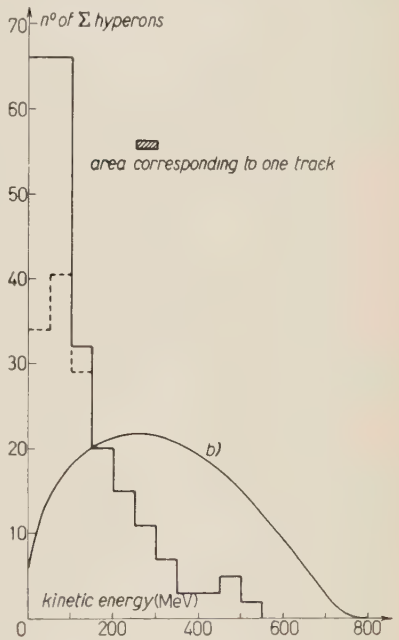

Fig. 2.

(3) *Alvarez's Report at the 1959 Annual International Conference on High Energy Physics at Kiev.*

(4) M. ALSTON, L. W. ALVAREZ, P. EBERHARD, M. L. GOOD, W. GRAZIANO, H. K. TICHO and S. WOJCICKI: *Proc. of the 1960 Annual International Conference on High Energy Physics at Rochester*, p. 445; *Phys. Rev. Lett.*, **5**, 520 (1960).

(*) *Note added in proof.* – More recent results give an estimate $< 4\%$ for the percentage of the decay mode $Y^* \to \Sigma + \pi$ (M. H. ALSTON and M. FERRO-LUZZI: *Rev. Mod. Phys.*, **3**, 416 (1961) and UCRL 9587).

3. – The above mentioned calculations neglect all the processes occurring in the nucleus. These processes can be distinguished in two types: those occurring after the Σ-hyperon production (scattering and absorption of Σ-hyperons) and those preceding the production process (scattering and charge exchange of the primary K^--mesons).

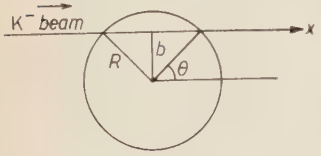

Fig. 3.

On can make a very simple calculation using a one dimensional diffusion equation in the nucleus.

The nucleus is considered as a sphere of radius $R = r_0 A^{\frac{1}{3}}$ (Fig. 3).

In order to obtain the fraction of charged Σ-hyperons emerging from the nucleus, we solve the diffusion equation:

$$\mathrm{d}N_\Sigma = N_K(x)\delta\,\mathrm{d}x - N_\Sigma(x)\gamma\,\mathrm{d}x\,, \tag{3}$$

where: $N_\Sigma(x)$ is the number of Σ at the distance x inside the nucleus;

$1/\delta$ is the K^--meson's mean free path in nuclear matter for production of charged hyperons;

$1/\gamma$ is the mean free path for $\Sigma \to \Lambda$ conversion in nuclear matter.

The number $N_K(x)$ of K^--mesons at the distance x is given by an exponential function:

$$N_K(x) = N_0 \exp[-\mu x]\,,$$

where: $1/\mu$ is the mean free path for production of charged and neutral hyperons in nuclear matter. In this way we take into account that a non-negligible amount of Σ-hyperons is produced by reemitted K^- and $\bar{K}^0$-mesons.

A straightforward calculation gives the following expression for the fraction f_Σ of charged hyperons emerging from the nucleus:

$$f_\Sigma = \frac{\delta}{\bar{\mu} - \gamma}\,[g(\gamma R) - g(\bar{\mu} R)]\,, \tag{4}$$

where:

$$g(y) = \frac{1 - (1 + 2y)\exp[-2y]}{2y^2}\,.$$

The reason for which in eq. (4) we use the mean values of δ and μ, will be explained later.

The energy distribution of the emerging Σ-hyperons is strongly modified by the processes inside the nucleus. On the contrary the spectral distribution

of those Σ-hyperons produced in a primary collision and emerging without suffering scattering depends only on the production process. Using a similar diffusion equation we can evaluate this percentage, f_0, and we obtain:

$$f_0 = \frac{\delta}{\alpha - \beta} [g(\beta R) - g(\alpha R)] , \tag{5}$$

where: $1/\alpha$ is the K^--meson's total mean free path in nuclear matter;

$1/\beta$ is the Σ-hyperon's total mean free path in nuclear matter.

In the preceeding calculations the biggest approximation is the use of a one-dimensional model.

This hypothesis is however justified by the fact that the direction of Σ-hyperons lies, in almost 90% of the cases, within the forward cone, as it is indicated by simple two-body kinematics calculations taking into account the Fermi motion of the nucleus. The same holds for the laboratory angular distribution of the re-emitted K^--mesons, according to recent experimental results [5], as will be discussed later.

To obtain from eqs. (4) and (5) the values of the fractions f_Σ and f_0 for the average emulsion nucleus ($A = 49$, $Z = 22$, $r_0 = 1.2 \cdot 10^{-13}$ cm) we must know the values of α, β, δ, γ, μ. Some of the related cross-sections are fairly well known while, unfortunately, for the others the available experimental information is still very poor. Moreover the K^--meson cross-sections are energy-dependent. While eq. (5) involves only the primary K^--mesons of a definite kinetic energy, $T_K = 750$ MeV, in eq. (4) we must use the values corresponding to the average energy of primary and re-emitted K^- mesons.

The processes in which a K^- (or a $\bar{\theta}^0$) meson is re-emitted in a collision with a nucleon, are the following:

a) coherent diffraction scattering;

b) incoherent elastic scattering;

c) inelastic re-emission with π production.

In order to evaluate the mean kinetic energy of re-emitted K^--mesons, we assumed an isotropic angular distribution in the centre of mass for process *b*), and we used a black sphere model for process *a*). To test the validity of our computation and to find the best values for the involved parameters, we have compared the results of the same black sphere computation for a kinetic

[5] V. Cook, B. Cork, T. F. Hoang, D. Keefe, L. T. Kerth, W. A. Wenzel and T. F. Zipf: *Proc. of the 1960 Annual Intern. Conference on High Energy Physics at Rochester*, p. 456.

energy of 1.5 GeV with the angular distribution experimentally obtained by COOK *et al.* [5]. Combining the results of computations for processes *a*) and *b*), we obtained for the K -mesons re-emitted in these processes a mean kinetic energy in the laboratory system of about $T_K = 600$ MeV. The K-mesons emitted through process *c*) have certainly a lower kinetic energy. We do not know the influence of process *c*) on the final results, and we will do all the calculations neglecting it. We shall take into account this approximation in the conclusion of our work and we shall make there some considerations on the possible weight of process *c*).

A great uncertainty exists at present about the values of the parameters μ and δ as functions of energy, owing to the lack of experimental data. The cross-sections for production of hyperons have been determined from hydrogen bubble chamber work [3] at 305 MeV/c and 1.15 GeV/c. The cross-sections for the production of hyperons in the interactions of K -mesons in flight with neutrons have not yet been determined.

We made an estimate of f_Σ introducing for the cross-section $\sigma_{\bar{\delta}}$ the value 8 mb (*).

As to the cross-section σ_γ relative to the $\Sigma \to \Lambda$ conversion, no direct determination has been done so far. We can obtain it indirectly from the knowledge of the total cross-section σ_β of charged Σ-hyperons (that was assumed to be equal to that of nucleons of energy in the range between 100 MeV and 500 MeV; $\sigma_\beta = 50$ mb) and from the cross section of Σ-hyperon scattering given by STANNARD [6] (**).

$$\sigma_\gamma = \sigma_\beta - \sigma_{\text{scatt}} = (25 \pm 10) \text{ mb} .$$

We carried on the calculations for three different values of the parameters μ and γ, that are the most uncertain.

The parameters α and δ entering in eq. (5) refers to the energy $T_K = 750$ MeV and are known [6,3]

(*) Alvarez's data [3] give for K^- interactions on protons:

$$\sigma_\delta = 4 \text{ mb} \quad \text{at} \quad T_K = 750 \text{ MeV} ,$$

$$\sigma_\delta = 18 \text{ mb} \quad \text{at} \quad T_K = 200 \text{ MeV} .$$

We have tentatively chosen an intermediate value, taking into account the energy of the primary K^- beam and an estimated mean kinetic energy of about 600 MeV for the K^- mesons re-emitted in processes *a*) and *b*).

[6] F. R. STANNARD: UCRL-9389 (September 1960).

(**) From the values, given by Stannard, of $\Sigma^\pm$ scattering cross sections on protons, we evaluated the $\Sigma^\pm$ scattering cross sections on neutrons according to charge independence.

The numerical results are collected in Table I.

TABLE I.

σ_μ (mb)	f_Σ	f_0	f_{scatt}	$f_{\text{re-em}}$
		$\sigma_\gamma = 15$ mb		
15	18	1.2	2.8	14
20	15	1.2	2.8	11
25	12.5	1.2	2.8	8.5
30	11	1.2	2.8	7
		$\sigma_\gamma = 25$ mb		
15	11.5	1.2	1.4	8.9
20	10	1.2	1.4	7.4
25	8	1.2	1.4	5.4
30	7	1.2	1.4	4.4
		$\sigma_\gamma = 35$ mb		
15	9	1.2	0.6	7.2
20	7.5	1.2	0.6	5.7
25	6	1.2	0.6	4.2
30	4.5	1.2	0.6	2.7

Column 3 indicates the fractions of Σ emitted from primary K^--mesons which suffered scatterings before emerging, and column 4 the fraction of Σ produced by re-emitted K^--mesons (*).

4. – Even with the uncertainties in the choice of the various parameters involved, Table I clearly exhibits some interesting features.

a) The fraction of emerging Σ-hyperons experimentally determined is 16.4% (1). This value agrees rather well with the maximum value of f_Σ which appears in column 1: this indicates that the mean $\sigma_{\bar{\delta}} = 8$ mb used in eq. (4) cannot be further lowered. This is in agreement with the fact that a considerable percentage of the emerging Σ-hyperons are produced by secondary K-mesons, of lower energy, as it is also shown by column 4, and that the cross-section for charged Σ-hyperon production strongly decreases with increasing K^--meson energy.

(*) This fraction was obtained by a diffusion equation derived in a similar way as eqs. (4) and (5).

b) The percentage of Σ-hyperons directly produced in a primary collision is not very high (column 2). In Table II we give again the last three columns of Table I expressed as percentages of the total number of emerging $\Sigma^{\pm}$-hyperons.

TABLE II.

σ_μ	f_0'	f'_{scatt}	$f'_{\text{re-em}}$
		$\sigma_{\pi^-} = 15$ mb	
15	7	15.5	77.5
20	8	19	73
25	9.6	22	68.4
30	11	25	64
		$\sigma_{\pi^-} = 25$ mb	
15	10	12	78
20	12	14	74
25	15	17.5	67.5
30	17	20	63
		$\sigma_{\pi^-} = 35$ mb	
15	13	7	80
20	16	8	76
25	20	10	70
30	26.5	13	60.5

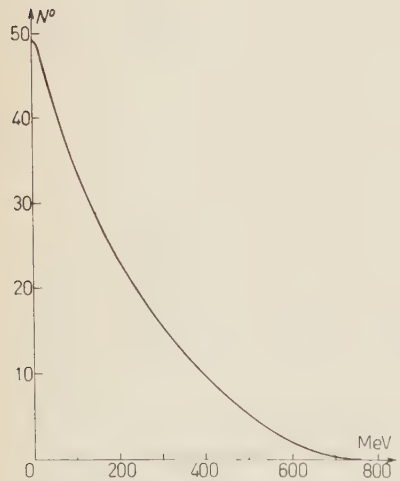

Fig. 4.

These figures should allow us to evaluate the energy spectrum of the emitted $\Sigma^{\pm}$-hyperons. A detailed calculation would be easy to carry out, but it would be of little significance owing to the considerable uncertainty in the parameters and especially to the difficulty of estimating the weight of inelastic K-meson re-emission. However a rough estimate of the energy spectrum according to the percentage of Table II ($f'_{\text{re-em}} = 73\,\%$, $f'_{\text{scatt}} = 19\,\%$, $f'_0 = 8\,\%$) seems to be not very far from the experimental spectrum except for the peak at very low energies (Fig. 4). This is probably due to the fact that an inelastic

K-meson re-emission with pion production (process *c*) of Section 3) occurs rather frequently.

If it is so, this process will give rise to a non negligible number of Σ produced by secondary Σ^--mesons of kinetic energy lower that the mean value of 600 MeV we used in our calculation. This fact will modify our results in the sense that the value of σ_{Σ^-} will be greater than 8 mb, and that a greater number of Σ-hyperons of very low energy will be emitted. These are only qualitative considerations, but will change the results of our calculation in the right way to give a better agreement both with observation *a*) of this section, and with the experimental energy spectrum.

* * *

We would like to thank Dr. A. E. WERBROUCK for his helpful suggestions and discussions.

RIASSUNTO

Partendo dai risultati sperimentali ottenuti nelle prime due parti di questo lavoro, viene presa in esame la percentuale di iperoni Σ carichi emessi nelle interazioni di K^- da 1.15 GeV/c. Viene inoltre data una giustificazione della distribuzione in energia di questi Σ, tenendo conto dei vari processi dentro il nucleo.

Mass Difference of Neutral K Mesons (*).

V. L. Fitch and P. A. Piroué

Princeton University - Princeton, N. J.

R. B. Perkins

Princeton University - Princeton, N. J.
Los Alamos Scientific Laboratory - Los Alamos, N. Mex.

(ricevuto il 26 Giugno 1961)

Summary. — The mass difference ΔM between the K_1^0 and K_2^0 mesons has been investigated by producing K^0 mesons and observing the $\overline{K}^0$ component of the K^0-$\overline{K}^0$ admixture as a function of time. The $\overline{K}^0$'s were sampled by using the charge exchange process and detecting the resulting K^- mesons. The best value for the mass difference is $\Delta M = 1.9 \pm 0.3 \hbar/\tau_1 c^2$ where τ_1 is the mean life of the K_1^0. However, selected high mass-differences ($\Delta M > 10$) are also consistent with the data.

1. – Introduction.

We describe here an experiment designed to measure the mass difference ΔM between the K_1^0 and K_2^0 mesons in the range of $0 < \Delta M < 10\hbar/\tau_1 c^2$, where τ_1 is the mean life of the K_1^0 meson (10^{-10} s). That a mass difference between the K_1^0 and K_2^0 would, under the proper circumstances, appear as an interference effect in the relative abundance of K^0 and $\overline{K}^0$ was first suggested by Serber and discussed in the paper of Pais and Piccioni (1). It is pointed out in this paper that the relative intensity, I, of the K^0 or $\overline{K}^0$ as a function

(*) This work was supported by the joint program of the Office of Naval Research and the U. S. Atomic Energy Commission.

(1) A. Pais and O. Piccioni: *Phys. Rev.*, **100**, 1487 (1955).

of the elapsed time t from the moment of production of a K^0 is given by

$$I\left(\frac{\overline{K}^0}{K^0}\right) = \frac{1}{4}\left[1 + \exp\left[-t/\tau_1\right](\mp)\, 2\exp\left[-t/2\tau_1\right]\cos\Delta\omega t\right], \tag{1}$$

where

$$\Delta\omega = \frac{\Delta M c^2}{\hbar} = \frac{\mu}{\tau_1},$$

and where the K_2^0 decay rate has been neglected. It has become customary in the literature to express the mass difference in units of the width of the K_1^0 mass, *i.e.*, $\Delta M = \mu\hbar/\tau_1 c^2$.

A mass difference between the K_1^0 and K_2^0 can be expected since the lifetimes of the two particles are different. Indeed, the principal interest in the mass difference stems largely from its being the only known instance where a self-energy due to the weak interactions is susceptible of experimental determination. In addition, a convincing demonstration of a small mass difference would rule out the possibility of transitions involving a strangeness change of 2. Such transitions permit a rapid mixing of K^0 and $\overline{K}^0$ giving rise to a large apparent mass difference between K_1^0 and K_2^0 ([2]).

GOOD has suggested ([3]) a different effect sensitive to the mass difference. He has shown that the angular distribution of the K_1^0 mesons regenerated in material placed in a K_2^0 beam is sensitive to the mass difference. This method has been employed in the experiment of MULLER *et al.* ([4]).

Various other ramifications of the mass difference and the determination of its sign have been discussed by several authors ([5-7]). The initial mass difference measurement ([8]), of limited statistical accuracy, utilized the interference effects given by eq. (1). In this measurement the K^0 and $\overline{K}^0$ components were sampled as a function of time by observing strangeness conserving interactions. TREIMAN and SACHS ([9]) have pointed out that the leptonic decay modes also sample these components. In particular, within the framework of

([2]) L. B. OKUN and B. PONTECORVO: *Žhur. Èksp. Teor. Fiz.*, **32**, 1587 (1957); [Translation: *JETP*, **5**, 1297 (1957)].

([3]) M. L. GOOD: *Phys. Rev.*, **110**, 550 (1958).

([4]) F. MULLER, R. W. BIRGE, W. B. FOWLER, R. H. GOOD, W. HIRSCH, R. P. MATSEN, L. OSWALD, W. M. POWELL, H. S. WHITE and O. PICCIONI: *Phys. Rev. Lett.*, **4**, 418 (1960).

([5]) W. F. FRY and R. G. SACHS: *Phys. Rev.*, **109**, 2212 (1958).

([6]) I. Y. KOBZAREV and L. B. OKUN: *Žhur. Èksp. Teor. Fiz.*, **39** 605 (1960); [Translation: *JETP* **12**, 426 (1961)].

([7]) N. N. BISWAS: *Phys. Rev.*, **118**, 866 (1960).

([8]) E. BOLDT, D. O. CALDWELL and Y. PAL: *Phys. Rev. Lett.*, **1**, 150 (1958).

([9]) S. B. TREIMAN and R. G. SACHS: *Phys. Rev.*, **103**, 1545 (1956).

the $\Delta I = \frac{1}{2}$ rule, the K^0 decays to $e^+(\mu^+)+\pi^-+\nu$ and the $\overline{K}^0$ decays to $e^-(\mu^-)+\pi^++\bar{\nu}$. Since this method was proposed the decay rates for the leptonic modes have been measured and found to be relatively small [10,11]. In condensed material the interaction rate is substantially higher than the decay rate. For this reason it appears most feasible to measure the K^0-$\overline{K}^0$ admixture through the strong interactions and this is the technique employed in the present experiment.

As seen from eq. (1) the interference effects are damped with a time constant of $2\tau_1$ corresponding to a distance of approximately 2.4 in. for particle momentum of 500 MeV/c. Since it is necessary to make observations close to the point of production, and therefore in a region of high background, it was the design of this experiment to charge exchange the neutral $\overline{K}^0$ mesons to K^- meson and with their relatively long lifetimes let them carry away the information from the region of high background. The experimental apparatus consisted of a source of K^0 mesons (5.3 GeV protons striking a Pt target in the bevatron), a converter variable in distance from the target ($1\frac{1}{4}$ in. to 5 in.) for charge exchanging the neutral mesons, and a detector of K^- mesons in a region of relatively low background approximately 18 ft. from the target. The energy of the proton beam and the angle of observation from the target were chosen to be highly unfavorable for the direct production of K^- and $\overline{K}^0$ mesons.

2. – Apparatus.

The K-mesons were produced in a $1\frac{1}{2}$ in. long, $\frac{1}{2}$ in. wide, and $\frac{1}{4}$ in. thick platinum target bombarded by protons with a mean energy of 5.3 GeV. The target was located in the west straight section of the bevatron and the K's were observed on the inside radius at an angle of 84° with respect to the proton beam. Rather than move a single converter back and forth relative to the target, we chose to use different converters at different distances in order that the converters subtend a constant solid angle at the center of the target. Furthermore, to enhance any effect originating in the converter an absorber which shadowed the detector from direct radiation from the target was used. This so-called shadow bar was 2 in. thick in the K beam direction, $\frac{1}{2}$ in. high, and $2\frac{1}{2}$ in. long, and was made of uranium. The target, converter, shadow-bar assembly is shown schematically in Fig. 1.

(10) M. Bardon, K. Lande, L. M. Lederman and W. Chinowsky: *Ann. Phys.*, **5**, 156 (1958).

(11) D. Neagu, E. O. Okonov, N. I. Petrov, A. M. Rosanova and V. A. Rusakov: *Proceedings of the 1960 Conference on High Energy Physics* (New York, 1960), p. 603.

It was necessary to plunge the target assembly into the beam region of the bevatron with each pulse. The mechanical arrangement was such as to make it possible to place any of the four converters in position by a remote switch. To obtain data at additional positions it was necessary to remove the target assembly and install a new set of converters. In these changes one of the converters was always held at a fixed position to provide a means of checking that no systematic effects occurred. Three sets of converters were used during two runs of the experiment at the bevatron. The first set was of copper, $\frac{1}{2}$ in. thick, which subtended horizontally a half-angle of $11\frac{1}{2}°$. The vertical half-angle was 60° except for the converter at the largest distance which, for mechanical reasons, was made to subtend a half-angle of 50°. The converters were spaced at intervals of $1\frac{1}{4}$ in. from the center of the target. The second set consisted of four $\frac{1}{4}$ in. thick tantalum converters also spaced at $1\frac{1}{4}$ in. intervals from the target. In this case the horizontal and vertical half-angles were $11\frac{1}{2}°$ and 50°. The third set of converters was similar to the second set except that they were located at $1\frac{1}{4}$, $1\frac{7}{8}$, $3\frac{1}{8}$, and $4\frac{3}{8}$ inches from the target. Note that the first converters in the second and third sets are identical.

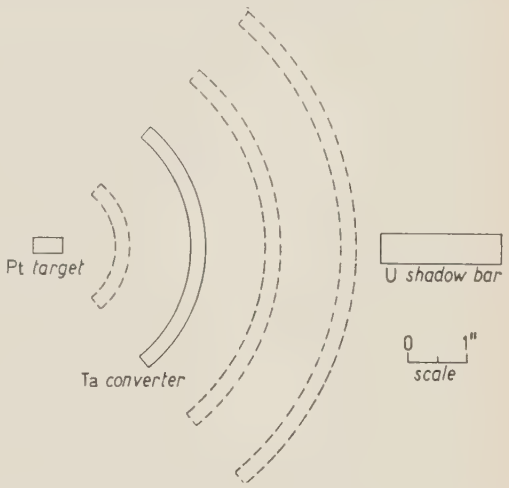

Fig. 1. – Layout of the target, converter, and shadow bar, elevation view. The proton beam entered the target on a line perpendicular to the plane of the figure.

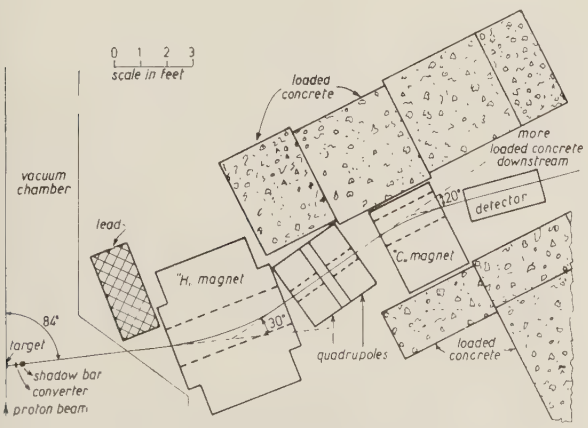

Fig. 2. – Plan view of the experimental arrangement at the bevatron.

The K-mesons were selected by momentum analysis, velocity selection, and range. Fig. 2 shows a plan view of the experimental arrangement within the magnet ring at the bevatron. The K beams from the target assembly are first

momentum-analysed (~ 540 MeV/c) in a 18 in.$\times$36 in. H magnet. They are then focussed at a point approximately 20 ft. from the target by two 6 in. aperture quadrupoles. Additional momentum analysis is provided by a 12$\times$24 in. C magnet placed after the focussing magnets for beam cleaning purposes. It is necessary for the detector to cover the image of the largest converter. For this reason the vertical and horizontal magnifications were chosen to be 0.4 and 1 respectively. In addition to the shielding shown in the plan view, the detector was enclosed on all sides by iron loaded concrete.

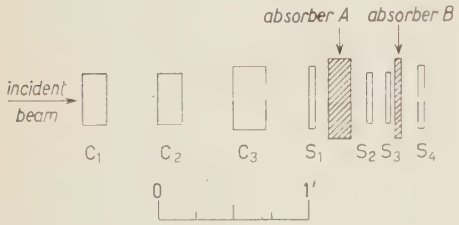

Fig. 3. – Arrangement of the counters in the K-detector. Scintillation counter S_2 defined the beam and was 2-in.$\times$4-in.$\times\frac{1}{2}$-in.

Fig. 3 shows the counter arrangement used to detect the K-mesons. Velocity selection was done using both Čerenkov and dE/dx counters. Čerenkov counters C_1 and C_2 are each sensitive to particles with velocities between the Čerenkov threshold and the velocity at which the radiation is totally internally reflected ($0.62 < \beta < 0.78$ for the carbon disulphide radiation) ([12]). Čerenkov counter C_3 (threshold $\beta = 0.75$) is operated in anticoincidence to reject those π-mesons which may have been detected in C_1 and C_2. Following the Čerenkov counters, four scintillation counters, denoted by S_1, S_2, S_3 and S_4 imposed a range requirement on the K-mesons in the beam. Counters S_1, S_2, and S_3 were operated in coincidence and S_4, run in anticoincidence, set the maximum range accepted. Counters S_2 and S_3 served as dE/dx counters. The output of S_2 and S_3 was fed to a fast integral discriminator which was set to eliminate about 80% of the minimum ionizing π-mesons. The K-meson stopping in absorber B was signaled by a $C_1C_2C_3'S_1S_2S_3S_4'$ coincidence (prime denotes anticoincidence). Absorber B in the case of run I was $\frac{1}{4}$ in. thick, in run II, $\frac{1}{2}$ in. thick. The thickness of copper absorber A could be varied remotely. That the overall detection system was effective is seen from the differential range curves for

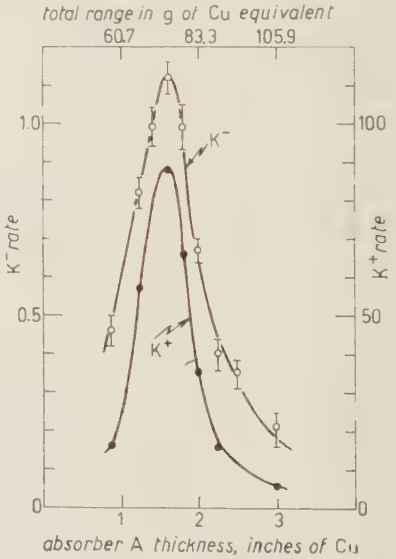

Fig. 4. – Differential range curves of K^+ and K mesons.

([12]) D. RITSON: *Techniques of High Energy Physics* (New York, 1961), p. 322.

both K^- and K^+-mesons originating in the target, shown in Fig. 4. The small background seen in the K^- range curve is due largely to beam particles. This background decreased proportionately when the shadow bar was inserted to attenuate the beam directly from the target. The ratio of the number of K^- to K^+ mesons coming directly from the target was approximately 0.01. The shadow bar attenuated the K^+ beam by a factor of ~ 10. Taking the number of K^0's equal to the number of K^+'s at the target the background level of K^- mesons was $\sim 10^{-3}$ of the number of K^0's at the target. The π-meson rate was given by a $S_1S_2S_3$ coincidence with the S_2 and S_3 discriminators set to a low value. The π^-/K^- ratio was approximately 10^4 at the detector.

It was important to minimize the number of protons which traversed the target, recirculated around the bevatron, and struck the converter structure. To this end a large target was placed 180° around the machine at a smaller radius to absorb the recirculating protons. During the long period in which the protons were allowed to strike the target, there was a substantial energy variation in the proton beam. For this reason data were recorded in three tandem time channels corresponding to mean energies of 5.0, 5.4, and 5.7 GeV. The final data showed no difference within statistics at the various incident proton energies. They were therefore combined.

The circulating beam striking the target was monitored by two separate counter telescopes which viewed the target directly from outside the magnet ring. The π and K rates were normalized to the monitor rate.

3. – Data.

The number of K^+, K^-, and (for checking purposes) $\pi^\pm$ was recorded in a large large number of relatively short runs for the various converter positions. The sum of all the data is shown in Fig. 5. The ratio of K^- to K^+ is used not only to aid in removing systematic effects but also because any charge exchange of the K^0 component is thereby included. As is seen from eq. (1) the mass difference effects have an opposite phase in the K^0 and $\overline{K}^0$ components. Taking

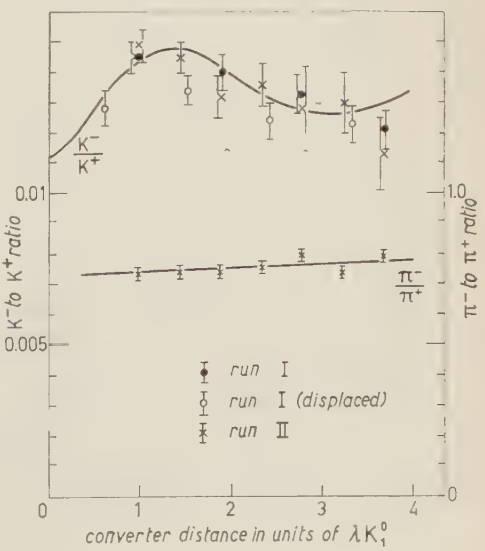

Fig. 5. – Experimental results. The curve through the K^-/K^+ points is the best fit as determined from a least-squares analysis. The π^-/π^+ points are fitted visually.

the ratio therefore emphasizes any mass difference effect that may be occurring.

The most striking evidence for the occurrence of the charge exchange process comes when the shadow bar is inserted into the beam. The K^-/K^+ ratio increases by about 30% when the shadow bar is in place. One would expect the ratio to decrease due to the greater absorption of the K^- mesons unless conversion was actually taking place in the material placed in the beam.

A possible explanation lies in the production of K^-'s by Λ's and Σ's originating in the target. This, however, requires the production of Λ^0's with a momentum of 1.5 GeV/c at 90°, a highly unlikely event. Furthermore, the data point closest to the target is good evidence against this possibility.

For comparison, the π^-/π^+ ratio is shown as a function of converter distance. The essential flatness of this curve indicates that no gross systematic effect was taking place.

Included in Fig. 5 are data (displaced data) obtained by moving the first set of converters $\frac{5}{8}$ in. closer to the target. This changed the solid angle subtended by the various converters and for that reason the data from these displaced converters are treated on a different basis.

Two corrections have been made before computing the ratio. The first one is for multiple scattering around the shadow bar. The correction is negligible in the copper converter data except for that converter closest to the shadow bar. The corrections in the case of the tantalum converters closest to the shadow bar are quite substantial. However, the ratio K^-/K^+ is quite insensitive to this correction—a correction made with fair accuracy. The velocity difference between the π and K mesons leads to a difference in the multiple scattering which makes it easy to pinpoint and check the magnitude of this effect. The second correction is made only to the data from the displaced copper converter nearest the target. This correction, which raised the plotted point about one-half the length of the error bar, comes from the beam which goes through the target, recirculates around the bevatron and strikes the converter. A radial profile of this recirculating beam was obtained by leaving the converters in place and moving the target about 10 ft. downstream in the same straight section of the machine. The number of K's was then recorded as a function of the converter as in the normal course of the experiment. The number of recirculating protons falls off very rapidly as one goes to radii smaller than the target radius and it was necessary to correct only the data from the converter closest to the target.

To interpret the structure seen in Fig. 5 in terms of a mass difference it is necessary to know the velocity of the pertinent K^0's. The velocity spectrum of K^0 mesons which give rise to the charged mesons detected depends on the details of the charge exchange process in the copper and tantalum converters. Since little is known of these details we have estimated the average velocity

(and its rms deviation) from the following considerations. The detector selects charged K-mesons of approximately 540 MeV/c. The neutral K-mesons which cast, by charge exchange, K^+'s into this momentum channel must possess momenta between approximately 540 MeV/c and the maximum momentum of the production spectrum. Assuming the charge exchange cross-section to be independent of energy lost in the process the number of K^0-mesons effective in the experiment is given by the production spectrum above approximately 540 MeV/c. In the design of the experiment a production spectrum given by phase space was used. As a check the number of K^+-mesons at 540, 635, and 730 MeV/c was measured. The measurements at 635 and 730 MeV/c were made by raising the magnet currents appropriately and degrading the energy of the K-mesons with carbon and aluminum absorbers before they entered the velocity and range-sensitive detector. The results have therefore been corrected for absorption and multiple scattering in the degrader and for the fact that a given momentum interval corresponds to a larger range interval

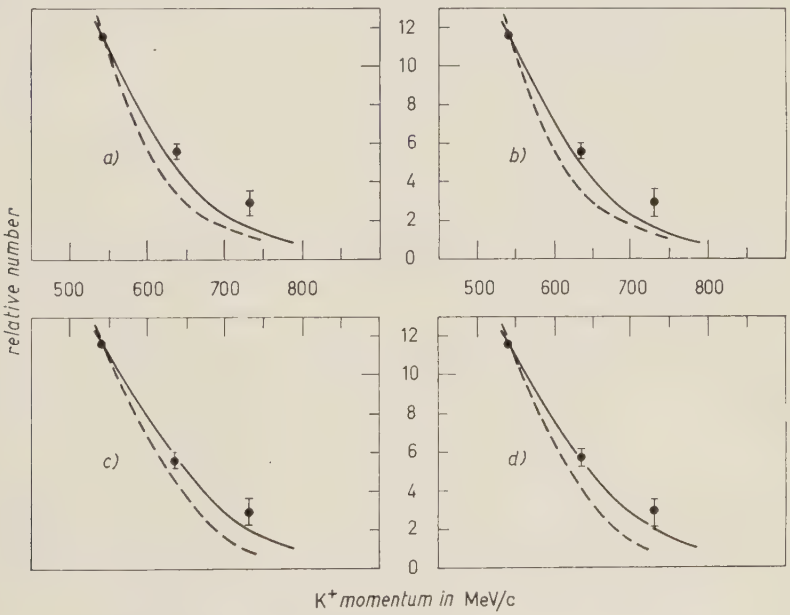

Fig. 6. – Production spectrum measurements compared with the results of various phase space calculations. The relative number is proportional to the differential cross section for the production of K^+ at 90° in the laboratory. The solid line refers to the reaction $p+n \rightarrow \Lambda^0+K^++n$ for a proton energy of 5.8 GeV. The broken line refers to the reaction $p+n \rightarrow \Sigma^0+K^++n$ for a proton energy of 4.8 GeV. A Gaussian distributed Fermi momentum with a mean energy of 19.3 MeV was used along with a matrix element $|H|$ which expresses various angular and momentum dependences, *viz.* (*a*) $|H|^2=1$, (*b*) $|H|^2=\cos^2\bar{\theta}$, (*c*) $|H|^2=\bar{\gamma}^2-1$, and (*d*) $|H|^2=\cos^2\bar{\theta}(\bar{\gamma}^2-1)$. The angle $\bar{\theta}$ and relativistic factor γ are c.m. values for the K meson. The measurements were made at a mean energy of 5.3 GeV and at an angle of 84°.

at higher momentum. Confidence in the correction was established by checking with π-mesons which have a somewhat higher absorption cross-section and show nearly the same multiple scattering at these momenta. The results are shown in Fig. 6 along with the results of the phase space calculations for a variety of matrix elements (*) ([13]).

It is observed that the measured K^+ flux extends to a higher momentum than the phase space calculations suggest. Presumably, the extra contribution is due to secondary scattering processes in the producing nucleus. Using the measured spectrum we obtain for the average momentum over 540 MeV c. $p/M = \gamma\beta = 1.30 \pm 0.20$. We consider this to give an upper limit to the velocity spread.

A separate estimate of the velocity spectrum was made by assuming the charge exchange process to be completely elastic involving individual nucleons in the nucleus with 20 MeV Fermi energy. Isotropic charge exchange over the angular interval subtended by the converter gives $\gamma\beta = 1.18 \pm 0.08$. In the analysis of the data the latter mean momentum was used since that model is probably closer to reality but with a more generous error as indicated by the first estimate, *viz.*: 1.18 ± 0.15.

4. – Results and conclusions.

The K^+ rate, after multiple scattering correction, proved to be nearly constant. For this reason we have fitted the K^-/K^+ data to the function,

$$(2) \qquad a + \frac{b}{2\Delta x}\int_{x-\Delta x}^{x+\Delta x} (\exp[-x] - 2\exp[-x/2]\cos\mu x)\,\mathrm{d}x \simeq$$

$$\simeq a + b\left(\exp[-x] - 2\,\frac{\sin\mu\,\Delta x}{\mu\,\Delta x}\exp[-x/2]\cos\mu x\right),$$

where x is the distance between the converters and the target measured in units of the mean decay length of K_1^0 meson in the laboratory, μ the mass difference in units of $\hbar/\tau_1 c^2$, Δx the uncertainty in the distance due to the

(*) A number of experiments have relied on the phase space calculations in the interpretation of the data, *e.g.* PANOFSKY *et al.*: *Phys. Rev.*, **109**, 1353 (1958), and BARDON *et al.* ([10]). To our knowledge this is the first time these have been even roughly checked in this energy region. Applied to the results of BARDON *et al.*, on the lifetime of the K_2^0 it suggests that their value should be reduced somewhat because of the higher average velocity of the K mesons than is given by phase space.

([13]) These calculations follow those of M. M. BLOCK, E. M. HARTH and R. M. STERNHEIMER: *Phys. Rev.*, **100**, 324 (1955).

finite thickness of the target and converters and the velocity spread of the K particles, a and b two constants to take into account the unknown background and magnitude of the effect. A least squares fit was performed separately for run I and II. There was essentially no difference in the results. Therefore, the data from the two runs were combined. Fig. 7 shows the χ^2 probability of the fit as a function of the mass difference. The best fits are for $\mu = 1.9$ as well as for discrete values between 10 and ∞. The displaced data points of Fig. 5 run I were not used since they were taken under somewhat different conditions, as discussed before. The point closest to the target however, constitutes a strong argument against a high mass-difference, *i.e.*, $\mu \gtrsim 30$. Isolated values of μ between 10 and 30 where the wavelength of the interference effect is a multiple of the spacing between the data points are acceptable. The best fit in the interval $0 < \mu < 10$ is for $\mu = 1.9 \pm 0.3$ where most of the error arises from the uncertainty in the velocity.

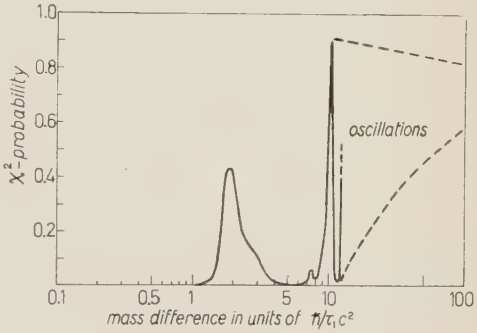

Fig. 7. – The χ^2 probability as a function of the mass difference.

These results are to be compared with those of CAMERINI *et al.* [14] $\mu = 1.5^{+0.3}_{-0.2}$ and with those of MULLER *et al.* [4] using the method suggested by GOOD, $\mu = 0.85^{+0.4}_{-0.25}$.

At this mass difference, $\mu = 1.9$, the least squares analysis yields $b/a = 0.11 \pm .03$. Using this result one can estimate the cross-section for the charge exchange process, $\bar{K}^0 + n \to K^- + p$ in the converter nuclei, assuming isotropy in the c.m. system and an equal number of K^0 and K^+ mesons at production. This yields a cross-section per nucleus of $0.05 \times \sigma_{\text{geometric}}$.

* * *

It is impossible for laboratory visitors to conduct an experiment of this extent without the most helpful co-operation of the host laboratory, in this case the Lawrence Radiation Laboratory. It is with great pleasure that we acknowledge the interest and encouragement given by Dr. E. LOFGREN, Pro-

[14] R. W. BIRGE, R. P. ELY, W. M. POWELL, H. HUZITA, W. F. FRY, J. A. GAIDES, S. V. NATALI, R. B. WILLMAN and U. CAMERINI: *Proceedings of the 1960 Conference on High Energy Physics* (New York, 1960), p. 601.

fessor E. McMillan, and the staff of the bevatron. We thank Messrs. Canton Kilpatrick, and Valledon for an ingenious target arrangement. We also thank Mr. Stuart L. Meyer for much assistance during run I.

RIASSUNTO (*)

Si sono studiate le differenze di massa ΔM fra i mesoni K_1^0 e K_2^0, producendo mesoni K^0 ed osservando la componente $\bar{K}^0$ della miscela K^0-$\bar{K}^0$ in funzione del tempo. Si campionarono i $\bar{K}^0$ servendosi del processo di scambio di carica e individuando i mesoni K^- risultanti. Il miglior valore della differenza di massa è $\Delta M = (1.9 \pm 0.3)\hbar/\tau_1 c^2$ in cui τ_1 è la vita media del K_1^0. Tuttavia, alcune opportune elevate differenze di massa ($\Delta M > 10$) concordano con i dati.

(*) *Traduzione a cura della Redazione.*

IL NUOVO CIMENTO Vol. XXII, N. 6 16 Dicembre 1961

Mesic Decays of Hypernuclei from K^- Capture.

III. – Caracteristics of the Parent Stars (*).

D. Abeledo and L. Choy

Physics Department Northwestern University - Evanston, Ill.

R. G. Ammar (**), N. Crayton, R. Levi Setti
M. Raymund and O. Skjeggestad

The Enrico Fermi Institute for Nuclear Studies,
The University of Chicago - Chicago, Ill.

(ricevuto il 15 Luglio 1961)

Summary. — 422 K^-- and 13 Σ^--capture stars emitting mesic hyperfragments (MHF) have been studied in an attempt to understand the mechanism of hyperfragment production. 123 K^- stars emitting ^{8}Li fragments were also considered. Several criteria were used to separate K^- captures in C, N, O and Ag, Br. Lower limits for the proportion of MHF produced in C, N, O are 57%, 73%, 84%, and 94% for H_Λ, He_Λ, Li_Λ and MHF of $Z \geqslant 4$. For ^{8}Li, this lower limit is 75%. An overall frequency of $(1.05 \pm 0.05) \cdot 10^{-2}$ MHF/K^--capture and $(3.8 \pm 1.4) \cdot 10^{-2}$ HF/Σ^--capture is obtained. The energy spectrum of the pions emitted in the capture stars indicates that a substantial fraction of the emitted bound Λ's originates in Σ-conversion processes. Indication of bound-Λ production from multinucleon K^--capture processes was obtained, important in the case of H_Λ. The momentum spectra for different hypernuclear species are very similar and the spectra of He_Λ and Li_Λ are, in turn, comparable with the momentum spectra of He and ^{8}Li respectively. Hyperfragments are emitted preferentially opposite to the direction of emission of an associated pion or fast proton. The backwards-forward (B/F) ratio is for π, MHF events, 1.8 ± 0.4. Two models for the production of hyperfragments are proposed. According to the first (« trapped-Λ ») the Λ

(*) Research supported by the National Science Foundation, by the U. S. Atomic Energy Commission through Argonne National Laboratory subcontract, and by the U. S. Air Force Office of Scientific Research, Contract No. AF 49(638)-209.

(**) Now at Northwestern University, Evanston, Ill.

created in the elementary process is trapped in the nuclear potential well of the parent nucleus. The HF is then emitted in the process of nuclear de-excitation. In the second model (« prompt-HF ») the HF is emitted promptly following the K^- or Σ^- interaction with a group of nucleons. It is concluded that both mechanisms may contribute. The occurrence of both processes can explain essentially all the salient features of hyperfragment emission.

Introduction.

The study of hypernuclear binding energies and of the branching ratios in the charged mesic decay modes of light hypernuclei have been the subject of two preceding reports (EFINS-NU Collaboration, Parts I and II [1]). In an attempt to obtain information relevant to the mechanism of hyperfragment production, we present here the results of an analysis of the parent K -absorption stars.

Analysis of individual hyperfragment (HF) parent stars has been already used as an auxiliary method in the identification of hypernuclei [2-5]. Systematic investigations on the HF production in K absorption have been reported by SCHNEPS *et al.* [6], SACTON [7], GORGÈ *et al.* [8] and by OVERSETH [9]. Both π^--mesic (MHF) and non-mesic (NMHF) decays were included in these works which all refer to nuclear emulsion studies. In addition, a considerable amount of information on the production of HF following K^- capture in He, has been given by the He-bubble chamber collaboration group [10].

The main source of material at our disposal is the sample of 376 MHF from K^- stars which were analysed in Parts I and II. These events originated

[1] R. G. AMMAR, R. LEVI SETTI, W. E. SLATER, S. LIMENTANI, P. E. SCHLEIN and P. H. STEINBERG: *Nuovo Cimento*, **15**, 181 (1960), part I; **19**, 20 (1961), part II.

[2] F. C. GILBERT, C. E. VIOLET and R. S. WHITE: *Phys. Rev.*, **103**, 248 (1956).

[3] B. P. BANNIK, U. G. GULIAMOV, D. K. KOPYLOVA, A. A. NOMOFILOV, M. I. PODGOREETSKII, B. G. RAKHIMBAEV and M. USMANOVA: *Sov. Phys. JETP*, **7**, 198 (1958).

[4] P. H. FOWLER: *Phil. Mag.*, **3**, 1460 (1958).

[5] P. E. SCHLEIN and W. E. SLATER: *Nuovo Cimento*, **21**, 213 (1961).

[6] J. SCHNEPS, W. F. FRY and M. SWAMI: *Phys. Rev.*, **106**, 1062 (1957).

[7] J. SACTON: *Kiev Conference* (1959), reported by E. H. S. BURHOP: UCRL-9354.

[8] V. GORGE, W. KOCH, W. LINDT, M. NIKOLIĆ, S. SUBOTIC-NICOLIĆ and H. WINZELER: *Nucl. Phys.*, **21**, 599 (1961).

[9] O. E. OVERSETH: *Bull. Am. Phys. Soc.*, **6**, 39 (1961).

[10] *Helium Bubble Chamber Collaboration Group, Proc. of the 1960 Annual International Conference on High Energy Physics at Rochester.*

in K^- captures in nuclear emulsion of standard gelatin concentration. An additional 46 MHF produced in a stack with twice the standard gelatin concentration (2× diluted emulsion) have been analysed for the purpose of the present study. With these statistics, one can attempt a description of the production features of individual hypernuclear species.

In Section **1-6** of this paper, the experimental results are presented. Particular emphasis is placed on a determination of the fractions of MHF produced in light (C, N, O) and heavy elements (Ag, Br) of the emulsion and on a comparison of the characteristics of MHF emission with those of ordinary nuclear fragments, such as He and ^{8}Li.

In Section **7** the data are examined with reference to several mechanisms which may play a role in the emission of hyperfragments.

1. – Emulsion stacks and measurements.

Three distinct stacks were employed in this work, the individual pellicles comprising each stack all having an area of 10 cm × 15 cm. They differed in the following essentials:

Stack A consisted of 59 K-5 pellicles of thickness ~1200 μm (EFINS),

Stack B consisted of 59 K-5 and 71 L-4 pellicles of thickness ~ 600 μm (NU),

Stack C consisted of 40 K-5 pellicles with twice the normal gelatin content and of thickness ~600 μm (EFINS).

The stacks were exposed to an enriched K^- beam (300 MeV/c) at the Berkeley Bevatron in December 1957. Further details concerning the properties of stacks *A* and *B* and the scanning for the detection of hyperfragments have been already reported in Part I and II. It is worth-while to repeat here that only for stack *A* were all grey and black prongs from each capture traced to their end in the stack.

The measurements reported here have been made on 422 stopping K 's yielding MHF as well as 123 K -capture stars yielding ^{8}Li fragments. At least two observers made a careful search for the emission of a fast pion for both kinds of primary stars. The blob density at plateau ranged between about 12 and 19 blobs/100 μm in the various stacks employed. But the stacks of lower minimum blob density were not used in determining the frequency of associated charged pions and their energy spectrum.

For all the 545 selected stars, the ranges of the grey and black prongs were measured and their identity ascertained even in those cases in which the particle did not come to rest in the stack. All light tracks (g^* 1.5) were inter-

preted as pions. In addition, for stack A, the energy spectrum of the associated pions with dip angle $< 30°$ was determined from either range or ionization measurements. The space angles between the direction of emission of a pion or « fast » proton (range > 1 cm), and that of the MHF, ^{8}Li, or stable prongs with a range $\leqslant 150\ \mu$m, were also measured (see Section 5).

2. – Hyperfragments from light and heavy elements.

In attempting to distinguish between K^- captures in the light (C, N, O) and heavy (Ag, Br) elements of the emulsion, we followed the approach already extensively used in the analogous problem for π^- captures ([11-13]) and in one instance already applied to the K^- absorption problem by GROTE *et al.* ([14]).

The parameters which differentiate captures in C, N, O from captures in Ag, Br are: *a*) the minimum energy with which charged particles are emitted, due to the different repulsive Coulomb potentials of the two groups of parent nuclei, *b*) the fraction of Auger electrons associated with the capture stars, and *c*) the prong number distribution of the capture stars. All the MHF parent stars have been analysed using these three criteria.

a) The theoretical effective height of the Coulomb barrier for Ag and Br is approximately 4.2 MeV and 9.6 MeV for protons and α-particles respectively ([15]). However, experimentally, slightly lower values, of ~ 3.3 and ~ 6.5 MeV for protons and α-particles have been reported as a result of studies of π^--induced disintegrations in emulsion nuclei ([13]), and the latter values have been adopted here. They correspond, in our emulsions, to proton ranges of 75 μm and α-particle ranges of 30 μm. The emission from K^- stars of protons or α-particles with ranges shorter than these values may therefore be interpreted as evidence for a capture in a light nucleus of the emulsion.

In order to make full use of the barrier height criterion, one should of course be able to discriminate protons, deuterons, tritons, from α-particles and heavier nuclear fragments. No such discrimination has been attempted here. We thus considered as captures in light elements only those stars with a prong of range $< 30\ \mu$m. This obviously implies that in this region there should not be a noticeable contribution of heavy fragments ($Z > 2$) from cap-

([11]) D. H. PERKINS: *Phil. Mag.*, **40**, 601 (1949).

([12]) M. G. K. MENON, H. MUIRHEAD and O. ROCHAT: *Phil. Mag.*, **41**, 584 (1950).

([13]) M. DEMEUR, A. HULEUX and G. VANDERHAEGHE: *Nuovo Cimento*, **4**, 509 (1956).

([14]) C. GROTE, I. KUNDT, U. KRECKER, K. LANIUS, K. LEWIN and H. W. MEIER: *Nuovo Cimento*, **14**, 532 (1959).

([15]) E. SEGRÈ: *Experimental Nuclear Physics*, vol. **2** (1953), p. 174.

tures in Ag and Br. An indication that this effect is indeed negligible is given by the known frequency and energy spectra of emission of ^{8}Li from K$^-$ capture (see Section 4·2). Our choice of the lowest barrier heights as well as our choice of the lowest cut-off range (because of lack of discrimination between charges 1 and 2) are both of such a nature as to make the number of events labelled « captures in light elements », only a lower limit to the true number.

Fig. 1 is a plot of the range distribution of the shortest prongs associated with K$^-$ stars emitting various species of MHF. A lower bound of 2 μm was imposed on this range distributions in order to minimize the contribution of recoils from captures in heavy nuclei.

The shaded area in the figure represents the cases in which the MHF itself was the shortest prong. It was also assumed that separation between captures in light and heavy elements could be achieved for these events using the barrier criterion. Minimum emission energies from Ag and Br were derived from the adopted values for $Z=1$, and 2, in proportion to the MHF charge. As can be seen in Fig. 1, the fraction of MHF parent stars which must have originated in C, N, O is large and seems to increase with the Z of the hypernucleus emitted. Lower limits for such fractions are approximately 57% for H_Λ, 73% for He_Λ, 84% for Li_Λ and 94% for $Z \geqslant 4$ hyperfragments. For MHF of $Z \geqslant 3$, these fractions are mainly given by the hyperfragment range distribution. Analogously, from the range distribution of ^{8}Li, which will be discussed later (4.2) one obtains that at least 75% of these fragments must originate in K$^-$ captures in C, N, O. Very similar results have been obtained by ALUMKAL *et al.* [16]

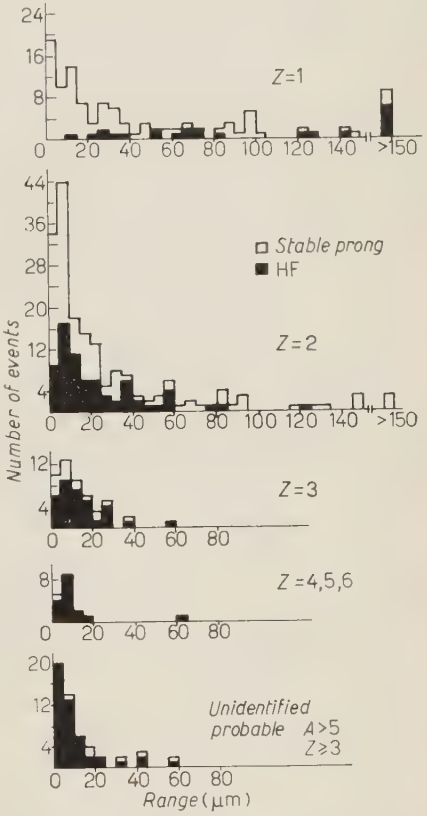

Fig. 1. Range distribution of the shortest prong ($R > 2$ μm) of K$^-$-capture stars emitting mesic hyperfragments. The shaded area is the distribution of the MHF ranges, for those events in which the shortest prong was the MHF itself.

[16] A. ALUMKAL, A. G. BARKOW, G. KANE, R. E. MCDANIEL and Z. O'FRIEL: *Nuovo Cimento*, **17**, 316 (1960).

for the related process of ^{8}Li emission following π^- capture in nuclear emulsion.

b) The fraction of Auger electrons accompanying the capture of negative charged particles in nuclear emulsion has been often employed to yield the proportion of captures in light and heavy elements of the emulsion respectively. While the yield of Auger electrons from mesonic captures in C, N, O amounts to only a few percent and may be neglected for our purpose here, the yield of Auger electrons from K captures in Ag and Br is probably greater than 50% ([17]). An exact knowledge of this yield is not required however if one compares the frequency of Auger electrons from MHF parent stars with that of a random sample of K$^-$ captures. According to a recent calculation by HILL ([18]) for K-5 emulsion of standard concentration, a random sample of K -meson captures should contain captures in light and heavy elements in ratios of about 1:1.67.

The 216 MHF parent stars in stack A have been studied for presence of Auger electrons of more than 3 grains, and for the presence of blobs. 7 stars with Auger electrons and 5 with blobs were found thus giving a relative frequency of $(6 \pm 2)\%$ of both Auger electrons and blobs. A search for random electron tracks spuriously associated with the MHF decay points indicates a background of $\sim 1\%$. An analogous search on a random sample of 160 K$^-$ captures has given a relative frequency of $(31 \pm 4)\%$ associated Auger electrons and blobs. Although these two values may not represent the true yields because of loss of the fastest Auger electrons, their ratio should be free from such loss.

On the basis of the above results, the fraction of MHF production in Ag, Br is about 12%. Thus method *b*) yields information which is compatible with the conclusions obtained using the Coulomb barrier criterion.

c) Further support to the result that most of the MHF are produced by captures in the light elements of the emulsion can be derived from a study of the prong number distributions of the MHF parent stars. It is well known that π^- captures in C, N, O lead generally to the emission of a larger number of prongs than captures in Ag, Br ([12,13]). That a similar behaviour is presented by K$^-$-capture stars, in the average, has been shown by GROTE *et al.* ([14]).

The prong number distribution of the MHF parent stars and of the ^{8}Li parent stars is shown in Fig. 2, where distinction is made among parent stars of the various hypernuclear species. Also shown is the distribution obtained by GROTE *et al.* for a random sample of K -captures stars attributed to light

([17]) E. H. S. BURHOP: *The Auger Effect* (Cambridge, 1952).
([18]) R. D. HILL: preprint (1961).

elements on the basis of the Coulomb barrier criterion; the histogram labelled in Fig. 2 « Total—C, N, O » refers to the difference between the prong number distribution for all stars and that for captures in C, N, O, thus representing a sample enriched with captures in Ag, Br. It is quite evident from the figure that the prong number distributions of the MHF parent stars and that of K^- captures in light elements have very close similarity. The difference of these distributions from that referring to captures mostly in heavy elements is well marked. One may also notice that the average number of prongs from MHF stars decreases with increasing hyperfragment charge which is consistent with the picture of prevailing MHF production in C, N, O. In conclusion, all the information from the various methods of approach *a*, *b*, and *c*, is internally consistent and points toward an overwhelming fraction of MHF being produced in light elements, this effect being particularly marked for MHF of $Z > 2$.

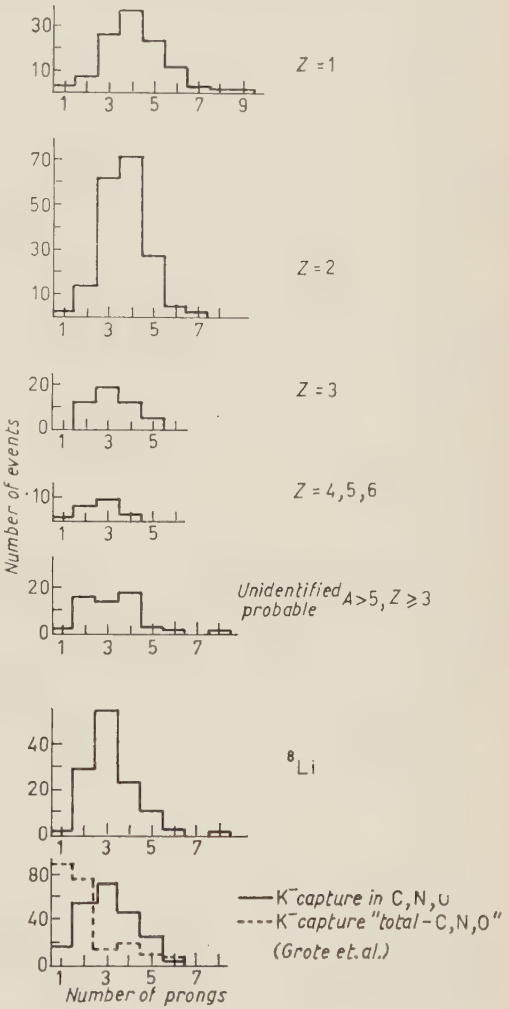

Fig. 2. – Prong number distribution of the parent stars of MHF's of $Z = 1, 2, 3$ and greater. Also included are the prong number distribution for ^{8}Li emitting stars and for K^- captures in light elements of the emulsion, the latter as given by GROTE *et al.* [14].

3. – Frequency of hyperfragment production.

3·1. *Mesic hyperfragments from* K^- *stars.* – The numbers of MHF observed for the various hypernuclear species in this experiment, are given in Table I where distinction is made among the emulsion stacks employed. The numbers

TABLE I. – *Frequency of mesic hyperfragments from* K^- *capture in nuclear emulsion.*

Hyper-nuclide	Stack *A*		Stack *B*		Stack *C* (2× diluted)		Adopted Q^-	$\bar{P}_{em.} \cdot 10^2$
	from K^-	from Σ^-	from K^-	from Σ^-	from K^-	from Σ^-		
$^3H_\Lambda$	15	0	4	0	3	0	0.5 ± 0.5	0.15 ± 0.06
$^4H_\Lambda$	41+(9)	3	23+(6)	1	10+(1)	0	[a]	0.46 ± 0.15
$^4He_\Lambda$	11+(5)	1	7+(5)	1	2+(2)	0	1.5 ± 0.4	0.49 ± 0.10
$^5He_\Lambda$	45+(26)	1	43+(27)	(1)	8+(6)	0	[b]	1.5 ± 0.3
$^7He_\Lambda$	4	0	1	0	1	0		
Li_Λ	30	2	17	0	3	0		
Be_Λ	4	0	5	0	0	0	8 ± 2	3.7 ± 1.0
B_Λ	3	0	1	0	1	0	[c]	
C_Λ	3	1	0	0	1	0		
$A > 5$	21	1	21	1	8	0		
Observed no. of MHF	216	9	160	4	46	0		
No. MHF corrected for geometrical loss	216		180		53			
No. of K^- star (excluding K_ϱ)	17 070		17 000		3 727			
Corrected no. K^-	18 925		18 845		4 132			
Frequency of MHF from K^-	$(1.14 \pm 0.07)\%$		$(0.96 \pm 0.07)\%$		$(1.28 \pm 0.17)\%$			

(*a*) This value of Q^- is obtained on the basis of 2 identified non-mesic decays of $^{3,4}H_\Lambda$ [19] and 4 π^--mesic $^{3,4}H_\Lambda$ [1] in the same range and dip interval taken from the same sample of K^- stars.

(*b*) See ref. [20].

(*c*) Q^- estimated from the known frequency of HF production in K^- capture stars [8,19,21], by subtracting the contribution of H_Λ and He_Λ.

of hyperfragments produced by K and Σ^- capture are indicated separately. Correction for geometrical loss of events applies only to stacks *B* and *C*, since for the stack *A* all grey and black prongs from each capture star were traced. Due to the longer average HF range, this loss affects mostly the hydrogen hyperfragments. The scanning efficiency for MHF detection, as determined from repeated scans, was at least 0.9 or better for all MHF configurations as

[19] R. G. AMMAR, N. CRAYTON, K. P. JAIN, R. LEVI SETTI, J. E. MOTT, P. E. SCHLEIN, O. SKJEGGESTAD and P. K. SRIVASTAVA: *Phys. Rev.*, **120**, 1914 (1960).

[20] P. E. SCHLEIN: *Phys. Rev. Lett.*, **2**, 220 (1959).

[21] J. SACTON: *Nuovo Cimento*, **18**, 266 (1960).

reported in Part II. Since, however, the scanning loss of MHF events has been found to arise mainly in the loss of the capture star itself, about the same fractional loss affects both the number of MHF's and the number of stars examined, except possibly in some of the rare decay modes with configurations that are difficult to detect.

Only stars with number of prongs ≥ 1 were recorded in the area scanning of all stacks. The numbers of stars given in Table I have therefore been corrected to include the number of zero-prong K^- stars (K_0) using for their frequency the value $(0.098 \pm .01)$ ([22]).

The frequency of MHF production per K^- capture is then $(1.14 \pm 0.07) \cdot 10^{-2}$ and $(0.96 \pm 0.07) \cdot 10^{-2}$ for stacks *A* and *B* respectively (for standard emulsion concentration). A value of $(1.28 \pm 0.17) \cdot 10^{-2}$ obtains for stack *C* (diluted emulsion). It is of interest to compare the relative frequency of MHF production in standard and diluted emulsion respectively with that expected on the basis of the known chemical compositions. If one takes 0.85 as the ratio of the capture rates for K^- in heavy and light elements in $2\times$ diluted emulsion (obtained from the data of HILL ([18])) and assumes that $\sim 80\%$ of an MHF are produced in light elements, one expects an increase in HF yield il the diluted emulsion by a factor 1.24, not inconsistent with the observed value of 1.2 ± 0.2.

3·2. *Hyperfragments from* Σ^- *stars.* – Table I also contains the numbers of MHF produced by Σ^- captures in our sample. Although the actual number of Σ^-'s is not determined here, it will be assumed that $\sim 2\%$ of the K^- captures emit Σ^-'s which in turn come to rest and produce a star with at least one prong ([22]). Correcting this figure for Σ_0's ([23]), we obtain that a total of 2460 Σ^- hyperons should have come to rest in our stacks. The yield of MHF per Σ^- capture is thus $(0.5 \pm 0.2) \cdot 10^{-2}$, somewhat lower than that obtained for K^- captures (*).

Out of a sample of 140 identified Σ^- captures producing $\geq$ one prong, 2 MHF and 13 NMHF were found. Correcting again for the undetected Σ_0's, one finds for the total HF yield the values $(3.8 \pm 1.4) \cdot 10^{-2}$ HF/Σ^- capture.

3·3. *Hyperfragment emission probabilities.* – In order to estimate the hyperfragment emission probabilities (P_{em} = number of HF/number of bound plus unbound Λ's produced) from the observed MHF yields, additional information

([22]) EUROPEAN K^- COLLABORATION: *Nuovo Cimento*, **12**, 91 (1959); **13**, 690 (1959), Part I; **14**, 315 (1959), Part II.

([23]) EUROPEAN K^- COLLABORATION: *Nuovo Cimento*, **19**, 1077 (1961).

(*) *Note added in proofs.* – Similar results have been recently obtained by J. SACTON, M. J. BENISTON, D. H. DAVIS, B. D. JONES, B. SANJEEVAIAH and J. ZAKRZEWSKI: preprint (1961).

is required on *a*) the total Λ yield from K⁻ capture stars in nuclear emulsion (*), *b*) the non-mesic/π^--mesic ratio (Q^-) for the various hypernuclear species, and *c*) the ratio of π^0- to π^--mesic decays. Column 8 of Table I indicates the values of Q^- adopted for H_Λ, He_Λ and heavier. Corrections to take into account the π^0 decay modes, according to DALITZ and LIU (24), have been introduced to derive the $\bar{P}_{em}$ given in the last column of Table I. The approximate value 0.7 was used for the fraction of K⁻ captures in nuclear emulsion nuclei yielding Λ-particles (22). The values of $\bar{P}_{em}$ thus obtained refer to the *average* of the emission probabilities for the various emulsion nuclei. With a knowledge of the correct K⁻-capture rates and Σ yields in C, N, O and Ag, Br separately, and using our results on the MHF production in light and heavy elements one could estimate P_{em} for the two groups of nuclei. Such P_{em} will, however, entirely reflect the striking difference already discussed for the rate of MHF production in C, N, O and Ag, Br.

As can be seen from Table I, the average emission probability increases with the mass of the hyperfragments, and thereby with the binding energy B_Λ. It can also be noticed that $\bar{P}_{em}$ for $^4H_\Lambda$ and $^4He_\Lambda$ are approximately the same, as one could anticipate for mirror hypernuclides (on the rather crude assumption that Q^- is identical for $^4He_\Lambda$ and $^5He_\Lambda$).

A further quantity which can be estimated from our data in a few instances is the yield of specific hypernuclides relative to the yield of the corresponding nuclear cores. The ratio of these quantities, r_{HF}, can be estimated for $^5He_\Lambda$ and $^9Li_\Lambda$. On the assumption that ^4He represent $\sim 40\%$ of the visible nuclear fragments from K⁻ capture in C, N, O (as discussed further in 4·3), we obtain for $^5He_\Lambda$ (having $B_\Lambda \sim 3.0$ MeV), $r_{HF} \sim 0.03$. The corrected number of ^8Li (hammer tracks) produced by K⁻ captures in our stacks is 150 ± 15. This may be compared with 6 identified mesic decays of $^9Li_\Lambda$ in the same volume. Taking as lower limit of Q^- ($^9Li_\Lambda$), the value of 4 (21), we obtain for $^9Li_\Lambda$ (having $B_\Lambda \sim 7.2$ MeV), $r_{HF} \sim 0.24$, apparently much larger than the above results for $^5He_\Lambda$.

4. – Spectra of emission of mesic hyperfragments and ordinary fragments.

4·1. *Momentum and velocity spectra of* MHF. – Making use of the range-energy relation for heavy ions of HECKMAN *et al.* (25) the momentum and velocity of each identified hypernucleus has been determined. Histograms for these quantities are displayed separately in Fig. 3 for various hypernuclear species. The distributions are corrected for geometrical loss of events for those

(*) Not including the Λ's from the decay $\Sigma^0 \to \Lambda + \gamma$.

(24) R. H. DALITZ and L. LIU: *Phys. Rev.*, **116**, 1312 (1959).

(25) H. H. HECKMAN, B. L. PERKINS, W. G. SIMON, F. M. SMITH and W. H. BARKAS: *Phys. Rev.*, **117**, 544 (1960).

stacks where only events contained in a single plate were recorded (dashed contour). The loss of very low energy events due to difficulty in separating primary and secondary stars should be confined to the regions of momenta below 40, 80, 130 and 230 MeV/c for H_Λ, He_Λ, Li_Λ and $Z \geq 4$, 5, 6 hypernuclei respectively, corresponding to a range of ~3 μm. Since it has been previously shown that the majority of the MHF originate in the light emulsion nuclei, a comparison of the momentum spectra should be almost unaffected by Coulomb effects, at least in the region accessible to observation.

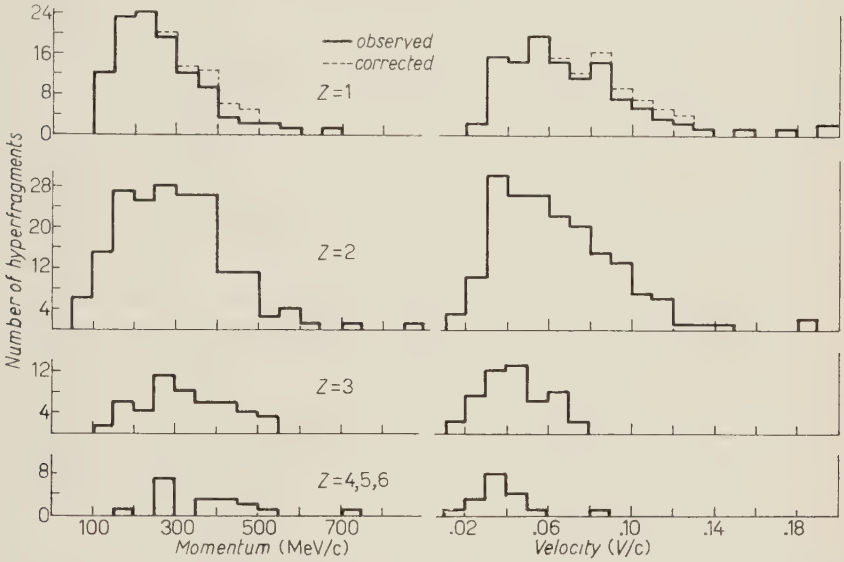

Fig. 3. – Momentum and velocity spectra of MHF's from K^- captures at rest in nuclear emulsion. The broken line, part of the spectrum for $Z=1$, represents the correction for geometrical loss of events in part of the stacks employed.

The momentum spectra for the various hypernuclides show considerable similarity with the indication of a slight increase in the average momentum with increasing Z. This may be partly accounted for by the cut-off at low momenta mentioned above. The velocity spectra, obviously determined by the momentum spectra, show conversely a marked shift toward lower velocities for increasing Z.

Table II contains the average emission energies for the various hyper-

TABLE II. – *Average kinetic energy of hyperfragments from* K^- *capture.*

Hypernuclei	$^3H_\Lambda$	$^4H_\Lambda$	$^4He_\Lambda$	$^5He_\Lambda$	Li_Λ	Be_Λ	B_Λ	C_Λ
Average energy in MeV	20.1	9.1	16.3	10.4	7.8	9.1	6.3	7.2

nuclides. Large fluctuations are expected for these values due to the importance of the high energy tail of the Maxwell-like HF energy distributions. The average MHF emission momentum for all hypernuclear species is 294MeV/c.

4·2. *Comparison of* Li_Λ *and* ^8Li *emission spectra.* – A total of 123 ^8Li (hammer tracks) were collected from the sample of K^--capture stars dealt with in this investigation. Their range distribution is given in Fig. 4. As previously mentioned, in Section 2·1, we estimate that at least 75% of these events originate in the light elements of the emulsion (from the fraction of ^8Li with $R \leqslant 21$ μm). Since the same conclusion was reached in the case of Li_Λ hyperfragments, a comparison of the range distributions of the two kinds of fragments is meaningful. Thus Fig. 4 also contains the range distribution of the 50 Li_Λ events, normalized to the area of ^8Li, The similarity of the two distributions is apparent.

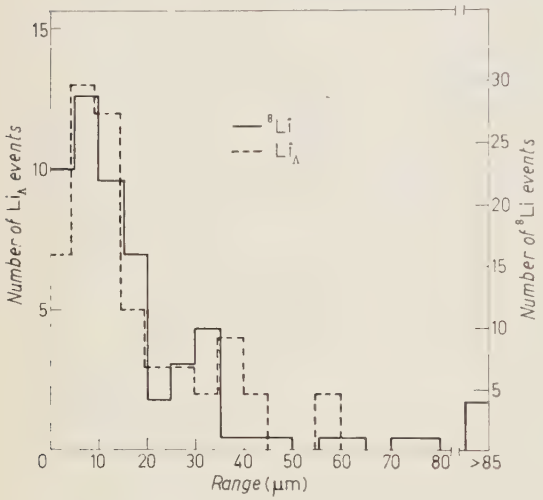

Fig. 4. – Range distributions for Li_Λ and ^8Li events, normalized to the same area.

4·3. *Comparison of* He_Λ *and* He *emission spectra.* – In view of the likeness noted for the Li_Λ and ^8Li spectra, it is of interest to investigate if other hyperfragments show a similar behaviour relative to the «stable» fragment of similar charge. Although a direct identification of other nuclear fragments was not attempted here, it can be shown that the majority ($\sim 70\%$) of the stable prongs having $R \sim 150$ μm from MHF parent stars, are He nuclei. Their range distribution and that of He_Λ are essentially identical, even without correcting the former for the background contributed by H and $Z \sim 2$ isotopes. An estimate of the effect of such background is however presented in the following.

The relative contributions of H, He and heavier isotopes among the products of K^- captures in C, N, O can be estimated on the basis of the known yields of such particles from π^--captures in C, N, O ([26]) and of the yields from

([26]) G. VANDERHAEGHE and M. DEMEUR: *Suppl. Nuovo Cimento*, **4**, 931 (1956); P. AMMIRAJU and L. M. LEDERMAN: *Nuovo Cimento*, **4**, 283 (1956).

disintegrations of C nuclei produced by 330 MeV protons ([27]). The nuclear excitation energies, for these two cases, are in fact quite comparable with the nuclear excitation observed in K^- captures ((30÷50) MeV) (*). Thus it is assumed that H, He and heavier isotopes are emitted in K^- captures in the proportion 46%, 50% and 4% respectively. For H and He, the relative contributions in the range interval (2÷150) μm have been estimated on the basis of a phase space calculation of their energy spectra ([12]). The corresponding range spectra, for an average 4-body break-up of C nuclei, at excitation energies of 30 and 50 MeV, are shown in Fig. 5*a*. The shape of these spectra so

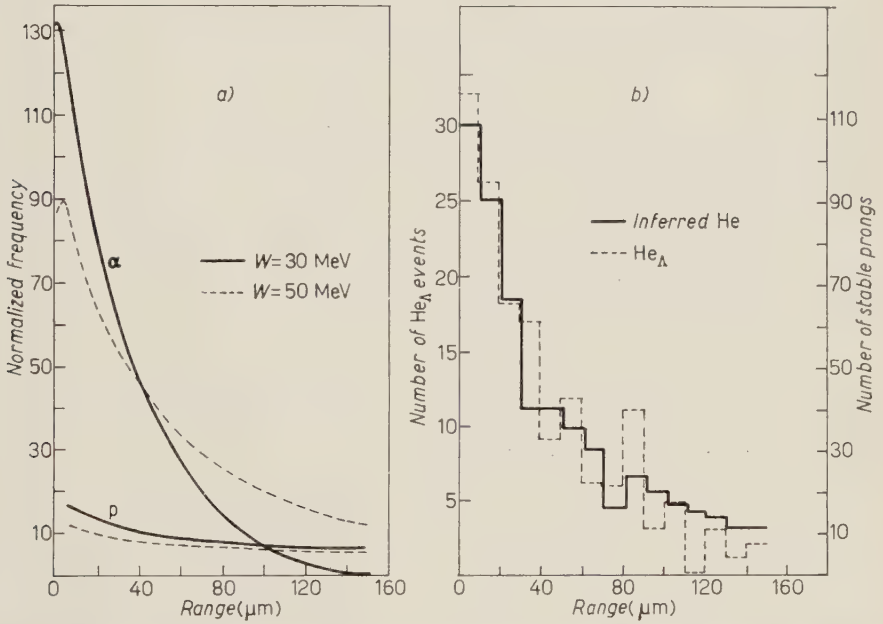

Fig. 5. – *a*) Range spectra of protons and α-particles from a 4-body break-up of C nuclei, for two nuclear excitation energies. The energy spectrum is taken from phase space considerations as

$$P(E)\,\mathrm{d}E = \mathrm{const}\left(W - \frac{M}{M-m}\,E\right)^{(3N/2-4)} E^{\frac{1}{2}}\,\mathrm{d}E\,,$$

where W is the excitation energy neglecting binding energies, M the mass of the parent nucleus, N the number of disintegration products, E and m the kinetic energy and mass of the emitted fragment respectively. The spectra are normalized to an α/p ratio of 1/1. *b*) Range spectrum of He_Λ and of the stable prongs of range $\lesssim 150$ μm after subtracting for proton background on the basis of Fig. 6*a* and for $Z > 2$ background as described in the text. The full line histogram is then attributed to He fragments.

([27]) W. H. Barkas and H. Tyren: *Phys. Rev.*, **89**, 1 (1953).

(*) The average visible energy (pions excluded) for the sample of MHF parent stars considered here is ~ 31 MeV per H_Λ and ~ 28 MeV per He_Λ parent star.

derived is also in qualitative agreement with the experimental data from π^- stars in C, N, O obtained by VANDERHAEGHE and DEMEURS [26]. We have thus subtracted from our raw spectrum (542 prongs of $R < 150\,\mu$m) a total H contamination of 20%, according to Fig. 5*a*. In order to subtract the contribution of $Z \geqslant 2$ isotopes from the remaining spectrum, we have assumed for these, on the average, a range spectrum similar to the one observed for ^{8}Li. This correction amounts to about 10% of the events contained in the raw spectrum.

The range spectrum of the stable prongs, after applying the above corrections, should therefore reproduce the He spectrum and is presented in Fig. 5*b*, together with the analogous spectrum for the He_Λ events. The shape of the two spectra is again remarkably similar.

5. – Angular correlations among the products of K$^-$-capture stars.

The space angle θ between the directions of emission of the MHF and associated pion or fast ($E \geqslant 52$ MeV) proton was measured for 155 events. No attempt was made to discriminate between pions and fast protons for events in stack *B* (45 events). A frequency histogram in units of $\cos\theta$ for these events is shown in Fig. 6. As can be seen the distribution is asymmetric, the

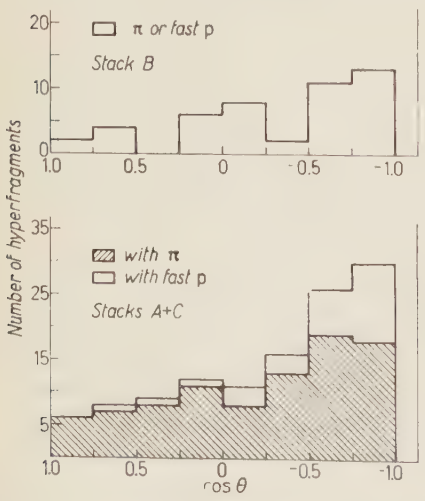

Fig. 6. – Distribution of the angle θ between the direction of emission of the MHF and that of an associated pion or fast proton.

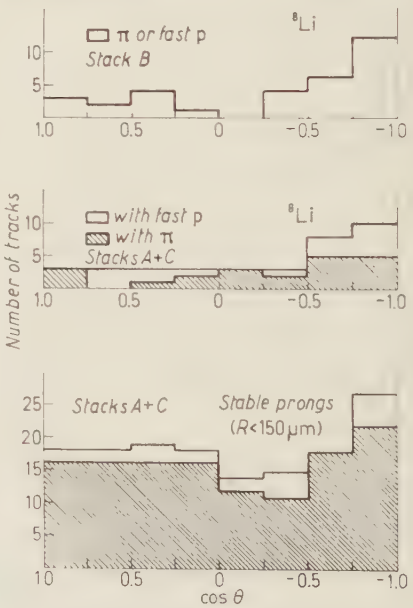

Fig. 7. – Distribution of the angle θ between the direction of emission of ^{8}Li fragments and an associated pion or fast proton. Also indicated is the θ distribution for stable prongs of range $\leqslant 150\,\mu$m which were emitted from the MHF parent K$^-$ captures.

pions and fast protons being preferentially emitted opposite to the hyperfragment. The backwards/forward ratio B/F (backwards being the interval $\theta > 90°$) equals 1.8 ± 0.4 for the events with associated pion, 8 ± 4 for those with associated fast proton. For both protons and pions, the average B/F is 2.5 ± 0.4. Our result for the B/F ratio of fast protons confirms previous similar observations by SACTON (7) who found a value of 7.5 ± 2.5 for protons with $E > 35$ MeV.

Analogous distributions for the angle θ between pions or fast protons and the ^{8}Li direction of emission are displayed in Fig. 7. This figure also contains a histogram of θ for all stable prongs with $R \leq 150$ μm emitted by the MHF parent stars. Some anisotropy is observed in the case of ^{8}Li ($B/F = 2.1 \pm 0.5$ for all events) while the stable prongs seem to be emitted isotropically with respect to pions and fast protons.

We have further attempted to detect possible correlations between θ and the pion or fragment momenta. No correlation among these quantities was found, with perhaps an exception in the scatter plot of θ *vs.* the fragment momentum, given in Fig. 8*a*. This plot indicates a slight tendency for the MHF of higher momenta to be emitted at larger θ angles, B/F being 2.8 ± 0.9 for $P \geq 300$ MeV/c and 2.2 ± 0.6 for $P < 300$ MeV/c respectively. An analogous plot for the ^{8}Li events is shown in Fig. 8*b*, yielding $B/F = 2.2 \pm 0.8$ for $P \geq 300$ MeV/c and $B/F = 1.6 \pm 0.6$ for $P < 300$ MeV/c.

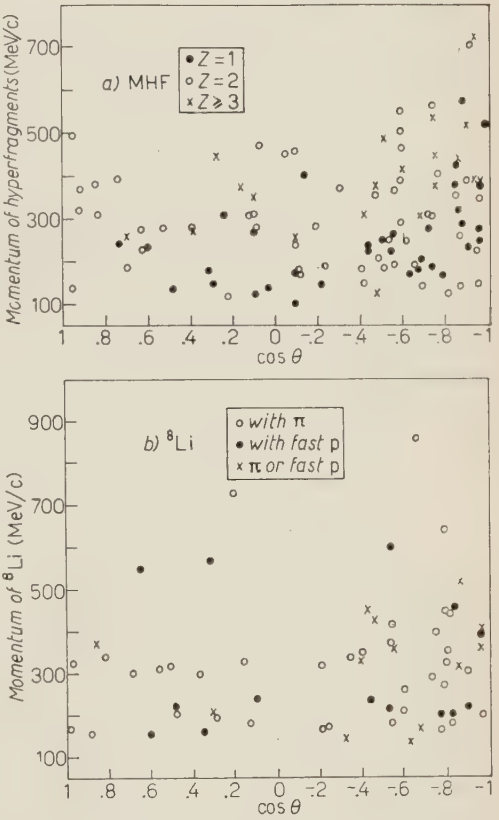

Fig. 8. – Plot of the angle θ between hyperfragment and pion or fast proton momenta, *vs.* the hyperfragment momentum. The same for ^{8}Li events.

6. – Primary reactions involved in MHF formation in nuclear emulsion.

The elementary interactions which, upon K^- captures in complex nuclei, may yield Λ-particles « available » for HF formation, are the following:

(1) $$K^- + \mathcal{N} \to \Lambda + \pi \text{ (direct-}\Lambda\text{ production)}$$

(2) $$K^- + \mathcal{N} \to \Sigma + \pi$$
$$\Sigma \downarrow$$
$$\Sigma + \mathcal{N} \to \Lambda + \mathcal{N} \text{ } (\Sigma\text{-conversion})$$

(3) $$K^- + 2\mathcal{N} \to \Lambda + \mathcal{N} \text{ (direct-}\Lambda\text{ from multinucleon capture)}$$

(4) $$K^- + 2\mathcal{N} \to \Sigma + \mathcal{N}$$
$$\Sigma \downarrow$$
$$\Sigma + \mathcal{N} \to \Lambda + \mathcal{N}.$$

It has been recently pointed out that a resonant state (Y^*) exists for the $\Lambda\pi$ system ([28]). Evidence has been presented for copious Y^* production, following multinucleon K^- capture in deuterium and helium ([29,30]). If this isobar is also abundantly produced following K^- capture in heavier elements, one should consider together with the above reactions, as sources of Λ's, the following processes:

(5) $$K^- + \text{nucleus} \to Y^* + \text{nuclear fragments}$$
$$Y^* \downarrow$$
$$Y^* \to \Lambda + \pi$$

and possibly $$Y^* + \mathcal{N} \to \Lambda + \mathcal{N} \text{ } (Y^*\text{ conversion}), \text{ etc.}$$

Several authors ([22,31]) have determined the relative frequency of occurrence of processes (1), (2), (3), (4) in emulsion nuclei. No re-evaluation of the emulsion data has however been presented, as yet, to include reactions via Y^* formation, such as reaction (5). An appreciable yield of the latter would obviously affect the conclusions reached so far: *e.g.* while the emission of a pion has been taken as evidence of K^- capture on single nucleons, it can be seen from (5) that this criterion does not hold any longer if Y^* formation is allowed to play a role. We have not attempted here such a re-analysis of the published data bearing on this subject.

In the analysis of the MHF parent stars, we tried to determine the relative yield of hyperfragment formation following the elementary processes (1) through (4). The same approach as that taken by the Bern Group ([31]) has

([28]) M. Alston, L. W. Alvarez, P. Eberhard, M. L. Good, W. Graziano, H. K. Ticho and S. G. Wojcicki: *Phys. Rev. Lett.*, **5**, 520 (1960).

([29]) O. Dahl, N. Horwitz, D. H. Miller, J. J. Murray and P. G. White: *Phys. Rev. Lett.*, **6**, 142 (1961).

([30]) Helium Bubble Chamber Collaboration Group: *Nuovo Cimento*, to be published.

([31]) Y. Eisenberg, W. Koch, M. Nikolić, M. Schneeberger and H. Winzeler: *Nuovo Cimento*, **11**, 351 (1959); *Helv. Phys. Acta*, **33**, 221 (1960).

been adopted for the classification of the primary stars. The basis for the classification is, in our case, the frequency of charged pion emission, their energy spectrum and the frequency of occurrence of fast protons among the K⁻-capture products.

Table III contains the numbers of MHF parent stars emitting a pion, a fast proton ($E \geqslant 52$ MeV), and also a pion together with a fast proton. Only the data from stack *A* are included; for this stack, the average plateau ionization was 16.4 blobs/100 microns.

TABLE III. – K^- *capture stars emitting* MHF (*stack A*).

Hypernuclide	Number of events	Number of events with π	Number of events with π and fast p	Number of events with fast p ($E \geqslant 52$ MeV)
H_Λ	65	15	3	16
He_Λ	90	42	4	8
Li_Λ	30	7	0	5
Be_Λ, B_Λ, C_Λ	10	5	0	1
$A > 5$	21	5	0	4
Total	216	74	7	34
% of stars	—	34.2 ± 3.5	3.2 ± 0.9	15.7 ± 2.8

As can be seen from Table III, the parent stars of He_Λ emit pions in $(47 \pm 6)\%$ of the cases while for the H_Λ parent stars this fraction is $(23 \pm 6)\%$. This different yield could be the effect of a loss of faster pions from H_Λ parent stars. On the other hand, the yield of fast protons associated with H_Λ emissions is $(24 \pm 6)\%$ to be compared with $(9 \pm 3)\%$ for the He_Λ parent stars. Since the majority of fast protons (unaccompanied by a pion) should originate in our case in multinucleon K^- captures, the above observed differences in pion and fast proton yields *both* indicate a rate of H_Λ production higher than the rate of He_Λ production in multinucleon captures.

If indeed the multinucleon K^--capture rate in Ag, Br is substantial, as suggested by the results of ALEXANDER *et al.* [32] the observation of a high multinucleon capture rate among the H_Λ parent stars could simply reflect the fact that more H_Λ than He_Λ are emitted from the heavy elements of the emulsion. This is not inconsistent with the results presented in Section 2·1.

[32] G. ALEXANDER, Y. EISENBERG, M. FRIEDMAN and D. KESSLER: *Proc. of the 1960 Annual Intern. Conference on High Energy Physics at Rochester*, p. 432.

The statistics on pion and fast proton emission for species with $Z \geq 3$ is obviously insufficient for a discussion on the above lines.

The overall fraction of MHF parent stars emitting a pion, including all species, is $(34.2 \pm 3.5)\%$. Although a loss of the fastest pions may affect this result, it is difficult to assess such a loss by comparing this values with those obtained by the European K^- collaboration [22] and the the Bern Group [31] in view of the noticeable differences pointed out for *e.g.* the parent stars of H_Λ and He_Λ. The overall fraction of MHF parent stars emitting protons of $E > 52$ MeV is $(15.7 \pm 2.8)\%$. This number, in conjunction with the fraction of stars yielding a pion and a fast proton $(3.2 \pm 0.9)\%$ indicates that at least $\sim 10\%$ of the events arise from multinucleon K^- capture [31].

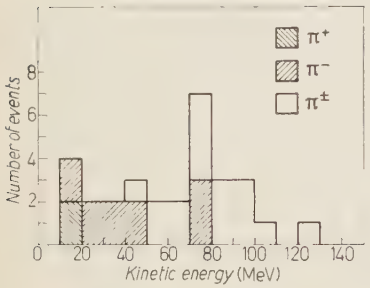

Fig. 9. – Energy spectrum of the pions with dip angle $\leq 30°$, emitted by MHF parent stars. The unshaded area corresponds to those pions whose energy was determined from ionization measurements.

Additional information as to the primary process leading to HF formation can be obtained from a study of the energy spectrum of the pions emitted by the HF parent stars. Such a spectrum for the 30 pions (out of 74) with dip angle $\leq 30°$ is shown in Fig. 9. 13 of these pions were brought to rest in the stack, two of which were positively charged. The energy of the remaining 17 pions was determined from ionization measurements and in all cases to better than 15%. The average pion energy is 60.6 MeV, and the average momentum is 138 MeV/c. The majority of the pions have energies below 90 MeV, the approximate lower bound of the pion spectrum from direct-Λ production (process (1) above) which is expected to peak at $\sim (120 : 180)$ MeV On the other hand the pions from Σ production are expected to peak in the region of 40 to 80 MeV. Thus our data can be interpreted as evidence that the Σ conversion contributes significantly to the process of HF production. Only a few pions can be attributed to direct-Λ production; the highest pion energy observed here is 125 MeV. Although the loss due to the low ionization of the stack may considerably affect the spectrum in this region, it should be pointed out that a large Λ production via Y* would have the effect of suppressing the pion spectrum at energies greater than about 120 MeV.

In conclusion, even with our limited statistics, it can be said that all the elementary processes (1) through (4) seem to contribute to MHF production, with the additional possibility that Λ production via the Y* isobar may be present. The relative contributions of these processes may differ for specific hypernuclear species produced; in the average, however, these contributions are consistent with those observed for a random sample of K capture stars [22,31].

7. – Discussion of the experimental results.

We will attempt in this section to correlate the experimental results presented in the preceding paragraphs with the expectation from possible models of hyperfragment production. The main results which have to be accounted for by such models can be summarized as follows:

a) with the exception of H_Λ, for which the production in Ag, Br may be important, all the other hypernuclides emerge preferentially from captures in C, N, O;

b) the lambdas bound in hyperfragments originate from all elementary processes conventionally defined as direct-Λ production, Σ-conversion and multinucleon capture;

c) the momentum spectra of emission for the various hypernuclides present marked similarity;

d) the emission spectra of He_Λ and Li_Λ are, within statistics, identical to those of the ordinary fragments He and ^{8}Li respectively;

e) hyperfragments are emitted preferentially opposite to an associated pion or fast proton. This effect is more pronounced for the latter case.

Although there may be several conceivable models of HF production, we will pay qualitative attention to two of them which explain several of the features noted above:

i) a model in which the lambda created in the elementary process is trapped in the nuclear potential well of the nucleus in which it is produced. The HF emission is then a result of the subsequent nuclear de-excitation;

ii) a model in which the hyperfragment is emitted promptly following the K^- or Σ^- interaction with a group of nucleons.

7·1. « *Trapped-*Λ » *model.* – According to this picture, the lambda which is produced by the K^- interaction with one or more nucleons of the capturing nucleus, may then be found in a bound state of the nucleus itself. Since the depth of the Λ-nucleon potential is of order (30÷40) MeV ([33]) and since a substantial fraction of the Λ's are produced with energies lower than this value, one may expect this capture process to be rather frequent. The Λ-capture process is then followed by nuclear de-excitation in a time short compared

([33]) R. H. Dalitz and B. W. Downs: *Phys. Rev.*, **111**, 967 (1958).

with the Λ lifetime. For excitation energies of $\lesssim 100$ MeV (visible energy release in MHF parent stars ~ 30 MeV) the de-excitation process may be quite different for light and heavy nuclei respectively. In fact, the observation of predominant HF emission from C, N, O is not surprising on the above assumptions. It is to be expected that the Coulomb barrier for Ag and Br would suppress quite effectively the emission of multiply charged hyperfragments at these low excitations. For example, on the basis of the evaporation model, the frequency of emission of ^{8}Li is for Ag and Br, at 100 MeV, already of order 50 times smaller than the observed frequency from a random sample of K stars in emulsion.

On the other hand the same amount of excitation energy is sufficient to cause the complete break-up of a light nucleus such as C, N, O. The Λ will then be found among the nuclear debris, either as a free particle or bound to a fragment to yield a hyperfragment.

The system of a Λ bound in a « silver » or « bromine » nucleus after nuclear de-excitation has occurred is to all effects a heavy hyperfragment which is likely to undergo non-mesonic decay. In no case is a visible track expected to reveal the formation of such a heavy HF.

In the framework of the present model, the energy distribution of both hyperfragments and ordinary nuclear fragments is expected to depend mainly on the excitation energy of the light parent nuclei. Neglecting specific final state interaction effects, the energy spectra of *e.g.* He_Λ and Li_Λ should be comparable to those of He and ^{8}Li respectively. This is indeed in agreement with the results presented in Fig. 4 and 5. In the very crude approximation of energy spectra determined by phase space only, it seems also possible to achieve a satisfactory fit with the experimental energy distributions. The curves of Fig. 5*a*, show a phase space spectrum for He fragments emitted in a random 4-body break-up of carbon, for excitation energies of 30 and 50 MeV. Such curves already bracket the qualitative features of the experimental spectrum; a more detailed comparison should average the partial contributions from the three nuclei in question, C, N, O, as well as contain the effect of a variation in the excitation energy and break-up modes. The information available is however insufficient for such a detailed calculation.

Another feature which can be explained by a statistical break-up of light nuclei is the similarity of the momentum spectra for various hypernuclear species. For a given excitation energy, and for $A > 4$, in fact, the phase space momentum spectra are rather insensitive to the mass of the fragment being considered. This can be seen, for example, from the relation for the momentum corresponding to the mode of the distribution, valid for a 4-body break-up:

$$p\,(\text{mode}) = \text{const} \cdot \left| \frac{2}{3} W m \left(1 - \frac{m}{M}\right) \right|^{\frac{1}{2}},$$

where W is the excitation energy, M the mass of the parent nucleus and m the mass of the fragment. Furthermore, one sees that a difference, for example between He and Li distributions, will be smeared out when combining distributions from the break-up of all the elements C, N, O.

The angular distributions of the emitted fragment, relative to the associated pion or fast proton, can partly be accounted for by assuming that the break-up occurs while the nucleus is in motion [34]. The prompt emission of a pion or of a fast proton in the elementary process of Λ creation, may in fact impart to the nucleus momenta mostly in the range $(100 \div 300)$ MeV/c. Fragments emitted isotropically in the rest frame of the recoiling nucleus will then exhibit in the laboratory an anisotropic distribution. This will give a backward-forward ratio greater than unity, for the relative direction of emission of HF and pion or fast proton.

While for direct-Λ production (reaction (1) and (3) of Section 6) the momentum transfer to the nucleus will, in general, be determined by the pion or nucleon momentum respectively, this may not be the case when the Λ arises from Σ-conversion (reactions (2) and (4) of Section 6). In the latter case, the additional momentum transferred to the nucleus by the secondary process of Σ-conversion may in fact smear out the effect of the original momentum transfer from the primary process. Thus the average momentum transfer is expected to be smaller than the average pion or fast proton momenta observed. Assuming, for example, an average momentum transfer of 100 MeV/c to a C nucleus (velocity acquired $= 0.01c$), and on the basis of the observed HF energy distributions, one would expect an average B/F ratio of ~ 1.8 for all hyperfragments. A comparable value (1.8 ± 0.4) is indeed observed for the MHF emitted together with a pion. For much higher momentum transfers, such as those appropriate to the emission of fast protons at the moment of Λ creation, one also obtains a value of B/F comparable with the observations.

On the basis again of momentum transfer to a C nucleus of order 100 MeV/c and of the observed energy distribution of ^{8}Li, one would expect for this isotope a B/F ratio of about 1.9 consistent with the observed value 1.8 ± 0.4. For ^{4}He of $E < 18$ MeV ($R < 150$ μm) under the same assumptions, one would expect $B/F \sim 1.6$. On the other hand, one finds $B/F \sim 1.0 \pm 0.2$ for the stable prongs of $R < 150$ μm. Although these two values are not in agreement it may be that the two numbers are not directly comparable because the stable prongs of $R < 150$ μm may contain, in addition to ^{4}He, a contamination of order 20% of H isotopes, a probable sizable proportion of ^{3}He and as much as 10% of isotopes heavier than He. Furthermore this discrepancy would diminish if an average momentum transfer lower than 100 MeV/c were assumed, while

[34] O. Skjeggestad and S. O. Sørensen: *Phys. Rev.*, **113**, 1115 (1959).

still preserving an agreement, within statistics, for the MHF and ^{8}Li B/F ratios.

We thus conclude that the « trapped-Λ model » accounts quite satisfactorily for the gross features of HF emission following K⁻ capture in nuclear emulsion.

7·2. « *Prompt*-HF » *model.* – The possibility of such a model is suggested by the reaction

$$K^- + {}^4He \rightarrow {}^4He_\Lambda + \pi^- ,$$

observed in the Helium Bubble Chamber ([10]), in which, within the experimental errors, the total available energy is apparently shared by the two bodies. Additional evidence, of a somewhat less stringent nature, is provided by the observation of

$$K^- + {}^4He \rightarrow {}^1H_\Lambda + \pi^0 \quad \text{(Ref. ([10]))} .$$

$$\left.\begin{aligned} K^- + {}^{12}C &\rightarrow {}^{12}B_\Lambda + \pi^0 \\ \Sigma^- + {}^{12}C &\rightarrow {}^{12}B_\Lambda + n \end{aligned}\right\} \text{(Ref. ([5]))} .$$

However it is extremely difficult to measure the total energy release in this case, so that one can only infer that the visible energy release is consistent with the one expected for two-body reactions.

Extending this idea, it is not inconceivable that reactions of this type could take place within a nucleus, involving only a limited number of nucleons. On this basis, the hyperfragment and the pion or fast proton would be emitted opposite to each other, if it were not for the perturbing effect of the neighboring nucleons. Additional smearing of both energy and angular distributions will arise from the two step process of Σ-production and conversion.

The prevalent HF emission from light nuclei can again be at least partly explained by this picture: if the available energy (~ 170 MeV) is to be shared between a pion and a hyperfragment, the HF energy is already comparable with the Coulomb barrier for Ag and Br for $^5He_\Lambda$ and will of course be smaller for heavier hypernuclides. Thus one can expect suppression in the emission of HF from heavy nuclei, following pion producing captures. One would expect however that K⁻ captures not yielding pions may contribute for some HF production even in Ag and Br. If the available energy in the latter case (~ 300 MeV) is shared by a nucleon and a hyperfragment, practically all hypernuclear species that have been observed could be imparted energy in excess of the Coulomb barrier of Ag and Br. Thus this mechanism could account at least for some features of H_Λ production. As already pointed out, the parent stars of this hypernuclide exhibit a high yield of fast protons, accompanied by a low yield of pions. The lower limit of production in C, N, O could

only be placed at about 57 %. This is some evidence that multinucleon capture in heavy elements contributes here, and that the above mechanism of HF production may well play a role (see 2·2).

The similarity of the momentum spectra of different HF species, as well as the similarity between the spectra of HF and ordinary nuclear fragments

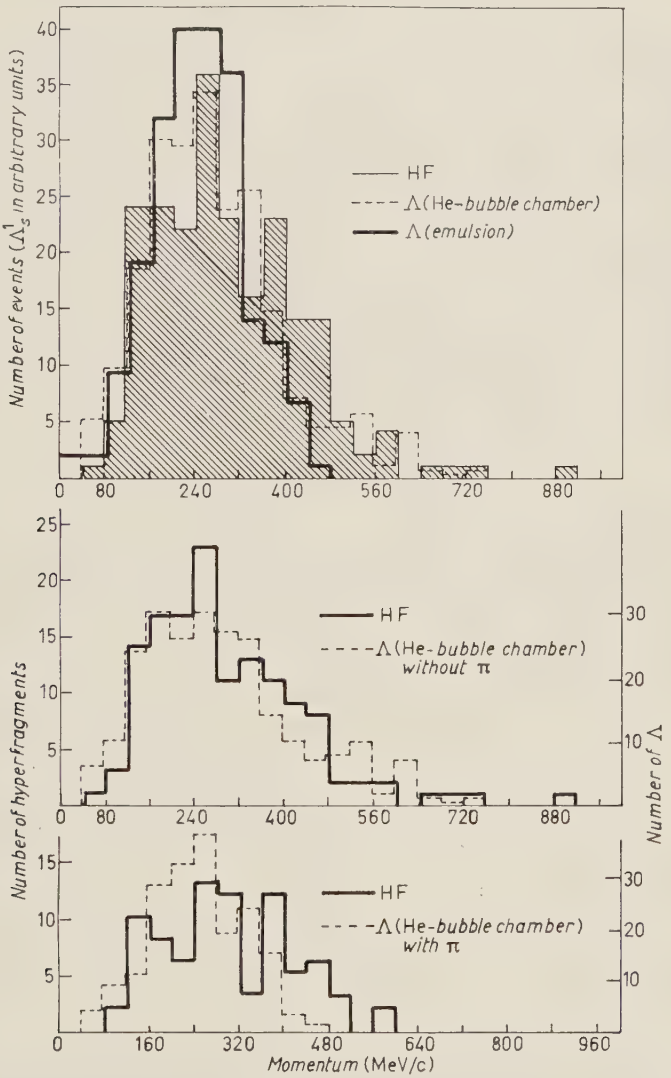

Fig. 10. – Momentum distribution of MHF from K^- captures in nuclear emulsion, compared with the momentum spectra of free Λ's from K^- captures in He ([10]) and nuclear emulsion ([35]). The MHF momentum spectra for events produced with or without a pion are also compared with the corresponding distributions for free Λ's from K^- captures in He.

should now be examined in relation to the « prompt-HF » model. It may be of interest in this connection to examine also the momentum spectrum of the free Λ's emitted following K^- captures in He and in nuclear emulsion.

Fig. 10 shows comparison of *a*) the momentum spectrum of all HF's with the spectrum of the free Λ's from K^- captures in He ([10]) and nuclear emulsion ([35]), *b*) the momentum spectrum of free Λ's (from He) and HF's accompanied in the capture by no pion emission and *c*) the same comparison as in *b*) for those captures in which a pion is emitted. As seen in Fig. 10, the momentum spectra of free Λ's and hyperfragments are rather similar, in particular if one considers the free-Λ data from the He experiment. The average Λ momenta expected from a single nucleon K^- capture is about 250 MeV/*c*, while is about 580 MeV from a 2-nucleon capture. In addition, the Λ's from Σ^- conversion may have momenta in the range (0 ÷ 500) MeV/*c*. The hyperfragment momenta from a 2-body production reaction (upper limits in the « prompt-HF » model neglecting momentum and energy transfer to neighboring nucleons) are surprisingly similar for all HF species and in the range (270÷280) MeV/*c* for emission of π and HF, in the range (700÷800) MeV/*c* when the HF is balanced by a nucleon. The final state interaction with the other nucleons in the nucleus where the K^- capture occurs is likely to yield lower average values. No attempt has been made to calculate an expected momentum spectrum; the possibility of producing HF's by this mechanism following Σ-conversion adds considerable complexity to the problem. The purpose of the above discussion is mainly to show that one cannot exclude, in the framework of the proposed model, that different hypernuclear species may be produced with very similar momentum spectra and that, in turn, these spectra may be comparable with the free-Λ spectrum.

On the other hand such a model cannot satisfactorily account for two important features of the data. In the first place, there is lack of a strong correlation between the angle *θ* and the HF momentum, which one would otherwise expect if such a production mechanism were dominant, due to the presence of final state interaction. As a result of such an interaction one would expect the HF's of higher momenta to have been least affected before escape from the nucleus and therefore to be emitted at large angles with respect to the π or fast proton. The HF's of lower momenta would instead have suffered secondary interactions and therefore lost their correlation with the pion or fast proton direction.

([35]) C. J. Mason: UCRL-9297 (unpublished); J. Bogdanowicz, A. Filipkowski, A. Krzywicki, E. Marquit, E. Skrzypczak, A. Wroblewski and J. Zakrzewski: Polish Academy of Science Report no. 107/V1; Bologna-Munich-Parma Collaboration and Munich-Turin Collaboration: *Proc. of the 1960 Annual Intern. Conference on High Energy Physics at Rochester*, presented by K. Gottstein, p. 440.

Secondly, if such a model were dominant, one would not expect the close similarity between the momentum spectra of He_Λ, ^4He and of Li_Λ, ^8Li except as an accident.

A possible further objection to such a model may lie in the fact that for such a mechanism the K would have to interact with a large aggregate of nucleons (*e.g.* Li) present within a larger nucleus.

7·3. *Conclusions.* – The previous two models are by no means the only possible production mechanisms. One could, for example, conceive of the prompt production of an « excited HF » which subsequently dissociated into the detected HF together with other nuclear fragments. Alternatively one may have a « pick-up » model in which a Λ picks up a group of nucleons when all are moving with small relative velocity. The discussion of the previous section has not been exhaustive but was mainly intended to show that many of the gross features of HF production may be accounted for in terms of two simple models with rather crude assumptions which are not however implausible. The models presented are not mutually exclusive and it is possible that even for a given hypernuclear species, more than one production process is operative.

* * *

We would like to thank Professors R. H. Dalitz and V. L. Telegdi at the Enrico Fermi Institute for Nuclear Studies for much appreciated criticism and advice. In addition, we would like to thank Professors L. M. Brown, R. H. Capps and J. H. Roberts at Northwestern University for their continued encouragement and helpful discussions during various phases of the present work.

We are greatly indebted to Dr. E. J. Lofgren and the Bevatron Staff for making this experiment possible and for their co-operation during the exposure of the stacks.

RIASSUNTO

Nel tentativo di interpretare il meccanismo di produzione degli iperframmenti, si sono studiate 422 stelle di cattura da K^- e 13 stelle di cattura da Σ^-; in entrambi i casi tali stelle danno origine a iperframmenti che si disintegrano con emissione di un mesone π^- (MHF). Si sono inoltre studiate 123 stelle da K^- emittenti frammenti di ^8Li. Diversi criteri hanno permesso una separazione delle catture di K^- in C, N, O da quelle in Ag, Br. I limiti inferiori alle frazioni di MHF prodotti in C, N, O sono 57%, 73%,

84% e 94% per H_Λ, He_Λ, Li_Λ e MHF di $Z \geqslant 4$. Per l'^{8}Li, tale limite inferiore è 75%. In totale, si ottiene una frequenza relativa di $(1.05 \pm 0.05) \cdot 10^{-2}$ MHF [cattura di K^- e di $(3.8 \pm 1.4) \cdot 10^{-2}$ HF] cattura di Σ^-. Lo spettro di energia dei pioni emessi dalle stelle di cattura suggerisce che una frazione considerevole delle particelle Λ emesse in uno stato legato proviene da processi di conversione di iperoni Σ. Si è ottenuta qualche prova della produzione di Λ legate da processi di cattura di K^- con più nucleoni, in particolare nel caso dell'H_Λ. Gli spettri di impulso per specie ipernucleari differenti sono molto simili tra loro, inoltre, gli spettri per l'He_Λ e Li_Λ sono comparabili rispettivamente con quelli dell'He e dell'^{8}Li. Gli iperframmenti sono emessi di preferenza in direzione opposta a quella di emissione di un pione o protone veloce. Il rapporto indietro/avanti (B/F) per eventi (π, MHF), è 1.8 ± 0.4. Si propongono due modelli per la produzione di iperframmenti. Secondo il primo di questi (Λ catturata) la Λ creata nel processo elementare viene catturata nella buca di potenziale del nucleo d'origine. L'iperframmento è in seguito emesso nel processo di diseccitazione nucleare. Nel secondo modello (emissione immediata), l'iperframmento è emesso direttamente a seguito della cattura di un K^- o di un Σ^- da parte di un gruppo di nucleoni. Si conclude che entrambi i meccanismi possono contribuire. Il verificarsi di entrambi i processi riesce a spiegare essenzialmente tutte le osservazioni relative all'emissione di iperframmenti.

IL NUOVO CIMENTO Vol. XXII, N. 6 16 Dicembre 1961

Nuclear Resonance Fluorescence in Solid ^{60}Co Sources.

M. Giannini, D. Prosperi and S. Sciuti

Centro di Studi Nucleari della Casaccia - Roma
Scuola di Perfezionamento in Fisica dell'Università - Roma

(ricevuto il 19 Luglio 1961)

Summary. — As well known, the compensation required for restoring the resonant conditions can be performed by means of the motion that the emitting nucleus might have as the result of one or more preceding transitions. Nuclear resonance cross-section in ^{60}Co solid sources exhibits a strong dependence from the mean life of the second excited level of ^{60}Ni, from which start the 1.17 MeV γ-rays involved in the compensation. A simple model in which the attenuation is related to this mean life is described. Analysing the experimental results obtained by us with a solid ^{60}Co source the second level mean life turns out to be $\leqslant 5 \cdot 10^{-12}$ s. This procedure seems to allow mean life estimates concerning a level leading, through a cascade, to the ground state, any time a situation similar to the $^{60}Co \rightarrow {}^{60}Ni$ decay occurs.

1. – Introduction.

It is well known that nuclear resonance fluorescence studies cover many fields of research. Lifetime measurements in ranges not attainable with electronic methods ($\tau_\gamma \leqslant 10^{-12}$ s) can be performed by this technique.

Among the compensation methods employed for restoring the resonance condition, the simplest is that using the motion that the emitting nucleus might have as the result of one or more preceding transitions. This method has been successfully employed by several authors [1] under the obvious condition that at least a fraction of the γ-rays is emitted before the compensation

[1] E. Pollard and D. E. Alburger: *Phys. Rev.*, **74**, 926 (1948); M. Schopper: *Zeit. f. Phys.*, **144**, 476 (1956); N. A. Burgov: *Soviet Phys. JETP*, **6**, 502 (1958); F. R. Metzger: *Prog. Nucl. Phys.*, **7**, 53 (1959).

be destroyed by the collisions of the recoiling nuclei with the surrounding source material. When employing this technique, a gaseous source is generally more convenient than liquid or solid ones because it is characterized by longer collision times. Further the shape of the emission line is easier to evaluate for gaseous sources. The knowledge of this shape is requested because the cross-section of the process is proportional to the fraction of γ-rays emitted in the energetic region of the absorption line.

In liquid or solid sources the collision times are of the order of 10^{-13} to 10^{-14} s; therefore only if the mean life of the studied level is $< 10^{-12}$ s a reduced resonance effect can still be observed. The attenuation effects appearing in liquid or solid sources are always more complex than those in gases; anyway self-absorption experiments [2] can avoid the need to evaluate them. The experimental difficulties introduced by the above-mentioned attenuations have been overcome by OFER and SCHWARZSCHILD [3] who employed strong radioactive sources and drastic shieldings. In all the cases studied by the authors the compensation was due to only one preceding decay; for $\tau_\gamma \sim 10^{-12}$ s they obtained cross-sections by about a factor fifty smaller than those corresponding to gaseous sources.

The mean life of the first excited level in ^{60}Ni (1.33 MeV) has been measured by many authors employing gaseous sources. In this case both the recoils due to the β-decay of ^{60}Co and to the 1.17 MeV γ-transition are required in order to attain the correct Doppler shift. METZGER [4] measured a cross-section of $\simeq 3 \cdot 10^{-26}$ cm^2 and a mean life $\tau_\gamma = (1.1 \pm 0.2) \cdot 10^{-12}$ s, BURGOV [5], found $\tau_\gamma = (1.0 \pm 0.3) \cdot 10^{-12}$ s, AKKERMAN *et al.* [6] obtained $\tau_\gamma = (1.14 \pm 0.37) \cdot 10^{-12}$ s.

Liquid ^{60}Co sources have been also employed. KAIPOV and SHUBNYI [7] have found a cross-section $\sigma = 1.76 \cdot 10^{-27}$ cm^2 to which corresponds a collision time of about $5 \cdot 10^{-14}$ s.

The collision time for ^{60}Co solid sources is about hundred times smaller than the measured mean life. Further in ^{60}Co the energy losses due to collisions take place all along two recoil processes. The γ-ray fraction satisfying the resonance conditions is strongly reduced and the resonance effect is therefore not easily detectable. In this case an attenuation bigger than those

(2) F. R. METZGER: *Phys. Rev.*, **110**, 123 (1958); S. OFER and A. SCHWARZSCHILD: *Phys. Rev.*, **116**, 725 (1959).

(3) S. OFER and A. SCHWARZSCHILD: *Phys. Rev. Lett.*, **3**, 384 (1959).

(4) F. R. METZGER: *Phys. Rev.*, **103**, 983 (1956).

(5) N. A. BURGOV, YU. V. TERECHOV and G. E. BIZINA: *Soviet Phys. JETP*, **9**, 1146 (1959).

(6) K. AKKERMAN, D. K. KAIPOV and YU. K. SHUBNYI: quoted in (5).

(7) D. K. KAIPOV and YU. K. SHUBNYI. *Soviet Phys. JETP*, **12**, 615 (1961).

found by OFER and SCHWARZSCHILD is expected; tentatively one can expect a cross-section of the order of $3 \cdot 10^{-26} \cdot (1/50)^2 \simeq 10^{-29}$ cm (see Section 8).

A very interesting characteristic shown by the particular compensation processes occurring in solid or liquid ^{60}Co sources is the strong dependence of the attenuation from the mean life of the second excited level from which start the 1.17 MeV γ-rays involved in the compensation. In order to take advantage of this fact we have developed a simple model in which the attenuation is related to this mean life. Analysing the experimental results obtained by us with a solid ^{60}Co source it appears that the second level mean life has a magnitude $\tau_\gamma \leqslant 5 \cdot 10^{-12}$ s. This procedure seems to allow mean life estimates concerning a level leading, through a cascade, to the ground state, any time a situation similar to the ^{60}Co $\rightarrow$ ^{60}Ni decay occurs.

2. – Experimental results.

The experimental set up is shown in Fig. 1. A ^{60}Co solid source (2.8 C) was employed. The measurement consisted in comparing the γ-intensities scattered respectively by Ni and Cu plates both 0.85 cm thick. The surface intercepted by the γ-beam was ~ 200 cm^2. The mean scattering angle was about 120°. The scattered γ-ray spectra, examined by means of a 200 channel pulse-height analyser are shown in Fig. 2 and 3. The contribution to the 1.33 MeV peak due to elastic scatterings (RAYLEIGH and THOMSON) is by an order of magnitude bigger than that due to the resonance fluorescence (difference between curves in Fig. 2 and 3). In the 1.17 MeV region the main contribution is due to the elastic scattering; the difference between the curves in this region is chiefly due to the Compton edge of 1.33 MeV resonant peak. A rather intense peak due to 1.46 MeV ^{40}K γ-rays is also shown. This peak clearly appears also in the inferior curves (Fig. 2 and 3), representing the background spectra obtained without the scatterers. By subtracting the background one obtains the curves *a* and *b* of Fig. 4 showing the γ-ray spectra scattered by Ni and Cu. The curve *c* is the difference between the two superior curves *a* and *b*. The intensity of the γ-rays scattered by Ni and Cu are respectively (356 ± 6) and (323 ± 6) photons per hour as a result of two sets

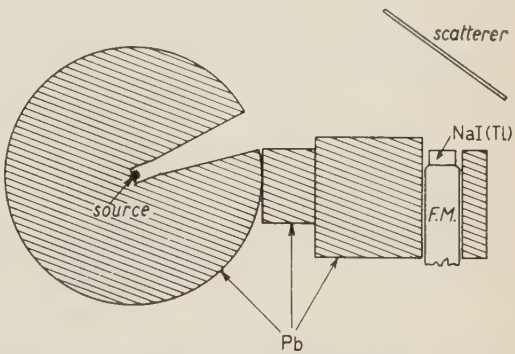

Fig. 1. - Schematic diagram for experimental arrangement.

of measurements. The resonant effect turns out to be bigger than the difference between the above quoted values (33 ± 9) because it is partially

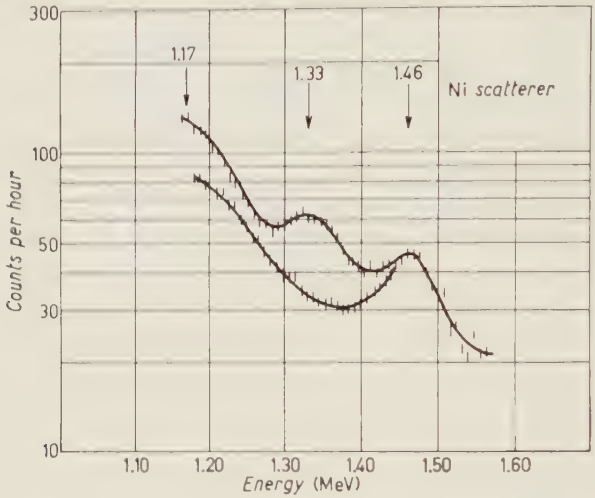

Fig. 2. – Upper curve: spectrum of γ-rays scattered by a Ni target. Lower curve: spectrum without the scatterer. The 1.46 MeV peak is due to ^{40}K.

masked by the bigger elastic scattering in Cu. The corrected difference is (40 ± 9) photons/hour.

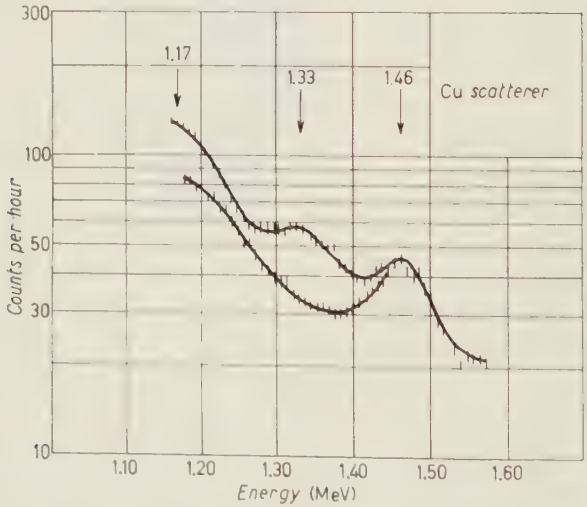

Fig. 3. – Upper curve: Spectrum of γ-rays scattered by a Cu target. Lower curve: spectrum without the scatterer. The 1.46 MeV peak is due to ^{40}K.

The resonant scattering cross-section can be deduced by comparison with the elastic scattering cross-section in Cu, whose magnitude turns out to be

$(1.01 \pm 0.43)\cdot 10^{-30}$ cm² from our experimental data (1.33 MeV and $\theta = 120°$). The latter cross-section can also be derived from the results of CINDRO and ILAKOVAC (8) employing an

$$E_\gamma^{-3}\,\frac{1-\cos^2\theta}{\sin^3(\theta/2)}$$

dependence according to the explicit Franz formula (9). In this way one obtains $(1.07 \pm .32)\cdot 10^{-30}$ cm². Averaging the above results one gets

$$\frac{d\sigma_{el}^{Cu}}{d\omega}(\theta = 120°, E_\gamma = 1.33\,\text{MeV}) = (1.05 \pm 0.25)\cdot 10^{-30}\,\text{cm}^2\,.$$

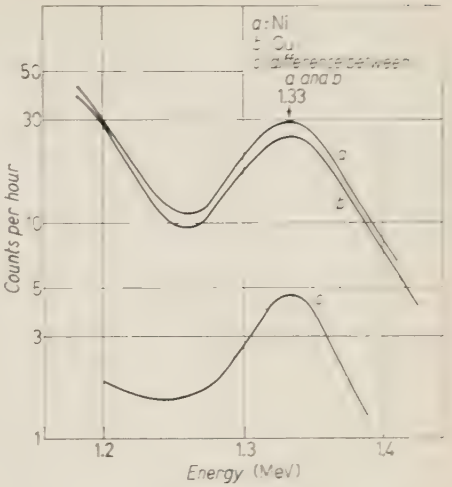

Fig. 4. – Curves *a* and *b*: spectra of γ-rays scattered by Ni and Cu (background subtracted). Curve *c*: difference between *a* and *b*.

From this values and from the ratio 1.10 ± .03 between the scattered intensities one has (*)

$$\frac{d\sigma_{NRF}}{d\omega}(\theta = 120°) = (0.49 \pm .13)\cdot 10^{-30}\,\text{cm}^2\,;$$

$$\sigma_{NRF} = \frac{d\sigma}{d\omega}\,\frac{\overline{W}\,4\pi}{W(120°)} = (8.9 \pm 2.4)\cdot 10^{-30}\,\text{cm}^2\,.$$

The theoretical angular correlation $W(\theta)$ employed in the above formula was calculated by assuming a $0^+ \to 2^+ \to 0^+$ transition.

3. – Interaction between the recoiling nuclei.

Some authors (3,10) have schematized the recoil phenomena by assuming that all the collisions take place at a distance R from the initial position of the radioactive atom. The atom can freely recoil as far as it reaches the surface of a sphere of radius R where it looses all its energy (absorbing hard sphere model). In resonance phenomena characterized by a single decay compen-

(8) N. CINDRO and K. ILAKOVAC: *Nucl. Phys.*, **5**, 647 (1958).

(9) W. FRANZ: *Zeit. f. Phys.*, **98**, 314 (1935).

(*) In the calculation the following data were employed: fraction of resonant atoms in Ni = 0.262; ratio between atomic densities in Ni and Cu = 1.082.

(10) K. ILAKOVAC: *Proc. Phys. Soc.* (*London*), A **67**, 601 (1954).

sation one can assume that the recoil velocity should be exactly $v = E_\gamma/Mc$ *i.e.* the velocity required for the compensation. Then the time interval effective for the emission of a resonant γ-ray is $t_c = R/v$; all the γ-rays emitted after t_c do not contribute to the process. These arguments were employed by the above-mentioned authors in order to take into account the effect of the collisions by introducing into the theoretical cross-section the attenuation factor $(1 - \exp[-t_c/\tau_\gamma])$. This procedure is not a realistic one. In fact the model implies that the recoil velocity keeps constant along the whole path R and then suddenly drops to zero. In practice in solid sources, before the drop, the velocity decreases continuously as long as the recoiling atom gets away from its equilibrium position ([11]). Therefore the compensation conditions can be satisfied only by nuclei with an initial speed equal or bigger than v at the instant in which they reach this velocity. The model is still appliable if the following conditions are fulfilled: *a*) the velocity behaviour can be considered linearly decreasing with the distance from the equilibrium position; *b*) a radius R can be defined in correspondence of which the velocity suddenly drops; *c*) the emission spectrum can be considered nearly constant in the energy interval available for the compensation. For liquid sources similar considerations are required; the attenuation phenomena are now dependent upon the mean free path and the interaction laws with the surrounding nuclei.

For ^{60}Co the above-mentioned considerations must be modified. In fact the total recoil is released in two distinct steps by the β-decay and by a first γ-transition with a mean life τ_{γ_1}. The probability that the second γ-transition, with a mean life τ_{γ_2}, can give rise to the resonance depends on τ_{γ_1} as already pointed out. In order to evaluate such a dependence we have extended the absorbing hard sphere model to ^{60}Co.

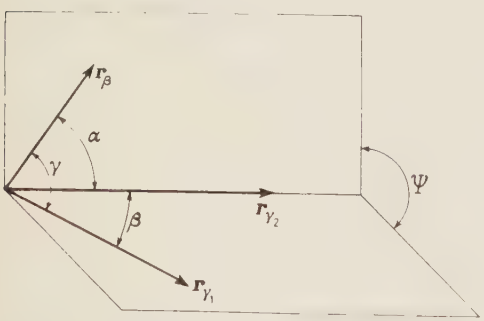

Fig. 5. – Recoil momenta and angles required in order to describe the ^{60}Co decay.

Let $\boldsymbol{r}_\beta$, $\boldsymbol{r}_{\gamma_1}$, $\boldsymbol{r}_{\gamma_2}$, α, β, γ and ψ be respectively the three recoil momenta taken away by the ^{60}Ni nuclei in their successive decays and the four angles characterizing the process (Fig. 5). Then we can express the Doppler energy increment ΔE_{γ_2} of the second γ-ray in terms of the nuclear recoils $\boldsymbol{r}_\beta$ and $\boldsymbol{r}_{\gamma_1}$:

$$\Delta E_{\gamma_2} = -\frac{m_0}{M} E_{\gamma_2}(E_{\gamma_1} \cos\beta + r_\beta \cos\alpha) .$$

([11]) J. B. GIBSON, A. N. GOLAND, M. MILGRAM and G. H. VINEYARD: *Journ. Appl. Phys.*, **30**, 1322 (1959).

where m_e and M are respectively the masses of electron and the recoiling nucleus; energies and momenta are expressed in $m_e c^2$ and $m_e c$ units. In order to take into account the interactions dissipating the recoil velocities one can introduce an attenuation function $\mathscr{A}(r_\beta, \alpha, \beta, \psi)$ expressing the probability that the Doppler increment ΔE_{γ_2} keeps constant until the second γ-ray is emitted. Now let $P(r_\beta)$ be the distribution function of the nuclear recoils due to the β-decay and $W(\cos\beta)$ the γ_1-γ_2 angular correlation. Then the attenuated cross-section can be written in a general way:

$$(1)\qquad \sigma_{\mathrm{FRN}} = \frac{\sigma_0 \sqrt{\pi}\, \Gamma_2}{8\pi\, \Delta_s} \int_0^{r_\beta^{\max}} P(r_\beta)\, \mathrm{d}r_\beta \int_0^{2\pi} \mathrm{d}\psi \int_0^{\pi} \sin\alpha\, \mathrm{d}\alpha \cdot$$

$$\cdot \int_0^{\pi} W(\cos\beta)\, \mathscr{A}(r_\beta, \alpha, \beta, \psi) \exp\left[-\frac{m_e}{M}\frac{E_{\gamma_2}}{\Delta_s}(E_{\gamma_2} + E_{\gamma_1}\cos\beta + r_\beta \cos\alpha)\right] \sin\beta\,,$$

where Γ_2 is the level width concerning the second γ-ray and Δ_s is the Doppler thermal width at the scatterer temperature. In the present hypothesis one can easily calculate the $\mathscr{A}(r_\beta, \alpha, \beta, \psi)$:

$$(2)\qquad \mathscr{A}(r_\beta, \alpha, \beta, \psi) = \int_0^{S/r_\beta} \lambda_1 \exp[-\lambda_1 t]\left\{1 - \exp[-\lambda_2 g(r_\beta, \alpha, \beta, \psi, t)]\right\} \mathrm{d}t\,,$$

where

$$S = R\,\frac{M}{m_e c}\,, \qquad \lambda_{\gamma_{1,2}} = \frac{1}{\tau_{\gamma_{1,2}}}\,,$$

$$g(r_\beta, \alpha, \beta, \psi, t) = \frac{1}{r_\beta^2 + E_{\gamma_1}^2 + 2\tau_\beta E_{\gamma_1}\cos\gamma}\left[-(r_\beta^2 + r_\beta E_{\gamma_1}\cos\gamma)t + \right.$$

$$\left. + \sqrt{(r_\beta^2 + r_\beta E_{\gamma_1}\cos\gamma)^2 t^2 - (r_\beta^2 t^2 - S^2)(r_\beta^2 + E_{\gamma_1}^2 + 2r_\beta E_{\gamma_1}\cos\gamma)}\right]$$

$$\cos\gamma = -\cos\alpha\left(\frac{E_{\gamma_2}}{E_{\gamma_1}} + \frac{r_\beta}{E_{\gamma_1}}\cos\alpha\right) + \sin\alpha\cos\psi\sqrt{1 - \frac{E_{\gamma_2}}{E_{\gamma_1}} + \frac{r_\beta}{E_{\gamma_1}}\cos\alpha}\,.$$

Substituting in (1) the exponential function with a Dirac δ-function, one gets

$$(3)\qquad \sigma_{\mathrm{FRN}} = \frac{\Gamma_2}{E_{\gamma_1}\cdot E_{\gamma_2}}\,\sigma_0\,\frac{M}{m_e}\,\frac{0.4762}{8}\,\mathscr{I}\,,$$

where

$$\mathscr{I} = \int_{\arccos\left(\frac{E_{\gamma_1} - E_{\gamma_2}}{r_\beta^{\max}}\right)}^{\pi} \sin\alpha \cdot \mathrm{d}\alpha \cdot \int_{\frac{E_{\gamma_2} - E_{\gamma_1}}{|\cos\alpha|}}^{\pi} W\left(\frac{E_{\gamma_2}}{E_{\gamma_1}} + \frac{r_\beta}{E_{\gamma_1}}\cos\alpha\right) P(r_\beta)\, \mathrm{d}r_\beta \int_0^{2\pi} \mathscr{A}(r_\beta, \alpha, \psi)\, \mathrm{d}\psi\,.$$

The angle β has been eliminated through relation $\cos\beta = -(E_{\gamma_2}/E_{\gamma_1} - \cos r_{\beta} E_{\gamma_1})$. The numerical factor $0.4762/8$ comes out from the normalization of the various probability functions. The triple integral, $\mathscr{I}$, has been numerically evaluated by the « Istituto per le Applicazioni del Calcolo » of the « Consiglio Nazionale delle Ricerche ». For ^{60}Co under the conditions $R < 10$ Å and λ_{γ_1} of the same order of magnitude or less than λ_{γ_2} one can write

$$\mathscr{I} = 2\pi S \lambda_{\gamma_2} I(\mu) ,$$

where

$$\mu = \frac{S\lambda_{\gamma_1}}{E_{\gamma_1}} .$$

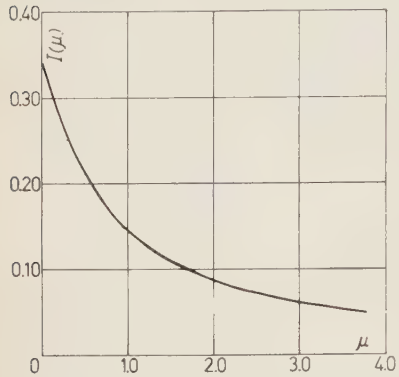

Fig. 6. – Graph of $I(\mu)$ introduced in eq. (4).

The graph representing $I(\mu)$ is shown in Fig. 6.

The cross-section attenuation cannot be anymore expressed by the factor $A = (1 - \exp[-t_c/\tau_{\gamma_2}]) \sim (1/\tau_{\gamma_2})(R/v)$ (see the beginning of the this paragraph). In the present case as it can be easily calculated from eq. (3) and from the knowledge of the corresponding cross-section obtained for $\mathscr{A}(r_\beta, \alpha, \beta, \psi) = 1$, one can write

$$A = \frac{R^2}{\tau_{\gamma_1} \cdot \tau_{\gamma_2}} I(\mu) \cdot 10^{-11} \tag{4}$$

which can roughly be thought of as the product of the two attenuation factors $(R/\tau_{\gamma_1} v) \cdot (R/\tau_{\gamma_2} c)$.

4. – Conclusions.

The above discussed model can be applied to the experimental results already reported above. In order to evaluate τ_{γ_1} from (4) it is necessary to estimate the collision radius R. In the simple case concerning only one preceding decay the R values found by OFER and SCHWARZSCHILD lie between 1 and 3 Å. In the present case the absorption line lies on the rapidly decreasing part of the emission line. The nuclei possessing an initial speed higher than the compensation value are very few; therefore the fraction that can give rise to the compensation at a distance R will be correspondly low. The critical cases must be described introducing a collision radius R smaller than that found by OFER and SCHWARZSCHILD. For ^{60}Co one can obtain a superior limit for τ_{γ_1} introducing a radius $R = 2$ Å obtained by averaging OFER and SCHWARZSCHILD's data. The limiting value is therefore $\tau_{\gamma_1} \sim 4 \cdot 10^{-12}$ s. We

have disregarded the possibility of employing KAIPOV and SHUBNYI's data because the nuclear resonance fluorescence in liquid sources is complicated by molecular phenomena which further attenuate the cross-section. The uncertainty in recoiling mass evaluation, the possible excitation of the molecular degrees of freedom, the difficulties in evaluating the proper mean free path, the possible persistence of the velocity after the first collision are reasons which reduce the possibility of obtaining reliable estimates of τ_{γ_1} from (4). Our τ_{γ_1} estimate is in agreement with the results obtained by electronic techniques ([12]), but seems to be lower than the values suggested by the systematics of nuclear levels (10^{-11} to 10^{-12} s).

In conclusion, a close connection seems to exist between the attenuation and the mean lives τ_{γ_1} and τ_{γ_2}. If τ_{γ_1} has a value sufficiently bigger than the collision time such a connection can be easily studied; inversely if the mean lives are known the above connection can give information on some structural properties of the employed source.

* * *

The authors wish to express their gratitude to Dr. WOLF GROSS of the « Istituto per le Applicazioni del Calcolo » of the « Consiglio Nazionale delle Ricerche » for having evaluated the triple integral $\mathscr{I}$.

Thanks are due also to Dr. M. CHIARA RAMORINO of C.N.E.N. for having carried out part of the measurements.

([12]) Z. BAY, V. P. HENRY and F. MCLERNON: *Phys. Rev.*, **97**, 780 A (1954); **97**, 561 (1955); M. R. LEMMER and M. A. GRACE: *Proc. Phys. Soc.*, A **67**, 1051 (1954); C. F. COLEMAN: quoted by W. D. ALLEN and P. A. EGELSTAFF: *Nature*, **175**, 1027 (1955).

RIASSUNTO

Com'è noto, la compensazione necessaria per ripristinare le condizioni di risonanza può essere ottenuta sfruttando il rinculo lasciato ad un nucleo in seguito ad uno o più decadimenti precedenti. La sezione d'urto di risonanza nucleare nelle sorgenti solide di ^{60}Co presenta una forte dipendenza dalla vita media del secondo livello eccitato del ^{60}Ni da cui partono i raggi γ da 1.17 MeV partecipanti alla compensazione. Si descrive un semplice modello in cui l'attenuazione viene espressa in funzione di questa vita media. Analizzando i risultati sperimentali da noi ottenuti con una sorgente solida di ^{60}Co si deduce per la vita media del secondo stato eccitato un valore inferiore od uguale a $5 \cdot 10^{-12}$ s. Questo procedimento permette di effettuare stime di vite medie per i livelli che decadono allo stato fondamentale attraverso una cascata, ogni qualvolta sia verificata una situazione analoga a quella del decadimento ^{60}Co$\rightarrow$^{60}Ni.

Monte Carlo Calculations on Interactions of 300 MeV Protons with Carbon.

E. Abate, G. Bellini, E. Fiorini and S. Ratti

Istituto di Fisica dell'Università - Milano
Istituto Nazionale di Fisica Nucleare - Sezione di Milano

(ricevuto il 2 Agosto 1961)

Summary. — Monte Carlo calculations on interactions of 300 MeV protons with carbon nuclei have been performed by means of a Remington Rand Univac U.T.C. electronic computer. In the first part of the calculations nuclear cascades of collisions on bound nucleons were studied. The same calculations were then repeated with the assumption that each cascade nucleon has a non-zero probability (30% and 40%) of colliding with an α-cluster instantaneously formed inside the nucleus. The treatment of the cascade was carried out with both the assumptions of a Fermi and of a gaussian distribution of nucleon momenta inside the nucleus. The results obtained were the percentages of cascades as functions of the number of collisions and of the number and nature of fast secondaries, the angular and energy distributions of the fast secondaries, and the excitation-energy distributions of the residual nuclei. The comparison of the results of the calculations with the few available experimental data gives the best agreement if the hypothesis of the existence of clusters inside the nucleus is adopted. The assumption that the momentum distribution of the nucleons is gaussian leads to absurd results concerning the energy spectrum of fast secondary nucleons and the spectrum of excitation energies of the residual nuclei. If, instead, one assumes a Fermi momentum distribution, the calculated spectra are reasonable and in agreement with experimental data.

Introduction.

According to the mechanism proposed by Serber [1] the interaction of a high-energy proton ($\gtrsim 100$ MeV) with a complex nucleus can be separated into two stages: a fast stage and a slow evaporation stage. In the fast stage

[1] R. Serber: *Phys. Rev.*, **72**, 1114 (1947).

the particle initiates a cascade of nucleon-nucleon collisions inside the nucleus; fast neutral and charged particles are emitted. During the evaporation stage the nucleus, excited by the cascade, loses its energy through a process very similar to the evaporation that occurs in low-energy nuclear reactions. The energies of the evaporation prongs are exponentially distributed, with a negligible percentage of nucleons emitted with energies greater than 30 MeV. If a prong has an energy less than 30 MeV, it is impossible to decide by experimental observations whether it was emitted during the fast or the slow stage of the interaction.

The fast part of the interaction can be described as follows: the incoming particle penetrates some distance into the nucleus and collides with a nucleon: each of the two partners of the collision either undergoes a further collision or escapes from the nucleus. This cascade process gives rise to the emission of a number of charged and neutral particles.

If this energy of the incoming particle is high enough, each of the collisions in the cascade can be studied classically because the wave lengths of the cascade nucleons are small with respect to the nuclear radius. In other words it is possible to define, in a classical sense, a trajectory of the incident and struck nucleon inside the nucleus. In addition the range of nuclear forces is small in comparison with the collision mean free path of the cascade nucleons; this makes it possible to consider the interaction as formed by many single collisions. The assumption of this model of the interaction (Goldberger model ([2])) seems to be reasonable enough, in the limits of the impulse approximation, at least for high-energy (>100 MeV) incoming nucleons ([3]).

Several authors have studied interactions of protons with energies between 100 and 2000 MeV with nuclei ranging from ^{27}Al to ^{238}U ([4-8]).

They used the Monte Carlo method to make a statistical investigation of the development of the cascade according to the Goldberger model. The calculated results seem to be in good agreement with the experimental ones, at least as far as nuclear transparency, distribution of various interaction types and angular distribution of the fast emitted protons are concerned. J. Combe ([8]) extended the Monte Carlo calculations to high-energy (340 MeV) nuclear interactions on light nuclei (C, N, O); but the results obtained are in disagreement

([2]) M. L. Goldberger: *Phys. Rev.*, **74**, 1296 (1948).

([3]) C. F. Chew and G. C. Wick: *Phys. Rev.*, **85**, 636 (1952).

([4]) G. Bernardini, E. T. Booth and S. J. Lindenbaum: *Phys. Rev.*, **82**, 307 (1951); **85**, 826 (1952); **88**, 1017 (1952).

([5]) G. C. Morrison, A. Muirhead and W. G. Rosser: *Phil. Mag.*, **44**, 1326 (1954).

([6]) H. McManus, W. T. Sharp and H. Gellman: *Phys. Rev.*, **93**, 924 (1954).

([7]) N. Metropolis, R. Bivins, M. Storm, A. Turkevitch, J. M. Miller and G. Friedlander: *Phys. Rev.*, **110**, 185 (1958).

([8]) J. Combe: *Suppl. Nuovo Cimento*, **3**, 182 (1956); *Ann. de Phys.*, **13**, 468 (1958).

with the experimental data ([8-10]). In order to explain the discrepancies COMBE introduced the cluster hypothesis of CÜER and COMBE ([11]); according to these authors the cascade nucleons could collide on clusters of the type ^{2}H, ^{3}H, ^{3}He, ^{4}He temporarily formed inside the nucleus. The effect of collisions with clusters would be expected to be appreciable only in interactions with light nuclei, where the cascade is likely to consist of one, two or three collisions. In heavy nuclei the more numerous collisions with single nucleons dominate the picture, especially as the momentum transfer in collisions with clusters is generally small. Thus information concerning the existence of clusters can be obtained only from results on interactions in light nuclei.

Combe's calculations show qualitatively that the existence of clusters affects the angular and energy distributions of the emitted particles in the sense suggested by the comparison with experimental data.

The existence of clusters inside the nucleus has been confirmed recently by experimental results on the direct emission of α-particles and deuterons in interactions of high-energy nucleons ([12-16]). Obviously, to interpret these results we must assume that the clusters have a non-zero mean life ([17]). Other experiments seem to confirm the cluster hypothesis indirectly: MCKEAQUE ([18]) found the same number of backward grey tracks in light and heavy nuclei of nuclear emulsion struck by 950 MeV protons; WILKINSON ([19]) noticed a considerable percentage of Σ^- emitted without pions in stars from K^- absorption in complex nuclei. Both these results can be easily interpreted on the basis of the existence of clusters.

Owing to the contributions that the existence of clusters could bring to the knowledge on the structure of nuclear matter, we thought it would be worth-while to apply, by means of an electronic computer, the Monte Carlo method to the analysis of high-energy nuclear interactions in light nuclei. Specifically, we chose to investigate collisions of 300 MeV protons with carbon nuclei. In the first part of this paper we discuss the nuclear model, and the parameters used in the calculations. In the next section calculations on pure

([9]) J. COMBE: *Journ. de Phys. et Rad.*, **16**, 445 (1955).
([10]) E. FIORINI and S. RATTI: *Nuovo Cimento*, **14**, 961 (1959).
([11]) M. CÜER and J. COMBE: *Compt. Rend.*, **240**, 1527 (1955).
([12]) M. CÜER and A. SAMMAN: *Journ. Phys. et Rad.*, **19**, 1, 13 (1958).
([13]) L. AZHGIREY, I. K. VZOROV, V. P. ZRELOV, M. G. MESCHERYAKOV, B. S. NEGANOV and A. P. SHABUDIN: *Soviet Phys. JETP*, **6**, 911 (1958).
([14]) M. Q. BARTON and J. H. SMITH: *Phys. Rev.*, **110**, 1143 (1958).
([15]) V. I. OSTROUMOV and R. A. FILOV: *Soviet Phys. JETP*, **10**, 3, 459 (1960).
([16]) V. I. OSTROUMOV, N. A. PERFILOV and R. A. FILOV: *Soviet Phys. JETP*, **12**, 1 (1961).
([17]) YU. I. SEREBRENNIKOV: *Dissertation*, Leningrad Polytech. Inst. (1959).
([18]) R. MCKEAQUE: *Proc. Roy. Soc.*, A **236**, 104 (1956).
([19]) D. H. WILKINSON: *Phil. Mag.*, **4**, 215 (1959).

nucleon-nucleon cascades are described; calculations for collisions partly against clusters are reported in Sections 3 and 4. In the last part of the paper the calculated distributions, namely the percentages of the various types of interactions, the angular and energy distributions of fast secondary particles and the distributions of excitation energy in residual nuclei are discussed in comparison with the experimental data.

Obviously the use of a statistical model for interactions in light nuclei is a quite crude approximation; we think however that this approximation is justified by the difficulty of working out a more suitable nuclear model. Our results should be compared with more complete experimental data than the present ones; we hope that such a comparison, together with the hypothesis of collisions on clusters, will provide a starting point for the development of a more refined model.

1. – Nuclear model and parameters used for the computations.

In a first treatment of the problem a completely degenerate Fermi nuclear model was adopted. As it is well known, according to this model the nucleus consists of a completely degenerate gas of nucleons contained in a spherical potential well whose depth can be obtained by adding the binding and the Fermi energies for a nucleon and then subtracting from this sum the Coulomb energy for protons. Values of 7.5, 21 and 3.5 MeV were assumed for the binding, maximum Fermi and Coulomb energies respectively. For the nuclear radius we assumed $R = 1.35 \cdot 10^{-13} A^{\frac{1}{3}}$ according to the recent data by SETH [20] on low-energy neutron scattering. In the initial part of the calculations we consider the interaction to consist purely of a cascade of nucleon-nucleon collisions; later on we introduce the hypothesis that collisions with clusters occur in a proportion of the cases.

The Pauli principle, which forbids all those collisions in which one or both of the secondaries have an energy lower than the Fermi energy, has been applied. Moreover we took into account that a cascade nucleon leaving the nucleus with an energy lower than 30 MeV is experimentally not distinguishable from an evaporation prong; therefore the calculation stops for all those secondaries leaving the point of collisions with an energy lower than the well depth increased by 30 MeV. These secondaries cannot give rise to further collisions with secondaries distinguishable from evaporation nucleons.

The interaction mean free path in nuclear matter has been calculated using the values of the total scattering cross-sections σ_{pp} and σ_{pn} obtained by METRO-

[20] K. K. SETH: *Rev. Mod. Phys.*, **30**, 442 (1958); *Can. Journ. Phys.*, **37**, 1199 (1959).

POLIS *et al.* (7) from experimental data. It should be noted that the cross-section σ_{pn} obtained by METROPOLIS is in good agreement also with the more recent experimental data of FOWLER *et al.* (21). The differential cross-sections in the center-of-mass system have been calculated by means of the following relation (7):

$$\frac{\mathrm{d}\sigma}{\mathrm{d}\Omega} = K(A\cos^4\theta + B\cos^3\theta + 1)\,, \tag{1.1}$$

where K is an interaction constant and A and B depend on the type of colliding particles and on the energy available in the center-of-mass system.

The interaction mean free path of a nucleon $\mathcal{N}$ in nuclear matter is given by

$$\left|\frac{1}{\lambda}\right|_{\mathcal{N}} = \left|\frac{1}{\lambda_p}\right|_{\mathcal{N}} + \left|\frac{1}{\lambda_n}\right|_{\mathcal{N}}. \tag{1.2}$$

We calculate $|1/\lambda_p|_{\mathcal{N}}$ and $|1/\lambda_n|_{\mathcal{N}}$ starting from the relativistic invariant reported by MØLLER (22); one has

$$\left|\frac{1}{\lambda_i}\right|_i = n_i\int_0^{\pi}\sigma_{ii}(|\boldsymbol{v}-\boldsymbol{u}|^2 - |\boldsymbol{v}\wedge\boldsymbol{u}|^2)^{\frac{1}{2}}\frac{\sin\theta}{2}\,\mathrm{d}\theta\,, \tag{1.3}$$

$$\left|\frac{1}{\lambda_i}\right|_j = n_i\int_0^{\pi}\sigma_{ij}(|\boldsymbol{v}-\boldsymbol{u}|^2 - |\boldsymbol{v}\wedge\boldsymbol{u}|^2)^{\frac{1}{2}}\frac{\sin\theta}{2}\,\mathrm{d}\theta\,, \tag{1.4}$$

where all the combinations can be obtained by putting $i=p$, $j=n$ or $i=n$, $j=p$; the vectors $\boldsymbol{v}$ and $\boldsymbol{u}$ are the velocities of the incoming and target nucleon, respectively, in the laboratory system and n is the density of protons or nucleons inside the nucleus. If one indicates as β the velocity of the incoming nucleon (in units of the velocity of light), as β_m the average velocity of a Fermi gas nucleon before the collision and as β_r the velocity of the incoming particle with respect to the target nucleon, one has

$$\frac{1}{\lambda}\Big|_i = \int_0^{\pi}\{n_i\sigma_{ii}(\beta_r) + n_j\sigma_{ij}(\beta_r)\}\left|1 + \frac{\beta_m^2}{\beta_r^2} - 2\,\frac{\beta_m}{\beta}\cos\theta - \beta_m\sin^2\theta\right|^{\frac{1}{2}}\frac{\sin\theta}{2}\,\mathrm{d}\theta\,, \tag{1.5}$$

(21) J. L. FOWLER and J. E. BROLLEY: *Rev. Mod. Phys.*, **28**, 103 (1956).

(22) C. MØLLER: *General property of the characteristic matrix in the theory of elementary particles*, in *Kgl. Dan. Videnskab. Selsk.* (1946).

where n_i and n_j must be changed during the cascade to take into account the nucleons that leave the nucleus. The change of λ_N *vs.* the energy of the incoming proton is shown in Fig. 1.

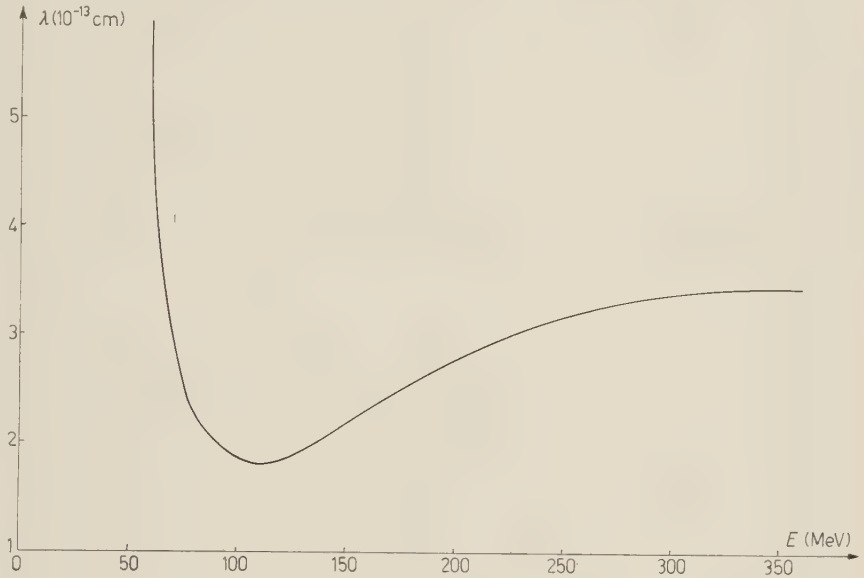

Fig. 1.

It should be noted that formulae (1.3) and (1.4) have a general validity; the expression $\sigma\left[|\boldsymbol{v}-\boldsymbol{u}_i|^2-|\boldsymbol{v}\wedge\boldsymbol{u}|^2\right]^{\frac{1}{2}}$ reduces to the monomial $\beta_r\sigma(\beta_r)$, used by METROPOLIS, only if $\boldsymbol{v}$ and $\boldsymbol{u}$ are parallel. The Pauli principle has not been taken into account in the calculation of the interaction mean free path: it will be shown that this principle can easily be applied to each single collision of the cascade.

The angle i between the directions of motion of the incident and target nucleon (forward direction: $i<90°$) is distributed according to the following spectrum:

$$(1.6)\qquad f_{ik}(i)\,\mathrm{d}i=\{\delta_{ik}\sigma_{ii}(\beta_r)+(1-\delta_{ik})\sigma_{ij}(\beta_r)\}\left[|\boldsymbol{v}-\boldsymbol{u}|^2-|\boldsymbol{v}\wedge\boldsymbol{u}|^2\right]\frac{\sin i}{2}\,\mathrm{d}i\,,$$

where k can be equal to i or j and $\delta_{ik}=1$ if $k=i$ and $\delta_{ik}=0$ if $k\neq i$. In (1.6) we used as $\boldsymbol{u}$ the average velocity of the nucleons inside the nucleus. The spectrum (1.6) for i-i collisions is reported in Fig. 2 for incoming particle energies of 50 and 300 MeV.

The type of target nucleon (proton or nucleon) is selected on the basis of the ratio $M=|1/\lambda_p|/|1/\lambda_m|$ given by (1.3) and (1.4), where n_i has been cal-

culated taking into account the number of nucleons struck in the preceding collisions. The change of the ratio M for a proton is shown, as a function of energy, in Fig. 3.

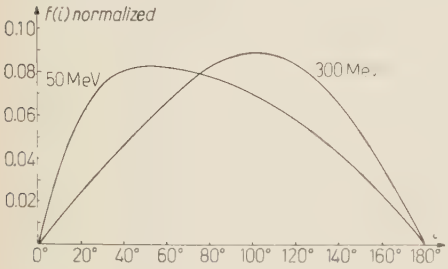

Fig. 2.

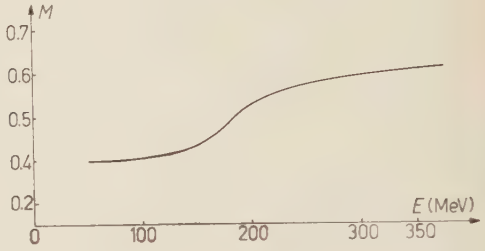

Fig. 3.

According to the Fermi distribution the density of nucleons is constant in phase space for energies lower than the Fermi energy, and drops to zero for higher energies. Therefore the momenta p of the struck nucleons have been selected at random out of a spectrum:

$$\mathrm{d}P \quad \frac{3}{p_{\max}^3} p^2 \mathrm{d}p \,. \tag{1.7}$$

where $\mathrm{d}P$ is the probability that a nucleon have a momentum between p and $(p+\mathrm{d}p)$.

In the second part of the calculations the Fermi distribution has been substituted by a gaussian distribution ([23]) of the nucleon momenta on the basis of the analysis of HENLEY ([24]) and WOLFF ([25]) and according to the experimental data obtained by CLADIS *et al.* ([26]) for carbon nuclei.

The random selection of the target-nucleon momentum has been obtained out of a distribution

$$\mathrm{d}P' = \frac{1}{\alpha^3 \pi^{\frac{3}{2}}} p^2 \exp\left[\frac{-p^2}{\alpha^2}\right] \mathrm{d}p \,. \tag{1.8}$$

where α corresponds to an energy of 19.3 MeV.

The application of the exclusion principle is quite difficult in this case because the energy levels are not completely occupied. We calculated therefore, for each level, the ratio between the probabilities that the level be oc-

([23]) K. A. BRUECKNER, R. J. EDEN and N. C. FRANCIS: *Phys. Rev.*, **98**, 1445 (1955).
([24]) E. M. HENLEY: *Phys. Rev.*, **85**, 204 (1952).
([25]) P. A. WOLFF: *Phys. Rev.*, **87**, 434 (1952).
([26]) J. B. CLADIS, W. N. HESS and B. J. MOYER: *Phys. Rev.*, **87**, 425 (1952).

cupied or not in a gaussian distribution. This ratio has been assumed to be equal to the probability that the collision be forbidden at that energy: the forbiddeness of the collision is decided at random, using this ratio.

2. – Details of the calculations for pure nucleon-nucleon cascades.

The Monte Carlo analysis of pure nucleon-nucleon cascades was carried out according to the block diagram shown by the solid-line part of Fig. 4. The interaction was reconstructed through the following steps:

1) A cartesian co-ordinate system ($0xyz$) with origin in the center of the nucleus and z-axis oriented along the direction of motion of the in-

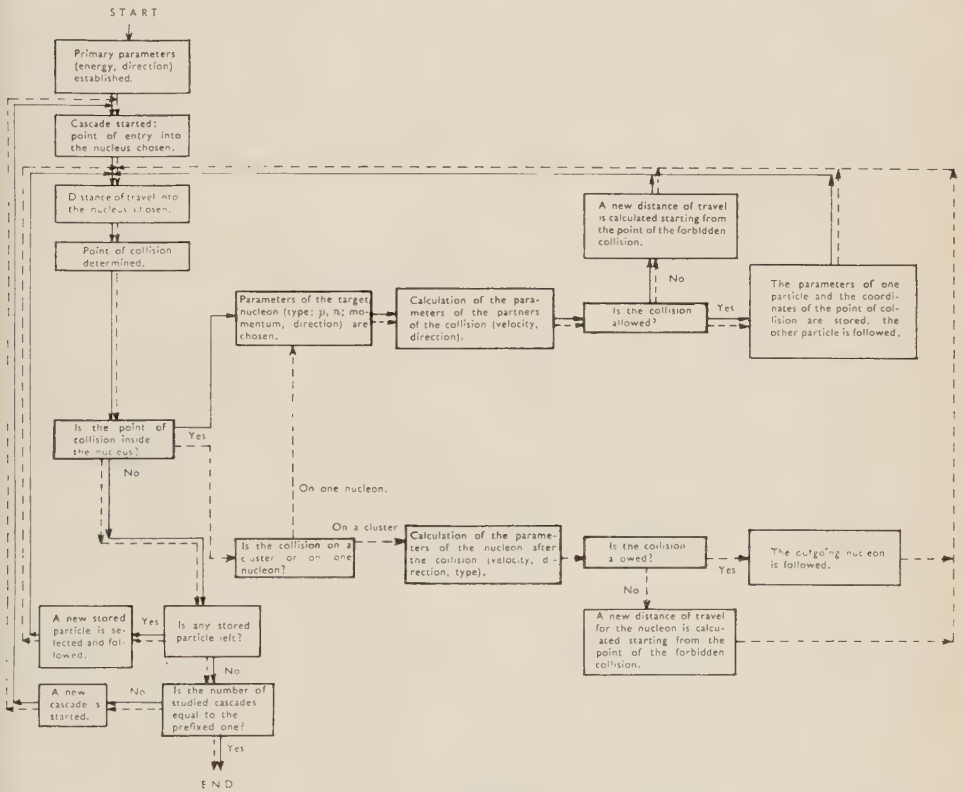

Fig. 4.

coming nucleons is fixed. The x- and y-co-ordinate of the point of entrance into the nucleus are selected at random from a uniform distribution between $-R$ and R, where R is the nuclear radius; the condition $x^2 + y^2 < R^2$ is checked and the corresponding z-co-ordinate calculated.

2) The distance of travel d of the particle inside the nucleus is calculated by means of the relation

$$\frac{d}{\lambda} = -\ln \xi \,, \tag{2.1}$$

where ξ is a number chosen at random from a uniform distribution between 0 and 1, and λ is given by (1.5).

3) The position of the collision is examined to see if it is inside or outside the nucleus. If it is outside, a new stored cascade particle is selected (see step 9); if no more cascade particles are left in the storage, a new interaction is initiated starting again from step 1. If the point of collision is inside the nucleus, the calculation goes on to step 4.

4) The charge of the target nucleon is chosen on the basis of the ratio M defined in the preceding section.

5) The momentum of the target nucleon is chosen according to the integral distributions calculated from (1.7) and (1.8) for a Fermi or a gaussian distribution, respectively.

6) The angle i between the directions of motion of the incoming and target nucleons is chosen out of the integral distribution calculated from (1.6).

7) The dynamics of the collision are calculated relativistically in the center-of-mass system, using a cartesian co-ordinate system with z-axis oriented along the direction of motion of the incoming particle. The directions of motion of the two outgoing particles are determined in polar co-ordinates θ and η. The former of these angles is selected out of an integral probability distribution obtained from (1.1), the latter out of an uniform distribution in the interval 0 to 2π. All the co-ordinates are then transformed back to the laboratory system.

8) The charge of the two outgoing nucleons is established. If the incoming and the target nucleons are of a different type a random choice is made to know which, out of the possible two, is the direction of motion of the proton and of the neutron.

9) The Pauli principle is applied. If forbiddeness results the computer forgets the collision and a new distance of travel from the point of collision is calculated, going directly to 2). If the collision is allowed the data of one of the two particles are stored and those of the other one are sent to 2), to follow its further history.

Random numbers must be selected out of a uniform distribution between 0 and 1, in order to establish the various parameters of the calculations. These

numbers have been generated through the congruential method ([27]), which seems particularly simple and suitable to our purpose. According to this method we multiplied by 10^{-10} the numbers of the sequence:

$$A_{n+1} = A_n M \ \text{(modulus } 10^{10}) , \tag{2.2}$$

where A_{n+1} and A_n are 10-figure integral numbers. As it is well known in number theory the operation (2.2) means: the number A_n of the sequence is multiplied by the fixed factor M; the number A_{n+1} is given by the last 10 figures of this product. The number $M = 7\,992\,538\,801$ has been used as fixed factor. In order to check the reliability of this method 10 000 numbers generated in this way were analysed: they turned out to be uniformly distributed between 0 to 1 within statistical deviations.

The quantities which were not uniformly distributed, were selected in the following way. If a is the quantity that must be selected and $f(a)$ is the corresponding normalized distribution function let us consider the quantity P given by

$$P = F(a) = \int_0^a f(a)\,\mathrm{d}a , \tag{2.3}$$

where P has a value between 0 and 1. The random selection of a can be done by sorting a value P out of an uniform distribution between 0 and 1 reversing the function $F(a)$ at the value P. The following method was employed when the function $F(a)$ was impossible or too difficult to be inverted: two numbers N_1 and N_2 were selected independently from a uniform distribution in the interval 0 to 1. The number N_1 was multiplied by the maximum value of a and N_2 by the maximum value of $f(a)$: the two values so obtained define a point in the $a/f(a)$ plane. If this point happens to be below the curve $f(a)$ the product of N_1 by the maximum value of a is assumed to be a random selected value of a; otherwise the selection of N_1 and N_2 is repeated until the above mentioned condition is fulfilled.

Non-relativistic calculations on pure nucleon-nucleon cascades were carried out before starting the relativistic treatment. In this way the reliability of the program, especially as far as the random selections were concerned, was checked and comparison with non-relativistic results of other authors performed. Following this, all the calculations were carried out relativistically; only relativistic results will be considered in the following sections.

([27]) *Simposium on Monte Carlo Method*, University of Florida (1954).

3. – Nuclear model and parameters for collisions on clusters.

The treatment of cascades involving collisions on clusters requires the use of new assumptions concerning the nature of clusters, for the results of experiments and of calculations carried out so far are very vague and do not lead to a definite and detailed model.

For this reason we thought it would be reasonable to perform the calculations with very naive assumptions; our only task is to examine the changes in the distribution of the characteristics of the fast secondary nucleons, which occur when the hypothesis of collisions on clusters is introduced. It seems to us that calculations on a more detailed model will be worth-while only when more complete experimental data have become available. The only type of clusters we considered were α-particles.

This simplifying assumption is reasonable for a first model because the probability of a cluster of a given type being formed inside the nucleus increases very sharply with its binding energy ([28]); the α-particle therefore seems to be the most probable one. The momentum as well as the effect of possible further collisions of the struck clusters have been neglected. The calculations were performed assuming probabilities of 30% and 40% for collisions on clusters. These values were chosen both

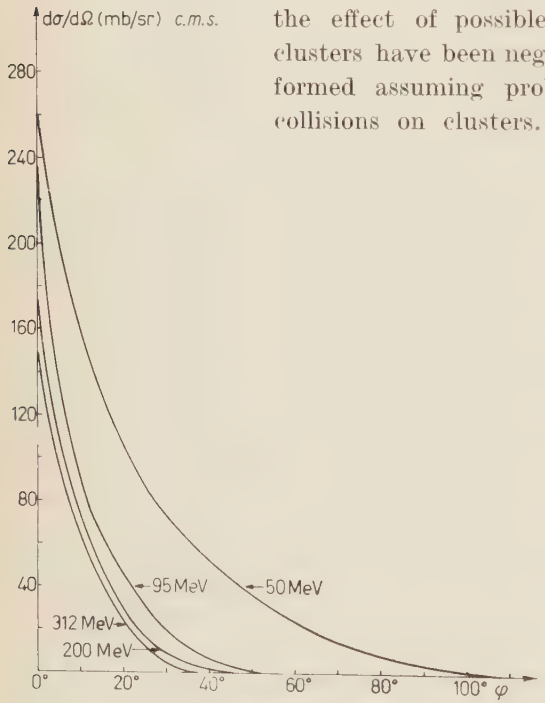

Fig. 5.

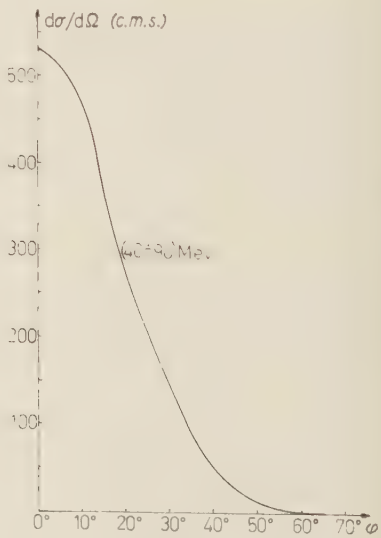

Fig. 6.

([28]) A. WILDERMUTH and C. KANELLOPOULOS: Theoretical Study Division, CERN-59 (23 Giugno 1959).

on the basis of the percentage suggested by other authors ([8,12,29]) and from our own results. The distributions of CHAMBERLAIN *et al.* ([30]), SELOVE and TEEM ([31]) and EISBERG ([32]) were used to determine the differential cross-section for proton-α collisions (Fig. 5). The neutron-alpha differential cross-section was obtained from the data of TANNENWALD ([33]) (Fig. 6) for energies between 40 and 90 MeV and from the function calculated by HEIDMANN ([34])

$$\frac{\mathrm{d}\sigma}{\mathrm{d}\Omega} = 4.5 \exp\left[-7.86\theta^2\right] \cdot 10^{-25} \text{ cm}^2/\text{sr}\,, \tag{3.1}$$

for higher energies.

4. – Details of calculations for cascades with nucleon-cluster collisions.

The block diagram of our calculations on cascades formed by nucleon-nucleon and nucleon-alpha collisions is shown by the dotted-line part of Fig. 4. Only the further history of the nucleon is followed in collision on clusters, because only the data on secondary nucleons will be compared with the experimental results.

The position of the point of collision is determined in the same way as for pure nucleon-nucleon cascades. The type of collision is then determined by means of random selection on the basis of the probability assumed for collision on clusters. The calculations for collisions with a nucleon are performed in the same way as in Section 2. If the collision happens to be against a cluster:

a) The dynamics of the collision are calculated and the angles θ and φ determined. The former is selected from a probability curve based on the distribution functions reported in the preceding section; the latter from a uniform distribution.

b) The exclusion principle is applied to the collision. If the collision is allowed the further history of the secondary nucleon is followed, if the collision is forbidden the calculations are repeated, starting from the point of collision.

The calculation on cascades with collisions on clusters have been carried out both for a Fermi and for a gaussian momentum distribution.

([29]) P. E. HOGDSON: *Nucl. Phys.*, **8**, 1 (1958).
([30]) O. CHAMBERLAIN, E. SEGRÈ, R. TRIPP, C. WIEGAND and T. YPSILANTIS: *Phys. Rev.*, **96**, 807 (1954); **102**, 1696 (1956).
([31]) W. SELOVE and E. J. M. TEEM: *Phys. Rev.*, **112**, 1658 (1958).
([32]) R. EISBERG: *Phys. Rev.*, **102**, 1104 (1956); *Bull. Am. Phys. Soc.*, **1**, 19 (1956).
([33]) P. E. TANNENWALD: *Phys. Rev.*, **87**, 205 (1952); **89**, 508 (1953).
([34]) J. HEIDMANN: *Phil. Mag.*, **41**, 444 (1950).

5. – Results on fast cascade secondaries.

The calculations were carried out by means of an electronic computer (Remington Univac U.T.C.). The standard treatment of the cascade according to each of the various hypotheses involved about one-thousand interactions. The obtained data will be discussed by investigating how the various assumptions affect the results, and by comparison, when possible, with the available experimental data.

5·1. *Number of collisions.* – The distributions of the numbers of collisions per cascade are given in Table I.

TABLE I. – *The cascades percentage according to their number of collisions.*

N	J. COMBE [8] (%)	F. 0% c. (%)	F. 30% c. (%)	F. 40% c. (%)	G. 0% c. (%)	G. 30% c. (%)	G. 40% c. (%)
1	60	41.37	42.66	42.16	40.45	40.62	43.83
2	30	26.35	26.40	27.20	25.35	25.40	22.78
3	10	16.76	15.47	13.38	14.26	15.03	14.56
4	—	9.60	8.37	8.70	8.95	8.37	9.18
5	—	5.92	6.91	8.27	10.99	10.56	9.65

N: number of collisions;
F. 0% c.: Fermi distribution without clusters (1050 events).
F. 30% c.: Fermi distribution (30% probability of collision on cluster, 1520 events);
F. 40% c.: Fermi distribution (40% probability of collision on cluster, 1520 events);
G. 0% c.: Gaussian distribution without clusters (1100 events);
G. 30% c.: Gaussian distribution (30% probability of collision on clusters, 1050 events);
G. 40% c.: Gaussian distribution (40% probability of collision on clusters, 610 events).

These results refer to zero, 30 and 40% probabilities for collisions on clusters, with both Fermi and gaussian distributions of the nucleon momenta. The percentages obtained do not seem to be noticeably affected by the different assumptions. One should note, however, the remarkable disagreement between our percentages and those assumed, *a priori*, by COMBE on the basis of qualitative considerations of CÜER and COMBE [11]. We conclude that the usual assumption of considering an interaction with a light nucleus as formed by a single collision is not realistic. For the sake of completeness the percentages of cascades formed by different numbers of collisions for events with one or two charged prongs are reported in Table II. The results of Table II also show that it is unjustified to assume that only one nucleon-nucleon collision took place if there is only one outgoing fast prong. The process giving rise to the single fast secondary cannot, therefore, be treated as an elastic nucleon-nucleon interaction.

TABLE II. – *Cascades percentage formed by different number of collisions for events with one or two charged prongs.*

N	Cascade type	G. 0% c. (%)	F. 0% c. (%)	F. 30% c. (%)	G. 30% c. (%)	F. 40% c. (%)	G. 40% c. (%)
1	$(p; p'kn)$	46.65	44.8	50.9	50.15	49.8	53.00
	$(p; 2p'kn)$	30.03	32.9	21.2	21.89	22.1	20.60
2	$(p; p'kn)$	27.85	28.2	24.6	25.82	27.5	23.60
	$(p; 2p'kn)$	25.60	28.7	32.2	24.89	24.3	20.60
3	$(p; p'kn)$	12.66	13.5	13.3	13.43	11.9	12.60
	$(p; 2p'kn)$	16.72	19.8	21.6	19.74	19.1	18.30
4	$(p; p'kn)$	6.87	8.1	6.1	5.97	5.9	6.20
	$(p; 2p'kn)$	12.97	11.6	13.9	12.02	17.6	17.60
5	$(p; p'kn)$	5.97	5.4	5.1	4.63	4.8	4.50
	$(p; 2p'kn)$	14.68	7.0	11.1	21.46	16.9	22.90

N: number of collisions;
G. 0% c. Gaussian distribution without clusters (1100 events);
F. 0% c. Fermi distribution without clusters (1050 events);
F. 30% c. Fermi distribution (30% probability of collision on clusters, 1080 events);
G. 30% c. Gaussian distribution (30% probability of collision on clusters, 1050 events);
F. 40% c. Fermi distribution (40% probability of collision on clusters, 620 events);
G. 40% c. Gaussian distribution (40% probability of collision on clusters, 610 events).

It seems worth-while to point out that the percentage of collisions on clusters in a cascade is not equal to the probability that an individual collision shall take place with a cluster; this is shown in Table III.

TABLE III. – *Cascades percentage according to their number of collisions with clusters.*

N_c	F. 30% c. (%)		F. 40% c. (%)		G. 30% c. (%)		G. 40% c. (%)	
0	43.94	43.94	30.39	30.39	40.42	40.42	30.96	30.96
1	41.97		46.85		44.35		46.45	
2	11.13		16.87		11.68		15.17	
3	1.67	56.06	4.02	69.61	2.30	59.58	5.21	69.04
4	1.18		1.61		0.86		1.26	
5	0.10		0.26		0.38		0.59	

N_c: number of collisions on clusters;
F. 30% c.: Fermi distribution (30% probability of collision on clusters, 1080 events);
F. 40% c.: Fermi distribution (40% probability of collision on clusters, 1050 events);
G. 30% c.: Gaussian distribution (30% probability of collision on clusters, 620 events);
G. 40% c.: Gaussian distribution (40% probability of collision on clusters, 610 events).

5·2. *Percentage of the various types of interactions.* – In Fig. 7 we give the calculated frequency distributions of cascades with various number of charged secondaries together with the experimental results of COMBE (9) and our-

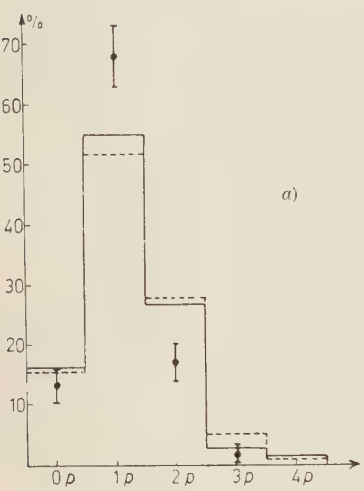

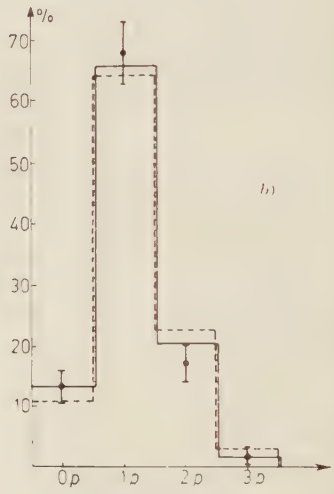

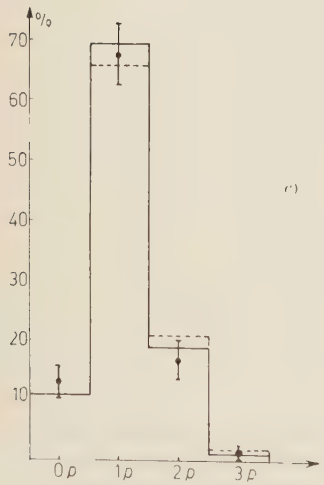

Fig. 7. – Percentage of various interaction types. *a*) —— Fermi distribution without clusters (979 events); – – Gaussian distribution without clusters (1070 events); ϕ experimental data (10). *b*) —— Fermi distribution (30% probability of collision on clusters, 1012 events); - - Gaussian distribution (30% probability of collision on clusters, 1049 events); ϕ experimental data. *c*) —— Fermi distribution (40% probability of collision on clusters, 632 events); – – Gaussian distribution (40% probability of collision on clusters, 700 events); ϕ experimental data.

selves (10). It can be seen that the results of the calculations are very sensitive to the assumption concerning the presence of clusters, and that they clearly favour the cluster hypothesis. More exact quantitative conclusions cannot be drawn with confidence, but we are tempted to say that the assumption of a Fermi momentum distribution with a 40% probability of collision on clusters gives the best agreement with the experimental data.

The percentages of cascades as functions of the numbers of their neutral and charged secondaries are reported in Table IV; no experimental data are available, so far, for comparison with these results.

TABLE IV. – *Cascades percentage according to the number of their neutral and charged secondaries.*

Cascade type	F. 0% c. (%)	G. 0% c. (%)	F. 30% c. (%)	G. 30% c. (%)	F. 40% c. (%)	G. 40% c. (%)
(0p, 1n)	11.64	11.423	10.01	8.48	8.17	8.23
(0p, 2n)	3.88	3.65	2.28	2.57	2.50	2.37
(0p, 3n)	0.61	0.37	0.1	0.2	0	0.32
(1p, 0n)	21.75	20.13	39.04	37.56	46.97	42.24
(1p, 1n)	29.42	26.873	24.58	22.28	20.66	21.83
(1p, 2n)	3.47	4.49	2.18	2.86	1.97	2.06
(1p, 3n)	0	0.187	0	0.48	0	0.16
(2p, 0n)	18.69	17.51	15.85	15.16	14.08	14.56
(2p, 1n)	7.35	7.96	3.87	5.82	4.21	5.22
(2p, 2n)	0.61	2.15	0.5	1.14	0	0.95
(2p, 3n)	0.2	0.37	0	0.2	0	0.16
(3p, 0n)	1.74	2.34	1.19	1.72	1.05	0.95
(3p, 1n)	0.41	1.4	0.3	0.86	0.39	0.95
(3p, 2n)	0.1	0.562	0	0.1	0	0
(4p, 0n)	0.1	0.37	0.1	0	0	0
(4p, 1n)	0	0.09	0	0	0	0
(4p, 2n)	0	0.09	0	0	0	0

F. 0 % c.: Fermi distribution without clusters (979 events).
G. 0 % c.: Gaussian distribution without clusters (1068 events);
F. 30 % c.: Fermi distribution (30 % probability of collision on clusters, 1039 events);
G. 30 % c.: Gaussian distribution (30 % probability of collision on clusters, 1049 events);
F. 40 % c.: Fermi distribution (40 % probability of collision on clusters, 760 events);
G. 40 % c.: Fermi distribution (40 % probability of collision on clusters, 760 events).

5·3. *Angular distributions of charged secondaries with respect to the primary.* – The angular distribution of the outgoing proton with respect to the primary particle is reported in Fig. 8 for interactions with a single charged secondary prong. Obviously the introduction of collisions on clusters increases the prob-

ability of small angle secondaries. Comparison with our experimental data [10] again favours the hypothesis of collision with clusters, and again the 40% level of the probability of collision with a cluster seems to provide the best fit.

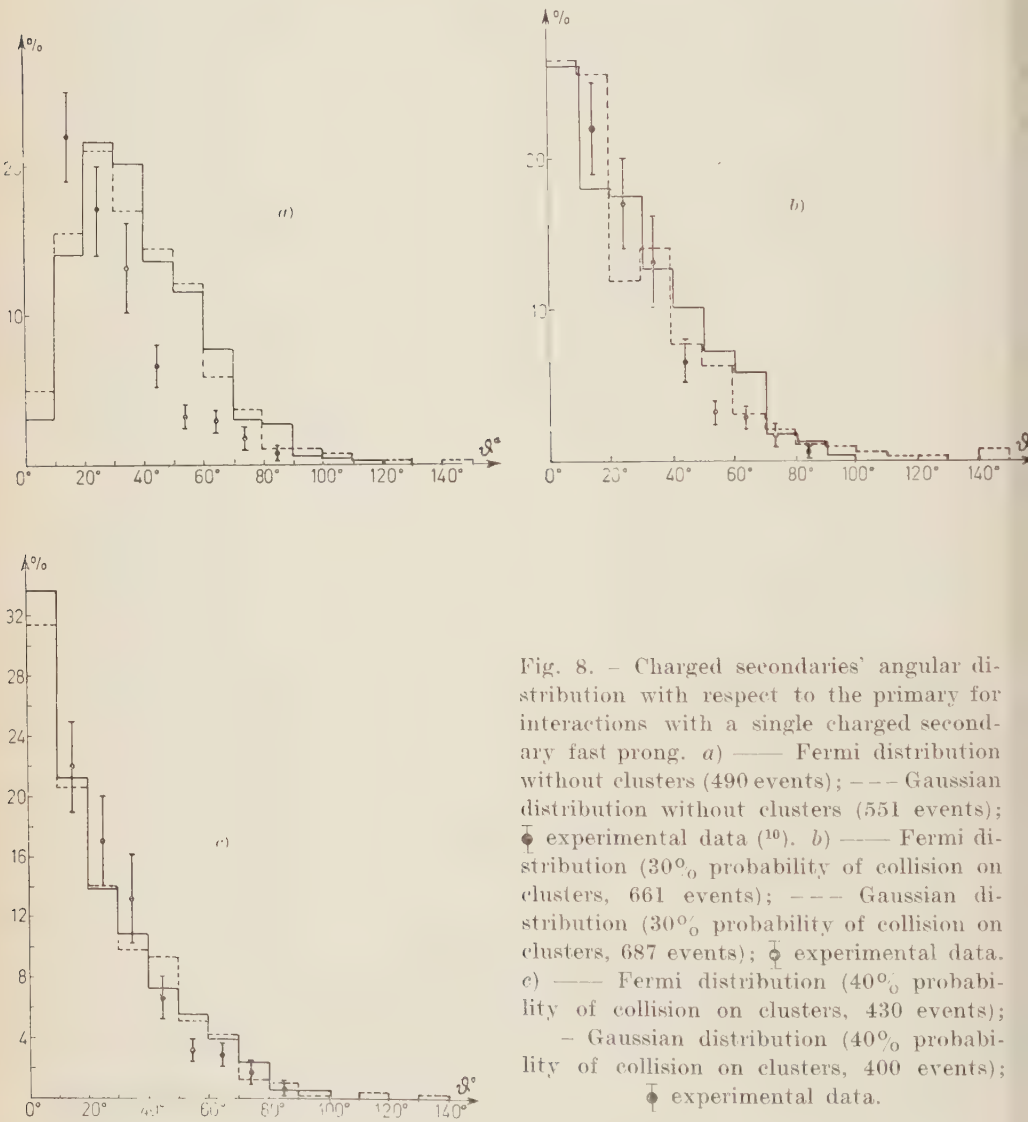

Fig. 8. – Charged secondaries' angular distribution with respect to the primary for interactions with a single charged secondary fast prong. *a*) —— Fermi distribution without clusters (490 events); – – – Gaussian distribution without clusters (551 events); ⊕ experimental data [10]. *b*) —— Fermi distribution (30% probability of collision on clusters, 661 events); – – – Gaussian distribution (30% probability of collision on clusters, 687 events); ⊕ experimental data. *c*) —— Fermi distribution (40% probability of collision on clusters, 430 events); – Gaussian distribution (40% probability of collision on clusters, 400 events); ⊕ experimental data.

It should be noted that there is very little difference between the calculated histograms for Fermi and gaussian momentum distributions, respectively.

The angular distributions, with respect to the primary, of the charged outgoing particles in interaction of any multiplicity are shown in Fig. 9.

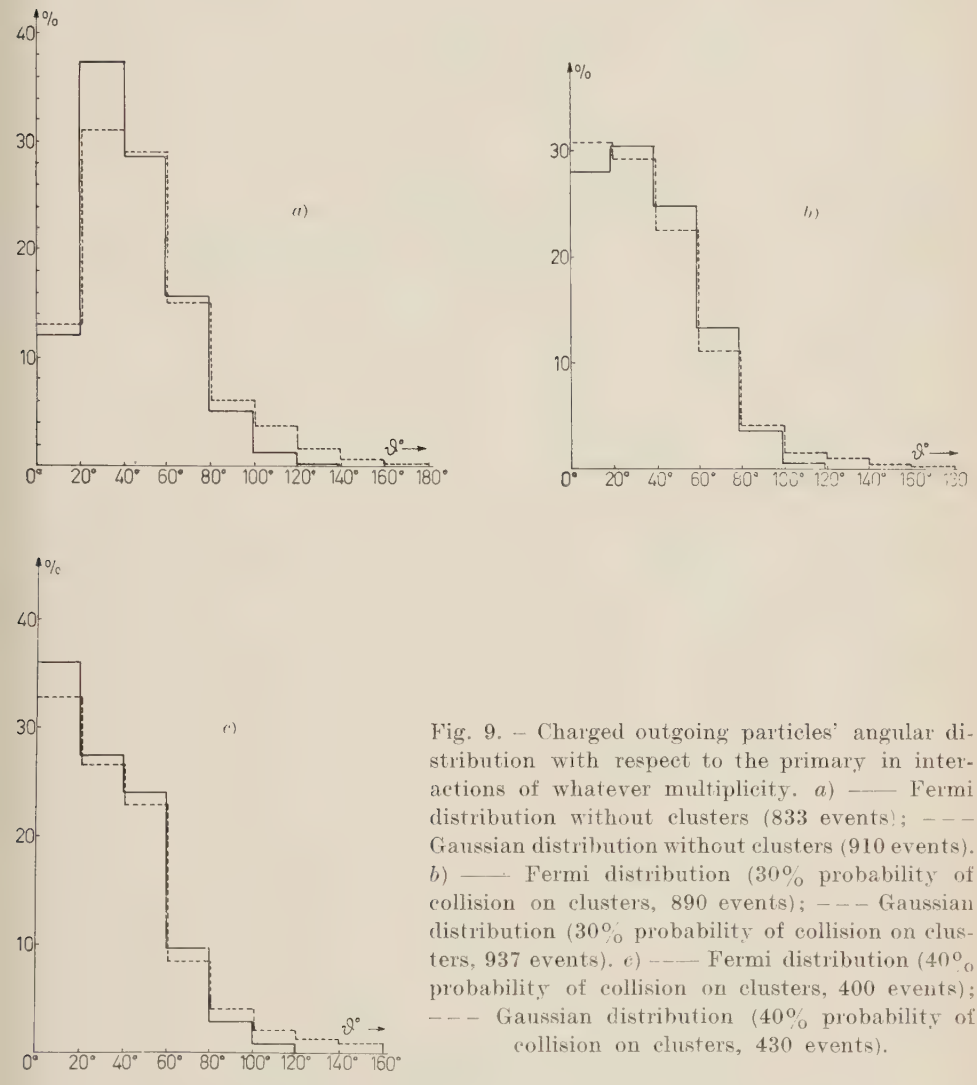

Fig. 9. – Charged outgoing particles' angular distribution with respect to the primary in interactions of whatever multiplicity. *a*) —— Fermi distribution without clusters (833 events); – – – Gaussian distribution without clusters (910 events). *b*) —— Fermi distribution (30% probability of collision on clusters, 890 events); – – – Gaussian distribution (30% probability of collision on clusters, 937 events). *c*) —— Fermi distribution (40% probability of collision on clusters, 400 events); – – – Gaussian distribution (40% probability of collision on clusters, 430 events).

5·4. *Angular distributions of neutral secondaries.* – Angular distributions of neutral secondary particles for events with a single prong and events with any multiplicity are reported in Fig. 10 and 11 respectively. No comparison is possible, so far, with experimental data.

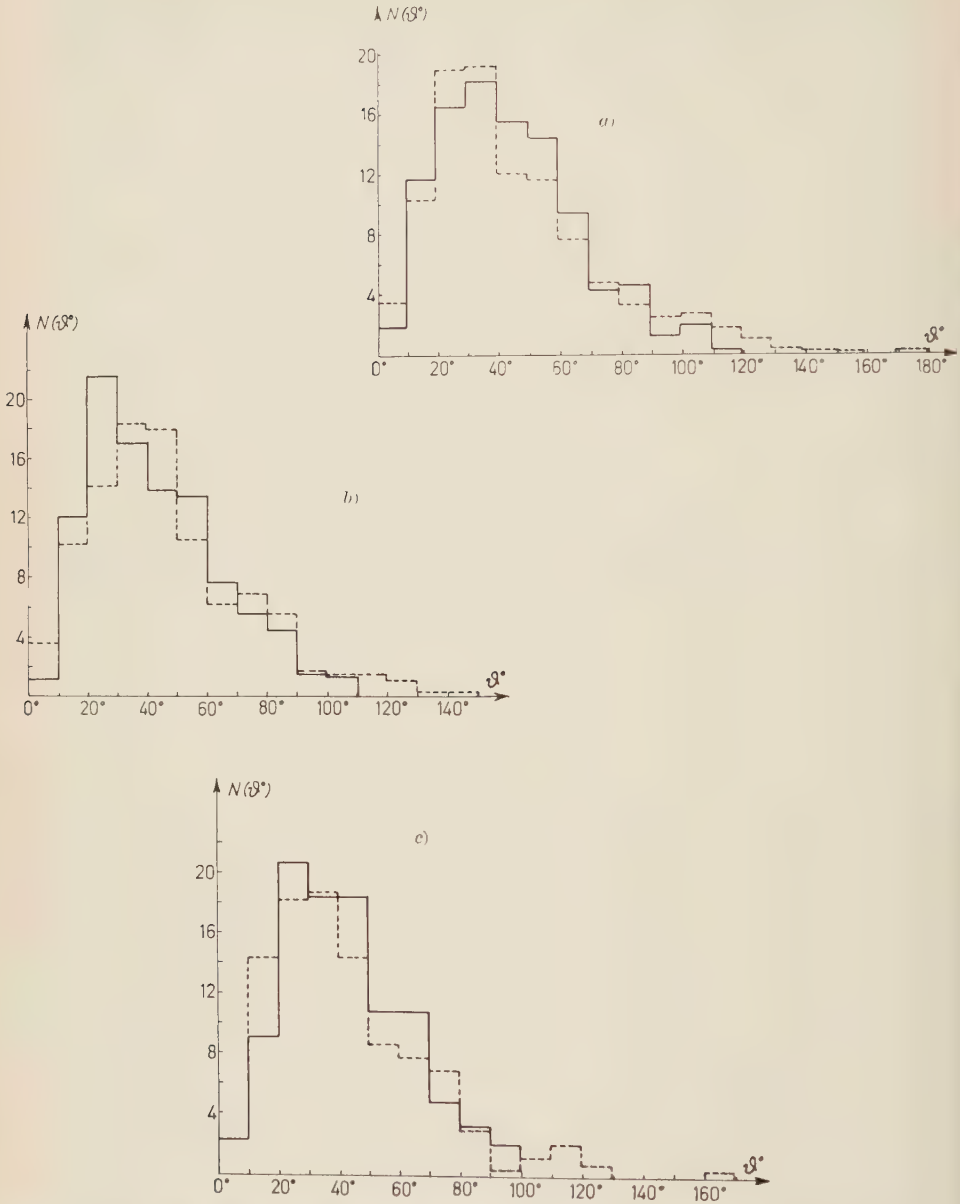

Fig. 10. Neutral secondary particles' angular distribution, with respect to the primary, for events with a single prong. *a*) —— Fermi distribution without clusters (840 events); – – – Gaussian distribution without clusters (810 events). *b*) —— Fermi distribution (30% probability of collision on clusters, 830 events); – – – Gaussian distribution (30% probability of collision on clusters, 850 events). *c*) —— Fermi distribution (40% probability of collision on clusters, 400 events); – – – Gaussian distribution (40% probability of collision on clusters, 450 events).

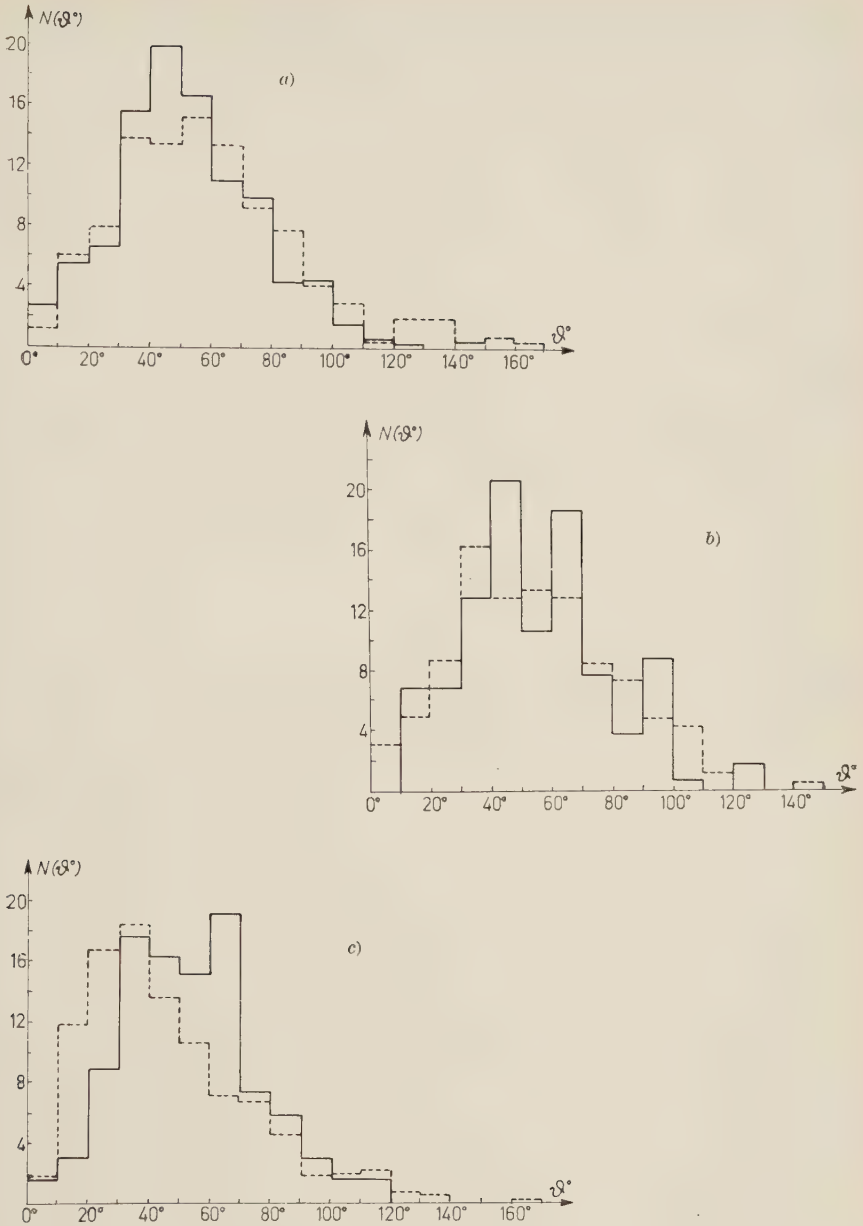

Fig. 11. – Neutral secondary particles' angular distribution, with respect to the primary, for events with whatever multiplicity. *a*) —— Fermi distribution without clusters (970 events); – – – Gaussian distribution without clusters (950 events). *b*) —— Fermi distribution (30% probability of collision on clusters, 950 events); – – – Gaussian distribution (30% probability of collision on clusters, 480 events). *c*) —— Fermi distribution (40% probability of collision on clusters, 490 events); – – – Gaussian distribution (40% probability of collision on clusters, 480 events).

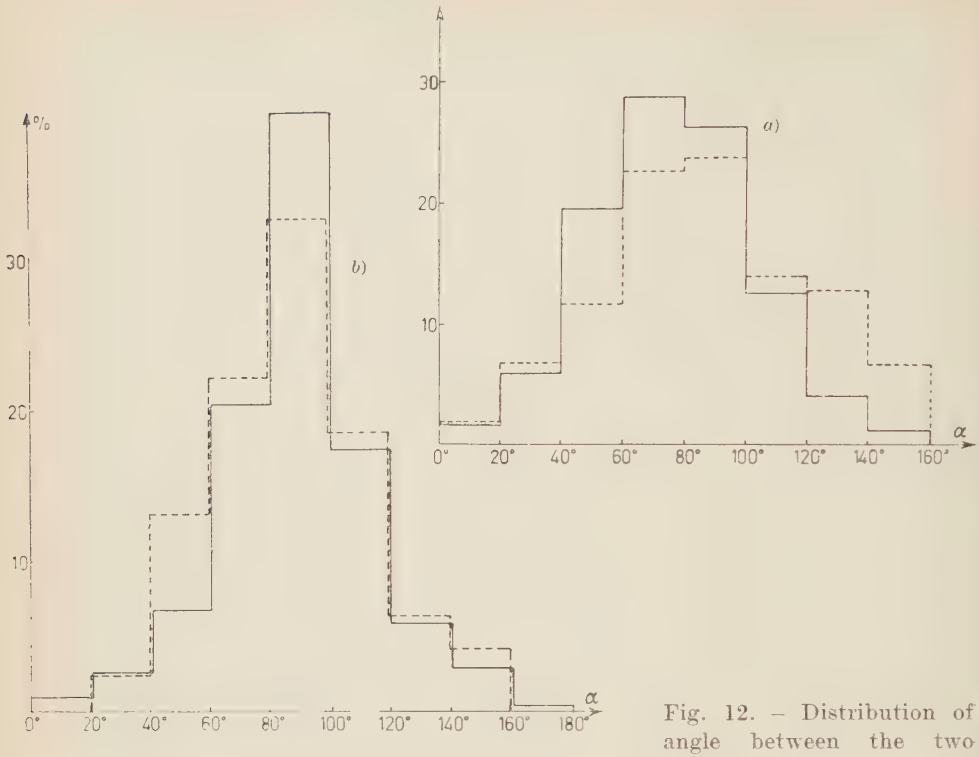

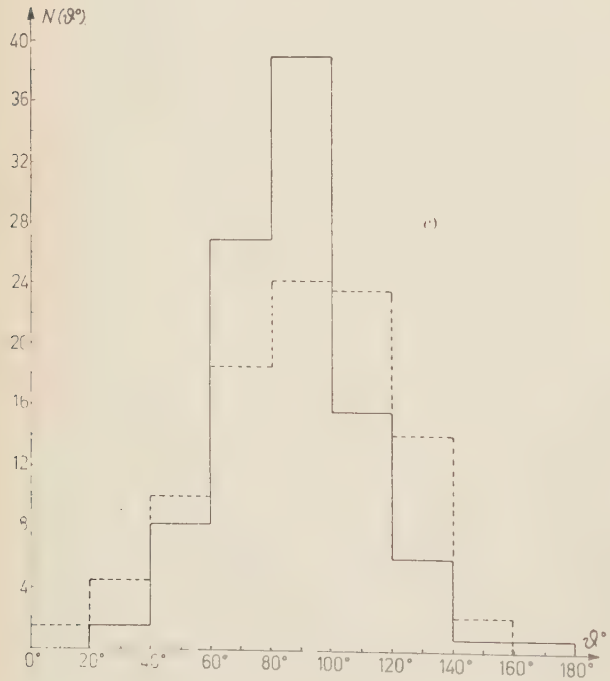

Fig. 12. – Distribution of angle between the two charged prongs in two charged secondaries events. *a*) —— Fermi distribution without clusters (246 events). $(57 \pm 5)\%$ events: $< 90°$; – – – Gaussian distribution without clusters (286 events). $(55 \pm 4)\%$ events: $< 90°$. *b*) —— Fermi distribution (30% probability of collision on clusters, 214 events). $(55 \pm 5)\%$ events: $< 90°$; – – – Gaussian distribution (30% probability of collision on clusters, 236 events). $(57 \pm 5)\%$ events: $< 90°$. *c*) —— Fermi distributrion (40% probability of collision on clusters, 134 events). $(57 \pm 6)\%$ events: $< 90°$; – – – Gaussian distribution (40% probability of collision on clusters, 131 events). $(45 \pm 6)\%$ events: $< 90°$.

5·5. *Distributions of the angle between the two charged prongs in events with two charged secondaries.* – The distributions of the angle formed by the two protons in interactions in which two fast charged secondary particles are emitted are given in Fig. 12. Combe's calculations on pure nucleon-nucleon cascades give for these angles a gaussian distribution with a maximum at 90°. A small shift of the maximum towards small angles seems to appear in our calculated distributions: the various assumptions on clusters and on the momentum distributions do not seen to affect noticeably the percentage of angles lower than 90°.

This shift can be accounted for by relativistic effects which, at 300 MeV primary energy, are counteracted somewhat by the variation of the collision probability with angle shown in Fig. 2. It is worth pointing out that at lower energies there would be an even more pronounced forward collimation because the collision probability then depends quite strongly on the angle (Fig. 2).

The percentages of events with angle lower than 90°, reported in Fig. 12, agree with the value 68 ± 12 obtained experimentally ([10]).

6. – Excitation energy of residual nuclei and energy distribution of fast secondaries.

The excitation energies E_{exc} of the residual nuclei were calculated by means of the following expression ([7]):

$$E_{\text{exc}} = E_i - \sum_{h=0}^{n} T_h^0 - n_n E_{Bn} - (n_p - 1) E_{Bp} , \tag{6.1}$$

where E_i is the energy of the incoming particle (in the laboratory system), T_h^0 is the energy of an outgoing cascade particle (in the laboratory system), E_{Bn} and E_{Bp} are respectively the energy of neutron and of proton secondaries, n_n and n_p are the numbers respectively of neutron and of proton secondaries. We subtracted 1 from n_p in order to take into account the energy gained by the primary particle when entering the nucleus.

6·1. *Fermi momentum distribution.* – The spectra of nuclear excitation energies for a Fermi distribution of nucleon momenta inside the nucleus are shown in Fig. 13. The average excitation energies E_{exc} are (39 ± 0.8) MeV, (28 ± 1) MeV and (22 ± 1.2) MeV for zero, 30% and 40% probability of collision on cluster respectively.

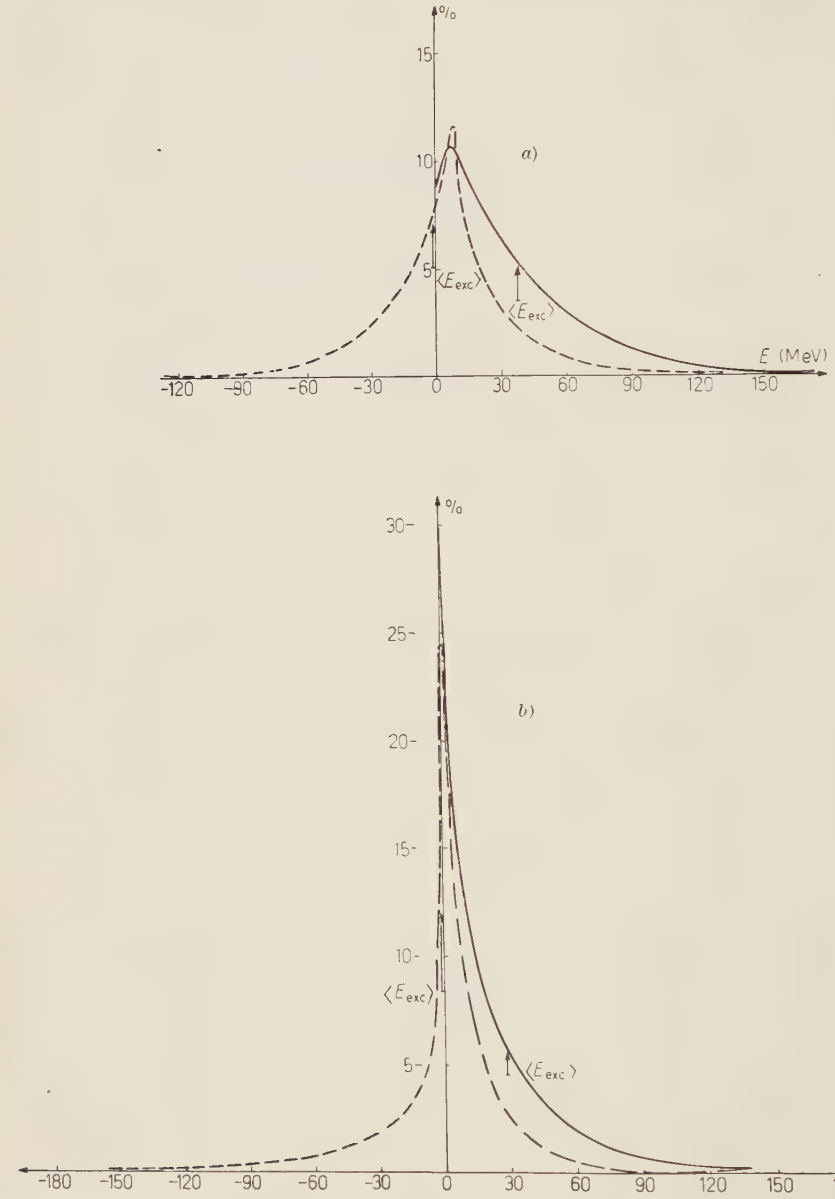

Fig. 13. – Nuclear excitation energies distribution. *a*) —— Fermi distribution without clusters (978 events); – – – Gaussian distribution without clusters (970 events). *b*) —— Fermi distribution (30% probability of collision on clusters, 950 events); – – – Gaussian distribution (30% probability of collision on clusters, 930 events).

E. E. Gross ([35]) obtained esperimentally the average value (27 ± 5) MeV by bombarding carbon nuclei with 190 MeV protons. When comparing with the present results, one should keep in mind that the Monte Carlo calculations

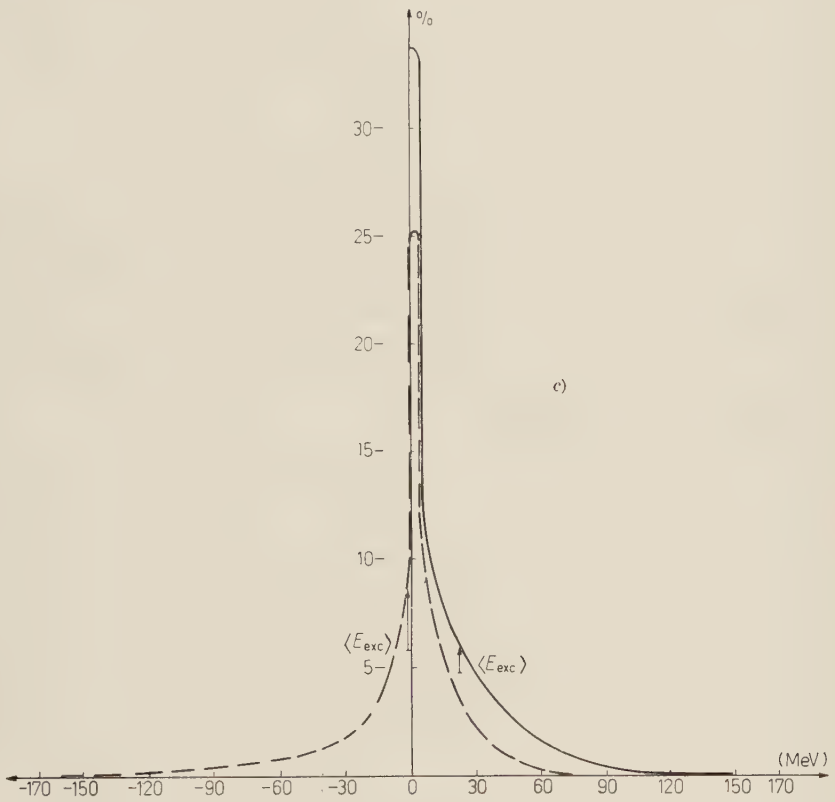

Fig. 13. – Nuclear excitation energies distribution. *c*) —— Fermi distribution (40% probability of collision on clusters, 758 events); – – – Gaussian distribution (40% probability of collision on clusters, 700 events).

of McManus, Sharp and Gellman ([6]), have shown that the average excitation energy increases only slowly with increase in primary energy (less than twice for 5 times increase of the primary energy); therefore this comparison also confirms the validity of the clusters' hypothesis. The energy spectra of Fig. 13 resemble maxwellian curves with maxima between 5 and 10 MeV for pure

([35]) E. E. Gross: *Bull. Am. Phys. Soc.*, **2**, 14 (1957).

nucleon-nucleon cascades and between 0 and 5 MeV if interactions on clusters are considered. This shift of the maximum seems reasonable if one remembers

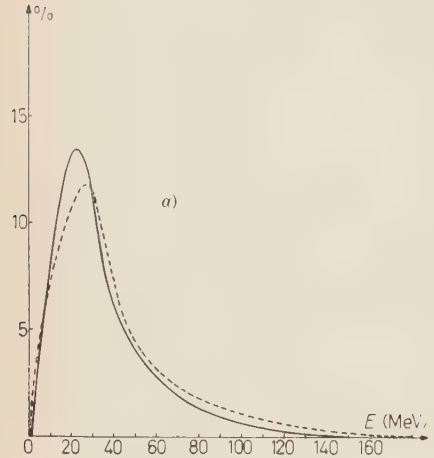

Fig. 14. – Nuclear excitation energy distributions for interactions of the type: —— (p, n); – – – (p, p'). *a*) Fermi distribution without clusters. *b*) Fermi distribution (30% probability of collision on clusters). *c*) Fermi distribution (40% probability of collision on clusters).

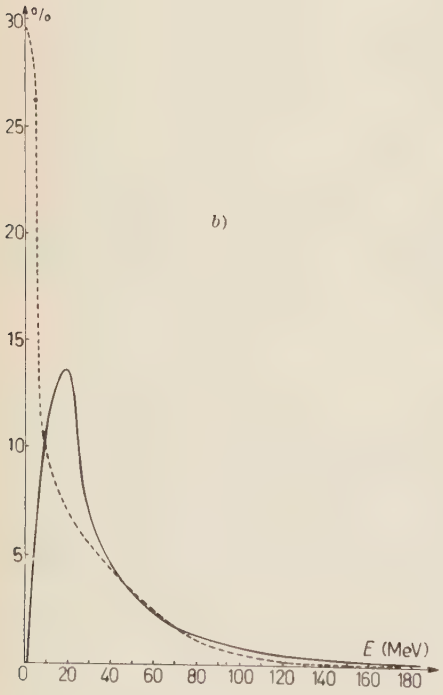

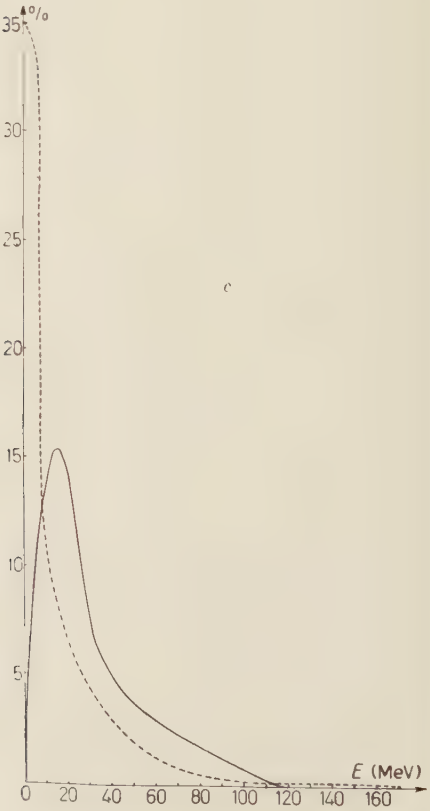

that collisions on clusters give rise to a lower energy dissipation in the nucleus. The excitation energy spectra for interactions of different type, as (p, p), (p, n), (p, 2p), (p, pn) and (p, 2n) are shown in Fig. 14 and 15; the corresponding

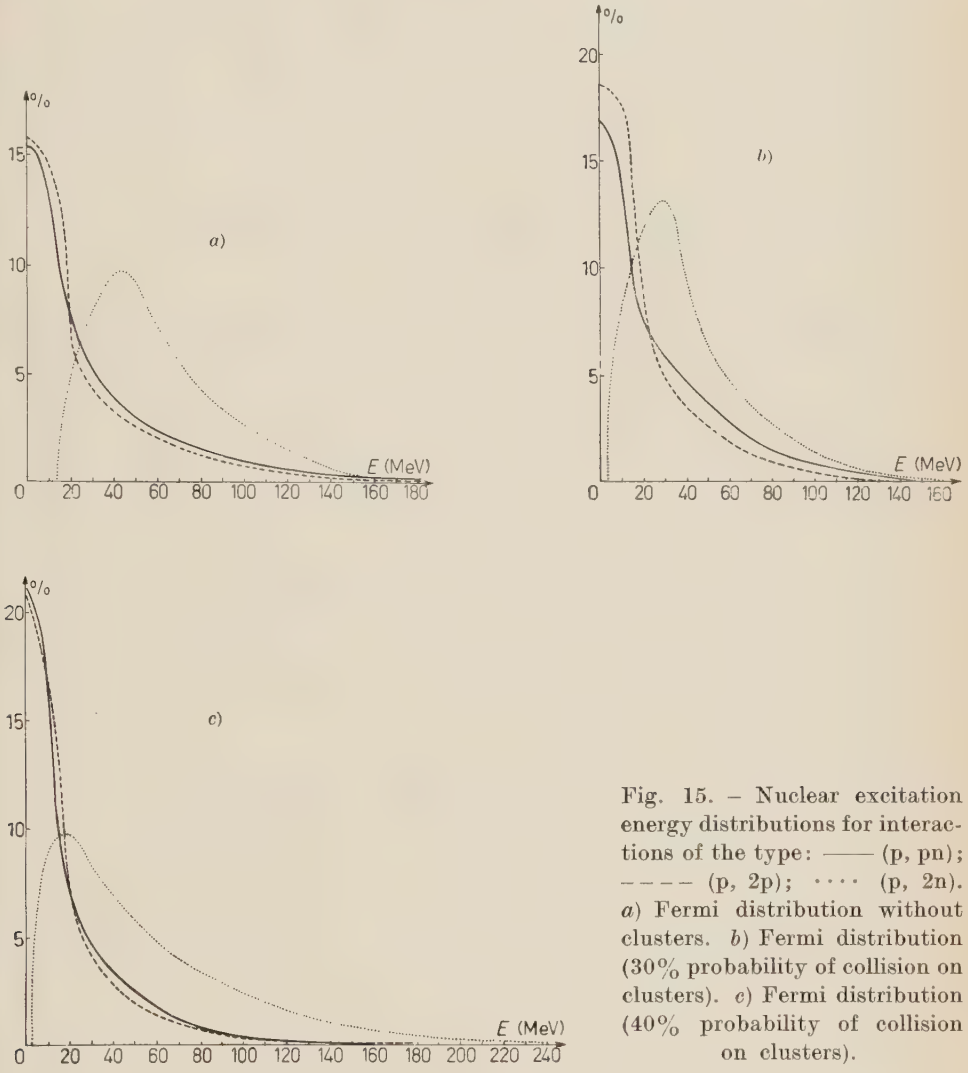

Fig. 15. – Nuclear excitation energy distributions for interactions of the type: —— (p, pn); – – – – (p, 2p); · · · · (p, 2n). *a*) Fermi distribution without clusters. *b*) Fermi distribution (30% probability of collision on clusters). *c*) Fermi distribution (40% probability of collision on clusters).

average excitation energies are given in Table V. The energy spectra of fast secondary prongs for various angles of emission are shown in Fig. 16; these distributions are discussed below in comparison with those obtained with a gaussian distribution.

TABLE V. – *Average nuclear excitation energies.*

Interaction type	F. 0% c.	F. 30% c.	F. 40% c.
for all types	39.00	28.00	22.00
1p	39.11	17.19	12.16
2p	32.16	24.13	22.27
1p 1n	31.84	26.81	24.11
1n	36.09	32.30	26.71
2n	59.50	45.79	59.76

F. 0% c.: Fermi distribution without clusters.
F. 30% c. Fermi distribution (30% probability of collision on clusters);
F. 40% c.: Fermi distribution (40% probability of collision on clusters).

6·2. *Gaussian momentum distribution.* – Calculations based on a gaussian distribution of the nuclear momenta ([26,29,36-42]) were carried out taking into account the Pauli principle in the way described in Section 1. The kinetic energy distributions of fast outgoing nucleons are shown by the dotted curves of Fig. 16. We note that, both for the Fermi and for the gaussian distribution, the momomentum spectra of fast secondary prongs are noticeably affected by the existence of clusters only at small angle of emission ($< 30°$) of the outgoing particle. This is quite reasonable if one takes into account that even if the cluster hypothesis is adopted most of the interactions with a wide-angle secondary are against a nucleon (see Section 5·3). The small-angle momentum distribution and, to a less extent, the overall distribution of Fig. 16 show that the hypothesis of clusters favours interactions with small loss of energy of the proton to the nucleus.

Let us now take into consideration the effects of Fermi and gaussian distributions on the curve of Fig. 16; the two assumptions do not lead to very different results if one considers that parts of the spectrum corresponding to energies of the secondary which are quite different from those of the primary particle. The effect of the gaussian distribution in this region of the spectra is essentially to smear out the two peaks given by the Fermi distribution at the beginning and at the end of the spectrum (small and wide angle of emis-

([36]) J. HADLEY and H. YORK: *Phys. Rev.*, **80**, 345 (1950).
([37]) L. AZHGIREY, I. K. VZOROV, V. P. ZRELOV, M. G. MESCHERYAKOV, B. S. NEGANOV and A. F. SHABUDIN: *Soviet Phys. JETP*, **33**, 1185 (1952).
([38]) C. RICHMAN and H. WILCOX: *Phys. Rev.*, **78**, 496 (1950).
([39]) J. WILCOX and B. MOYER: *Phys. Rev.*, **99**, 875 (1955).
([40]) J. MCEVEN, W. GIBSON and P. DUKE: *Phil. Mag.*, **2**, 231 (1957).
([41]) L. S. AZHGIREY, I. K. VZOROV, V. P. ZRELOV, M. G. MESCHERYAKOV, B. S. NEGANOV, R. M. RYMDIN and A. F. SHABUDIN: *Nucl. Phys.*, **13**, 238 (1959).
([42]) W. SELOVE: *Phys. Rev.*, **101**, 231 (1950).

sion, respectively). The experimental data of CLADIS *et al.* [26] obtained at angles of 30° and 40° cannot give us any help in the choice of the model; in

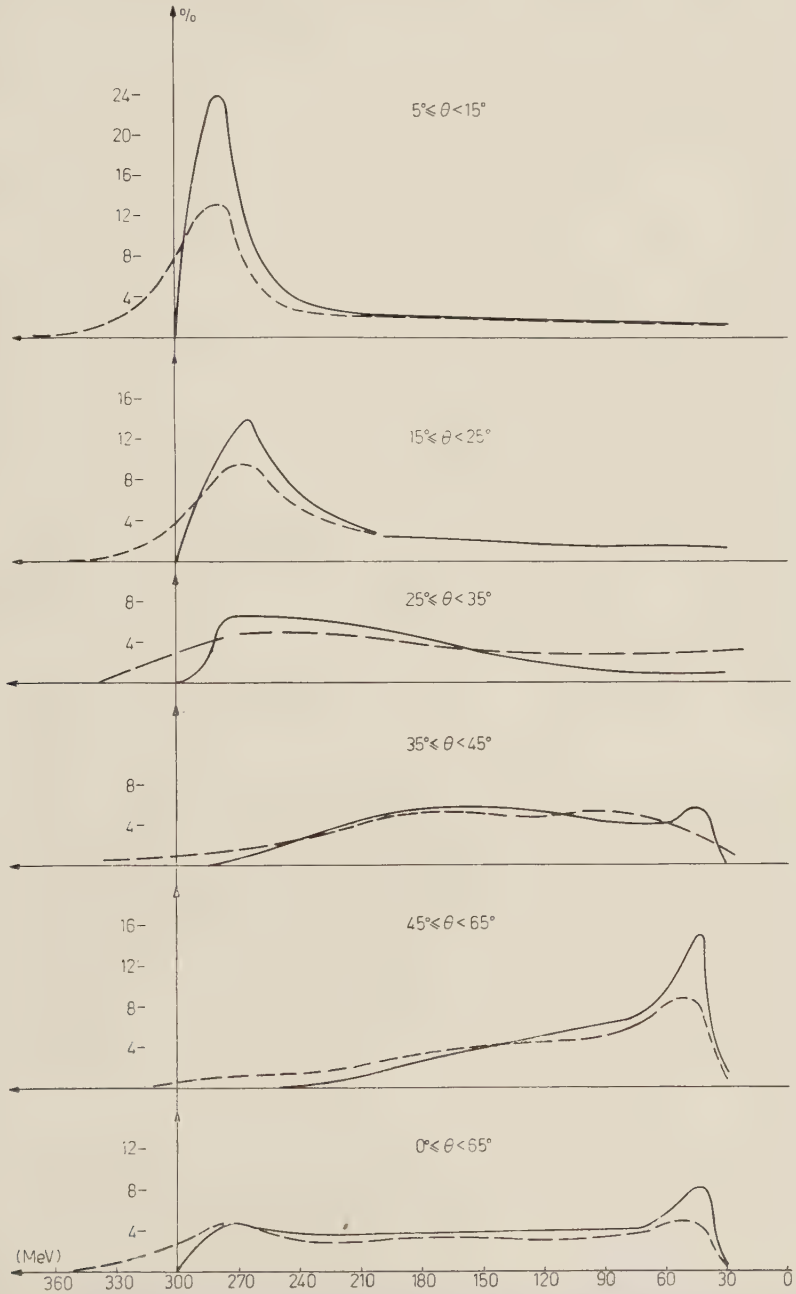

Fig. 16. – Energy spectra of fast secondary protons for different angles of emission. I: —— Fermi distribution without clusters; – – – Gaussian distribution without clusters.

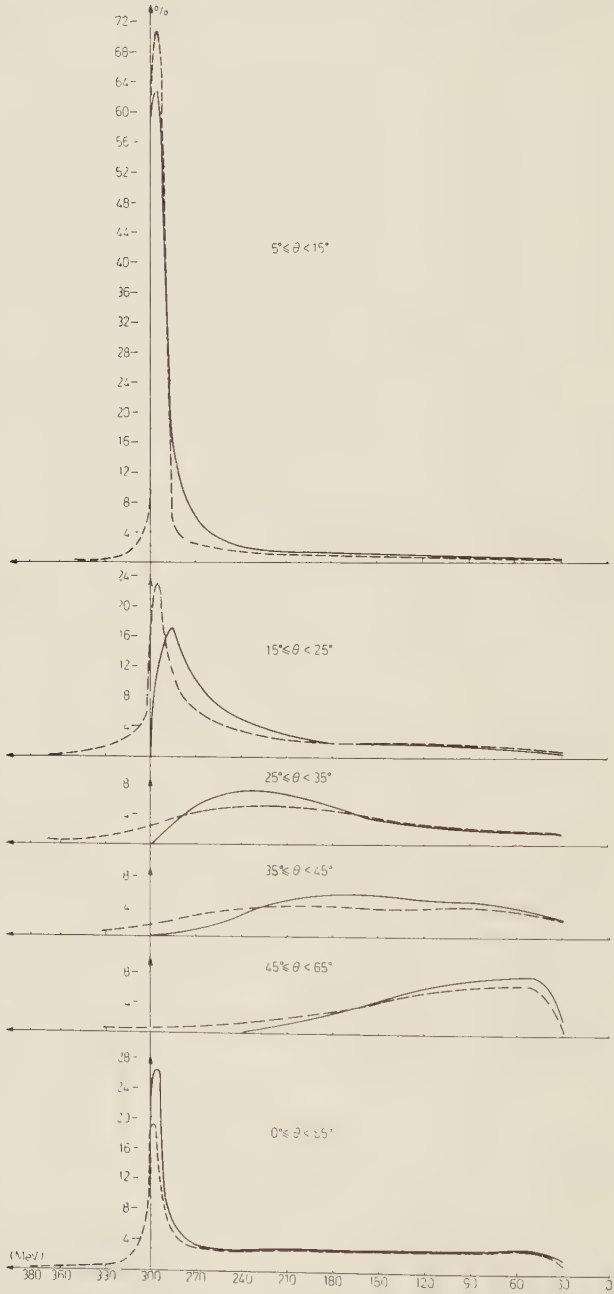

Fig. 16. – Energy spectra of fast secondary protons for different angles of emission. II: —— Fermi distribution (34,28% probability of collision on clusters); – – – Gaussian distribution (34.28% probability of collision on clusters).

fact they agree with the curves obtained with both the Fermi and the gaussian distributions, with and without clusters. The Fermi and gaussian distributions affect the high-energy left end of the spectra in Fig. 16 in strikingly different ways; however the curve calculated for a gaussian distribution extends to energies of the secondary higher than that of the primary. In this case, clearly, the nucleus can lose its excitation energy during the fast part of the interaction by transferring energy to the cascade particles. In fact, owing to the incomplete filling of the lowest levels, a struck nucleus can transfer energy to a cascade particle by jumping into a lower level.

The possibility of a bombarding particle gaining energy in its passage through the nucleus seems quite disturbing to us; it could perhaps be checked with an appropriate experiment. Much more disturbing are the consequences of the gaussian distribution on the excitation energy spectra (Fig. 13). Here the difference of the curves obtained on the basis of the two models are more noticeable, the tail at negative excitation energies is quite pronounced and the mean excitation energy is near to zero, both for pure nucleon-nucleon cascades and for cascades with collisions on clusters. This result is obviously absurd and in complete disagreement with the experimental data ([35]).

Therefore, while the gaussian model gives no better agreement with some experimental data than the Fermi model, it leads to absurd conclusions as far as other data are concerned.

7. – Conclusions.

On the basis of the results of our calculations we conclude that:

a) The angular distributions of the charged secondaries with respect to the primary and the percentages of cascades of different types are very sensitive to the hypothesis of collision on clusters. On the other hand they do not seem to be much affected by different assumptions on momentum distribution of the nucleons. The best agreement between the experimental angular and size distributions of the disintegration stars is obtained with a Fermi-type momentum distribution of the nucleons and with the assumption that the probability of a cascade particle colliding with an α-particle cluster within the nucleus is of order of 30 to 40%.

b) The distribution of the angle between the two secondary protons in interactions with two fast secondary particles is not sensitive to the assumptions made concerning the momentum distributions or the probability of collisions with clusters. For all these assumptions it seems that angles less than 90° are more probable; this can be accounted for, at least for high energy, by relativistic effects.

c) The energy spectrum of the fast secondary nucleons is quite sensitive to the cluster hypothesis only for secondaries with small angles of emission, and is very strongly affected by the type of momentum spectrum assumed when the energy of the secondary is near to that of the primary. The choice of hypothesis also (Fermi or gaussian distribution) strongly affects the excitation energy spectra of the residual nuclei; here the gaussian distribution leads to quite absurd results, as a fairly high percentage of interactions with negative excitation energy results in a mean excitation energy near to zero. The existing experimental data on the energy distributions of fast secondaries do not allow us to decide between a gaussian or a Fermi distribution of nuclear momenta; but the nuclear-excitation-energy spectra obtained with the former are in complete disagreement with the experimental data.

* * *

It is a pleasure to acknowledge the help of the Centro Calcolo dell'Università di Milano and of the Centro Elettronico della Società Remington Rand, particularly of Drs. G. BORTONE and M. CAVEDON. Thanks are also due to Prof. A. J. HERZ for many helpful discussion and to Dr. L. BODINI and Mr. L. GABBA for help during the calculations. The assistance and active interest throughout all this work by the theoretical-physics group of the University of Milan, and particularly by Drs. R. CIRELLI and G. M. PROSPERI, are gratefully acknowledged.

RIASSUNTO

Si sono studiate in questo lavoro le interazioni di protoni di 300 MeV di energia su nuclei di carbonio applicando un metodo di Montecarlo a mezzo di una calcolatrice elettronica Remington Univac U.T.C. In una prima parte dei calcoli si sono studiate cascate costituite solamente da interazioni nucleone-nucleone; successivamente si sono studiate le interazioni assumendo che ciascun nucleone della cascata avesse una probabilità diversa da zero (30% e 40%) di urtare contro una sottostruttura α, formatasi istantaneamente in seno al nucleo. La trattazione della cascata è stata svolta sia sulla base di una distribuzione alla Fermi, che di una distribuzione gaussiana delle quantità di moto dei nucleoni in seno al nucleo. I nostri risultati si riferiscono alle percentuali delle cascate distinte in base al numero delle collisioni ed alla natura dei secondari veloci uscenti, alle distribuzioni angolari ed energetiche dei nucleoni veloci, alle energie di eccitazione dei nuclei dopo la cascata. Il confronto dei risultati dei nostri calcoli coi dati sperimentali è in accordo con l'ipotesi di esistenza di sottostrutture in seno al nucleo. L'assunzione di una distribuzione gaussiana delle quantità di moto dei nucleoni porta a risultati assurdi nelle distribuzioni delle energie di eccitazione dei nuclei e delle energie dei secondari veloci. Se invece si assume una distribuzione alla Fermi gli spettri che si ottengono sono ragionevoli ed in accordo con i dati sperimentali.

IL NUOVO CIMENTO Vol. XXII, N. 6 16 Dicembre 1961

Statistical Emission in Nuclear Reactions and Nuclear Level Density (*).

E. Erba (**)

Istituto di Fisica dell'Università - Milano

U. Facchini

Istituto di Fisica dell'Università - Milano
Laboratori C.I.S.E. - Milano

E. Saetta Menichella

Laboratori C.I.S.E. - Milano

(ricevuto l'8 Agosto 1961)

Summary. — The statistical model in nuclear reactions has been developed extensively in the past decades, mainly by V. Weisskopf. However a clear understanding of the experimental situation regarding low and medium energy nuclear reaction is not yet settled. The interpretation is complicated by the fact that often the reactions proceed via other mechanisms, for instance direct effects. In the present work an attempt is made to show the possibility of explaining a certain group of nuclear reactions with a statistical model. The experiments discussed refer to: *a*) resonance measurements for slow neutrons; *b*) energy spectra of particles emitted in the reactions (n, p) and (n, n′) and (p, n) for incident energies ranging between 4 and 16 MeV; *c*) cross-sections of (n, p) and (n, n′) at 14 MeV. From the set of experiments discussed it is possible to obtain a consistent table of the *a* parameter of nuclear level density formula.

1. – Introduction.

The statistical model for nuclear reactions, developed especially by Weisskopf (1), describes one of the basic mechanisms of nuclear reactions at low and medium energies.

(*) This work has been supported by the « Consiglio Nazionale delle Ricerche ».

(**) Borsa di studio del « Consiglio Nazionale delle Ricerche ».

(1) F. Friedman and V. Weisskopf: *Niels Bohr and the Development of Physics* (London, 1955), p. 135.

The statistical formulation contains as a main term the expression of the nuclear level density. In fact the energy spectra of protons, neutrons and α-particles emitted in medium-energy reactions are directly related, through the statistical formulae, to such level densities.

An independent source of knowledge for nuclear level densities are the measurements of slow neutrons resonances. In a number of papers that appeared in recent years the neutron resonances and various nuclear reactions have been analysed under the statistical point of view ([2-13]). However, the various parameters that enter the model and the field of validity of the model itself are still not well defined. The purpose of the present paper is to try to bring into one picture the conclusions obtained from the various experiments: the experiments discussed refer particularly to:

a) the measurements of the total cross-sections for slow neutrons in the resonance areas of about 110 nuclei,

b) energy spectra of particles emitted in the reaction (n, p) (n, n′) and (p, n), for incident energies ranging between 4 and 16 MeV (56 spectra),

c) cross-sections of (n, p) and (n, n′) reactions at 14 MeV energy for medium and heavy nuclei (32 and 33 nuclei, respectively).

2. – Nuclear level density.

The most used formula representing the density of nuclear levels has been introduced by BETHE ([12]) and is based on the «equidistant spacing model» of the nucleus.

This formula has been also developed by other authors ([6-11]) and here we report the formula as used by LANG and LE COUTEUR ([6]).

([2]) N. O. LASSEN and N. O. ROY PULSEN: *International Conference on Low-Energy Nuclear Physics in Paris* (July 1958).

([3]) T. D. NEWTON: *Can. Journ. Phys.*, **34**, 804 (1936).

([4]) A. G. W. CAMERON: *Can. Journ. Phys.*, **36**, 1040 (1958).

([5]) J. M. B. LANG and K. J. LE COUTEUR: *Proc. Phys. Soc.*, A **67**, 586 (1954).

([6]) K. J. LE COUTEUR and D. W. LANG: *Nucl. Phys.*, **13**, 32 (1959).

([7]) L. COLLI, U. FACCHINI, I. IORI, G. M. MARCAZZAN and A. M. SONA: *Nuovo Cimento*, **13**, 730 (1959) (I).

([8]) U. FACCHINI, I. IORI and E. MENICHELLA: *Nuovo Cimento*, **16**, 1109 (1960) (II).

([9]) D. L. ALLAN: *Nuclear Phys.*, **24**, 274 (1961).

([10]) D. B. THOMSON (Advisor L. CRANBERG): *Thesis*: *Nuclear Level Densities and Reactions Mechanisms from Inelastic Neutron Scattering* (Los Alamos Scientific Laboratories, 1960).

([11]) T. ERICSON: *Adv. in Phys.*, **9**, no. 36, 425 (1960).

([12]) H. A. BETHE: *Rev. Mod. Phys.*, **9**, 69 (1937).

([13]) J. BLATT and V. WEISSKOPF: *Theoretical Nuclear Physics* (New York, 1952).

The density of the levels $\varrho(E, j)$ of the nucleus, containing A nucleons at excitation energy E and with spin j, is obtained assuming that the nucleus consists of two groups of nucleons (N neutrons and Z protons) distributed in two sets of states. The spacing of the states of the nucleons in a region around the top of the distribution is assumed to be constant and respectively g_p^{-1} for protons and g_n^{-1} for neutrons. The pairing interactions is introduced through the « effective excitation energy » U given by

$$U = E + \Delta ,$$

where Δ is a negative term representing the pairing energy of the last two protons when Z is even, of the last two neutrons when N is even, the sum of both pairing energies for even-even nuclei; Δ is zero for odd-odd nuclei.

$\varrho(E, j)$ is given by the formula

$$(1) \qquad \varrho(E, j) = \frac{6^{-\frac{1}{2}}}{2^{\frac{3}{2}}} \pi\hbar^3(2j+1) \frac{\exp\left[-(j+\frac{1}{2})^2/2ct\right]}{12} g_0^{\frac{1}{2}} \mathscr{I}^{-\frac{3}{2}} \frac{\exp\left[2\sqrt{aU}\right]}{(U+t)^2} ,$$

where

$$(2) \qquad g_0 = g_n + g_p , \qquad a = \frac{\pi^2}{6} g_0 .$$

The thermodynamic temperature t is obtained from the relation

$$(3) \qquad U = at^2 - t .$$

$\mathscr{I}$ is the moment of inertia of the nucleus and c is given by

$$c = \frac{\mathscr{I}}{\hbar^2} .$$

The momenta of inertia appears in formula (1), in close connection with the spin-dependence of $\varrho(E, j)$.

3. – Resonance of slow neutrons.

In reactions with slow neutrons we have well-defined and separate resonances corresponding to well-defined and separate levels of the compound nucleus.

The average spacing D_{obs} between these resonances gives directly the level spacing of the compound nucleus at a given E for determined values of j.

Though no special hypotheses are formulated, it may be supposed that

all the possible levels, in accordance with the rules of the conservation of spin and parity, are excited and therefore D_{oss}^{-1} represents the density of the nuclear levels of the compound nucleus at excitation energy E and with given value of the spin j. The binding energy of the neutron B_n gives with good approximation the excitation energy E of the compound nucleus.

Taking into account the spin I of the target nucleus we have

$$(4) \qquad \begin{cases} D_{\text{oss}}^{-1} = \frac{1}{2} \cdot \varrho(E, j = \frac{1}{2}); & I = 0 . \\ D_{\text{oss}}^{-1} = \frac{1}{2} \cdot [\varrho(E, I + \frac{1}{2}) + \varrho(E, I - \frac{1}{2})]; & I \neq 0 . \end{cases}$$

Since the initial state has a well-defined parity, the observed levels have only one of the two possible parities. Therefore we introduced in formulae (4) the factor $\frac{1}{2}$ which is due to the hypothesis of the equiprobability of the two parities for nuclear levels. For the few cases where the l value of neutrons is different from zero, the necessary alterations have been used.

The measurements made by various groups and reported in BNL reports and in other papers (see Table I) give the value D_{oss} for a number of nuclei. We have restricted our analysis to 110 nuclei having resonances at neutron energy below 200 keV.

From formulae (1)–(5) we can obtain the value of g_0.

We have introduced for $\mathscr{I}$ the value $\frac{2}{5} MAR^2$ (M mass of nucleons), corresponding to a rigid nucleus following the advice of ERICSON ([11,14]). R has been chosen equal to $1.4A^{\frac{1}{3}}$ fermi. Varying $\mathscr{I}$ by 10% to 30%, the set of

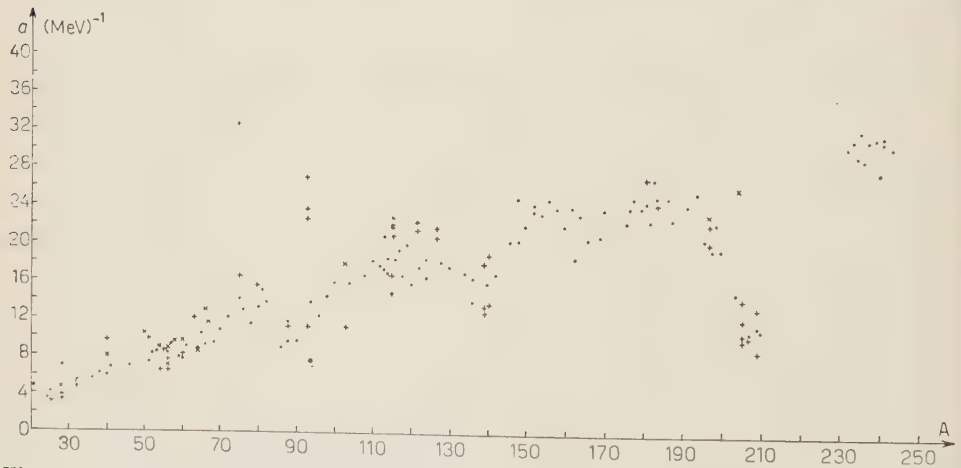

Fig. 1. – Values of a (MeV^{-1}) as a function of mass number A; • a from D_{oss}, · a from spectra ($U > 5.5$ MeV), + a from spectra ($U \leqslant 5.5$ MeV).

([14]) T. ERICSON: *Proc. of the Int. Conf. on Nucl. Structure* (Kingston, 1960), p. 697.

TABLE I.

Compound nucleus	I target spin	$\lvert B_n \rvert$ (MeV)	$\lvert \Delta \rvert$ (MeV)	D_{obs} (eV)	Reference	a_{calc} (MeV^{-1})
^{20}F (*)	1/2	6.605	0	$5 \cdot 10^4$	(*a*)	4.80
^{24}Na (*)	3/2	6.995	0	$2.01 \cdot 10^5$	(*a*)	3.48
^{25}Mg (*)	0	7.331	2.10	$3.46 \cdot 10^5$	(*a*)	4.19
^{28}Al (*)	5/2	7.724	0	$4 \cdot 10^3$	(*a*)	6.94
^{32}P	1/2	7.937	0	$5 \cdot 10^4$	(*b*)	4.76
^{36}Cl	3/2	8.577	0	$1 \cdot 10^4$	(*b*)	5.47
^{38}Cl	3/2	6.110	0	$2.78 \cdot 10^4$	(*a*)	6.03
^{40}K	3/2	7.798	0	$1.12 \cdot 10^4$	(*a*)	5.93
^{41}Ca	0	8.360	1.51	$1.95 \cdot 10^4$	(*a*)	6.80
^{46}Sc	1/2	8.766	0	$2 \cdot 10^3$	(*b*)	6.85
^{51}V	6	11.040	1.47	$1.26 \cdot 10^3$	(*a*)	7.18
^{52}V	7/2	7.304	0	$2 \cdot 10^3$	(*b*)	8.06
^{53}Cr	0	7.943	1.44	$2.9 \cdot 10^4$	(*a*)	8.28
^{56}Mn	5/2	7.270	0	$2 \cdot 10^3$	(*b*)	8.28
^{57}Fe	0	7.642	1.45	$2.32 \cdot 10^4$	(*a*)	9.01
^{60}Co	7/2	7.497	0	$3 \cdot 10^3$	(*b*)	7.74
^{59}Ni	0	9.001	1.37	$2.57 \cdot 10^4$	(*a*)	7.77
^{61}Ni	0	7.823	1.37	$2.2 \cdot 10^4$	(*a*)	8.99
^{64}Cu	3/2	7.916	0	$1.4 \cdot 10^3$	(*a*)	8.65
^{66}Cu	3/2	7.061	0	$1.99 \cdot 10^3$	(*a*)	9.10
^{65}Zn	0	7.989	1.09	$1.85 \cdot 10^3$	(*a*)	10.31
^{68}Zn	5/2	10.199	2.61	$6.9 \cdot 10^2$	(*a*)	9.51
^{70}Ga	3/2	7.730	0	$3 \cdot 10^2$	(*a*)	10.64
^{72}Ga	3/2	6.960	0	$2.05 \cdot 10^2$	(*a*)	12.06
^{76}As	3/2	7.287	0	90	(*c*)	12.81
^{75}Se	0	8.020	1.42	≈ 200	(*c*)	13.94
^{78}Se	1/2	10.480	2.87	$3.93 \cdot 10^2$	(*a*)	11.46
^{81}Se	0	6.821	1.42	$1.5 \cdot 10^3$	(*a*)	14.96

TABLE I (*continued*).

Compound nucleus	I target spin	B_n (MeV)	Δ (MeV)	D_{obs} (eV)	Reference	a_{calc} (MeV^{-1})
^{80}Br	3/2	7.893	0	45	(*c*)	13.02
^{82}Br	3/2	7.648	0	34	(*a*)	13.77
^{86}Rb	5/2	8.580	0	$8.33 \cdot 10^2$	(*a*)	8.99
^{88}Rb	3/2	6.200	0	$1.18 \cdot 10^3$	(*a*)	11.46
^{88}Sr	9/2	11.120	2.47	~ 400	(*c*)	9.44
^{90}Y	1/2	6.850	0	$4.85 \cdot 10^3$	(*a*)	9.83
^{94}Nb	9/2	7.190	0	42.5	(*c*)	13.86
^{96}Mo	5/2	9.160	1.92	~ 200	(*c*)	12.16
^{98}Mo	5/2	8.290	2.39	~ 200	(*c*)	14.28
^{100}Tc	9/2	7.100	0	14	(*b*)	15.7
^{104}Rh	1/2	6.790	0	~ 75	(*c*)	15.69
^{108}Ag	1/2	7.210	0	27.5	(*c*)	16.51
^{110}Ag	1/2	6.820	0	17.5	(*c*)	18.01
^{112}Cd	1/2	9.290	2.68	34	(*c*)	17.49
^{113}Cd	0	6.420	1.38	~ 230	(*c*)	20.57
^{114}Cd	1/2	9.050	2.67	30.5	(*c*)	18.22
^{114}In	9/2	7.310	0	7	(*c*)	16.67
^{116}In	9/2	6.610	0	7	(*c*)	18.15
^{113}Sn	0	8.010	1.32	150	(*b*)	17.17
^{117}Sn	0	7.190	1.32	150	(*b*)	19.16
^{118}Sn	1/2	9.250	2.56	70	(*b*)	16.43
^{119}Sn	0	6.580	1,32	300	(*b*)	19.65
^{120}Sn	1/2	9.240	2.60	150	(*b*)	15.47
^{122}Sb	5/2	6.800	0	15	(*c*)	17.16
^{124}Sb	7/2	6.450	0	35	(*c*)	16.33
^{124}Te	1/2	9.400	2.28	15	(*c*)	18.08
^{128}I	5/2	6.706	0	11.68	(*d*)	17.91
^{130}I	7/2	6.485	0	17.56	(*a*)	17.48

TABLE I (*continued*).

Compound nucleus	I target spin	B_n (MeV)	l (MeV)	D_{obs} (eV)	Reference	a_{calc} (MeV^{-1})
^{136}Xe	3/2	7.904	1.65	~ 500	(*c*)	13.92
^{134}Cs	7/2	6.740	0	21	(*c*)	16.79
^{136}Ba	3/2	9.210	2.18	35	(*c*)	16.36
^{140}La	7/2	5.010	0	~ 500	(*c*)	15.63
^{142}Pr	5/2	5.840	0	110	(*b*)	16.61
^{143}Nd	7/2	7.580	2.18	25	(*c*)	20.02
^{148}Pm	5/2	5.000	0	5.37	(*a*)	24.89
^{148}Sm	7/2	8.120	1.9	7	(*c*)	20.09
^{150}Sm	7/2	8.010	1.9	3.3	(*c*)	21.77
^{152}Sm	5/2	8.400	2	1.3	(*a*)	23.05
^{152}Eu	5/2	6.480	0	0.725	(*c*)	23.88
^{154}Eu	5/2	6.560	0	1.1	(*c*)	22.94
^{156}Gd	3/2	7.860	1.96	2.1	(*c*)	24.48
^{158}Gd	7/2	7.930	2.01	2	(*b*)	23.49
^{160}Td	3/2	6.500	0	4	(*b*)	21.61
^{162}Dy	7/2	8.200	1.96	1.15	(*c*)	23.63
^{163}Dy	0	6.300	0.91	~ 200	(*c*)	18.17
^{164}Dy	7/2	7.600	1.97	5	(*c*)	22.83
^{168}Ho	7/2	6.400	0	6.55	(*b*)	20.18
^{170}Tm	1/2	6.000	0	7.5	(*c*)	23.39
^{169}Yb	0	6.800	1	~ 30	(*c*)	20.56
^{178}Lu	7/2	6.050	0	4.45	(*c*)	22.04
^{177}Lu	≈ 8	7.120	1.02	1.45	(*c*)	23.54
^{176}Hf	7/2	7.540	2.13	3.75	(*c*)	24.52
^{180}Hf	9/2	7.420	2.08	6	(*b*)	23.59
^{181}Ta	1	7.600	0.97	~ 1.5	(*c*)	24.02
^{182}Ta	7/2	6.070	0	5.6	(*c*)	22.10
^{183}W	0	6.180	1.23	~ 50	(*c*)	26.51

TABLE I (*continued*).

Compound nucleus	I target spin	$\lvert B_n \rvert$ (MeV)	l (MeV)	D_{obs} (eV)	Reference	a_{calc} (MeV^{-1})
^{184}W	1/2	7.460	2.14	15	(*c*)	24.72
^{187}W	0	6.450	1.23	75	(*a*)	24.69
^{186}Re	5/2	4.340	0	3	(*c*)	30.6
^{188}Re	5/2	5.900	0	7.5	(*c*)	22.23
^{192}Ir	3/2	6.080	0	$\sim$ 3.5	(*c*)	23.88
^{194}Ir	3/2	5.760	0	$\sim$ 3.5	(*c*)	24.99
^{196}Pt	1/2	7.920	1.59	35	(*c*)	20.33
^{198}Au	3/2	6.496	0	30	(*c*)	19.1
^{199}Hg	0	6.690	0.72	$\sim$100	(*c*)	21.95
^{200}Hg	1/2	8.000	1.33	$\sim$ 50	(*c*)	19.01
^{204}Tl	1/2	6.620	0	1000	(*b*)	14.67
^{207}Pb	0	6.730	0.80	$2.5 \cdot 10^4$	(*b*)	10.52
^{209}Pb	0	3.930	0.80	$4 \cdot 10^5$	(*b*)	11.23
^{210}Bi	9/2	4.640	0	$4 \cdot 10^4$	(*b*)	10.76
^{233}Th	0	5.070	0.80	19	(*b*)	29.82
^{234}U	5/2	6.770	1.45	0.64	(*b*)	30.60
^{235}U	0	5.240	0.81	15	(*b*)	28.87
^{236}U	7/2	6.400	1.39	0.65	(*c*)	31.58
^{237}U	0	5.420	0.81	16.5	(*b*)	28.49
^{239}U	0	4.760	0.81	19	(*c*)	36.25
^{238}Np	5/2	5.370	0	0.655	(*c*)	30.41
^{240}Pu	1/2	6.380	1.24	2.75	(*c*)	30.64
^{241}Pu	0	5.520	0.69	19.5	(*c*)	27.17
^{242}Pu	5/2	6.210	1.26	1.7	(*c*)	30.3
^{242}Am	5/2	5.480	0	0.43	(*b*)	30.95
^{244}Am	5/2	5.150	0	1.462	(*a*)	29.73

(*a*) B.N.L. 325 «Neutron Cross Sections», II ed. (1958).
(*b*) A. G. W. CAMERON: *Can. Journ. Phys.*, **36**, 1040 (1958).
(*c*) A. STOLOVY and J. A. HARVEY: *Phys. Rev.*, **108**, 353 (1957).
(*d*) T. D. NEWTON: *Can. Journ. Phys.*, **34**, 804 (1936).
(*) $l \neq 0$.

a values obtained does not change appreciably. J values have been taken from Cameron tables ([4]) and the binding energy of neutron from Wapstra tables ([15,16]). Table I contains all data related to the calculations with the necessary references.

The values of g_0 and of a have been obtained with electronic calculation.

Fig. 1 represents the values of a corresponding to each nucleus. These values show a regular behaviour with mass number A, and present the known minima ([3]) for values of A corresponding to nuclei having a magic neutron number ($A \simeq 90$, 140, 210). Analyses of the neutron resonance have been presented by other authors, namely Le Couteur and Lang ([6]), Newton ([3]) and Cameron ([4]).

The values obtained in the present paper are higher than the results given by these authors.

In fact all these authors did not account correctly for the moment of inertia ([17]).

4. – Statistical model for nuclear reactions: spectra of neutrons and protons.

The statistical model of nuclear reactions gives a simple formula for the energy spectrum of particles emitted in a nuclear reaction.

The essential assumption that should be satisfied in order to apply a statistical model to a nuclear reaction is the formation and decay of the compound nucleus as two independent processes.

The two basic quantities entering in the evaporation formula are the density of states of the nucleus and the inverse cross-section ([13]).

According to the statistical model ([13]) the « reduced spectra », *i.e.* the ratio between the differential cross-sections $\partial^2\sigma/\partial\varepsilon\partial\Omega$ and the inverse cross-section times the energy of the emitted particle at a fixed bombarding energy, is proportional to the density of the states of the residual nucleus:

$$\frac{1}{\varepsilon\sigma_c}\frac{\partial^2\sigma_c}{\partial\varepsilon\,\partial\Omega} \propto \sum_j (2j+1)\varrho(E, j)\,. \tag{5}$$

The sum is extended over the possible j values.

In the previous work ([7]) (I) we discussed the energy distribution of nucleons and α-particles emitted by various medium nuclei and in various re-

([15]) F. Everling, L. A. König, J. H. Mattauch and A. H. Wapstra: *Nucl. Phys.*, **18**, 529 (1960).

([16]) A. H. Wapstra: *Physica*, **21**, 367 (1955).

([17]) A. C. Douglas and N. MacDonald: *Nuclear Phys.*, **13**, 382 (1959).

actions and showed how a certain number of energy spectra are consistent with the statistical model. Generally, only backward spectra have been considered to avoid as much as possible the presence of direct effects, and only spectra corresponding to reactions in which the incident particles have energies below about (12 ÷ 16) MeV. In fact in these conditions the emission is nearly isotropic and direct effects are negligible. At higher energies of the incident particles (15 or 20 MeV and more) the spectra of emitted particles are not consistent with the statistical model and with the results at lower energies, the angular distributions being much picked forward and the direct effects being more notable here and can be observed even at backward angles.

By comparing the groups of « reduced spectra » corresponding to the same or neighbouring nuclei it was possible in a few cases of nuclei with $A \sim 40$ to 60 to build curves proportional to such state densities of the residual nucleus.

In particular, the comparison gave consistent result for (n, p) reactions at 14 MeV, for (p, p′) reactions at 11 MeV and for (α, α') reactions at from 12 to 16 MeV. Recently we have noticed that a group of (p, α) reactions [18] gives consistent results in agreement with the (α, α') ones.

A new set of measurements has recently been conducted on (n, p) reactions at 14 MeV by ALLAN [9] and by COLLI [19,20] and co-workers, while a group of (n, n′) reactions for medium and heavy nuclei has been investigated by THOMSON [10].

ALLAN studied backward spectra for 27 elements between Mg and Zn finding evaporation spectra practically free of direct effects.

THOMSON showed that for (n, n′) reactions with incident neutron energy ranging from 4 to 7 MeV, direct effects are not very important and the evaporation emission is clearly observed, when spectra obtained at various incident energies are compared.

We have collected in this paper all the spectra regarding nucleon emission discussed in (I), the more recent results on (n, p) and all the (n, n′) and (p, n) results at energies below 16 MeV.

The inverse cross-sections σ_r have been calculated using the Weisskopf [13] tables and taking as « effective nuclear radius » the value $R = r_0 A^{\frac{1}{3}}$ with $r_0 = 1.4$ fermi for neutrons and $r_0 = 1.5$ fermi for protons.

Taking into account that: 1) the expression of $\varrho(E, j)$ is given by (1), 2) the term $\exp[-(j+\frac{1}{2})^2/2\sigma t]$ is roughly equal to unity, 3) only few values

[18] R. SHERR and F. P. BRADY: communication at M.I.T. Meeting (April 1960) and to be published.

[19] L. COLLI, I. IORI, G. M. MARCAZZAN, F. MERZARI, A. M. SONA and P. G. SONA: *Nuovo Cimento*, **17**, 634 (1960).

[20] L. COLLI, G. M. MARCAZZAN, F. MERZARI, P. G. SONA and P. TOMAŠ: *Nuovo Cimento*, **20**, 928 (1961).

of j are permitted for the residual nucleus, the logarithmic derivative of formula (6) gives with a good approximation the a values, according to:

$$(6) \qquad -\frac{\mathrm{d}\ln\left((1/\varepsilon\sigma_c)\cdot(\mathrm{d}^2\sigma/\mathrm{d}\varepsilon\,\mathrm{d}\Omega)\right)}{\mathrm{d}\varepsilon} = \frac{1}{T} = \sqrt{\frac{a}{U}} - \frac{2}{U+t/2},$$

where t is given by (3) and $U = E+Q+\Delta-\varepsilon$.

To check the validity of this formula over the whole « reduced spectrum » the values of a can be obtained at different values of U.

However, in many cases the part of the spectra corresponding to high values of U contains multiple reactions, and the secondary particles mix and alter the shape of the evaporative spectrum of the primary particles.

At low U values the low number of levels and the presence of direct effects (low U values correspond to high energies of emitted particles) also alter the evaporative shape of the curve.

Due to these facts it is impossible to know with a good precision the slope of the level densities over the whole « reduced spectrum », and the U values useful for the calculation are restricted generally to an interval between about 3 and 10 MeV.

The values of a obtained from the various spectra at various U values are collected in Table II, and in Fig. 1 they are differently labelled being obtained at U values greater or smaller than 5.5 MeV (*).

The agreement between the a values obtained for a given spectrum at different U values is generally good and formula (1) can be regarded as a good approximation.

It must be remembered that formula (1) in a small range of values of U is not quite different from an exponential shape

$$(7) \qquad \varrho \sim C\exp\left[U/T\right],$$

with $T \simeq$ constant. This simple formula has been used by many authors to fit the level densities.

Comparing the a values obtained from the spectra with the ones obtained from the resonance of slow neutrons (Fig. 1) we note that a quantitative agreement is obtained between the two groups of results, and that particularly the deep minima at magic N nuclei and the average shape of the a curve *vs.* A are substantiated.

(*) The values of a given by Thomson are different from the present values by 50% due to the omission of the $(U+t)^{-2}$ term in the level density formula.

TABLE II.

Residual nucleus	Reaction	E_0 (MeV)	Reference	T (MeV)	U (MeV)	a_{calc} (MeV^{-1})
^{25}Na	n, p	14	(*a*)	2.10	2.80	3.2
^{28}Al	n, p	14	(*b*)	1.91	2.14	3.6
			(*a*, *b*)	1.80	4.14	4
			(*a*)	1.81	6.64	4.5
^{32}P	n, p	14	(*c*)	1.57	6.07	5.3
			(*a*)	1.75	7.07	4.9
^{40}K	n, p	14	(*a*)	1.01	5.46	9.7
			(*a*)	1.285	7.46	7.9
^{50}V	n, p	14	(*a*)	1.16	8.74	10.2
^{51}V	n, n′	7	(*d*)	0.90	3.53	9.4
					4.53	10.5
^{54}Mn	n, p	14	(*a*)	1.21	4.09	6.6
			(*a*)	1.125	6.09	8.7
			(*a*)	1.22	8.09	9.0
^{55}Mn	n, n′	7	(*d*)	1.00	3.68	8.2
					4.68	9.1
^{56}Mn	n, p	14	(*e*)	1.21	3.60	6.3
			(*e*)	1.31	6.10	6.9
			(*a*)	1.13	6.10	8.6
^{56}Fe	n, n′	7	(*d*)	0.95	1.23	7.1
					2.23	7.5
					3.23	8.4
^{58}Co	n, p	14	(*a*)	1.14	7.39	9.5
^{60}Co	n, p	14	(*a*)	1.10	4.97	8.1
					6.97	9.7
^{63}Cu	n, n′	7	(*d*)	0.79	3.56	11.3
					4.56	12.8

TABLE II (*continued*).

Residual nucleus	Reaction	E_0 (MeV)	Reference	T (MeV)	U (MeV)	a_{calc} (MeV^{-1})
^{64}Cu	n, p	14	(*a*)	1.18	6.79	8.6
^{66}Cu	n, p	14	(*a*)	0.88	6.15	12.8
^{67}Cu	n, p	14	(*a*)	1.07	8.71	11.6
^{75}As	n, n′	7	(*d*)	0.67	4.53	16.5
$^{78\text{-}80}$Se	n, n′	7	(*d*)	0.62	3.19	15.4
^{88}Sr	n, n′	7	(*d*)	0.80	3.53	11.1
^{93}Nb	n, n′	5	(*d*)	0.48	3.38	23.6
		6	(*d*)	0.49	4.38	26.9
		7	(*d*)	0.59	5.38	22.6
^{93}Mo	p, n	8	(*f*)	0.73	2.57	11.1
^{103}Pd	p, n	8	(*f*)	0.70	2.27	11.2
		16	(*g*)	0.85	8.27	16.4
		16	(*g*)	0.85	10.27	19.1
^{115}In	n, n′	4	(*d*)	0.40	1.71	21.8
		5	(*d*)	0.48	2.71	20.8
		6	(*d*)	0.52	3.71	21.9
		7	(*d*)	0.56	4.71	22.6
^{115}Sn	p, n	5	(*h*)	0.50	1.40	15.0
		8	(*h*)	0.50	2.40	18.4
			(*f*)	0.65	3.40	14.8
$^{121\text{-}123}$Sb	n, n′	4	(*d*)	0.40	1.74	22.0
		7	(*d*)	0.58	4.74	21.4
^{127}I	n, n′	4	(*d*)	0.41	1.80	21.6
		7	(*d*)	0.60	4.60	20.4

TABLE II (*continued*).

Residual nucleus	Reaction	E_0 (MeV)	Reference	T (MeV)	U (MeV)	a_{calc} (MeV^{-1})
^{139}La	n, n′	4	(*d*)	0.65	2.46	12.8
		5	(*d*)	0.69	3.46	13.6
		7	(*d*)	0.68	5.46	18.0
^{140}Ce	n, n′	5	(*d*)	0.60	2.25	13.8
		7			4.25	18.9
^{181}Ta	n, n′	7	(*d*)	0.52	5.03	26.7
$^{184\text{-}186}$W	n, n	7	(*d*)	0.50	3.87	24.0
^{197}Au	n, n′	4	(*d*)	0.47	2.39	20.2
		7	(*d*)	0.60	5.39	22.0
^{197}Hg	p, n	16	(*g*)	0.77	9.88	22.1
		16	(*g*)	0.77	10.88	23.7
$^{203\text{-}205}$Tl	n, n′	4	(*d*)	0.76	2.35	10.2
		5	(*d*)	0.81	3.35	10.6
		6	(*d*)	0.80	4.35	12.2
		7	(*d*)	0.78	5.35	14.3
^{205}Pb	p, n	16	(*g*)	0.71	9.50	24.7
		16	(*g*)	0.71	10.50	26.6
^{206}Pb	n, n′	7	(*d*)	0.92	4.68	10.3
^{209}Bi	n, n′	5	(*d*)	0.68	3.19	13.4
		7	(*d*)	1.05	5.19	8.9

(*a*) D. L. ALLAN: *Nuclear Phys.*, **24**, 274 (1961).
(*b*) L. COLLI, G. M. MARCAZZAN, F. MERZARI, P. G. SONA and P. TOMAŠ: *Nuovo Cimento*, **20**, 928 (1961).
(*c*) L. COLLI, I. IORI, G. M. MARCAZZAN, F. MERZARI, A. M. SONA and P. G. SONA: *Nuovo Cimento*, **17**, 634 (1960).
(*d*) *Thesis* by G. B. THOMSON (Advisor L. CRANBERG), Los Alamos Scientific Labor. (1960).
(*e*) P. V. MARCH and W. T. MORTON: *Phil. Mag.*, **3**, 143 (1958).
(*f*) Wash. 1026 (1959), p. 59.
(*g*) P. C. GUGELOT: *Phys. Rev.*, **81**, 51 (1951).
(*h*) Wash. 1026 (1959), p. 56.

We can reach the conclusion that the spectra collected from (p, n), (n, n′) and (n, p) reactions can be used to build a consistent set of a parameters and that the corresponding « reduced spectra » can represent the dependence of the level densities *vs.* U below 10 MeV.

5. – (n, p) cross-sections at 14 MeV.

In paper II we showed that all the cross-sections of (n, p) reactions for medium nuclei at 14 MeV known at that time can be shown to be in good agreement with the statistical model.

Before comparing the values of cross-sections with the evaporation model it should be a good rule to know the spectra of the particles emitted and the angular distribution of every particular reaction studied, to be sure that spectra and angular distribution are in agreement with the model; if they are not, it will be necessary to subtract in some way the contribution of direct effects. In the (n, p) reactions for medium nuclei (A from about 20 to 60), at 14 MeV, both the shapes of the spectra and the angular distributions of protons show the presence of direct effects, but either these effects are negligible or can be easily subtracted.

Bearing in mind these considerations we made in paper II a comparison between cross-sections for nuclei ranging between Mg and Sb with the evaporative model, introducing, as a first approximation, formula (7) for the density of nuclear levels, T being constant. The T values had been obtained from experimental (n, p) spectra. In particular it was shown in (II) how the introduction of the pairing energy increases by $\simeq 10$ times the calculated values of $\sigma(\mathrm{n}, \mathrm{p})/\sigma(\mathrm{n}, \mathrm{n}')$ for even A nuclei with respect to odd A nuclei, in agreement with experimental results. The nuclear radius was chosen as $R = 1.6 A^{\frac{1}{3}}$ fermi from a best fit consideration.

More extended calculations have been made by ALLAN [9]; the values of 27 cross-sections obtained by him through measurements of spectra of the protons are compared with the evaporation model, using three different formulae for the level densities.

In all cases he uses radius $R = 1.5 A^{\frac{1}{3}}$ fermi.

At first he found a good agreement between calculations and experiments, utilizing the level density formula (27) of LANG and LE COUTEUR [5] which is quite similar to formula (1). The values of a are assumed to be given by $a = A/8$; these values are not quite in good agreement with the a values deduced by the experimental spectra of protons (see Table II). ALLAN also showed how the use of formula (7) was not in good agreement (using r_0 1.5) because this formula tends to enhance the neutron emission. We can, on the

other hand observe, to explain the agreement found in paper II using formula (7), that the choice of $r_0 = 1.6$ enhances even the proton emission.

In order to complete the situation it is interesting to repeat the calculations following formula (1) using the a values of Fig. 1.

We have calculated the ratio between $\sigma(\mathrm{n}, \mathrm{p})$ and $\sigma(\mathrm{n}, \mathrm{n}')$ using the formula

$$\frac{\sigma(\mathrm{n}, \mathrm{p})}{\sigma(\mathrm{n}, \mathrm{n})} = \frac{\int_0^{\varepsilon_{\mathrm{p\,max}}} \varepsilon \sigma_{c\mathrm{p}} \exp\left[2\sqrt{aU}\right]/(U+t)^2 \, \mathrm{d}\varepsilon}{\int_0^{\varepsilon_{\mathrm{n\,max}}} \varepsilon \sigma_{c\mathrm{n}} \exp\left[2\sqrt{aU}\right]/(U+t)^2 \, \mathrm{d}\varepsilon}, \tag{8}$$

where: $\varepsilon_{\mathrm{p\,max}} = E_0 + Q + \Delta(\mathrm{n}, \mathrm{p})$,

$\varepsilon_{\mathrm{n\,max}} = E_0 + \Delta(\mathrm{n}, \mathrm{n}')$,

$U = \varepsilon_{\max} - \varepsilon$,

the meaning of the various symbols being evident. The values of a are taken from Table I or interpolated.

Values of σ_c are assumed, as stated in Section 2 above, to be with radius parameter 1.5 fermi for protons and 1.4 for neutrons. Q values have been calculated from Wapstra's tables [15,16].

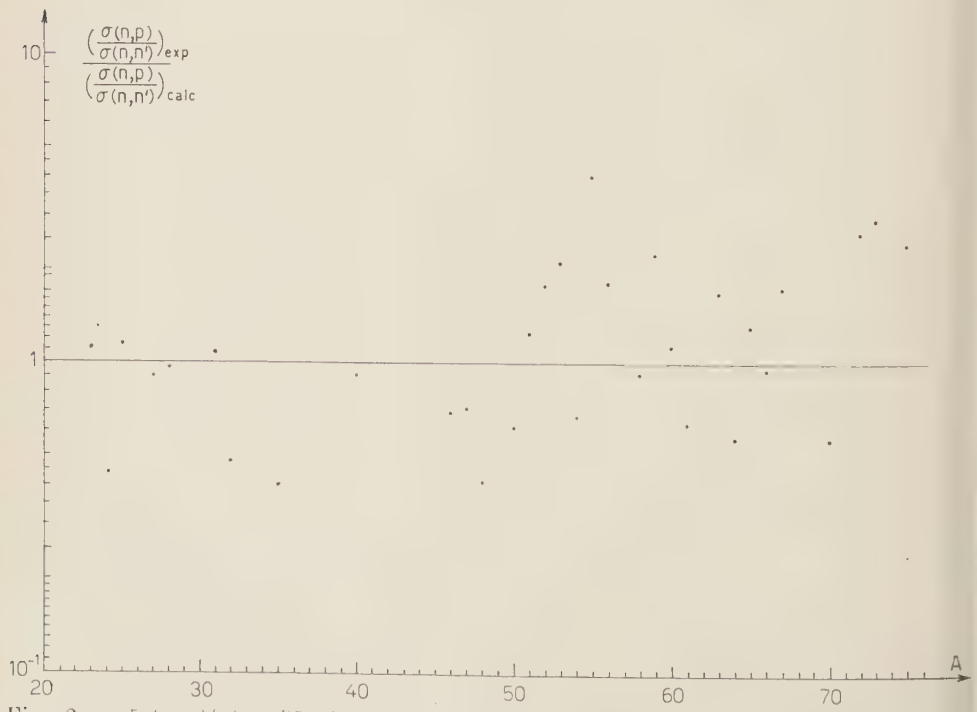

Fig. 2. – $[\sigma(\mathrm{n}, \mathrm{p})/\sigma(\mathrm{n}, \mathrm{n}')]_{\mathrm{exp}}/[\sigma(\mathrm{n}, \mathrm{p})/\sigma(\mathrm{n}, \mathrm{n}')]_{\mathrm{calc}}$ as function of mass number A for $20 < A \leqslant 75$.

Values of $\Delta(n, p)$ and $\Delta(n, n')$ have been taken from CAMERON [4].

The calculations have been performed electronically and the calculated values of the ratio $\sigma(n, p)/\sigma(n, n')$ have been compared with the experimental ratio.

We have considered a new set of experimental $\sigma(n, p)$ values obtained by averaging over all the known results; in particular, direct effects have been subtracted in lighter nuclei following the results of COLLI and co-workers [19,20] and when the direct cross-sections were known. For medium A nuclei $40 < A < 60$ direct effects are negligible and we have considered the total $\sigma(n, p)$ as due to evaporation [21].

The ALLAN [9] results obtained from measurements at backward angles have been also included.

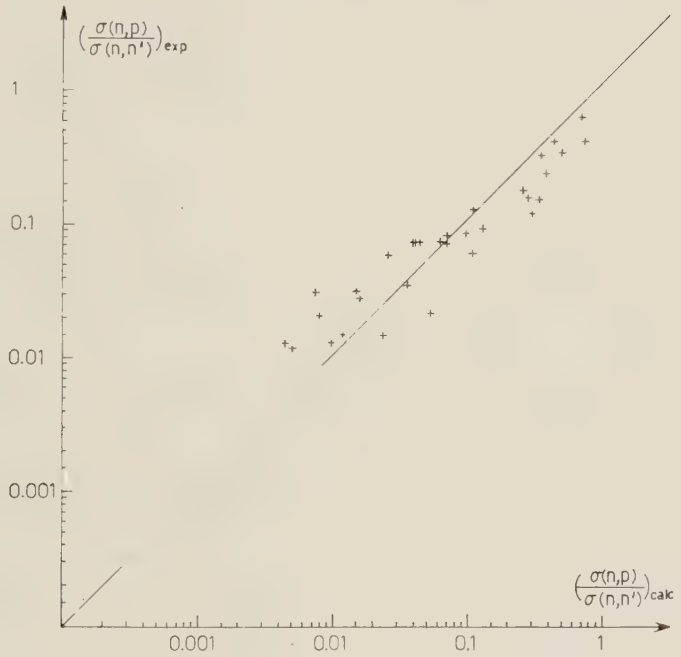

Fig. 3. – $[\sigma(n, p)/\sigma(n, n')]_{exp}$ as function of $[\sigma(n, p)/\sigma(n, n')]_{calc}$ for the same nuclei as in Fig. 2.

$\sigma(n, n')$ at 14 MeV have been obtained from total anelastic cross-sections [22] minus (n, p) cross-sections. (n, α) cross-sections have not been introduced, being negligible.

[21] L. COLLI, I. IORI, S. MICHELETTI and M. PIGNANELLI: *Evaporation Mechanism and Direct Effect in* n, p *Reactions on Medium Weight Nuclei*, to be published on *Nuovo Cimento*.

[22] M. H. MACGREGOR, W. P. BALL and R. BOOTH: *Phys. Rev.*, **108**, 726 (1957).

TABLE III.

Target nucleus	$\sigma(n, p)_{exp}$ (mb)	Reference	$\sigma(n, n')_{exp}$ (mb)	$\left(\frac{\sigma(n, p)}{\sigma(n, n')}\right)_{exp}$	E_0 (MeV)	$Q(n, p)$ (MeV)	$\Delta(n, p)$ (MeV)	$\Delta(n, n')$ (MeV)	a (MeV^{-1})	$\left(\frac{\sigma(n, p)}{\sigma(n, n')}\right)_{calc}$	$\frac{(\sigma(n, p)\ \sigma(n, n'))_{exp}}{(\sigma(n, p)\ \sigma(n, n'))_{calc}}$
^{23}Na	57	(*a*)	793	0.072	14	— 3.597	2.25	2.48	3.80	0.0645	1.12
^{24}Mg	114	(*a*, *b*)	756	0.151	14.05	— 4.734	0	4.58	3.48	0.34	0.44
^{25}Mg	67	(*a*)	813	0.0824	14	— 3.022	2.17	2.10	3.70	0.0719	1.15
^{27}Al	72	(*a*, *c*)	840	0.086	14	1.835	2.10	2.17	4.90	0.096	0.90
^{28}Si	243	(*a*)	717	0.338	14	— 3.857	0	4.30	5.54	0.35	0.965
^{31}P	120	(*a*, *d*, *e*)	920	0.13	14.1	— 0.694	2.13	1.74	5	0.1203	1.08
^{32}S	301	(*a*, *b*, *f*)	771	0.39	14.06	0.926	0	3.28	4.93	0.796	0.48
^{35}Cl	125	(*a*)	1005	0.12	14	0.615	1.54	1.75	5.4	0.301	0.40
^{40}Ca	485	(*a*, *g*)	755	0.64	14.25	0.539	0	3.23	7.36	0.70	0.91
^{46}Ti	203	(*a*)	1117	0.18	14	— 1.583	0	3.14	6.85	0.26	0.69
^{47}Ti	112	(*a*)	1218	0.092	14	0.183	1.29	1.73	7.65	0.13	0.71
^{48}Ti	29	(*a*)	1311	0.022	14	3.208	0	3.02	8.35	0.054	0.41
^{51}V	20	(*a*)	1370	0.015	14	1.683	1.73	1.47	8.55	0.012	1.25
^{50}Cr	265	(*a*)	1105	0.24	14	0.255	0	2.73	10.17	0.386	0.62
^{52}Cr	96	(*a*, *h*)	1304	0.074	14	— 3.211	0	2.91	8.06	0.0413	1.79
^{53}Cr	44	(*a*)	1366	0.032	14	— 1.74	1.32	1.44	8.28	0.0151	2.10
^{55}Mn	43	(*a*)	1387	0.031	14	— 2.038	1.44	1.32	8.66	0.0076	4.00
^{54}Fe	361	(*a*, *i*, *r*)	1059	0.34	13.83	0.094	0	2.92	7.70	0.517	0.66

^{61}Ni	22	(n)	1478	0.015	14.8	— 0.507	1.44	1.37	8.99	0.024	0.625
^{63}Cu	106	(a, q, r)	1414	0.075	14	0.716	1.37	1.44	12.06	0.045	1.67
^{65}Cu	19	(d)	1521	0.013	14.1	— 1.314	1.37	1.46	10.31	0.0097	1.30
^{64}Zn	212	(a, n, s, u, t)	1318	0.161	14	0.209	0	2.53	8.6	0.284	0.566
^{66}Zn	53	(a, l, n, t)	1497	0.035	14	1.847	0	2.55	10.95	0.037	0.94
^{67}Zn	43	(a, v)	1517	0.028	14	0.211	1.52	1.09	11.57	0.0163	1.72
^{70}Ge	93	(t)	1497	0.062	14	— 0.867	0	2.88	10.64	0.11	0.56
^{72}Ge	34	(t, v)	1576	0.021	14	— 3.21	0	2.87	12.06	0.0079	2.60
^{73}Ge	21	(t, v)	1609	0.013	14	— 0.77	1.47	1.36	13.4	0.00453	2.86
^{75}As	19	(t)	1621	0.012	14.1	— 0.4	1.36	1.47	16.5	0.005	2.40

(*a*) D. L. Allan: *Nuclear Phys.*, **24**, 274 (1961).
(*b*) L. Colli, I. Iori, G. M. Marcazzan, F. Merzari, A. M. Sona and P. G. Sona: *Nuovo Cimento*, **17**, 634 (1960).
(*c*) G. Brown, G. C. Morrison, H. Muirhead and W. T. Morton: *Phil. Mag.*, **2**, 785 (1957).
(*d*) S. G. Forbes: *Phys. Rev.*, **88**, 1309 (1952).
(*e*) J. A. Grundle, R. L. Henkel and B. L. Perkins: *Phys. Rev.*, **109**, 425 (1958).
(*f*) L. Allen jr., W. A. Biggers, R. J. Prestwood and R. K. Smith: *Phys. Rev.*, **107**, 1363 (1957).
(*g*) L. Colli, U. Facchini, I. Iori, G. M. Marcazzan, M. Pignanelli and A. M. Sona: *Nuovo Cimento*, **7**, 400 (1958).
(*h*) B. D. Kern, W. E. Thomson and J. M. Ferguson: *Nuclear Phys.*, **10**, 226 (1959).
(*i*) P. V. March and W. T. Morton: *Phil. Mag.*, **3**, 143 (1958).
(*j*) P. V. March and W. T. Morton: *Phil. Mag.*, **3**, 577 (1958).
(*l*) S. Yasumi: *Journ. Phys. Soc. Japan*, **12**, 443 (1957).
(*m*) G. W. McClure and D. W. Kent: *Journ. Franklin Institute*, **260**, 238 (1959).
(*n*) I. L. Preiss and R. W. Fink: *Nuclear Phys* , **15**, 326 (1960).
(*o*) I. Kumabe and R. W. Fink: *Nuclear Phys.*, **15**, 316 (1960).
(*p*) K. M. Purser and E. W. Titterton: *Austral. Journ. Phys.*, **12**, 103 (1959).
(*q*) L. Colli, R. Facchini, I. Iori, G. M. Marcazzan and A. M. Sona: *Nuovo Cimento*, **13**, 730 (1959).
(*r*) D. L. Allan: *Nuclear Phys.*, **10**, 348 (1959).
(*s*) Wash. 191 (1956), AEC.
(*t*) Cited in F. L. Ribe in *Fast Neutron Physics*, cap. V: *Neutron induced reactions*, to be published.
(*u*) A. H. Armstrong and L. Rosen: *Nuclear Phys.*, **19**, 40 (1960).
(*v*) F. N. Levkovski: *Sov. Phys. JETP*, **6**, 1174 (1958).

TABLE IV.

Target nucleus	$\sigma(n, p)$ (mb)	Reference	$\sigma(n, n')$ (mb)	$\left(\frac{\sigma(n,p)}{\sigma(n,n')}\right)_{exp}$	E_0 (MeV)	$Q(n, p)$ (MeV)	$\Delta(n, p)$ (MeV)	$\Delta(n, n')$ (MeV)	a (MeV $^{-1}$)	$\left(\frac{\sigma(n,p)}{\sigma(n,n')}\right)_{exp}$	$\frac{(\sigma(n,p)/\sigma(n,n'))_{exp}}{(\sigma(n,p)/\sigma(n,n'))_{calc}}$
^{103}Rh	11	(a)	1849	0.006	14	0.03	1.28	1.22	14.5	0.0024	2.5
^{109}Ag	11.7	(b)	1888	0.0062	14.25	0.32	1.38	1.36	17.26	0.0008	7.85
^{111}Cd	15	(a)	1895	0.0079	14	— 0.27	1.3	1.38	17.8	0.00072	11
^{112}Cd	10	(a)	1910	0.0052	14	3.25	0	2.68	17.49	0.000303	17.16
^{113}Cd	7.2	(a)	1917.8	0.00375	14	— 1.21	1.29	1.38	20.57	0.000113	33.2
^{115}In	15.5	(b)	1919.5	0.008	14.5	— 0.67	1.38	1.29	21.80	0.00017	47.06
^{127}I	11.7	(b)	2003.3	0.00584	14.5	0.098	1.04	1.2	20.98	$5.2 \cdot 10^{-4}$	11.23
^{136}Ba	38.3	(b)	2041.7	0.0187	14.5	— 1.79	0	2.18	15.14	$8.87 \cdot 10^{-4}$	21.1
^{138}Ba	2.2	(b)	2087.8	0.00105	14.5	4.04	0	1.67	14.95	$2.5 \cdot 10^{-5}$	42
^{139}La	2.33	(b)	2092.67	0.00111	14.5	1.6	1.13	0.54	14.82	$4.86 \cdot 10^{-5}$	22.84
^{140}Ce	12.1	(b)	2087.9	0.0058	14.5	2.99	0	1.75	16	$7.06 \cdot 10^{-5}$	80
^{142}Ce	9.4	(b)	2110.6	0.00445	14.5	4.19	0	1.81	16.61	$1.04 \cdot 10^{-5}$	428
^{142}Nd	13.5	(b)	2106.5	0.00641	14.5	— 1.37	0	1.97	16.61	$6 \cdot 10^{-4}$	10.68
^{143}Nd	11.5	(b)	2108.5	0.00545	14.5	0.15	0.6	1.43	17.46	$6.3 \cdot 10^{-4}$	8.7

^{183}W	8	(*a*)	2377	0.003	14.5	— 0.28	0.91	1.23	26.51	$1.18 \cdot 10^{-5}$	254
^{184}W	4.6	(*a*, *b*)	2385.4	0.0019	14.5	2.69	0	2.14	24.35	$4.2 \cdot 10^{-6}$	452
^{186}W	2.9	(*b*)	2402	0.0012	14.5	— 3.44	0	2.06	27.3	$4.9 \cdot 10^{-7}$	2449
^{187}Re	3.93	(*b*)	2406	0.0016	14.5	0.52	1.23	0.83	24.69	$2.7 \cdot 10^{-6}$	592
^{193}Ir	2.7	(*b*)	2447.3	0.0011	14.5	0.34	0.85	0.66	24.5	$4.67 \cdot 10^{-6}$	235
^{194}Pt	3.92	(*b*)	2451	0.0016	14.5	1.44	0	1.64	24.99	$8.64 \cdot 10^{-6}$	185
^{195}Pt	2.91	(*b*)	2457	0.0011	14.5	1.45	0.61	0.98	22.66	$2.06 \cdot 10^{-7}$	534
^{197}A	2.42	(*b*)	2472.6	0.001	14.5	0.04	0.98	0.61	21.98	$8.9 \cdot 10^{-6}$	112
^{200}Hg	3.63	(*b*)	2496.4	0.00145	14.5	1.52	0	1.33	19.01	$1.406 \cdot 10^{-5}$	103.1
^{201}Hg	2.12	(*b*)	2498	0.00085	14.5	0.72	0.9	0.72	17.9	$8.6 \cdot 10^{-6}$	98.8
^{205}Tl	6.8	(*b*)	2523	0.0026	14.5	0.87	0.72	0.52	18.75	$5 \cdot 10^{-6}$	522
^{209}Bi	1.33	(*b*)	2558.7	0.00052	14.5	0.16	0.80	0.81	11.19	$1.8 \cdot 10^{-4}$	2.88
^{235}U	1.86	(*b*)	2738	0.00068	14.5	0.61	0.64	0.81	28.87	$2.9 \cdot 10^{-7}$	2345
^{237}N	1.3	(*b*)	2749	0.000473	14.5	0.27	0.81	0.58	28.49	$7.6 \cdot 10^{-7}$	622
^{239}P	3	(*b*)	2762	0.0011	14.5	0.06	0.55	0.69	36.25	$2.26 \cdot 10^{-7}$	4867

(*a*) F. L. Ribe in *Fast Neutron Physics*, cap. V: *Neutron induced reactions*, to be published.
(*b*) R. F. Coleman, B. E. Hawker, L. P. O'Connor and J. L. Perkin: *Proc. Phys. Soc.*, **73**, 215 (1959).

Table III collects all the data related to such calculations and to the comparison. Fig. 2 reports the ratio

$$\frac{(\sigma(\mathrm{n,\,p})/\sigma(\mathrm{n,\,n'}))_{\mathrm{exp}}}{(\sigma(\mathrm{n,\,p})/\sigma(\mathrm{n,\,n'}))_{\mathrm{calc}}},$$

as a function of the mass number A.

The agreement shown in Fig. 2 is of the same kind as the one found in paper II and the one found by ALLAN.

Most of the experimental results agree more or less with the theoretical ones; for a group of nuclei (the same nuclei in all cases) the experimental proton emission is bigger by a factor of up to $2 \div 4$ than the theoretical one.

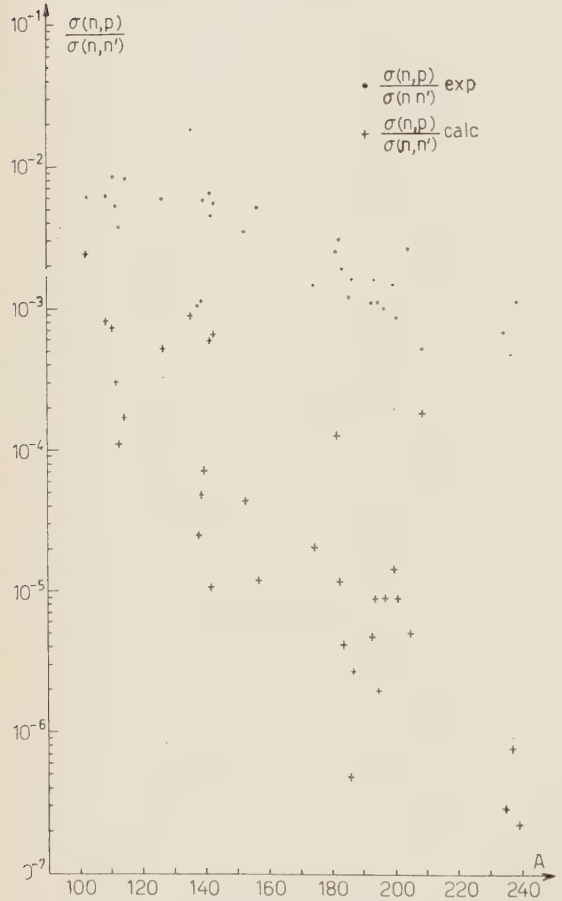

Fig. 4. - $[\sigma(\mathrm{n,\,p})/\sigma(\mathrm{n,\,n'})]_{\mathrm{e\ p}}$ and $[\sigma(\mathrm{n,\,p})/\sigma(\mathrm{n,\,n'})]_{\mathrm{calc}}$ as functions of mass number A for $90 < A < 240$.

It is not possible, however, to choose among the different sets of parameters: the spectra are not sufficiently known to permit such a choice and the same can be said for the barrier penetrations.

For the sake of coherency we should say that at least as a first approximation the present calculations should be preferred.

In making this choice, due regard was given to the consistency of the sets of experiments discussed in Sections 3, 4 and in the present section.

Fig. 3 represents the results in a different way: $(\mathrm{(n,\,p)/\ (n,\,n')})_{\mathrm{exp}}$ as function of $(\sigma(\mathrm{n,\,p})/\sigma(\mathrm{n,\,n'}))_{\mathrm{theor}}$: it is quite interesting to note how the biggest discrepancies ar found with the smallest values of the ratio $\sigma(\mathrm{n,\,p})/\sigma(\mathrm{n,\,n'})$; here the experimental values are about twice the calculated ones; it is to be observed that the direct effects for these small cross-sections can be relatively much more intense.

The calculations and the comparison have been extended for nuclei with $Z > 40$. Table IV contains the data relative to these nuclei. The calculated and the experimental values of $\sigma(n, p)/\sigma(n, n')$ for the various nuclei are shown in Fig. 4 as functions of A.

For these nuclei the experimental results are generally of a greater order of magnitude than the calculated ones, which shows that for these nuclei the direct effects are determinant. Practically the whole $\sigma(n, p)$ for these nuclei can be attributed to these effects.

6. – Conclusions.

The consistence of the whole group of experimental results discussed under the evaporation rules gives an experimental basis to the evaporation model and at the same time to the description of the excited nuclear levels by formula (1).

The evaporated energy spectra in the medium energy reactions studied do not correspond necessarily to a compound nucleus in a statistical equilibrium.

In fact at the excitation energies ranging from 10 to 20 MeV the width of levels, Γ, is assumed to be much greater than the level spacing D: $\Gamma \gg D$ and following the arguments of V. WEISSKOPF [1] the particles are emitted mostly before equilibrium is reached.

However in order to apply the « evaporation model » *i.e.* formula (6) the equilibrium is not necessary but the independence of entrance channels from exit channels is required and this independence is possible without equilibrium.

The values of g_0 have to be interpreted as « average densities » of the nucleons near the top of the energy distribution; of particular interest is the fact that these densities change in a regular way showing significant shell effects. The meaning of deep minima at $A \simeq 90$, 140, 210 corresponding to magic neutron nuclei is however not clearly understood [3,6].

The greater values of a correspond however to the highly deformed nuclei indicating for these nuclei a more dense population of nucleons at the top of the Fermi distribution.

Particularly, the set of parameters obtained will be useful in extending the calculation to other experiments and to more complicated situations.

* * *

We wish to express our thanks to Dr. T. ERICSON and Dr. D. L. ALLAN for useful discussions and we thank Dr. L. CRANBERG for sending us detailed results and for discussions.

RIASSUNTO

Il modello statistico delle reazioni nucleari è stato sviluppato da qualche decina di anni soprattutto da V. Weisskopf. Tuttavia non si ha ancora una chiara comprensione della situazione sperimentale riguardante le reazioni nucleari alle basse ed alle medie energie. L'interpretazione è complicata dal fatto che spesso le reazioni avvengono secondo altri meccanismi, per esempio effetti diretti. In questo lavoro si cerca di mostrare la possibilità di spiegare un certo gruppo di esperienze con un modello statistico. Le esperienze discusse sono: *a*) misure di risonanza per neutroni lenti; *b*) spettri energetici delle particelle emesse nelle reazioni (n, p) (n, n′) e (p, n) per energie incidenti tra 4 e 16 MeV; *c*) sezioni d'urto di reazioni n, p ed n, n′ a 14 MeV. Da queste esperienze è possibile ottenere una tavola di valori consistenti di a, parametro della formula della densità di livelli nucleari.

On a G. M. Counting Rate Increase Recorded at Balloon Altitude.

D. Brini, M. Galli and G. L. Tabellini

Istituto di Fisica dell'Università - Bologna

U. Ciriegi and A. Gandolfi

Commissione Ricerche Spaziali del C.N.R. - Sezione di Bologna

(ricevuto il 12 Ottobre 1961)

Summary. — A fast pulse of G.M. counts has been recorded in a balloon flight, near Bologna, under 120 $g \cdot cm^{-2}$ of residual atmosphere, between 0712 UT and 0714 UT on July 18, 1961, during a period of relatively high solar activity. In the interval of about two minutes the counting rose and decayed again to the normal value, reaching a maximum about 50% higher than the value corresponding to the absence of solar activity. Solar geophysical events of this period and the possible causes of our counting burst are here considered. Because of the peculiarity of the event it is difficult to state the type of particle responsible for our event. Among all the possible causes, the least improbable are that of solar photons with energies in the range of about 1 MeV up to a few 100 MeV, or that of solar protons with energies in the range (4 ÷ 8) GeV.

1. – Results.

During a recent period of a relatively high solar activity some balloons were launched up to the burst altitude, in order to test the Cosmic Ray intensity and to look for any variation.

The equipment used was composed essentially of some G.M. counters of total area of 24 cm^2, of a baroswitch and of a telemetering system elsewhere described ([1,2]). Pressure and G.M. total counts were recorded every 15 seconds

([1]) D. Brini, U. Ciriegi, A. Gandolfi and G. L. Tabellini: *Suppl. Nuovo Cimento*, **17**, 277 (1960).

([2]) D. Brini, U. Ciriegi, M. Galli, A. Gandolfi and G. L. Tabellini: *Ricerca scientifica*, **1**, 1 (1961).

intervals. During the flight on July 18, 1961, whose measurement period lasted from 0625 UT to 8000 UT, a very short count burst was detected between 0712 UT and 0714 UT, at an altitude corresponding to about 120 $g \cdot cm^{-2}$ of residual atmosphere while the sun was 34° 33′ above the horizon. The counting behaviour of the remaining flight time was quite similar to that of many other balloon flights, made in the same period, when the solar activity level was relatively low.

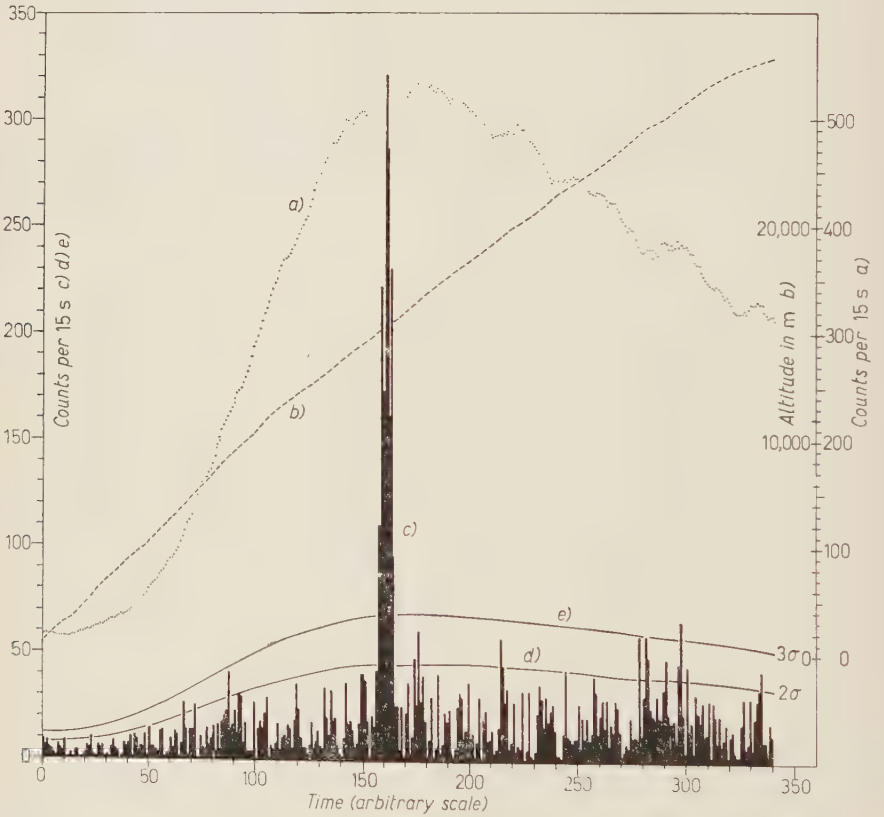

Fig. 1.

The results of our measurements have been summarized in Fig. 1, where we represent, *vs.* time:

a) the behaviour of the 11-term moving average of the 15 s series of G.M. made for the whole measurement period, except readings in the period 0712–0714 UT;

b) the altitude behaviour;

c) the absolute values of the deviation of each individual term from the corresponding term of the moving average;

d) *e*) the behaviours respectively of 2 and 3 standard errors, deduced from the 11-term moving average.

It can clearly be seen that the count burst has a sudden rise and a sudden decrease and reaches a maximum of about 150% the normal value.

We have looked for the possible causes of instrumental errors and of misfunctioning but nothing has arisen to justify such fast variations. Therefore we believe there is a high probability that this event is true.

2. – Probable correlations.

As mentioned above, at the moment of the balloon launch we were aware of the high solar activity.

a) A class 3 flare was observed at 0505 UT ([3,4]) although neither beginning nor end was seen. A class 2+ flare was observed between 0754 UT and 0837 UT. Another class 3+ flare was observed between 0921-UT and 1330 UT which has been associated to a strong PCA and to an injection of Cosmic Ray particles recorded at ground and balloon altitudes ([3,5,6]).

All these flares were observed in the same point of the solar disk.

We should mention that the same reference ([3]) reports that the « flare patrol » was not working between 0030 UT and 0750 UT.

b) Furthermore a type IV storm of solar radionoise emissions superposed to many type III storms was recorded between 1305 UT and 1800 UT in the (25÷41) MHz band ([5]). Observations of solar radionoise at 20, 545, 2 980 and at 9 100 MHz at Nera show no special events in the period 0510 UT–0800 UT ([7,8]).

c) The Earth's magnetic field recorded at the Aquila Observatory ([9]), slightly perturbed during the early hours of July 18, ($\pm 50\ \gamma$), showed a magnetic storm beginning at about 1100 UT.

([3]) *Solar Geophysical Data*, part B, CRPL-F 204 (National Bureau of Standards).

([4]) Map of the Sun: 1961 July 18, Fraunhofer Inst.

([5]) Preliminary Report of Solar Activity: TR 516, High Altitude Observatory, Boulder, Colorado.

([6]) Private communication (Kiruna Geophysical Observatory).

([7]) Private communication (Nera Observatory).

([8]) Solar Geoph. Data: July 1961, Netherlands P.T.T.

([9]) Private communication from Istituto Nazionale di Geofisica.

d) The riometer recording at the Microwave Center of Florence [10], having a quiet behaviour until the calibration time, beginning at 0652 UT, showed a certain degree of absorption when at 0730 UT it started recording again.

e) Cosmic Ray intensity, recorded every 15 minutes by scintillation monitors placed in this Institute with 450 $g \cdot cm^{-2}$ of absorber and without absorber, and the neutron monitor data at Deep River [3], showed no variations greater than some per mill in the interval 0700–0800 UT.

The above picture of solar-geophysical events around the period of our balloon flight does not allow us to make any correlation, but helps us in the discussion on the possible causes of our burst of G.M. counts.

3. – Discussion.

Taking into account the picture of the solar geophysical phenomena reported above, it is possible to reject some causes of our event in the following discussion.

a) Artificial radioactivity at 120 $g \cdot cm^{-2}$.

In our case no increase in the atmospheric radioactivity or nuclear explosions [11] could be correlated with our event.

This cause has to be considered because in the past similar events have been recognized as due to artificial radioactivity [12].

b) Electrons with energies smaller than 250 MeV and protons with energies smaller than 600 MeV, because they cannot reach 120 $g \cdot cm^{-2}$.

c) Electrons with energies greater than 4 GeV, corresponding to the geomagnetic cut-off at the latitude of Bologna because, in this case, our ground monitors should have recorded a detectable increase in the counting rate.

d) Primary protons of energies greater than about 8 GeV.

In fact, because of the multiplicity factors at 120 $g \cdot cm^{-2}$ and at ground, they certainly should have been recorded even at ground.

With protons of these energies the increase of 50% at 120 $g \cdot cm^{-2}$ should correspond to an increase, of our ground detectors, greater than 1.5%/15 minutes, that is the sensitivity limit due to the time resolution and to the statistics ($3 \cdot 10^5$ counts/h).

[10] Private communication.

[11] Private communication from Health Physics Lab. of Bologna Univ.

[12] H. T. MANTIS and J. R. WINCKLER: *Journ. of Geoph. Res.*, **65**, 3515 (1960).

e) Solar neutrons having a power law differential energy spectrum, with a negative exponent smaller than 1.5 and higher than 2.5. In fact, in this case, the burst of G.M. pulses should be more spread out in time. Such a conclusion can be drawn taking into account the neutron collision mean free path for production of protons with energies greater than the G.M. cut-off, the absorption mean free path of the primary neutrons and the neutron decay between the Sun and the Earth.

In addition, for the exponent smaller than 1.5, the increase should have been detected even at ground.

f) Solar photons and auroral photons with energies smaller than 0.5 MeV.

It is known that X-rays of such energies may be associated with auroral activity ([13,14]). But we have to exclude them because they cannot reach 120 $g \cdot cm^{-2}$.

g) Solar photons of energies greater than a few GeV.

In this case we should have a burst of secondary particles at ground.

The possibilities so far discarded have been discarded mainly from the instrumental point of view.

Strictly speaking, because of the rarity of the event and the poor knowledge of the interplanetary and solar physics, none of the remaining possible causes can be excluded.

However, many of them are difficult to maintain as, for example, that of the primary electrons or protons of energies smaller than the geomagnetic cut-off, entering the atmosphere through a sudden and strong deformation of the Earth's magnetic field.

Solar neutrons having a differential energy spectrum with an exponent in the range $1.5 \div 2.5$ could explain the temporal shape of our burst of G.M. pulses. But it is difficult to think of a generation mechanism for neutrons in the Sun not associated with charged particles not detectable on the Earth.

As far as we know about solar physics it is not impossible to admit, as a cause of our event, photons of energies in the range from 0.5 MeV up to some 100 MeV, or protons in the range $(4 \div 8)$ GeV. This conclusion is not inconsistent with the arguments of KORFF and HAYMES ([15]) and of PETERSON and WINCKLER ([16]) in connection with the discussion of events that have many aspects similar to ours.

([13]) K. A. ANDERSON: *Phys. Rev.*, **111**, 1397 (1958).
([14]) K. A. ANDERSON: *Journ. of Geoph. Res.*, **65**, 551 (1960).
([15]) S. A. KORFF and R. C. HAYMES: *Journ. of Geoph. Res.*, **65**, 3165 (1960).
([16]) L. PETERSON and J. R. WINCKLER: *Phys. Rev. Lett.*, **1**, 205 (1958).

RIASSUNTO

In un volo di pallone, effettuato il 18 Luglio 1961 durante un periodo di attività solare relativamente forte, è stato rivelato un impulso di conteggi fra le ore 0712 UT e le ore 0714 UT, con contatori G.M. Questo evento, corrispondente ad un aumento del conteggio di circa il 50% sul valore normale relativo a mancanza di attività solare, è avvenuto ad una quota di circa 120 $g \cdot cm^2$ di atmosfera residua. Sono stati presi in considerazione i fenomeni geosolari avvenuti nello stesso periodo di tempo e le possibili cause di questo evento. A causa della peculiarità dell'evento è difficile definire il tipo di particelle responsabili dell'evento stesso. Fra tutte le cause possibili le meno improbabili sono rappresentate da fotoni solari di energie comprese fra circa 1 MeV e poche centinaia di MeV, o da protoni solari di energie da 4 a 8 GeV.

Characteristics of Λ^0 Produced in Carbon Nuclei by 1.3 GeV π^-.

R. Cester (*)

Istituto Nazionale di Fisica Nucleare - Sezione di Torino
University of Princeton - Princeton, N. J.

(ricevuto il 15 Novembre 1961)

Summary. — The main purpose of this experiment was to derive information on the polarization of Λ^0 produced in carbon from the measurement of the decay asymmetries. This was done on 238 events originated by π^- of 1.3 and 1.2 GeV. The up-down asymmetry measured with respect to the plane $\boldsymbol{P}_{\pi\,\mathrm{i.c}} \times \boldsymbol{P}_{\Lambda^0}$ is $\overline{\alpha P}_\theta = -0.018 \pm 0.107$; the asymmetry (left-right) measured with respect to the plane $(\boldsymbol{P}_{\pi\,\mathrm{inc}} \times \boldsymbol{P}_{\Lambda^0}) \times \boldsymbol{P}_{\Lambda^0}$ is also very small $\overline{\alpha P}_\xi = +0.01 \pm 0.11$. This implies that the Λ^0 we measure has not, in most cases, been directly produced in the interaction of a 1.3 (or 1.2) GeV π^- with a nucleon of the carbon nucleus. Secondary strange particles are found to play an important role in the depolarization process. The forward-backward asymmetry with respect to the Λ^0 laboratory line of flight has also been measured. The result is found to be compatible with zero when the effect of scanning bias has been taken into account. From the analysis of the π^- stars from which a Λ^0 is emitted, information on the frequency of the various Λ^0 production channels is derived. In particular we set an upper limit to the cross-section for reaction $\Sigma^- + \mathrm{p} \to \Lambda^0 + \mathrm{N}$, $\sigma_{\Sigma^-\Lambda^0} \leqslant (38 \pm 24)$ mb. From the study of missing energy and momentum in two V events the lower limit to the frequency of secondary reactions is set to be 50%.

1. – Introduction.

In recent years the angular distribution of the particles originated from the decay of hyperons produced in hydrogen has been studied in order to detect parity non-conservation in weak interactions.

It was indeed pointed out by Lee, Yang *et al.* in 1957 [1] that if strange

(*) Present address: Istituto Nazionale di Fisica Nucleare, Sezione di Torino.

[1] T. D. Lee, J. Steinberger, G. G. Feinberg, P. K. Kabir and C. N. Yang: *Phys. Rev.*, **106**, 1367 (1957).

particle decay interactions are not parity-conserving, the particles from hyperon decay could be asymmetrically emitted with respect to the direction of the hyperon spin. The expected angular distribution has the form $1 + \alpha \bar{P} \cos\theta$ where θ is the angle between the decay particle momentum in the c.m. system and the hyperon spin direction, α is the asymmetry parameter defined as:

$$\alpha = 2 \operatorname{Re}(A^* B) / (|A|^2 + |B|^2),$$

A, B amplitudes for decay into s and p final states of the π-nucleon system and P is the average hyperon polarization.

If parity is conserved in strong interactions the Λ^0 can only be polarized along the normal to the production plane ([2]). For Λ^0 produced in hydrogen, in the process

$$\pi^- + p = \Lambda^0 + \theta^0 \tag{1}$$

the value of αP was carefully measured ([3,4]) as a function of the π^- energy [$\alpha \bar{P} = 0.4 \pm 0.1$ in our energy interval] and (at ~ 990 MeV π^- kinetic energy) as a function of the c.m. emission angle.

Independent measurements of α have been attempted; the more recent experiment gives a value ([5]) $\alpha = -.75^{-0.15}_{+0.50}$. The average value of the polarization along the normal to the production plane, for Λ^0 produced in hydrogen through reaction (1) is then very nearly 1.

Once parity non conservation in the Λ^0-decay has been established, the study of the up-down asymmetry in the Λ^0-decay can be used to analyse the degree of polarization of Λ^0 produced in reactions other than reaction (1). It seems rather useful from an operational point of view to see if complex nuclei as well as hydrogen, can be used as sources of polarized Λ^0's. In particular it seems important to carry on a polarization analysis for Λ^0's produced in carbon nuclei, since many of the operating bubble chambers are propane ones and therefore carbon events are and will be available in great number.

This paper reports on the characteristics of 145 Λ^0 produced by 1.3 GeV π^-

([2]) T. D. Lee and C. N. Yang: *Phys. Rev.*, **108**, 1645 (1957).

([3]) F. Eisler, R. Plano, A. Prodell, N. Samios, M. Schwartz, J. Steinberger, P. Bassi, V. Borelli, G. Puppi, G. Tanaka, P. Waloschek, V. Zoboli, M. Conversi, P. Franzini, I. Mannelli, R. Santangelo, V. Silvestrini, D. A. Glaser, C. Graves and M. L. Perl: *Phys. Rev.*, **108**, 1353 (1957). Also *Proc. Rochester Conf.* (1958), p. 147.

([4]) F. S. Crawford, M. Cresti, M. L. Good, K. Gottstein, E. M. Lyman, F. T. Solmitz, M. L. Stevenson and H. K. Ticho: *Phys. Rev.*, **108**, 1112 (1957).

([5]) J. Leitner, L. Gray, E. Harth, S. Lichman, J. Westgard, M. Block, B. Brucker, A. Engler, R. Gessaroli, A. Kovacs, T. Kikuchi, C. Meltzer, H. O. Cohn, W. Bugg, A. Pevsner, P. Schlein, M. Meer, N. T. Geimellini, L. Lendinara, L. Monari and G. Puppi: *Phys. Rev. Lett.*, **7**, 264 (1961).

on carbon nuclei; the polarization analysis has been carried out on a total of 259 Λ^0 including 118 events, at slightly different energies, previously measured by other laboratories.

From the polarization of Λ^0-particles as well as from the kinematics of the events and from the detailed study of the π^- star from which the Λ^0 is emitted, we deduce some information on the secondary reactions occurring in nuclear matter. In particular we set an upper limit to the frequency of the $\Sigma^- + n = \Lambda^0 + n$ conversion process.

2. – Experimental.

The experiment has been carried on making use of films obtained from the exposure of the 12 in. Columbia Propane bubble chamber to π^- of 1.3 and 1.2 GeV kinetic energy.

All of the 1.3 GeV film had been scanned twice ([6]) by the Columbia group in order to detect V shaped events, in the course of their early experiment to study strange particle production in hydrogen.

A re-examination of all the V shaped events was done by us and all the events which could be interpreted as production of Λ^0 in carbon (*) or hydrogen nuclei and which had not been previously analysed by the Columbia group, were carefully measured (**).

The data were processed on a I.B.M. 650 to get reconstruction of the event in space and momenta of the charged particles. Mean errors in the angular measurements were also computed. The events were then analysed to check their consistency with the kinematics of a Λ^0 decay and, once this was established, the direction of the Λ^0 was adjusted to fit coplanarity. The correction to be applied to the angles of the Λ^0 was due mainly to the incertainty in the measurement of the co-ordinates of the π^- interaction point from which the Λ^0 did originate. In no case the displacement of this point in the chamber exceeded 2 mm. The results of the analysis of 211 measured events are

([6]) F. Eisler, R. Plano, A. Prodell, N. Samios, M. Schwartz, J. Steinberger, P. Bassi, V. Borelli, G. Puppi, G. Tanaka, P. Waloschek, V. Zoboli, M. Conversi, P. Franzini, I. Mannelli, R. Santangelo, V. Silvestrini, D. A. Glaser, C. Graves and M. L. Perl: *Nuovo Cimento*, **10**, 468 (1958). Also *Proc. Rochester Conf.* (1958), p. 147.

(*) A Λ^0 was said to come from a carbon origin when: *a*) coming from a star from which an odd number of charged prongs and/or a charged baryon was emitted; *b*) when condition *a*) was not fulfilled but the kinematics of the event was found to be incompatible within the limits of error with that of an H-event.

(**) The measurement procedure and estimated errors on angle and momentum measurements were the same as reported in ([3]). Also the scanning efficiency was the efficiency in the H experiment since all the events measured by the Columbia group were independently reselected while re-examining the V shaped events records.

reported in Table I, together with the data concerning the 105 events measured by the Columbia group.

TABLE I.

$T_{\pi^-}=1.3$ GeV	Λ^0 from carbon		Λ^0 from (*) carbon poorly measured		θ^0 (**)	Λ^0 from wall	V^0 not identified	stars	H events		H events $K^-\pi^-\Lambda^0$
	ass. θ^0	single	ass. θ^0	single					ass. θ^0	single	
Present work	12	81	1	9	37	18	3	32	3	12	3
Columbia	27	25	2	3	—	—	—	—	26	32 (2 Σ^0)	—
Total	39	106	3	12	—	—	—	—	29	44	

(*) These events were only used for cross-section estimates.
(**) θ^0 unambiguously identified on the scan table where not measured and are not included in this figure.

The 1.2 GeV film has been completely scanned by the Pisa group which collaborated in the quoted experiment (6). A Puppi plot has been made for all hydrogen and carbon events.

The result of their analysis gave 197 Λ^0 originating in the chamber, 54 coming from a π^- interaction on an hydrogen nucleus. For 96 out of the 143 remaining events enough information was available to allow us to classify them as carbon events and to make use of them for the polarization analysis. In 43 of such events the associated θ^0 was decaying by its charged mode inside the chamber.

3. – Relative yields of Λ^0 from carbon and hydrogen nuclei.

The results obtained from the analysis of the events found in the 1.3 GeV π^- film allow a determination of the frequency of carbon events as compared to the frequency of hydrogen ones at this energy.

We will first discuss those events in which both θ^0 and Λ^0 are seen to decay through their charge mode inside the chamber (2 V events). Associated $\Lambda^0\theta^0$ production in hydrogen is due to reactions:

1) $\pi^- + p \to \Lambda^0 + \theta^0$.

2) $\pi^- + p \to \Sigma^0 + \theta^0$ followed by $\Sigma^0 \to \Lambda^0 + \gamma$.

For the 2 V events the two reactions can be separated; their relative frequency is known to be (6) $\sigma(\Lambda^0\theta^0)/\sigma(\Sigma^0\theta^0) = (0.32 \pm 0.06)/(0.24 \pm 0.06) = 1.33^{+0.78}_{-0.46}$.

Associated $\Lambda^0\theta^0$ production in carbon can be obtained through the following channels:

3) $\pi^- + \mathrm{p\,(bound)} \rightarrow \Lambda^0 + \theta^0 + (\pi)$ which can be followed by a rescattering of the particles in nuclear matter.

4) $\pi^- + \mathrm{p\,(bound)} \rightarrow \Sigma^0 + \theta^0 + (\pi)$ followed by $\Sigma^0 \rightarrow \gamma + \Lambda^0$.

5) $\pi^- + \mathrm{p\,(bound)} \rightarrow \Sigma^0 + \theta^0 + (\pi)$ followed by $\Sigma^0 + \mathrm{n} \rightarrow \Lambda^0 + \mathrm{n}$.

6) $\pi^- + \mathcal{N}\mathrm{(bound)} \rightarrow \Sigma^- + \theta^0 + (\pi)$ followed by $\Sigma^- + \mathrm{p} \rightarrow \Lambda^0 + \mathcal{N}$.

Even if both strange particles decay in the chamber it is not possible to separate the yields due to different channels, however the presence of a fast proton in $\sim 15\,\%$ of the cases indicates that secondary interactions occur in a significative part of the events.

To the events classified as carbon ones will also contribute reaction:

7) $\pi^- + \mathrm{p} \rightarrow \Lambda^0 + \theta^0 + \pi^0$.

occurring in hydrogen. This is however expected to occur in few percent (*) of the hydrogen associated productions and therefore we will not correct for this effect.

The ratio N carbon/ hydrogen of events in which both Λ^0 and θ^0 are seen to decay through their charged mode in the chamber are given in Table II.

TABLE II.

E_π (GeV)	$\frac{N\,(2\,\mathrm{V}^0\,\mathrm{in\,C})}{N\,(2\,\mathrm{V}^0\,\mathrm{in\,H})}$	$\frac{\sigma_\mathrm{C}\,(2\,\mathrm{V}^0)}{\sigma_\mathrm{H}\,(2\,\mathrm{V}^0)}$	$\frac{N\,(\Lambda^0\,\mathrm{in\,C})}{N\,(\Lambda^0\,\mathrm{in\,H})}$ (*)	$\frac{N_\mathrm{tot}\,(\Lambda^0\,\mathrm{in\,C})}{N_\mathrm{tot}\,(\Lambda^0\,\mathrm{in\,H})}$	$\sigma_\mathrm{C}\,(\Lambda^0)$ (**)
1.3	$\frac{42}{29} = 1.45$	3.9	$\frac{113}{48}$	$\frac{155}{77}$	5.27	$3.0^{+1.7}_{-1.2}$

(*) Single Λ^0 only.

(**) Taking for σ_{Λ^0} in H $(\sigma_{\Lambda^0} + \sigma_{\Sigma^0}) = 0.56$ mb. The errors were computed with the following assumptions: upper value $N_{\Sigma^0\mathrm{H}} = 2$; $N_{\mathrm{C\,cont}} = 0.52 \cdot 37$; lower value $N_{\mathrm{C\,cont}} = 0$; $N_{\Sigma^0\mathrm{H}} = (39 - 13)$, 13 being the number of events which are not compatible with the kinematics of $\pi^- + \mathrm{p} \rightarrow \Sigma^0 + \theta^0$; $\Sigma^0 \rightarrow \Lambda^0 + \gamma$.

The cross-section ratios are also given taking into account the relative abundance of carbon to hydrogen nuclei in propane (3/8).

(*) The frequency of reaction (7) is expected, from charge independence considerations, to be equal to the frequency of reaction $\pi^- + \mathrm{p} \rightarrow \Lambda^0 + \mathrm{K}^+ + \pi^-$, which was found to occur only in 3 out of the 75 H events.

Events in which a single Λ^0-decay is visible in the chamber can be attributed to hydrogen only if they are produced through the channels:

1) $\pi^- + p \to \Lambda^0 + \theta^0$.

8) $\pi^- + p \to \Lambda^0 + K^+ + \pi^-$.

If the Λ^0 is due to the decay of a Σ^0 produced in hydrogen the event will be attributed to H only if the decay γ is converted in the chamber. Two such events were found. As carbon events will be labelled all the following Λ^0 producing events:

3) $\pi^- + p$ (bound) $\to \Lambda^0 + \theta^0$.

4) 5) $\to \Sigma^0 + \theta^0$ followed by Σ^0 conversion or decay.

9) $\to \Sigma^- + K^+$ followed by Σ^- conversion.

6) $\pi^- + n$ (bound) $\to \Sigma^- + \theta^0$ followed by Σ^- conversion.

2) $\pi^- + p$ (free) $\to \Sigma^0 + \theta^0$ followed by $\Sigma^0 \to \gamma + \Lambda^0$, γ not converted.

(All of these reactions can be accompanied by the emission of one or two π's.)

Before giving the ratio between the carbon and hydrogen-produced Λ^0 we must correct for two effects:

a) Some of the Λ^0 produced in carbon will satisfy within the limits of error the kinematics of reaction 1). The percentage of such events can be deduced from the analysis of 2 V carbon events [6]. It was found that in $(44 \pm 8)\%$ of the 2 V's carbon events in which no extra prongs are visible at the π^- interaction point, the Λ^0 satisfy within the measurement errors the kinematics of an hydrogen event. If the θ^0 had not been seen, such events would have been classified as hydrogen ones.

b) The Λ^0 produced in hydrogen in reaction 2) must be separated from the ones coming from carbon nuclei. This can be done statistically using the quoted ratio

$$\frac{\sigma(\Lambda^0 \theta^0)}{\sigma(\Sigma^0 \theta^0)} = 1.3^{+0.8}_{0.5}.$$

The correct yields of single Λ^0 from hydrogen and carbon are therefore obtained solving the linear system:

$$N_{C\,stop} + N_{\Sigma^0 H} - N_{C\,cont} = 39\,,$$

$$N_H + N_{C\,cont} = 41\,,$$

$$N_H = 1.3\, N_{\Sigma^0 H}\,,$$

$$N_{C\,cout} = 0.44\, N_{C\,top}\,,$$

$$N_C = N_{C\,stop} + N_{C\,star}\,, \qquad N_{C\,tr} = 78.$$

The ratio of the total yields from carbon and hydrogen and the cross-section ratios are also given in Table II.

Since the cross-sections in H at this π energy are known ([6]), this allows an estimate of the cross-section for Λ^0 production in carbon.

The result, as reported in Table II, is in good agreement with the data obtained at slightly different energies ([7,8]).

4. – Characteristics of Λ^0 origins.

The 106 π^- stars from which a single Λ^0 was emitted have been analysed. The momentum of the charge prongs has been obtained from curvature and/or range measurements, the sign of the charge has been assigned and whenever possible, the particle identity has been established from range and/or ionization *vs.* momentum measurements.

The characteristics of the stars are reported in Table III (*). The main features which can be deduced are:

TABLE III.

Evaporation only	Fast protons with or without evaporation	π^- with of without evaporation			K^+ with or without evaporation		π^+ with or without evaporation	Stop
		21+(2)			11+(3)			
		with fast p	with K^+	with π^+	with fast p	with π^+		
22	8+(2)	6+(3)	11+(3)	2	3+(1)	1	3+(1)	37

The sum of the frequency of the reactions:

1) *a*) $\pi^- + p\,(\text{bound}) \rightarrow \Lambda^0 + K^+ + \pi^-$

b) $\rightarrow \Sigma^0 + K^+ + \pi^-$

is $\sim 10\,\%$ of all the Λ^0 producing reactions in carbon. From charge independ-

(7) T. BOWEN, J. HARDY, G. REYNOLDS, C. R. SUN, G. TAGLIAFERRI, A. WERBROUCK and W. A. MOORE: *Phys. Rev.*, **119**, 2030 (1960).

(8) H. BLUMENFELD, W. CHINOWSKY and M. LEDERMAN: *Nuovo Cimento*, **8**, 296 (1958).

(*) Numbers in parentheses indicate uncertain identification and are included for upper limits.

ence considerations we deduce that the frequency of the reaction:

2) $\pi^- + \mathrm{p\,(bound)} \rightarrow \Lambda^0 + \theta^0 + \pi^0$

is equal to the frequency of reaction 1 *a*) and therefore is $\leqslant 10\,\%$.

The remaining yield of π^- $(7+(5)/106)$ events are most probably due to reactions:

3) *a*) $\pi^- + \mathrm{n\,(bound)} \rightarrow \Lambda^0 + \theta^0 + \pi^-$

b) $\rightarrow \Sigma^0 + \theta^0 + \pi^-$.

From the percentage of stars from which a K^+ and no π^- are emitted we can deduce an upper limit for the conversion ratio of Σ^- to Λ^0 if we assume that such events are all due to reaction:

4) $\pi^- + \mathrm{p\,(bound)} \rightarrow K^+ + \Sigma^-$ followed by $\Sigma^- + p \rightarrow \Lambda^0 + n$

in nuclear matter. The total number of Λ^0 produced can indeed be written as:

$$N_{\mathrm{tot}\Lambda^0} = 155 = N_{\Lambda^0\mathrm{direct}} + N_{\Sigma^0\rightarrow\Lambda^0} + \mathrm{C.R.} \times N_{\Sigma^-} ,$$

where N_{Λ^0} direct are the Λ^0 directly produced, $N_{\Sigma^0\rightarrow\Lambda^0}$ are the Λ^0 originating from Σ^0 through conversion or decay, N_{Σ^-} are the produced in the reactions:

4) $\pi^- + p \rightarrow K^+ + \Sigma^-$.

5) $\pi^+ + \mathcal{N} \rightarrow \theta^0 + \Sigma^-$.

and C.R. is the probability for a Σ^- to be converted in the carbon nucleus of production.

From the number of « K^+ no π^- » stars we know that:

$$\mathrm{C.R.} \times N_{\Sigma^-K^+} \leqslant 14 \pm 4 .$$

It follows that:

$$\frac{\sigma_{\Lambda^0\,\mathrm{direct}} + \sigma_{\Sigma^0\rightarrow\Lambda^0}}{\mathrm{C.R.} \times \sigma(\Sigma^- \text{-} K^+)} + \left[1 + \frac{\sigma(\Sigma^-\theta^0)}{\sigma(\Sigma^- K^+)}\right] \geqslant 11^{+4}_{-2} ,$$

and substituting the know cross-sections values (*)

$$\mathrm{C.R.} \leqslant 0.2\ ^{+0.15}_{-0.11}$$

(*) The cross section for reaction (5) has been obtained from charge symmetry. The value taken is $\sigma_{\theta^0\Sigma^-}$ (0.15 ± 0.5) mb obtained by Brown *et al.* (9) at 1.1 GeV π^- energy. As can be checked the result is not very sensitive to this value.

(9) J. L. Brown, D. A. Glaser, D. I. Meyer, M. L. Perl and J. Van der Velde: *Phys. Rev.*, **107**, 906 (1957).

which corresponds to a total cross-section for the processes (7):

6) $\Sigma^- + p \to \Lambda^0 + n$,

$\sigma_{\Sigma^0 \to \Lambda^0} \leqslant (38 \pm 24)$ mb.

5. – Missing momentum analysis.

On 80 of the 2 V's events found both on the 1.2 and 1.3 GeV film, the Λ^0 and θ^0 momentum and angle of emission were measured with sufficient accuracy as to allow a meaningful estimate of missing energy and missing momentum.

On 28 of such events the missing energy (defined as: $W_{miss} = W_\pi - W_{\Lambda^0} - W_{\theta^0} + M_p$, where W is total energy and M_p is the proton mass) was found to be greater than the $\pi^\pm$ mass. There is no significative difference between the percentage of such events at the two energies (14/43 at 1.2 GeV and 14/37 at 1.3 GeV). If we average the results we obtain an upper limit for the percentage of events in which a π-meson is emitted $N_\pi / N_{total} \leqslant 35\,\%$.

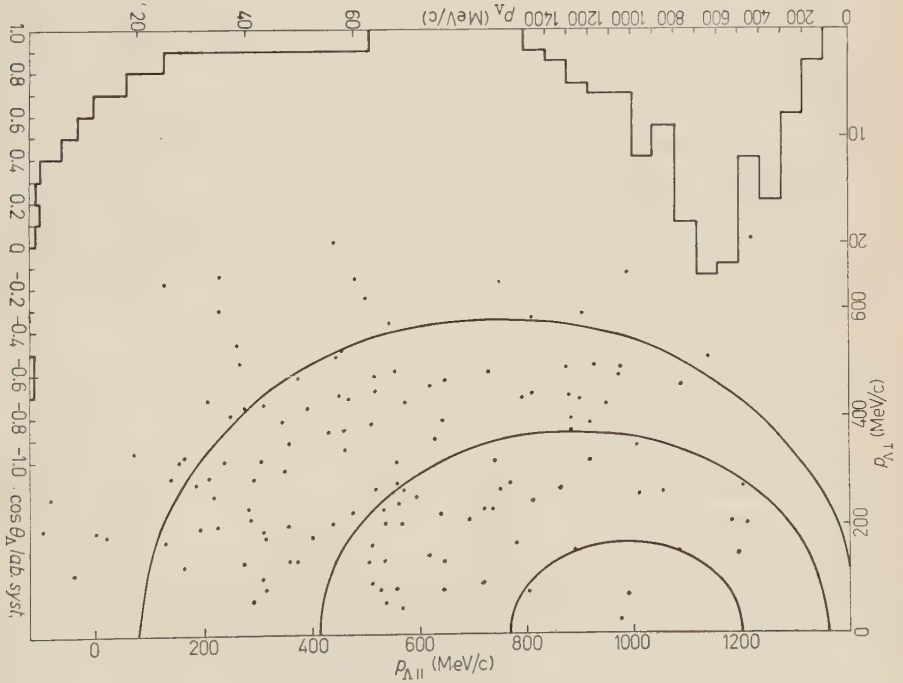

Fig. 1. – Distribution of 145 Λ^0 produced in carbon, as a function of laboratory momentum (p_Λ) and angle of emission (θ). The curves are momentum ellipses for the reaction $\pi^- + p \to \Lambda^0 + \theta^0$ with $E_{\pi^-} = 1.3$ GeV and $p_F = 0, +200, -200$.

On the remaining 52 events the missing momentum was estimated in order to see what percentage of such events is compatible with a one-nucleon reaction. The upper limit of the Fermi momentum of the target nucleon was taken to be $P_F = 250$ MeV/c. In 25 of the 52 events the missing momentum could be made to be < 250 MeV allowing for experimental errors. This sets a lower limit of 50% to the events in which a secondary interaction has occured inside the nucleus. The choice of the upper limit for the Fermi momentum is of course rather arbitrary but in most of the discarded events the missing momenta are well above this limit (Fig. 2). Moreover it must be pointed out that for the events compatible with one-nucleon reactions the missing momentum distribution is not isotropic (as should be expected for nuclear motion) but is peaked in the forward direction (13 events forward and 9 backward). This indicates that even this sample contains some event in which one of the strange particles has suffered a secondary collision. While the $\Sigma^0 \to \Lambda^0$ decays will reduce the forward peaking of the missing momentum distribution, this effect will not, in general, cause a double event to become incompatible with a single-nucleon interaction.

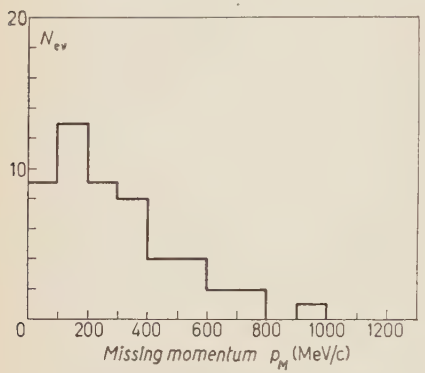

Fig. 2. – Missing momenta distribution (absolut value).

In Fig. 1 the distribution of all the 145 Λ^0 produced in carbon by 1.3 GeV π^- is given as a function of the momentum and production angle in the L.S. In Fig. 1 momentum ellipses for the reaction $\pi^- + p \to \Lambda^0 + \theta^0$ are also plotted for the cases in which the momentum of the target is $p_F = 0, -200, -200$ MeV c.

6. – Λ^0's polarization.

6·1. *Along the normal to the production plane.* – It is an experimentally well established fact [3,4] that a Λ^0 produced in the reaction 1) $\pi + p \to \Lambda^0 + \theta^0$ is polarized at least for π energies up to the one we are dealing with. The establishment of Λ^0 polarization was a by-product of the experiment to check parity nonconservation in the decay of Λ^0-particles. As is well known this experiment consisted in measuring the up-down asymmetry of the Λ^0-decay particles with respect to the Λ^0 production plane. The asymmetry has the form $1 + \alpha \overline{P} \cos\theta$ where θ is the angle between the decay particle (say the π^-) in the Λ^0 c.m. system and the normal to the production plane, α is the asymmetry coefficient defined as $\alpha = 2\,\mathrm{Re}\,(A^* \cdot B)/(|A|^2 + |B|^2)$ and P is the Λ^0

spin polarization along the normal to the production plane. The average value of αP in the π^- energy interval 910 to 1300 GeV is $\alpha\bar{P} \simeq 0.4 \pm 0.1$ ([3]). A recent independent measurement of the asymmetry coefficient gives the value ([5]) $\alpha = -0.75^{+0.50}_{-0.15}$ which leads to a value of the average polarization P very near to 1.

Recent experiments have measured the up-down asymmetry of Λ^0 produced by π^- in heavier elements (such as iron ([10]), lead ([7]), copper ([11]) and xenon ([12]) at π^- energies comparable with those of the H experiment, and Λ^0 produced in propane ([13]) at higher energies ($(7 \div 8)$ GeV); all these experiments gave a value of $\overline{\alpha P}$ compatible with zero. For the heavier elements this result was attributed to the depolarizing effect of secondary interactions inside the nucleus. The result in propane could be interpreted as an indication that the polarization of the Λ^0 produced in reaction 1) decreases with increase of the π^- beam energy. On the other side since most of the Λ^0 produced in propane arise from carbon nuclei one might wonder how much rescattering, in this small size nucleus, can be responsible for the result.

A re-examination of the existing data for Λ^0 produced in carbon give no conclusive result since such data are scanty and quite dishomogeneus. Since most of the working bubble chambers are propane ones, it seems important, from an operational point of view, to establish if one can use carbon nuclei as a source of polarized Λ^0.

The main purpose of this experiment was the polarization analysis of Λ^0 produced in carbon by π^- of 1.3 and 1.2 GeV, that is at an energy at which we know that the Λ^0 produced in H is polarized.

We define as production plane, the plane (*) $\hat{p}_1 \times \hat{p}_2$ where $\hat{p}_1$ and $\hat{p}_2$ are unit vectors along the direction of the incident π ($\hat{p}_1$) and of the emitted $\Lambda^0(\hat{p}_2)$ in the laboratory system. This is the true production plane only if the target nucleon is at rest. In a complex nucleus however the target nucleus is in motion due to Fermi momentum and the true production plane depends also upon $\boldsymbol{p}_F$ where $\boldsymbol{p}_F$ is the momentum vector of the target nucleon. WERBROUCK ([14]) has recently calculated the projection of the spin onto the direction $\hat{p}_1 \times \hat{p}_2$, as a function of the Λ^0 c.m. emission angle. The result of his calculation for 1.3 GeV and for a Gaussian distribution of the Fermi

([10]) E. BOLDT, H. S. BRIDGE, D. O. CALDWELL and Y. PAL: *Phys. Rev. Lett.*, **1**, 256 (1958). Also E. BOLDT: *Ph. D. Thesis.*

([11]) G. R. KALBFLEISCH: *Phys. Rev.*, **121**, 1544 (1961).

([12]) E. V. KURZNETZOV, I. A. IVANOVSKAYA, A. PROKESH and I. V. CHUVILO: *Proc. of the Rochester Conf. (1960)*, p. 384.

([13]) M. I. SOLOVIEV: *Proc. Rochester Conf. 1960*, p. 388.

(*) In what follows we will often — for brevity — refer to the plane defined by two vectors $\boldsymbol{a}$ and $\boldsymbol{b}$ and the normal to which is directed along $\boldsymbol{a} \times \boldsymbol{b}$ as to « the plane $\boldsymbol{a} \times \boldsymbol{b}$ ».

([14]) A. E. WERBROUCK: *Phys. Rev.*, **120**, 1463 (1960).

momentum:

$$W(p_F)\,dp_F = p_F^2 \exp\left[p_F^2/p_0^2\right] dp_F; \qquad \frac{p_0^2}{2M} = 14 \text{ MeV},$$

is reported in Fig. 3. If we take into account the Λ^0 c.m. angular distribution it turns out that only in $\sim 10\%$ of the cases the projection of the spin along the direction $\hat{p}_1 \cdot \hat{p}_2$ is $< 90\%$ of the spin value, the more affected being Λ^0 of very low and very high momentum.

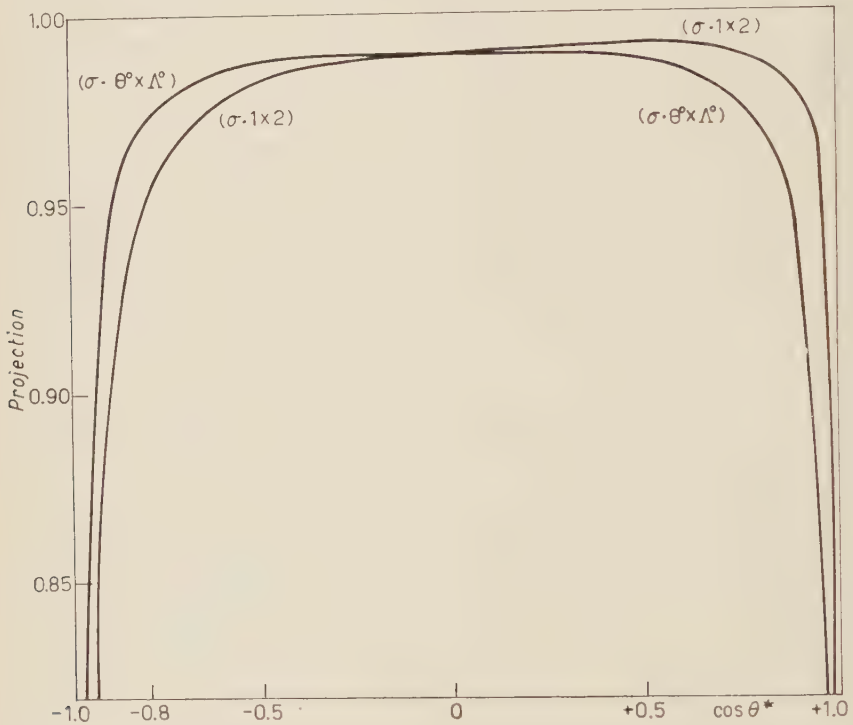

Fig. 3. – Spin projection along the directions $\boldsymbol{p}_1 \times \boldsymbol{p}_2$ and $\boldsymbol{p}_0 \times \boldsymbol{p}_\Lambda$ as a function of the c.m. Λ^0 production angle.

In Table IV are reported the results of the asymmetry measurements. Columns III and IV refer to the up-down asymmetry which is given in terms of the pseudoscalar:

$$\cos\theta = \frac{\boldsymbol{p}_3 \cdot (\hat{p}_1 \times \hat{p}_2)}{p_3^* \, \hat{p}_1 \cdot \hat{p}_2}$$

where $\boldsymbol{p}_3$, $\boldsymbol{p}_3^*$ are momentum vectors of the decay π in the l.s. ($\boldsymbol{p}_3$) and in the c.m. system ($\boldsymbol{p}_3^*$).

beam energy (GeV)	Selection criteria	$\frac{\text{up}-\text{down}}{\text{up}+\text{down}}$	$\overline{\alpha P_\theta} = \frac{3}{N}\sum 2\cos\theta \pm \sqrt{\frac{3}{N}}$	$\frac{\text{Forw}-\text{Back}}{\text{Forw}+\text{Back}}$	$\overline{\alpha P_\varphi} = \frac{3}{N}\sum 2\cos\varphi \pm \sqrt{\frac{3}{N}}$	$\frac{\text{left}-\text{right}}{\text{left}+\text{right}}$	$\overline{\alpha P_\xi} = \frac{3}{N}\sum 2\cos\xi \pm \sqrt{\frac{3}{N}}$
1.3	All events	$\frac{70-72}{142}$	-0.02 ± 0.15	$\frac{80-62}{142}$	0.29 ± 0.11	$\frac{72-70}{142}$	-0.01 ± 0.15
	$700\leqslant P_\Lambda\leqslant 1170$	$\frac{25-21}{46}$					
	$300\leqslant P_\Lambda\leqslant 800$			$\frac{51-37}{88}$			
1.2	All events	$\frac{50-46}{96}$	$+0.22\pm0.18$	$\frac{51-45}{96}$	0.02 ± 0.18	$\frac{50-46}{96}$	$+0.04\pm0.18$
	$700\leqslant P_\Lambda\leqslant 1170$	$\frac{18-13}{31}$					
	$300\leqslant P_\Lambda\leqslant 800$			$\frac{38-31}{69}$			
1.5 [a]	All events	$\frac{10-11}{22}$	-0.03 ± 0.37	$\frac{8-6}{14}$ [a]	[a]	[a]	[a]
Total	All events	$\frac{130-129}{259}$	-0.018 ± 0.107	$\frac{139-113}{252}$	0.184 ± 0.11	$\frac{122-116}{238}$	$+0.01\pm0.11$
					(0.10 ± 0.11) [b]		
	$700\leqslant P_\Lambda\leqslant 1170$	$\frac{50-41}{91}$	$+0.15\pm0.18$				
	$300\leqslant P_\Lambda\leqslant 800$			$\frac{89-68}{157}$	$\pm0.257\pm0.137$		
					(0.10 ± 0.14) [b]		
	2 V's events plane $\hat{p}_\theta\times\hat{p}_\Lambda$	$\frac{35-31}{66}$	0.193 ± 0.21				

([a]) Cloud chamber data. (7) information on this sample is incomplete.
([b]) Corrected for scanning losses.

If in order to increase the statistical weight we use all the events (which seems quite reasonable due to the little spread in energies) we find no evidence that the Λ^0 is polarized along the direction $\hat{p}_1 \wedge \hat{p}_2$. Target motion can clearly not account for such a strong depolarization effect. The depolarization mechanism must be searched for in:

a) scattering of the incident π in nuclear matter, previous to the strange particles producing interaction;

b) secondary hyperon interactions.

An effort to separate the effects of *a*) and *b*) has been done defining for the 2 V events the plane $\hat{p}_{V^0} \wedge \hat{p}_{\Lambda^0}$ as the production plane. In this case only strange particle interactions are responsible for the depolarization, which appears to be still a rather large effect. The result is however affected by low statistics.

BOLDT *et al.* ([10]) and BOWEN *et al.* ([7]) have found a finite polarization for Λ^0 in the range of momentum $700 < p_\Lambda < 1000$ MeV/*c*. This is of course to be expected for two reasons:

1) The selection criteria favours directly produced Λ^0.

2) The depolarization of such events due to target motion is ~ 0.

There is an indication of such effect also in our data.

6·2. *In the production plane.* – SALMERON and ZICHICHI ([15]) re-examining a sample of cosmic ray-produced Λ^0 have found evidence of a forward-backward asymmetry in the c.m. angular distribution of the decay particles with respect to the Λ^0 laboratory line of flight. This has given rise to speculations whether this could be considered as an indication of parity non conservation in strong interactions. It is well known ([2]) in fact that if parity is conserved in reaction 1) the polarization of the Λ^0 (if any) should be directed along the normal to the production plane. The presence of a component of the polarization on the plane of production would indeed prove the existence of a parity non conserving term in strong interactions. F. S. CRAWFORD *et al.* ([16]) have found no evidence of forward-backward asymmetry for Λ^0 produced in hydrogen by π^- in the energy range $910 \leqslant E_{\pi^-} \leqslant 1300$ MeV.

The sample of Λ^0 studied by SALMERON and ZICHICHI differed from those studied by CRAWFORD *et al.* in two respects:

1) The energy of the primary particles.

2) The nucleus in which the Λ^0 was created.

([15]) R. A. SALMERON and A. ZICHICHI: *Nuovo Cimento*, **11**, 461 (1959).

([16]) F. S. CRAWFORD jr., M. CRESTI, M. L. GOOD, K. GOTTSTEIN, E. M. LYMAN, F. T. SOLMITZ, M. L. STEVENSON and H. K. TICHO: *Phys. Rev. Lett.*, **2**, 517 (1959).

The results could then be accounted for in two ways:

1) The reaction from which the Λ^0 was originating was essentially 1) (the nucleus being rather transparent to produced Λ^0). The backward-forward asymmetry arises from the energy-dependent parity nonconserving terms in interaction (1).

2) The measured Λ^0's originate mainly from secondary interactions inside the parent nucleus. In this case if the hyperon produced in the π primary interaction has spin directed along the normal to the production plane (as seems to be the case from the results of the H experiment) the secondary interaction, just because it changes the hyperon's direction of flight will give rise to a spin component along the Λ^0 line of flight. The presence of a finite forward-backward asymmetry on a sample of Λ^0 produced in complex nuclei could therefore be due to the characteristics of the secondary interactions and/or to the selection criteria of Λ^0 events.

Almost no detailed information is available about hyperon-nucleon interactions. As to selection criteria, in order to avoid identification difficulties one is forced to limit himself to the study of low momentum Λ^0 ($p_{\Lambda^0} \leqslant 1000$ MeV/c). In this way one will select preferentially backward emitted and secondary Λ^0. The more so, the upper the incident beam energy. For this reason, if a finite polarization along the laboratory Λ^0 line of flight should arise from such a selection criteria, this effect should be enhanced at high energies (*).

In the course of this experiment the forward-backward asymmetry has been measured on 252 Λ^0 originated in carbon nuclei. The results are reported in Table IV columns V and VI and in Fig. 4 in terms of the scalar

$$\cos\varphi = \gamma \frac{(\boldsymbol{p}_3 \cdot \hat{\boldsymbol{p}}_2) - \eta W_3}{\boldsymbol{p}_3^*},$$

where

$$\gamma = \frac{W_2}{M}, \qquad \gamma\beta = \eta = \frac{p_2}{M}, \qquad (W_2,\ W_3 \text{ total energies}).$$

There is a slight indication that a forward-backward asymmetry of the same sign as the one found at higher energies is present. If however one takes into account the loss of events in which a short π^- is emitted ($p_{\pi^-} \leqslant 60$ MeV/c), comparing the loss of such events with that expected for a c.m. isotropic distribution, one finds a result which is compatible within the limit of error with

(*) The author wishes to thank Dr. CIOCCHETTI for many clarifying discussions on this subject.

a zero forward-backward asymmetry (*). This way of correcting is questionable since it implies isotropy in the decay particle c.m. distribution. An independent way of estimating the loss of events with a short π^- was to check the frequency of such Λ^0 in the 2 V events where a Λ^0 has a much higher probability of detection, and to compare with the frequency in single Λ^0 events.

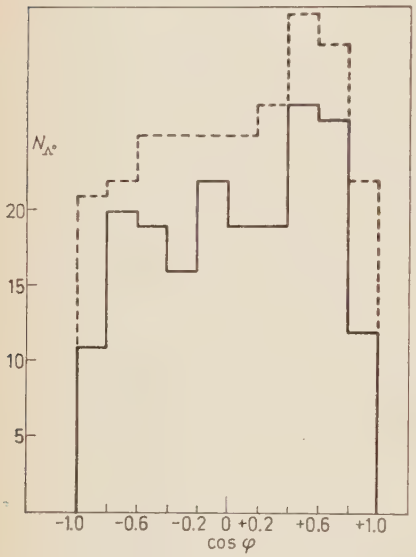

Fig. 4. – Distribution of Λ^0 as a function of cos φ where φ is the angle between the Λ^0 laboratory line of flight and the decay π^- line of flight in the Λ^0 c.m. system. Dotted line istogram, all events; full line istogram events with $300 \leqslant p_\Lambda \leqslant 800$ MeV/c.

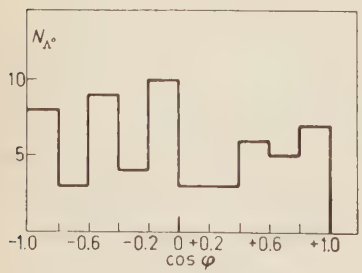

Fig. 5. – Distribution of Λ^0 as a function of cos φ (2 V events only).

The result was: 4/66 for 2 V events and 3/186 for single Λ^0 events. The limitations due to low statistics are evident, however it is a striking fact that the frequency of short $\pi^- \Lambda^0$ is much higher for 2 V events than for single Λ^0 events, and, moreover, is nearly that expected for an isotropic c.m. decay distribution (see also Fig. 5).

The conclusion is that we can not exclude that the forward-backward asymmetry we measure is explained by a Λ^0 detection bias.

The left-right asymmetry has been also measured in terms of the scalar

$$\cos \xi = \frac{\boldsymbol{p}_3 \cdot ((\hat{p}_1 \times \hat{p}_2) \times \hat{p}_2)}{\boldsymbol{p}_3^* |\hat{p}_1 \times \hat{p}_2|} .$$

The results are reported in columns VII, VIII of Table IV. The angular distribution is symmetrical. This does not mean much since the direction with respect to which the angle ξ is measured is not related significantly to any true right-left polarization at production, as a consequence of secondary interactions.

* * *

The main part of this experiment has been done at Princeton University. The author wishes to thank Dr. G. Reynolds for hospitality in his group and Dr. T. Bowen for his help and encouragement throughout

(*) This loss affects also cloud chamber results since the ionization of the two prongs is very similar and the events can be mistaken for large angle scattering. This kind of bias has not been taken into account by Salmeron and Zichichi.

the work. The author wishes also to thank the Columbia group for lending the film and the spatial reconstruction program and the Columbia and Pisa group for making their data available.

The author is also indebted to Drs. CIOCCHETTI, GARELLI, SEIDLIZ, SUN and WERBROUCK for many helpful discussions, to Dr. MARZARI for some help in analysing the data and to Miss JOAN WINTERS for her help in measuring and processing the data.

RIASSUNTO

Lo scopo principale di questa ricerca è lo studio della polarizzazione di Λ^0 prodotte in carbonio da π^- di 1.3 e 1.2 GeV. Per analizzare la polarizzazione media di queste Λ^0 si misurano le asimmetrie nella distribuzione angolare del π^- di decadimento nel c.m. del Λ^0. La distribuzione angolare è simmetrica rispetto al piano $\boldsymbol{P}_{\pi\,\mathrm{inc}} \times \boldsymbol{P}_{\Lambda^0}$ e al piano $(\boldsymbol{P}_{\pi\,\mathrm{inc}} \times \boldsymbol{P}_{\Lambda^0}) \times \boldsymbol{P}_{\Lambda^0}$. Questo implica che le Λ^0 che noi misuriamo non sono, in generale, prodotte direttamente nella interazione di un π^- primario con un nucleone del nucleo di carbonio. Si trova che le interazioni secondarie di particelle strane hanno un forte peso in questo processo di depolarizzazione. È stata anche misurata l'asimmetria avanti-indietro ($\alpha \boldsymbol{P}_q$) rispetto alla direzione del Λ^0 nel laboratorio. $\overline{\alpha P}_q$ è compatibile con 0 quando si siano corretti i risultati per tener conto delle perdite di scanning. Dallo studio delle stelle di π^- da cui viene emessa un Λ^0 si deducono informazioni sulla frequenza delle varie reazioni che danno origine a un Λ^0. In particolare si trova che la sezione d'urto per la reazione $\Sigma^- + \mathrm{p} \to \Lambda^0 + \mathrm{n}$ è $\sigma_{\Sigma^- \Lambda^0} \leqslant (38 \pm 24)$ mb. Dallo studio dell'energia e del momento mancanti negli eventi con 2 V^0 si apprende che la frequenza di reazioni secondarie nel nucleo di carbonio è $\geqslant 50\%$.

Scattering of High-Energy Nucleons by Heavier Nuclei.

T. TAKEMIYA

Department of Physics, University of Kyoto - Kyoto

Y. SAKAMOTO

Yoshida College, University of Kyoto - Kyoto

(ricevuto il 29 Aprile 1961)

In the previous paper (1), we have investigated the differential cross-sections of high-energy nucleons elastically scattered from heavier nuclei. In the analyses of the experimental data, we have found that, by using the impulse approximation, the experimental differential cross-sections are explained by superpositions of amplitudes for the scattering of nucleon by nucleons in the target nucleus which are multiplied by certain factors less than unity, and that the factors depend little on incident energies and mass numbers of medium and heavy weight nuclei. SASAKAWA (2) explained the fact by using a certain model. He called the model the independent pair model. His result does not depend on mass number and incident energies. On the other hand, KERMAN, MCMANUS and THALER (3) estimated the effects of pair correlations of target nucleons on the optical potential.

Their results do not depend almost on mass number but on incident energies for the nuclei heavier than about $A = 100$. The effects of correlations estimated by them act to decrease the magnitude of the cross-sections of the scattered nucleons at $(90 \div 150)$ MeV by only a few percent and to increase that at about 300 MeV by only a few percent. Then, even if one takes into account the effects of correlations, one cannot explain the discrepancies between the magnitudes of the experimental differential cross-sections and of the results calculated by using the optical model potential constructed by nucleon-nucleon scattering phase shifts which are equivalent to the results calculated in the framework of the impulse approximation.

Empirically, the observed differential cross-sections are given by the products of certain factors and the differential cross-sections calculated by using the impulse approximation. The factors do not depend on the scattering angles at forward small angles. In order to interpret this fact, we introduce the effective nuclear potential for target nucleus. The effective nuclear potential is constructed by a

(1) T. TAKEMIYA, T. SASAKAWA and Y. SAKAMOTO: *Prog. Theor. Phys.*, **24**, 1307 (1960).
(2) T. SASAKAWA: *Prog. Theor. Phys.*, **24**, 241 (1960).
(3) A. K. KERMAN, H. MCMANUS and R. M. THALER: *Ann. Phys.*, **8**, 551 (1959).

product of a factor $\exp[-x(\boldsymbol{r})/l]$ and U which is a parameter of RIESENFELD and WATSON [4] potential. The potential effectively perceived by the incident nucleon depends on the mean free path of the incident nucleon. The mean free path is related to the total cross-section of two-nucleon scattering, and depends on the incident energy. The mean free path is lengthened by the effects due to the Pauli principle. Generally, as the incident energy increases, the mean free path becomes larger and the potential effectively perceived by the incident nucleon becomes larger.

The effects of pair correlations of nucleons in target nuclei may be taken into account within the effective potential.

The mean free path l is given by [5]

$$l = \frac{1}{\sigma_2 \varrho_0} \frac{1}{\left(1 - \frac{7}{5}(E_F/E_i)\right)}, \tag{1}$$

where the second factor is caused by the Pauli principle, and σ_2 is the total cross-section of two-nucleon scattering defined by the optical theorem

$$\sigma_2 = \frac{4\pi}{kA} \operatorname{Im}\{(A + Z)A_1 + (A - Z)A_0\}, \tag{2}$$

where the notations A_1, A_0 etc., have usual meanings, ϱ_0 is the nucleon density of the nucleus defined by

$$\varrho_0 = \frac{3}{4\pi r_0^3}. \qquad (r_0 = 1.3 \cdot 10^{-13} \text{ cm}). \tag{3}$$

For the high energy nucleon elastically scattered from complex nuclei the potential may be constructed as follows

$$V(\boldsymbol{r}) = U\varrho(r) \exp\left[-\frac{x(\boldsymbol{r})}{l}\right], \tag{4}$$

where $x(\boldsymbol{r})$ is the distance measured from nuclear surface along the direction of the incident beam.

Then, the amplitude of the nucleon scattered by the nucleus is given by

$$f_{\text{eff}} = -\frac{(2\pi)^2}{\hbar^2} m \sum^{A} \int \exp[-i\Delta\boldsymbol{k}\cdot\boldsymbol{r}] U\varrho(r) \exp\left[-\frac{x(\boldsymbol{r})}{l}\right] \mathrm{d}\boldsymbol{r}. \tag{5}$$

Then, the factor $\lambda(E, A)$ is defined as

$$\lambda(E, A) = f_{\text{eff}}/f|_{\theta\sim 0}, \tag{6}$$

where

$$f = -\frac{(2\pi)^2}{\hbar^2} m \sum^{A} \int \exp[-i\Delta\boldsymbol{k}\cdot\boldsymbol{r}] U\varrho(r)\, \mathrm{d}\boldsymbol{r}.$$

[4] W. B. RIESENFELD and K. M. WATSON: *Phys. Rev.*, **102**, 1157 (1956).
[5] M. L. GOLDBERGER: *Phys. Rev.*, **74**, 1269 (1948).

$\lambda(E, A)$ gives the amplitude of high-energy nucleons elastically scattered by heavier nuclei at very small scattering angles. Then the differential cross-section is written as follow

$$\frac{\mathrm{d}\sigma}{\mathrm{d}\Omega} = |f_{\mathrm{eff}}|^2 = \lambda^2 |f|^2 . \tag{7}$$

The values of $\lambda(E, A)$ are shown in the Fig. 1 for the incident energies $E = 90$, 156, 310 and 340 MeV, respectively. The agreements between the experimental data and the results calculated by using eq. (7) are fairly good.

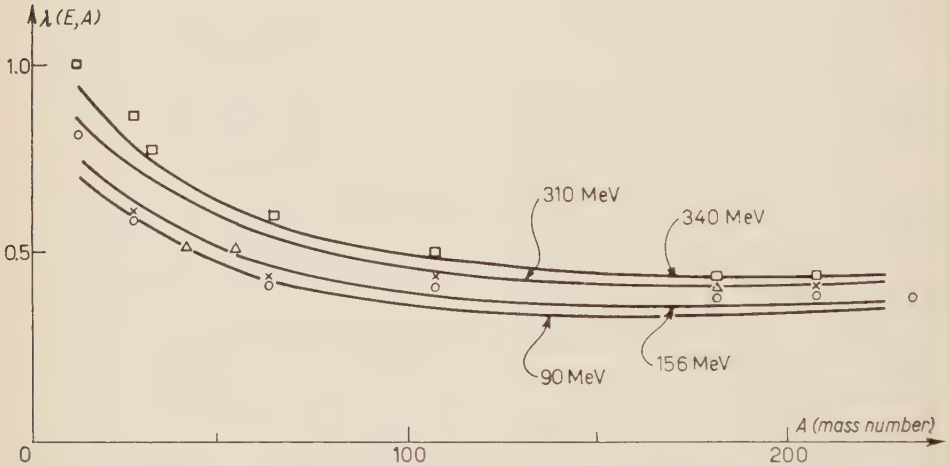

Fig. 1. – The solid curves show the values of $\lambda(E, A)$. ○, × etc., show the points of experimental data divided by the parameter of RIESENFELD and WATSON [4] times mass number of target nucleon. Values of $\lambda(E, A)$: ○ 95 MeV, × 135 MeV, △ 310 MeV, □ 340 MeV.

The mean free paths are rather insensitive to the incident energies in the region from 150 to 340 MeV. This presumably arises from two compensating effects: the importance of the Pauli principle in excluding collisions is small at high energies and this tends to decrease the mean free path of the incoming nucleon. On the other hand, the total elementary cross-sections decrease with increasing energy, this effects tending to increase the mean free path. Then the mean free paths are not so varied with the incident energies, therefore the factors $\lambda(E, A)$ are not so varied with energies.

In the above treatment, we have neglected the effect of multiple scattering, the error introduced by multiple scattering is $a_2/2k\bar{l}^2$ [6], where $\bar{l}$ = mean free path and a_2 = mean scattering length, and one obtains about 11% at 90 MeV, 6% at 156 MeV and 3% at 310 MeV, respectively. Then the effect of multiple scattering is expected to be small.

[6] G. F. CHEW and G. C. WICK: *Phys. Rev.*, **85**, 636 (1952).

Isotopic Spin Relations in Hyperon Production.

A. Salam
Imperial College - London

J. Tiomno
Centro Brasileiro de Pesquisas Físicas
Faculdade Nacional de Filosofia - Rio de Janeiro

(ricevuto il 12 Agosto 1961)

Experiments on Σ-K production on hydrogen for pion incident energies around 1 GeV seem to indicate that [1,2]

$$\sqrt{\sigma_+} + \sqrt{\sigma_-} \approx \sqrt{2\sigma_0}\,, \tag{1}$$

where:

$$\sigma_+ \to \pi_+ + \mathrm{p} \to \mathrm{K}_+ + \Sigma_+\,,$$

$$\sigma_0 \to \pi_- + \mathrm{p} \to \mathrm{K}_0 + \Sigma_0\,,$$

$$\sigma_- \to \pi_- + \mathrm{p} \to \mathrm{K}_+ + \Sigma_-\,.$$

Isotopic spin analysis would predict only an inequality whereas experiments seem to show an equality in (1).

The general amplitude $\pi + \mathcal{N} \to \mathrm{K} + \Sigma$ can be expressed as

$$(\mathcal{N}\,|\,A\boldsymbol{\pi}\cdot\boldsymbol{\Sigma} + iB\boldsymbol{\tau}\cdot\boldsymbol{\pi}\wedge\boldsymbol{\Sigma}\,|\,K)\,. \tag{2}$$

In perturbation calculations A and B are real. Thus the experimental results can be understood in the form that the non-i-spin-flip amplitude $A \approx 0$ and only the i-spin-flip amplitude B contributes to the production process at these energies.

If $A \approx 0$ we have even a more constringent relation there (1):

$$\sigma_+ \approx \sigma_- \approx \tfrac{1}{2}\sigma_0\,. \tag{3}$$

Relation (3) is indeed favored by the experimental results [2] (Fig. 1). In the following we try to find the implications of this result on the basis of simple perturbation ideas.

Assuming even Σ-Λ and K-π parities we have three graphs given in Fig. 2.

---

[1] F. S. Crawford, R. L. Douglass, M. L. Good, G. R. Kalbfleisch, M. L. Stevenson and H. K. Ticho: *Phys. Rev. Lett.*, **3**, 394 (1959).

[2] C. Baltay, H. Courant, W. J. Fickinger, E. C. Fowler, H. L. Kraybill, J. Sandweiss, J. R. Sanford, D. L. Stonehill and H. D. Taft: *Rev. Mod. Phys.*, **33**, 374 (1961).

These give

$$(4)\quad \begin{cases} A \sim \left(\dfrac{g_{K\Sigma\mathcal{N}} g_{\mathcal{N}\mathcal{N}\pi}}{p_{\mathcal{N}} \cdot p_\pi} + \dfrac{g_{K\Lambda\mathcal{N}} g_{\Lambda\Sigma\pi}}{p_\Sigma \cdot p_\pi} \right) (\gamma \cdot p_\pi) \\ B \sim \left(\dfrac{g_{K\Sigma\mathcal{N}} g_{\mathcal{N}\mathcal{N}\pi}}{p_{\mathcal{N}} \cdot p_\pi} \quad \dfrac{g_{K\Sigma\mathcal{N}} g_{\Sigma\Sigma\pi}}{p_\Sigma \cdot p_\pi} \right) (\gamma \cdot p_\pi) \end{cases}$$

It is interesting to mention that relation (5) corresponds to Gell-Mann's D-coupling in the unitary theory [3], as

$$g_{K\Sigma\mathcal{N}} = -\sqrt{3} g_{K\Lambda\mathcal{N}};$$

$$g_{\Lambda\Sigma\pi} = 2/\sqrt{3} g_{\mathcal{N}\mathcal{N}\pi}.$$

The angular distribution is however roughly isotropic.

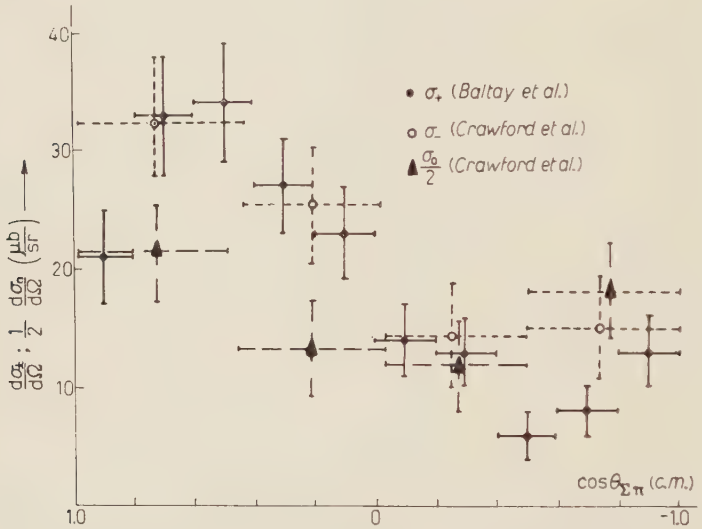

Fig. 1. – Angular distributions in $\pi_\pm + p \to K + \Sigma$ reaction at 1.08 GeV (Lab.). The Σ_0 cross-section is divided by 2.

where p's are the corresponding 4-momenta and we have neglected Λ-Σ mass difference. For the energy region considered $p_\Sigma \cdot p_\pi / p_{\mathcal{N}} \cdot p_\pi \approx \frac{2}{3}$. Thus we may conclude that

$$(5)\qquad \frac{g_{K\Sigma\mathcal{N}}}{g_{K\Lambda\mathcal{N}}} \approx -\frac{3}{2} \frac{g_{\Lambda\Sigma\pi}}{g_{\mathcal{N}\mathcal{N}\pi}}.$$

In addition to the three graphs of Fig. 2 there is a fourth graph (Fig. 3), with a K* exchange [4] which contributes

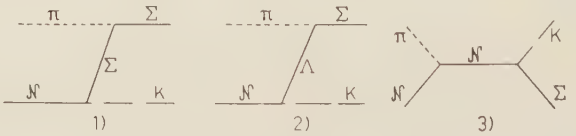

Fig. 2. – Feynman diagrams for Σ production.

(3) M. GELL-MANN: *The Eight-Fold Way*, California Institute of Technology report (1961).

(4) M. ALSTON, L. W. ALVAREZ, P. EBERHARD, M. L. GOOD, W. GRAZIANO, H. K. TICHO and S. G. WOJCICKI: *Phys. Rev. Lett.*, **5**, 520 (1960).

to both amplitudes A as well as B. If spin of K* is unity or if K* is scalar this will lead (as for K-Σ production ([5])) to a forward peaking of K-mesons. This

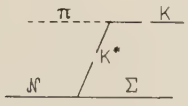

Fig. 3. – Diagram for Σ production with intermediate K*.

type of peaking does seem to show itself for a KΛ-production only at higher energies ($\gtrsim 1.3$ GeV ([2-5])). This seems to indicate that $N\Sigma K^*$ coupling is energy-dependent and our neglect of this around 1 GeV may be justified.

When Λ-Σ parity is odd an K-π even the experimental relation (1) can be obtained only if the K* graph is no longer neglected. The relations of coupling constant are not any more simple. The angular distributions of K's may now be peaked backwards at $E_\pi \approx 1$ GeV, the forward peak due to the K* graph becoming important at higher energies, as indicated by the experimental results ([1,2,6]).

* * *

We wish to thank Prof. R. G. Sachs for the hospitality of the Summer Institute for Theoretical Physics.

([5]) M. Gell-Mann and J. Tiomno: *Proc. of the 1960 Annual Intern. Conf. on High-Energy Physics at Rochester* (New York, 1960), p. 508; A. Salam and J. C. Ward: *Phys. Rev. Lett.*, **5**, 390 (1960). Also J. Tiomno, A. Videira and N. Zagury: *Phys. Rev. Lett.*, **6**, 120 (1961); M. Beg and P. DeCelles: *Phys. Rev. Lett.*, **6**, 145 (1961); C. Chan: *Phys. Rev. Lett.*, **6**, 383 (1961).

([6]) M. I. Soloviev: *Proc. of the 1960 Rochester Conference*, p. 388.

Total Inelastic Cross-Section for Negative Pions and Protons in Cu, Cd, and Pb at High Energies.

R. N. Peacock, B. Hahn, E. Hugentobler and F. Steinrisser

Department of Physics, University of Fribourg - Fribourg

(ricevuto il 13 Settembre 1961)

Total inelastic cross-sections have been measured in Cu, Cd and Pb absorbers for negative pions of 6.0, 11.3, 16 and 17.6 GeV/c, and for protons of 24 GeV/c. The three absorbers, each 15.0 mm thick, 70 mm deep, and about 30 mm long, were mounted on an aluminum alloy bracket in a 16 cm diameter Freon bubble chamber [1] as shown in Fig. 1. Using a collimated beam as large as the absorber assembly, data could be obtained simultaneously for all three metals. As contrasted to counter methods the use of a bubble chamber to measure cross-sections is tedious if good statistics are necessary, but it has the advantage that the processes causing absorption of the beam may be identified when desired.

The particle beams used were from the CERN proton synchrotron. In correcting the data the muon contamination of the pion beam was taken as 5^{0}_{0}. The proton beam was essentially pure. Further information on certain beams from the CERN proton synchrotron, and some absorption cross-sections measured by counter methods are given by von Dardel *et al.* [2] and by Ashmore *et al.* [3].

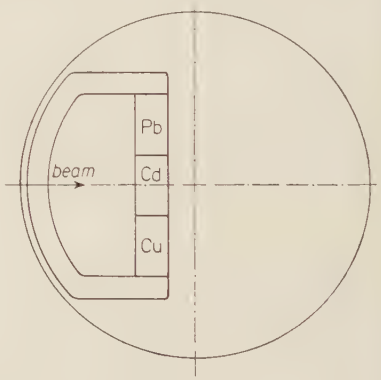

Fig. 1. Arrangement of the bubble chamber with absorbers in position.

The scanning procedure was simple. Using a suitable mask to identify the metals in projection, the number of

(1) B. Hahn, A. W. Knudsen and E. Hugentobler: *Suppl. Nuovo Cimento*, **15**, 236 (1960).

(2) G. von Dardel, D. H. Frisch, R. Mermod, R. H. Milburn, P. A. Piroué, M. Vivargent, G. Weber and K. Winter: *Phys. Rev. Lett.*, **5**, 333 (1960).

(3) A. Ashmore, G. Cocconi, A. N. Diddens and A. M. Wetherell: *Phys. Rev. Lett.*, **5**, 576 (1960).

entering particles and the number of inelastic events for each absorber were collected in a register system. In general the scanning was done with a single view since stereo was not necessary. Checks made by scanning a particular section of film using several people, and the good agreement of results obtained by different scanners, have confirmed that the scanning errors were small.

of the cross-sections may be obtained by averaging the r_0 values for the various metals at each momentum. The results are:

6.0 GeV/c: $r_0=(1.22\pm0.02)$ fermi;

11.3 GeV/c; $r_0=(1.21\pm0.03)$ fermi;

17 GeV/c; $r_0=(1.24\pm0.03)$ fermi;

24 GeV/c: $r_0=(1.24\pm0.02)$ fermi.

TABLE I. – *Inelastic cross-sections.*

Momentum GeV/c	Particle	Cu		Cd		Pb	
		σ_{inel} (mb)	r_0 (fermi)	σ_{inel} (mb)	r_0 (fermi)	σ_{inel} (mb)	r_0 (fermi)
6.0	π^-	675 ± 30	$1.16\pm.03$	1230 ± 50	$1.30\pm.04$	1610 ± 80	$1.21\pm.04$
11.3	π^-	616 ± 60	$1.11\pm.06$	1120 ± 80	$1.24\pm.06$	1830 ± 130	$1.29\pm.06$
16, 17.6	π^-	672 ± 40	$1.16\pm.04$	1240 ± 70	$1.31\pm.05$	1700 ± 120	$1.24\pm.06$
24	p	715 ± 20	$1.20\pm.02$	1146 ± 40	$1.25\pm.03$	1810 ± 60	$1.28\pm.03$
Cern results 24 GeV/c p		740 ± 20		1180 ± 25		1750 ± 30	

Results for the total inelastic cross-sections are shown in Table I. The errors stated are statistical only. The statistics obtained are not adequate to show a variation of the cross-section with energy, or a difference between the results for pions and protons. Values for r_0 are also given, computed assuming that the cross-sections obey a $\pi r_0^2 A^{\frac{2}{3}}$ law. The absorption cross-sections found for these metals by the CERN group [4] are included in the table for comparison.

Further evidence for the constancy

Thus, within statistical errors, the r_0 values are constant in the momentum range of 6 to 24 GeV/c.

The use of a Freon bubble chamber made it possible to include an estimate of the contribution of the processes

$$p+p\ (\text{or } n)\rightarrow p+p\ (\text{or } n)+\pi^0,$$

and

$$\pi^-+p\ (\text{or } n)\rightarrow \pi^-+p\ (\text{or } n)+\pi^0,$$

to the total inelastic cross-section [5]. As seen in the chamber these events

[4] A. ASHMORE, G. COCCONI, A. N. DIDDENS and A. M. WETHERELL: CERN Report SC 60-11 (much of the information in this report is included in the preceding reference).

[5] G. COCCONI, A. N. DIDDENS, E. LILLETHUN and A. M. WETHERELL: *Phys. Rev. Lett.*, **6**, 231 (1961).

are often indistinguishable from elastic scattering, especially when the interaction takes place in an absorber. However, the average pair conversion length in Freon for γ-rays of the energy concerned is about 16 cm, enabling detection of the inelasticity 60% of the time. Such events were detected in two steps: in the first, possible events with projected scattering angles greater than 10 mrad were recorded during the general scanning; in the second, a search was made for π^0 production without visible deflection of the entering track. For the latter method $3 \cdot 10^3$ negative pion tracks and 10^4 proton tracks were examined.

In the scanning of the 10^4 proton tracks nine electron pairs were found that were probably aimed at primary protons passing through the absorbers. All cases with electron pairs were examined on two views, but a background of electron pairs was present, making it somewhat difficult to be sure of the origin of a low-energy pair. Seven of these electron pairs were of low energy, 50 MeV or less. Only two pairs had an energy greater than 500 MeV, and one of them was accompanied by 50 mrad scattering of the primary proton. All events showed but a single electron pair, making it questionable that π^0-decay was the only source of electron pairs. Based on this data plus that from small angle one-prongs found in normal scanning, the processes

$$p+p\ (\text{or } n) \rightarrow p+p\ (\text{or } n)+\pi^0,$$

were assumed to contribute 2% of the total inelastic cross-section. The results for pions are the same.

The 311 one-prongs found in all negative pion scanning were carefully examined a second time for electron pairs. Twelve electron pairs were found, or, correcting for the pair conversion length, 7% of the one-prongs were inelastic. The projected scattering angle was required to be greater than 10 mrad, except for Pb at 6 GeV/c where only deflections greater than 20 mrad were accepted.

* * *

We would like to acknowledge the assistance of the staff of CERN, particularly Mr. J. GEIBEL, for making it possible to operate our chamber at the proton synchrotron. Dr. H. H. BINGHAM and Dr. H. FILTHUTH have been of especial help in setting up the beams. Miss G. JUNGO has helped with a considerable portion of the scanning.

On the Decay $\Sigma^0 \to \Lambda^0 + \gamma$ in the Charge-Independent Pion Interaction.

P. Prakash (*)

Centro Brasileiro de Pesquisas Físicas - Rio de Janeiro

(ricevuto il 23 Ottobre 1961)

Σ^0 is known to radiate rapidly into Λ^0 and a photon with a lifetime $\tau < 10^{-10}$ s. The decay is possible due to the anomalous $\Sigma^0\Lambda^0$ magnetic momentum generated by the pion and K meson-cloud around these particles, *e.g.*

$$\Sigma^0 + \pi^\pm \to \Sigma^\pm + \gamma \to \Lambda^0 + \gamma\,, \quad \Sigma^0 + K^- \to p + \gamma + \Lambda^0 + \gamma\,, \quad \Sigma^0 \to K^+ + \Xi^- \to \gamma + \Lambda^0 + \gamma\,.$$

The knowledge of this anomalous magnetic momentum is also important for the associated decay $\Sigma^0 \to \Lambda^0 + e^+ + e^-$ which has been proposed for the determination of the $\Sigma\Lambda$ parity [1].

The pion interaction in the charge-independent form and consequently in the Doublet Approximation [2] of Tiomno, Gell-Mann and Pais does give rise to an anomalous $\Sigma^0\Lambda^0$ magnetic moment and hence the decay $\Sigma^0 \to \Lambda^0 + \gamma$ contrary to the implied forbiddenness in Pais's paper [3]. The magnetic moment contributions being due to the isovector pion and Σ currents (in the usual charge-independent scheme) is expected to be of the order of magnitude of the nucleon magnetic moments where the main contribution is known to come from the isovector part (**).

The charge independent strong interaction of pions and baryons is written as

$$(1)\quad iG_1\bar{N}_1\boldsymbol{\tau}\gamma_5 N_1\cdot\boldsymbol{\pi} + iG_4\bar{N}_4\boldsymbol{\tau}\gamma_5 N_4\cdot\boldsymbol{\pi} + G_2(\bar{\Sigma}^+\Gamma\Lambda^0\pi^+ + \bar{\Sigma}^0\Gamma\Lambda^0\pi^0 + \bar{\Sigma}^-\Gamma\Lambda^0\pi^-) + \text{h.c.} +$$
$$+ iG_3[(\bar{\Sigma}^0\gamma_5\Sigma^- - \bar{\Sigma}^-\gamma_5\Sigma^0)\pi^+ - (\bar{\Sigma}^+\gamma_5\Sigma^- - \bar{\Sigma}^-\gamma_5\Sigma^+)\pi^0 - (\bar{\Sigma}^+\gamma_5\Sigma^0 - \bar{\Sigma}^0\gamma_5\Sigma^+)\pi^-]\,,$$

(*) Supported in part by the Conselho Nacional de Pesquisas of Brazil.

(1) G. Feinberg: *Phys. Rev.*, **109**, 1019 (L) (1958); G. Feldman and T. Fulton: *Nucl. Phys.*, 8, 106 (1958).

(2) J. Tiomno: *Nuovo Cimento*, **6**, 69 (1957); M. Gell-Mann: *Phys. Rev.*, **106**, 1296 (1957) and A. Pais: *Phys. Rev.*, **110**, 574 (1958).

(3) A. Pais: *Phys. Rev.*, **112**, 624 (1958).

(**) We can write the anomalous magnetic moment as $\mu = \mu_s + \mu_v T_3$ where T_3 is the third component of isospin matrix. Then for nucleons $\mu_p = \mu_s + \mu_v = 1.79$; $\mu_n = \mu_s - \mu_v = -1.91$ giving $\mu_s = -0.06$ and $\mu_v = 1.85$ in nuclear magnetons.

where $N_1 \left(\begin{matrix} P \\ n \end{matrix}\right)$ $N_4 \left(\begin{matrix} \Xi^0 \\ \Xi \end{matrix}\right)$ and Γ 1 or $i\gamma_5$. The doublet approximation is obtained by assuming (Λ, Σ and N having same parities) $\Gamma = i\gamma_5$, $G_2 = G_3 = G$, neglecting the mass difference between Σ and Λ and writing the mas two doublets (*) $N_2 = \left(\begin{matrix} \Sigma^+ \\ \Upsilon^0 \end{matrix}\right)$. $N_3 = \left(\begin{matrix} Z^0 \\ \Sigma^- \end{matrix}\right)$ where $\Upsilon^0 = (\Lambda^0 - \Sigma^0)/\sqrt{2}$ and $Z^0 = (\Lambda^0 + \Sigma^0)/\sqrt{2}$. The strong interaction can then be written as (**)

$$i[G_1 \bar{N}_1 \boldsymbol{\tau} \gamma_5 N_1 + G(\bar{N}_2 \boldsymbol{\tau} \gamma_5 N_2 + \bar{N}_3 \boldsymbol{\tau} \gamma_5 N_3) + G_4 \bar{N}_4 \boldsymbol{\tau} \gamma_5 N_4] \cdot \boldsymbol{\pi} \,. \tag{2}$$

The interaction with the electromagnetic field is written as

$$H_{\mathrm{em}} = -ie \left(\frac{\partial \pi^{+*}}{\partial x_\mu} \pi^+ - \pi^{+*} \frac{\partial \pi^+}{\partial x_\mu} \right) A_\mu + e^2 \pi^{+*} \pi^+ A_\mu^2 \,.$$

$$H'_{\mathrm{em}} = -ie(\bar{p} \gamma_\mu p + \bar{\Sigma}^+ \gamma_\mu \Sigma^+ - \bar{\Sigma}^- \gamma_\mu \Sigma^- - \bar{\Xi}^- \gamma_\mu \Xi^-) A_\mu \,.$$

The latter one can also be written in the form

$$H_{\mathrm{em}} \quad ie \left[\bar{N}_1 \gamma_\mu \left(\frac{1 + \tau_3}{2} \right) N_1 - \bar{N}_2 \gamma_\mu \left(\frac{1 - \tau_3}{2} \right) N_2 - \right.$$

$$\left. + \bar{N}_3 \gamma_\mu \left(\frac{-1 + \tau_3}{2} \right) N_3 + \bar{N}_4 \gamma_\mu \left(\frac{-1 + \tau_3}{2} \right) N_4 \right] A_\mu \,.$$

The last two terms in this form can be combined to give the form $-e \cdot \bar{\Sigma} \gamma_\mu \varrho_3 \Sigma A_\mu$, where $\boldsymbol{\varrho}$ are the isospin matrices for isospin one.

The anomalous magnetic moment λ calculated from the Feynman graphs shown in the Fig. 1 is given by the following:

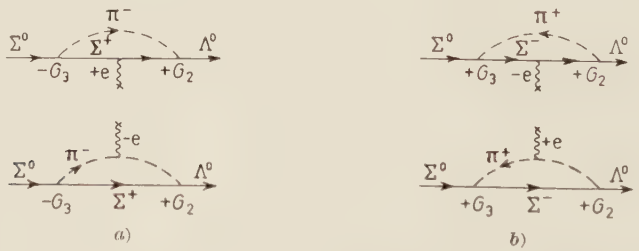

Fig. 1. – Feynman graphs contributing to the $\Sigma^0 \Lambda^0$ anomalous magnetic moment.

(*) When the relative parities of various baryons are different, a modified doublet theory can be developed using doublets which are eigenstates of parity. See a forthcoming paper.

(**) It may be remarked that this form of writing the strong interaction is more general than the usual charge-independent theory interaction (1). For if $G_2 \neq G_3$ we obtain for the Λ and Σ interaction an additional term of the form:

$$\{(-\bar{\Sigma}^- i\gamma_5 \Sigma^0 \pi^+ - \bar{\Sigma}^- i\gamma_5 \Sigma^0 \pi^-) + \text{h.c.} + (\bar{\Sigma}^+ i\gamma_5 \Sigma^+ + \bar{\Sigma}^- i\gamma_5 \Sigma^-) \pi_0 - (\bar{\Sigma}^0 i\gamma_5 \Sigma^0 + \bar{\Lambda}^0 i\gamma_5 \Lambda^0) \pi^0 + (\bar{\Sigma}^+ i\gamma_5 \Lambda^0 \pi^+ - \bar{\Sigma}^- i\gamma_5 \Lambda^0 \pi^-)\}.$$

For the same Σ and Λ parities $II = +$ (pion assumed pseudoscalar)

$$\lambda_+ = -\left(\frac{G_2 G_3}{4\pi}\right)\left(\frac{e}{2M}\right)\cdot\frac{1}{\pi} f(\eta) ,$$

where $\eta = m_\pi / M$ and

$$f(\eta) = 1 - \eta^2 \ln \eta + \frac{\eta^4 - 2\eta^2}{\sqrt{4\eta^2 - \eta^4}} \cos^{-1}\left(\frac{\eta}{2}\right).$$

We neglect the mass difference of Σ^0 and Λ^0.

For $II = -$ (*)

$$\lambda_- = +\left(\frac{G_2' G_3}{4\pi}\right)\left(\frac{e}{2M}\right)\frac{1}{\pi} h(\eta) ,$$

where

$$h(\eta) = -\ln \eta + \frac{\eta}{\sqrt{4 - \eta^2}} \cos^{-1}\left(\frac{\eta}{2}\right).$$

For $\eta = 0.121$ and

$$\left.\begin{aligned} II = + \qquad & \lambda_+ = -\left(\frac{G_2 G_3}{4\pi}\right)\left(\frac{0.849}{\pi}\right) \\ II = - \qquad & \lambda_- = +\left(\frac{G_2' G_3}{4\pi}\right)\left(\frac{2.204}{\pi}\right) \end{aligned}\right\} \text{ in units of } \left(\frac{e}{2M}\right).$$

Thus

$$\lambda_- / \lambda_+ = -2.595 (G_2' / G_2) .$$

The corresponding decay probability for the decay is

$$\frac{1}{\tau} \qquad \Gamma = \frac{1}{\pi} |\lambda|^2 \cdot \omega^3 ,$$

where ω is the energy of the photon.

For

$$II + \qquad \tau_+ = \left(4.38 \Big/ \left(\frac{G_2 G_3}{4\pi}\right)^2\right)\cdot 10^{-18} \text{ s} .$$

For

$$II - \qquad \tau_- = \left(0.65 \Big/ \left(\frac{G_2' G_3}{4\pi}\right)^2\right)\cdot 10^{-18} \text{ s} .$$

(*) G_2' being the $\Sigma\Lambda\pi$ coupling constant in this case.

For

$$\left(\frac{G_2 G_3}{4\pi}\right)^2 = \left(\frac{G_2' G_3}{4\pi}\right)^2 \simeq 3\,,$$

the life time is $\sim 1.46 \cdot 10^{-18}$ s for the same $\Sigma\Lambda$ parity while it is $\sim 0.33 \cdot 10^{-18}$ s in the case the parity is opposite.

* * *

The author is grateful to Professor J. Tiomno for suggesting the problem. The author acknowledges gratefully several useful discussions with him and Professor J. Leite Lopes.

π^+ Decay of a $^4He_\Lambda$ Hyperfragment (*).

Y. W. Kang, N. Kwak, J. Schneps and P. A. Smith
Department of Physics, Tufts University - Medford, Mass.

(ricevuto il 7 Novembre 1961)

In a stack of Ilford K-5 emulsion pellicles exposed to an enriched 800 MeV/c K^- beam at the Bevatron we have discovered an event which corresponds to the π^--mesonic decay of a $^4He_\Lambda$ hyperfragment. The hyperfragment emerged from an 11-prong star produced by a K^--meson of the beam. The hyperfragment track (F) had a range of 361 μm, was completely saturated, and showed scattering near the end which indicated that the fragment had come to rest. The fragment decayed into two particles; a particle of range 96.6 μm (track 1) and a π^+-meson (track 2) of range 1693 μm. The π^+-meson was identified by the fact that after coming to rest it underwent the characteristic π-μ-e decay, the range of the μ-meson being 589 μm. The measurements on this event are given in Table I.

There are only two possible interpretations for this hyperfragment decay. These are:

$$(1) \qquad {}^4He_\Lambda \to n + \pi^+ + {}^3H \,,$$

$$(2) \qquad {}^4He_\Lambda \to n + n + \pi^+ + {}^2H \,.$$

In the case of reaction (1) the Q value turns out to be 34.2 MeV and the binding energy of the Λ (1.5 ± 0.5) MeV (using $Q = 37.58$ MeV). In the case of (2), since there are two neutrons, we can only give limits on the Q value and binding energy. These are $19.9 < Q < 26.2$ and $3.4 < B < 9.6$. The measured binding energy of $^4He_\Lambda$ is (2.36 ± 0.12) MeV [1]. Any other interpretation of this event with one or more neutrons can be ruled out because the binding energies obtained are inconsistent with known values.

As a check on the identity of the hyperfragment we have made thickness measurements on track F, track 1, and a ^8Li track of dip angle 25° which was found in the same plate. Since the three tracks were nearby and were measured at the same time under equivalent conditions, we expect any uncertainties due to fluctuations in development or illumination will be unimportant. Each track was measured from a point beginning at 25 μm residual range to a point corresponding to 68 μm residual

(*) Supported by the U. S. Atomic Energy Commission.

(1) R. Ammar, R. Levi Setti, W. E. Slater, S. Limentani, P. E. Schlein and P. H. Steinberg: *Nuovo Cimento*, **15**, 181 (1960).

TABLE I. – *Measurements on tracks* F, 1, 2.

Track	Dip angle (degrees)	Angle in plane of emulsion (degrees)	Range (microns)	Identity	Energy (MeV)
F	+ 24.5	—	361	$^4He_\Lambda$	30.9
1	+ 15.4	0	96.6	^3H or ^2H	5.2 or 4.5
2	— 47.3	8.6	1693	π^+	8.4

range, a total of 64 measurements being made on each track. The mean values of the thickness were found to be (0.75 ± 0.01) μm for track *F*, $(0.66 \pm \pm 0.01)$ μm for track 1, and $(1.01 \pm \pm 0.01)$ μm for the ^8Li track. This result is consistent with the assignment of charge 2 for the hyperfragment track.

This π^+-mesonic decay of a hyperfragment in nuclear emulsion is only the second such decay which has been reported. The first was found in this laboratory three years ago (2), and could be interpreted as $^7Li_\Lambda \to n + \pi^+ + {}^6He$, $^7Be_\Lambda \to$ $\to n + \pi^+ + {}^6Li$, or $^5He_\Lambda \to n + n + \pi^+ + {}^3H$. Hyperfragment studies since then do not unambiguously indicate the existence of $^7Be_\Lambda$. Also, as DELOFF *et al.* (3) have pointed out, the probability of a $^5He_\Lambda$ hyperfragment undergoing π^+-decay is very small because the ^4He core is so tightly bound. Thus the $^7Li_\Lambda$ interpretation seems most likely.

Since the identification of a π^+-mesonic decay in emulsion is quite easy, it is fortuitous that the only two events which have been observed in emulsion were both in this laboratory. Therefore in attempting to obtain a rough estimate of the frequency of π^+-mesonic decay, we have tried to use all the data on π^- decays which have been reported in the literature by emulsion groups. The total number of π^--mesonic decays reported is about 400 (4). Thus the ratio of π^+ to π^- decays for all hyperfragments is, on the basis of two events, $2/400 = = 0.5 \cdot 10^{-2}$. For the case of $^4He_\Lambda$, DELOFF *et al.* (3) have calculated this ratio assuming that the π^+-decay arises from the Σ^+ virtual state of the Λ, and find that it is of the order of 10^{-2}. On the basis of our one π^+-decay of $^4He_\Lambda$, and some 60 π^--decays reported in the literature, the ratio is $1/60 = 1.6 \cdot 10^{-2}$.

DELOFF *et al.* also predict that the mesons from π^+-decays will generally be considerably less energetic than those

(2) J. SCHNEPS: *Phys. Rev.*, **112**, 1335 (1958).

(3) A. DELOFF, J. SZYMANSKI and J. WRZECIONKO: *Bulletin de l'Académie Polonaise des Sciences, Série des Sciences Mathématiques, Astronomiques et Physiques*, **7**, 521 (1959).

(4) S. LIMENTANI, P. E. SCHLEIN, P. H. STEINBERG and J. H. ROBERTS: *Nuovo Cimento*, **9**, 1046 (1958); C. GROTE: *Nuovo Cimento*, **10**, 652 (1958); P. L. JAIN: *Nuovo Cimento*, **10**, 557 (1958); W. E. SLATER: *Suppl. Nuovo Cimento*, **10**, 1 (1958); R. LEVI SETTI, W. E. SLATER and V. L. TELEGDI: *Suppl. Nuovo Cimento*, **10**, 68 (1958); F. BREIVIK, O. SKJEGGESTAD, S. O. SÖRENSEN and A. SELHEIM: *Nuovo Cimento*, **12**, 531 (1959); S. MORA and I. ORTALLI: *Nuovo Cimento*, **12**, 635 (1959); G. C. DEKA: *Nuovo Cimento*, **14**, 1217 (1959); J. SACTON: *Nuovo Cimento*, **15**, 110 (1960); R. AMMAR, R. LEVI SETTI and W. E. SLATER: *Nuovo Cimento*, **15**, 181 (1960); M. TAHER-ZADEH: *Nuovo Cimento*, **17**, 980 (1960); R. AMMAR, R. LEVI SETTI and W. E. SLATER: *Nuovo Cimento*, **19**, 20 (1961); P. E. SCHLEIN and W. E. SLATER: *Nuovo Cimento*, **21**, 212 (1961); Y. PRAKASH, P. H. STEINBERG, D. A. CHANDLER and R. J. PREM: *Nuovo Cimento*, **21**, 235 (1961). (This list does not include papers published before the World Survey of LEVI SETTI, SLATER and TELEGDI since most of their events are included in that survey).

from π^--decays. This is because the decay from a Σ^+ virtual state involves the change of a proton to a neutron in the hyperfragment core. It is interesting to note that the energy of the π^+-meson in these two events was relatively low, 13.8 MeV in the previously reported case, and 8.4 MeV in the present one.

* * *

The authors are grateful to Dr. E. J. LOFGREN and Dr. J. MURRAY for making possible the exposure at the Bevatron.

Energy-Dependence of Fragmentation Parameters.

D. E. Evans and R. R. Hillier

H. H. Wills Physical Laboratory, University of Bristol - Bristol

(ricevuto il 13 Novembre 1961)

One of the basic problems in the theory of the origin of the cosmic rays is the interpretation of their chemical composition as observed from the earth. It is possible to make an estimate of their composition at the source and the amount of interstellar hydrogen through which they have passed on their journey from the source to the earth by adopting some specific model for their propagation through space. Any model of this kind contains the so-called fragmentation parameters, P_{ij}, which are measures of the spallation products of heavy cosmic ray nuclei in interactions with interstellar hydrogen. Normally P_{ij}'s are calculated from an analysis of the fragmentation of cosmic ray nuclei in interactions with the nuclei of elements present in nuclear emulsion. It is usually assumed that the fragmentation parameters are independent of energy but we believe that evidence exists which shows that this is not true.

It is not easy to measure the energy-dependence directly. Most measurements of the P_{ij}'s have been made in emulsion stacks exposed at geomagnetic latitudes where the incident nuclei are all relativistic, since this facilitates charge measurements on the tracks. The incident nuclei have a wide range of energies but the fluxes are too small to allow separation into energy groups and at the same time to retain good statistics. The results averaged over the energy spectrum above 1.5 GeV/nucleon are not significantly different from those averaged over energies in excess of about 7 GeV/nucleon [1].

The fragmentation in flight of cosmic ray nuclei is merely an evaporation process taking place in a moving frame or reference, and is therefore exactly the same process as the evaporation of emulsion nuclei which have been excited by bombardment with fast protons. Mono-energetic beams of protons are available from particle accelerators and they have been used to study the energy-dependence of the evaporation process. Conclusions can be drawn about the parallel process of fragmentation in flight from these studies.

A parameter which has been used extensively to characterize the de-excitation of emulsion nuclei is the number, N_h, of tracks with grain density $> 1.4\, g_{\min}$, emerging from disintegrations. Fig. 1 shows the N_h distributions obtained by various investigators for incident

[1] C. J. Waddington: *Progr. Nucl. Phys.*, 8, 1 (1960).

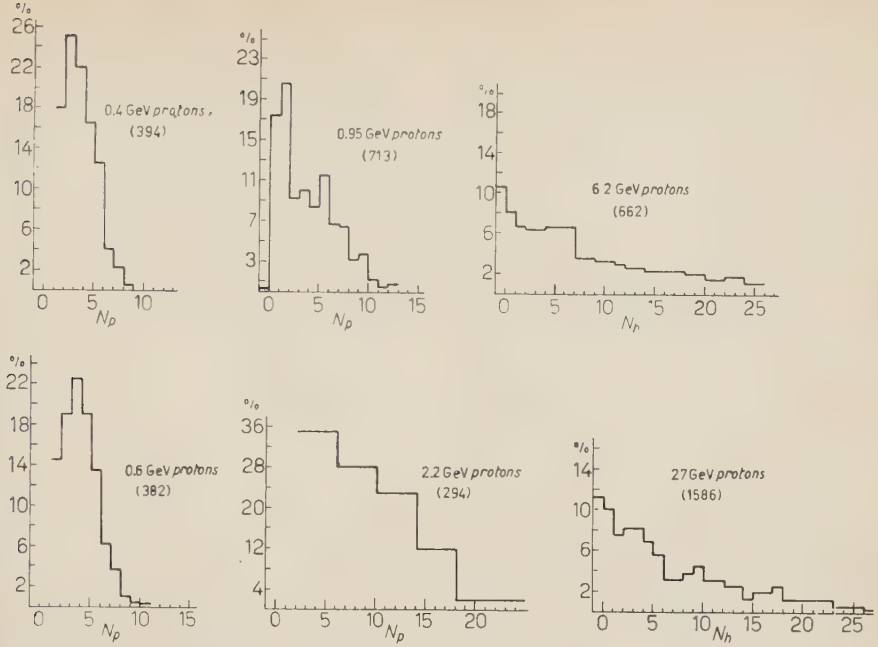

Fig. 1. – Prong distributions of stars produced in nuclear emulsion by artificially accelerated protons of the energy indicated. The number of individual events contributing to each histogram is shown in brackets. The parameters N_h and N_p are defined in the text.

proton energies of 0.4 ([2]), 0.6 ([3]), 0.95 ([4]), 2.2 ([5]), 6.2 ([6]) and 27 ([7]) GeV. The energy-dependence can be seen more clearly in the integral distributions, plotted semi-logarithmically in Fig. 2. The disintegrations produced by 0.4, 0.6 and 2.2 GeV protons were detected by area scanning, and a scanning inefficiency may account for the lack of stars with $N_h = 0, 1$ and 2. In the experiments using 0.4, 0.6, 0.95 and

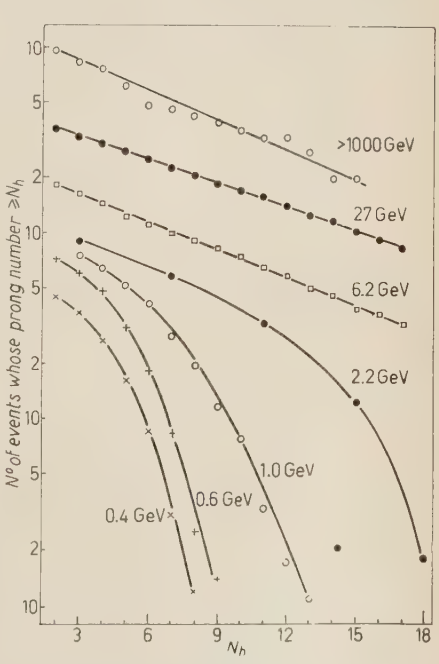

Fig. 2. – Integral prong distributions constructed from the differential distributions shown in Fig. 1. The curves have been moved up and down the ordinate scale for convenience.

([2]) A. D. Sprague, D. M. Haskin, R. G. Glasser and M. Schein: *Phys. Rev.*, **94**, 994 (1954).

([3]) W. O. Lock and P. V. March: *Proc. Roy. Soc.*, A **230**, 222 (1955).

([4]) W. O. Lock, P. V. March and R. McKeague: *Proc. Roy. Soc.*, A **231**, 368 (1955).

([5]) M. Widgoff, C. P. Leavitt, A. M. Shapiro, L. W. Smith and C. E. Swartz: *Phys. Rev.*, **92**, 851 (1953).

([6]) A. Barbaro-Galtieri, A. Manfredini, B. Quassiati, C. Castagnoli, A. Gainotti and I. Ortalli: *Nuovo Cimento*, **21**, 469 (1961).

([7]) A. Winzeler, B. Klaiber, W. Koch, M. Nikolić and M. Schneeberger: *Nuovo Cimento*, **17**, 8 (1960).

2.2 GeV protons, the authors measured N_p, the total number of tracks leaving the disintegration, rather than N_h; at 2.2 GeV there is an average of 0.5 light tracks per star, and at lower energies there are even fewer. However, the energy-dependence of the distributions is most marked at large values of N_h where distortions of the distributions due to the effects just described are expected to be least significant.

It is clear that the probability of an interaction producing a large number of prongs increases with increasing energy between 0.4 and 2.2 GeV/nucleon, and thereafter approaches a limit which has been reached by 6.2 GeV/nucleon. The change between 6.2 and 27 GeV appears to be negligible and indeed, the N_h distribution derived from the study of ultra-high energy ($>$ 1000 GeV) cosmic ray proton-induced events ([8]) suggests that the probability remains about constant to at least as high energy as this.

The fragmentation parameters cannot be calculated from the N_h distributions for emulsion nuclei, but it is very improbable that they should be independent of energy while the N_h distributions vary in the way shown above. It is not clear whether the energy-dependence is equally marked for both light and heavy nuclei.

If the fragmentation parameters are measured in the usual way by analysing the interactions of cosmic ray nuclei over a region of the energy spectrum, the results can be used without error to describe the propagation of these nuclei, provided that their energy is not changing. The results should not be used to calculate the propagation of nuclei in a different energy region. Moreover it is not correct to use one set of parameters to describe the acceleration of a group of nuclei from rest to relativistic energies.

* * *

We are grateful to Dr. H. H. Aly for helpful discussion.

([8]) B. P. Edwards, J. Losty, K. Pinkau, D. H. Perkins and J. Reynolds: *Phil. Mag.*, **3**, 237 (1958).

IL NUOVO CIMENTO Vol. XXII, N. 6 16 Dicembre 1961

A Note on Non-Linear Effects in Electrodynamics.

Z. Fried

U.S. Naval Ordnance Laboratory - Silver Spring, Md.

(ricevuto il 13 Novembre 1961)

Since the advent of lasers a new stimulus has been added to the study of non-linear effects in electrodynamics. The feasibility of producing a large flux of photons suggests many interesting experiments. Among these is the well-known [1] photon-photon scattering which as yet cannot be reached by the existing lasers. There are, however, other, not as well publicized non-linear effects which are amenable to the present day technology. These include the possibility of two or more photons interacting « simultaneously » with a given scattering center. Among the end products of such an encounter, several possibilities may materialize. The more spectacular are

(1) $$\gamma+\gamma+\mathrm{e}\to\gamma'+\mathrm{e}'\,,$$

(2) $$\gamma+\gamma+\mathrm{A}\to\mathrm{A}^*\,,$$

(3) $$\gamma+\gamma+\gamma+\mathrm{e}\to\gamma''+\mathrm{e}'\,,$$

(4) $$\mathrm{e}+\gamma+\gamma+\gamma\to\gamma'+\gamma+\mathrm{e}'\,.$$

If the incident photons have low energy *i.e.* $\omega\ll m$, the emerging photons will be of energy 2ω and 3ω in reactions (1) and (3). Reaction (2) corresponds to a two-photon excitation of an atom. Reactions (1) and (2) have been in effect observed [2,3].

It is the aim of this note to present results for reaction (1) based on perturbative expansion of the S-matrix in quantum electrodynamics and draw attention to some of the interesting kinematical features of reactions (3) and (4).

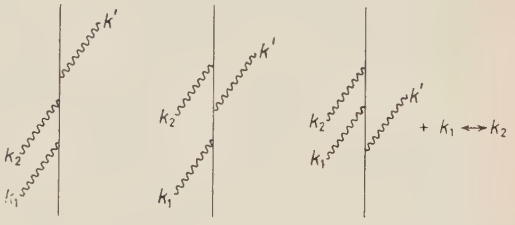

Fig. 1. – Feynman graphs for reaction (1).

[1] J. M. Jauch and F. Rohrlich: *The Theory of Photons and Electrons*, Chap. 13 (Cambridge, 1955), p. 295.

[2] P. A. Franken, A. E. Hill, C. W. Peters and G. Weinreich: *Phys. Rev. Lett.*, **7**, 118 (1961).

[3] W. Kaiser and C. G. R. Garrett: *Phys. Rev. Lett.*, **7**, 229 (1961).

The intrinsic rate to be computed from the theory for reaction (1) is the number of events per unit time per unit flux per unit density of the incoming photon beam. The relevant lowest order Feynman graphs are shown in Fig. 1. In the event that both incoming photons have identical momenta, and the electron is at rest, the differential rate for unpolarized incoming light and unpolarized target electrons summed over the polarization of the outgoing photon is given by

$$(5)\qquad \frac{\mathrm{d}R}{\mathrm{d}\Omega}(\omega,\theta)=\frac{r_0^3}{(2\pi)^2}\left(\frac{\omega'}{\omega}\right)^2\frac{1}{32\omega m}\cdot$$

$$\cdot\left[\left(\frac{\omega'}{4\omega}\right)(11-y-12y^2)+(2+5y^2-3y+5y^3-8y^4)+\left(\frac{\omega}{\omega'}\right)(7-2y-5y^2)+4\frac{\omega}{m}(1-y)(1-y^2)\right],$$

where ω is the energy of the incoming photons, $y=\cos\theta$, θ being the angle between incoming and outgoing photons, ω' is the energy of the emerging photon, r_0 is the classical electron radius, and $\hbar=c=1$:

$$(6)\qquad \omega'=\frac{2\omega}{1+(2\omega/m)(1-y)}\,.$$

The total rate for the above process in the low-energy limit, *i.e.* $\omega\ll m$, is given by

$$(7)\qquad R=\frac{r_0^3}{2\pi}\frac{29}{40\omega m}\,.$$

Since we have computed the reaction rate for (1), *i.e.* free electrons, our results cannot be compared directly with the experimental results of P. A. Franken *et al.* [2]. There are, however, still some worth-while points to make in connection with eq. (7):

a) The low energy rate for reaction (1) is proportional to [4] $1/\omega$. The $1/\omega$ dependence will also hold for scattering off a bound electron provided that there are no resonances.

b) Our results indicate that an anisotropic scattering medium is not essential for this non-linear effect. This is in disagreement with the statement of Franken *et al.* [2].

Furthermore, we would like to draw attention to the feasibility of detecting the following reactions:

$$(8)\qquad \gamma+\gamma+\gamma+\mathrm{e}\to\mathrm{e}'+\gamma'''\,.$$

$$(9)\qquad \gamma+\gamma+\gamma+\mathrm{e}\to\mathrm{e}'+\gamma''+\gamma\,.$$

A preliminary calculation of reaction (8) indicates that the number of events in the output should be of the same order of magnitude as that of reaction (1). Although the rate for reaction (8) is of higher order in the fine structure constant, the rate

[4] It si entirely possible that if we add up the transition rates for all the processes in which two incoming photons can participate to order e^6, the resulting $1/\omega$ term will cancel. This will be examined in a subsequent paper.

is proportional to $1/\omega^4$, and thus for presently available photon densities, reaction (8) should be detectable.

We now wish to draw attention to reaction (9). Here there are three incoming photons and two outgoing photons. In the outgoing photons γ'' has twice the frequency of γ and γ' has the same quantum number as γ.

The major contribution to such a final state will arise from the interference terms of the Feynman graphs shown in Fig. 2.

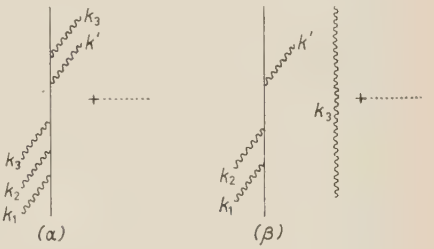

Fig. 2. – Feynman graphs for reaction (9).

These are the interference terms between amplitudes in which all three incoming photons scatter off the electron (α) and the amplitude (β) in which two of the photons interact with the electron and the third photon goes straight through. This interference term has the same power of e^2 as the transition rate for reaction (8). Its energy dependence at low ω is again $1/\omega^4$. Its sign, however, is negative. The important conclusion we can draw from this is that the double frequency output will not be strictly proportional to the (flux)$\times$(density). It will be of the form [5]:

$$N(2\nu) = \{A(\omega) - B(\omega)\,\text{density}\}\,\text{flux} \times \text{density}\,, \tag{10}$$

where $N(2\nu)$ is the number of events with outgoing photons having frequency 2ν.

* * *

The author has profited from discussions with Drs. W. M. Frank, H. R. Reiss and Mr. A. L. Licht of this Laboratory and Dr. I. Manning of the Naval Research Laboratory.

[5] This effect has been observed by J. A. Giordmaine (to be published). I am indebted to Dr. E. S. Dayhoff for bringing this reference to my attention.

A Coupled Analysis of the $I = \frac{3}{2}$, $J = \frac{3}{2}$, P and D Waves in Pion-Nucleon Scattering.

E. Galzenati and M. Pusterla

Istituto di Fisica Teorica dell'Università - Napoli
Istituto di Fisica Teorica dell'Università - Bari
Istituto Nazionale di Fisica Nucleare - Sottosezione di Napoli

(ricevuto il 15 Novembre 1961)

The partial wave amplitudes f^I_{l+} and $f^I_{(l+1)-}$ for pion-nucleon scattering corresponding to the same isotopic spin I and total angular momentum $J = l + \frac{1}{2}$, and to opposite parity, are coupled by analytic continuation in the w plane (w is the c.m.s. total energy) through Mac Dowell's symmetry [1]:

$$f_{l+}(w) = -f_{(l+1)-}(-w) .$$

The well-known relation [1,2] between $f^I_{l+}(w)$ and the partial wave projections of the invariant amplitudes suggests the introduction of another function $h^I_J(w)$, which allows to exhibit the threshold behaviour of $f^I_{l+}(w)$ and has the same analyticity properties [*] in the w-plane of the mentioned projections. We define

$$h^I_J(w) \qquad \frac{w \qquad f^I_{l\pm}(w)}{E + M \qquad k^{2l}} .$$

E = total energy of the nucleon in the c.m.s. [**];
M = mass of the nucleon;
k = c.m.s. momentum of the pion-nucleon system;
$J = l + \frac{1}{2}$.

In this letter we would like to point out a procedure which allows to obtain a phenomenological description of the dynamical singularities of $h^I_J(w)$, with particular regard to those related with the « short range » forces. This procedure exploits the fact that $h^I_J(w)$, on the two physical cuts for $w < -M-1$ and for $w > M+1$, is strictly related to the two partial wave amplitudes corresponding to different

[1] S. W. Mac Dowell: *Phys. Rev.*, **116**, 774 (1960).
[2] W. R. Frazer and J. R. Fulco: *Phys. Rev.*, **119**, 1420 (1960).
[*] For this analytical properties we refer to the various authors.
[**] We here are using units $\mu_\pi = 1$.

parity. The results can indicate an approximate behaviour of $h_J^I(w)$, that gives the correct experimental values in the two physical energy intervals where the waves are experimentally known and the elastic scattering is supposed to be dominant.

We here analyse the $h_{3/2}^{3/2}$ amplitude, which offers the possibility of correlating the resonating $P_{3\,\frac{2}{2}}^{3\,\frac{2}{2}}$ phase shifts with the very small positive $D_{3\,\frac{2}{2}}^{3\,\frac{2}{2}}$ wave, and allows the definition of two « short range » parameters. The problem of the $S_{\frac{1}{2}}$, $P_{\frac{1}{2}}$ phase shifts is important as well, and can be investigated by a similar method.

The dynamical equations for $h_{3/2}^{3/2}(w)$ can be written in the form of two coupled integral equations by using the N/D method ([3]). We shall show that it is possible to obtain effective range formulae for the low energy $P_{3\,\frac{2}{2}}^{3\,\frac{2}{2}}$ and $D_{3\,\frac{2}{2}}^{3\,\frac{2}{2}}$ elastic amplitudes by introducing parameters in the equations for the $N(w)$ and $D(w)$.

The insertion of the dynamical singularities is usually done in the numerator function $N(w)$, whereas the physical singularities are inserted in the denominator function $D(w)$. In an effective range approach it is possible to neglect a detailed description of the far-away contributions; therefore, we insert in the numerator function $N(w)$ only those singularities nearest to the physical regions for P and D waves, namely the Born term and part of the pion-pion contributions, which are the corresponding ones to the « long range » forces. The description of the « short range » interaction is taken into account by parameters introduced in the denominator function $D(w)$.

Previous calculations ([4]) showed that the « long range » contributions on the P wave can be reduced to the Born term, because the pion-pion pion interaction does not seem to modify significantly the situation. On the contrary, the nearest part of the Born term to the D wave does not give any effect, whereas the role of the pion-pion interaction looks very important ([5]). In order to take into account this situation in a simple form we approximate the long-range Born term on the P wave side by a pole at $w=+M$ with the correct residue, $R_1=-\frac{2}{3}f^2$, and the pion-pion interaction on the D wave side (which is distributed on a circle of radius $r=\sqrt{M^2-1}$) by an equivalent pole at $w=-M$, with appropriated residue R_2.

The unitarity integrals, which contribute to the $D(w)$ function, in the particular case of $h_{3/2}^{3/2}(w)$ are not convergent. Therefore we need three subtractions in $D(w)$ in order to make the integrals convergent. We then introduce in this way two parameters.

We finally obtain the following effective range formula for the P wave:

$$k^3 \operatorname{cotg} \delta_{33}^{P} = \frac{w}{E+M} \operatorname{Re} \frac{D(w)}{N(w)} = \frac{w}{E+M} \left| \frac{(w-M)\beta R_2}{w^2-M^2} - \frac{(w+M)\alpha R_1}{w^2-M^2} \right|^{-1} \cdot$$

$$\cdot \left\{ \frac{(w+M)\alpha + w(w-M)\beta - 2(w^2-M^2)}{2M^2} - w(w^2-M^2)[R_1 \mathscr{H}_1(w)\alpha + R_2 \mathscr{H}_2(w)\beta] \right\},$$

and for the D wave:

$$k^3 \operatorname{cotg} \delta_{33}^{D} = \frac{w}{E-M} \operatorname{Re} \frac{D(-w)}{N(-w)} = \frac{w}{E-M} \left| \frac{(w-M)\alpha R_1}{w^2-M^2} - \frac{(w+M)\beta R_2}{w^2-M^2} \right|^{-1} \cdot$$

$$\cdot \left\{ \frac{w(w+M)\beta + w(w-M)\alpha - 2(w^2-M^2)}{2M^2} + w(w^2-M^2)[R_1 \mathscr{H}_1(-w)\alpha + R_2 \mathscr{H}_2(-w)\beta] \right\}.$$

([3]) G. F. CHEW and F. E. LOW: *Phys. Rev.*, **101**, 1570 (1956).
([4]) S. C. FRAUTSCHI and J. D. WALECKA: *Phys. Rev.*, **120**, 1486 (1960).
([5]) J. BOWCOCK, N. COTTINGHAM and D. LURIÉ: *Nuovo Cimento*, **19**, 142 (1961).

where α and β are $D(M)$ and $D(-M)$, respectively,

$$\mathscr{H}_1 \quad \frac{1}{\pi} P(H_1 \quad H_2) \,, \qquad \mathscr{H}_2 \quad \frac{1}{\pi} P(H_1' \quad H_2') \,,$$

$$H_1 = \int_{M+1}^{\infty} \mathrm{d}W' \frac{(E'+M)k'^3}{w'^2} \frac{1}{(w'-M)^2(w'+M)(w'-w)}$$

$$H_2 = \int_{-\infty}^{-M-1} \mathrm{d}w' \frac{(E'+M)k'^3}{w'^2} \frac{1}{(w'-M)^2(w'+M)(w'-w)} \,,$$

and $H_{1,2}'$ are the integrals one gets from $H_{1,2}$ by interchanging $w'+M$ with $w'-M$.

The above written formulae become meaningful after we fit the parameters from the low-energy experimental values of D and P phase shifts, achieving in this way to constraint the analytical function $h_{3/2}^{2/2}(w)$ to have the wanted physical behaviour at low energies, specifically in the two intervals $-M-4.5 < w < -M-1$ and $M+3.3 > w > M+1$. To carry out a phenomenological preliminary evaluation of the parameters, we took R_2 as a parameter also, because the theoretical knowledge of the pion-pion interaction seems still uncertain. We therefore assumed three experimental conditions, which gave us three linear equations for the determination of α, β and R_2. Because of the inelastic effects, which may be present in the D wave experimental points, we took only the value at low energy ($w \simeq 9.75$).

In order to understand how to relate the parameters with the « short range » forces, we may notice that the insertion of experimentally consistent values of α and β determines the birth of poles (corresponding to zeros in $D(w)$) in the amplitude $h_{3/2}^{3/2}(w)$ in the complex w plane. These poles must not interfere with the singularities put in $N(w)$ and, in the approximation in which the numerator function deals only with « long range » contributions, have to fall within the region of the w plane occupied by the « short range » singularities. From the point of view of the analytical properties of $h_{3/2}^{3/2}(w)$ the « short range » poles provide a fairly good description of the branch lines if the corresponding discontinuity is peaking very strongly in certain points and is negligible otherwise. Therefore we cannot accept any spurious poles in the w complex plane, out of the mentioned region, in the parametrized solution.

The upper requirements restrict the range of values of α, β and R_2 very strongly. We find indeed two possibilities: $R_2 > 0$, $\alpha, \beta > 0$ or $R_2 > 0$, $\alpha > 0$, $\beta < 0$. The experimental fit makes us disregard the latter case because it provides an enormous increase of the $D_{3/2}^{3/2}$ phase shifts with the energy, in contraddiction with the experiment ([6]). The former case provides an acceptable solution with $R_2 = 0.069$ and parameters $\alpha = 0.37$, $\beta = 0.69$. For a fixed value of R_2, the numerical values of α and β may fluctuate of 10 and 20%, respectively: α is the most related with the $P_{3/2}^{3/2}$ resonance, whereas β and R_2 seem to tie down the order of magnitude and the sign of the $D_{3/2}^{3/2}$ wave phase shifts (*). It is interesting to point out how

([6]) W. D. WALKER, J. DAVIS and W. D. SHEPHARD: *Phys. Rev.*, **118**, 1612 (1960).

(*) The numerical values of the parameters so calculated need to be compared with those obtained by fitting independently the two waves: for consistency it is required that their ranges of variation are such to contain the values of the coupled solution.

the curves we obtain (Fig. 1, 2) deviate from the experimental points at higher energies for both $P_{3/2}^{3/2}$ and $D_{3/2}^{3/2}$ waves ([6,7]). To be more specific, for energies greater than the P wave resonance, corrective terms to the resonating formula of the « static theory » produce a shift from the Chew-Low plot in the opposite direction of that required by the experiment (in analogy with the Frazer-Fulco solution), whereas our D wave phase shifts, for energies greater than $\sim$ 370 MeV (kinetic energy in the laboratory), grow too rapidly. These effects may be related with the necessity of a more detailed description of the dynamical singularities and with the influence of the inelastic scattering channels.

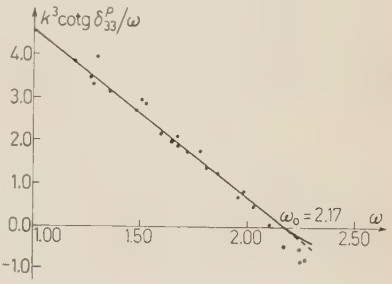

Fig. 1. – P-wave solution. • experimental points; dashed line Chew-Low plot; straight line = parametrized solution. $f^2 = 0.087$, $\omega = w - M$.

Nevertheless, in the low energy region, our approach gives the $D_{3/2}^{3/2}$ phase shifts essentially in terms of two parameters (α and R_2). It is well known that the CGLN-Wataghin D wave formula ([8]) contains the same number of parameters: however, we want to outline that our procedure takes into account explicitly the D wave unitarity integrals and makes use of one pole for the pion-pion contributions. On the other hand, the results give a most accurate fit with the experimental data, and allow to obtain definite conclusions about the sign and the order of magnitude of the residue of the pole on the D wave side. Finally, our procedure makes it possible to obtain information about the importance of the pion-pion contributions.

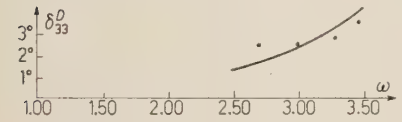

Fig. 2. – D-wave solution.

We would like to outline also that the value of the residue R_2 can be estimated theoretically from the data on the pion-pion interaction: this fact suggests a comparison between this evaluation and the results of our analysis. This comparison can definitively indicate whether well described « long range » contributions, associated with two « short range » parameters, can give a complete phenomenological description of the low energy $P_{3/2}^{3/2}$ and $D_{3/2}^{3/2}$ waves. A similar comparison can be established with the results obtained by other authors; in particular, the value of the residue R_2, including pion-pion contributions, can be related with the « discrepancy » introduced by HAMILTON *et al.* ([9]). Calculations on these latter points are now in progress.

* * *

We are indebted to Prof. S. FUBINI, Dr. R. STROFFOLINI and Dr. B. VITALE for their interest and for clarifying discussions.

([7]) S. W. BARNES and B. ROSE: *Phys. Rev.*, **117**, 226 (1960).

([8]) G. F. CHEW, M. L. GOLDBERGER, F. E. LOW and Y. NAMBU: *Phys. Rev.*, **106**, 1337 (1957).

([9]) J. HAMILTON and T. D. SPEARMAN: *Ann. Phys.*, **12**, 172 (1961); J. HAMILTON, P. MENOTTI, T. D. SPEARMAN and W. S. WOOLCOCK: *Nuovo Cimento*, **20**, 519 (1961).

IL NUOVO CIMENTO Vol. XXII, N. 6 16 Dicembre 1961

Diffraction Scattering of 1.6 GeV/c π^- on p for Small Momentum Transfer (*).

Saclay-Orsay-Bari-Bologna Collaboration

J. Alitti, V. Alles-Borelli, J. P. Baton, A. Berthelot,
U. Bidan, A. Daudin, B. Deler, O. Goussu, M. A. Jabiol,
F. Lévy, C. Lewin, M. Neveu-René, A. Rogozinski and F. Shively

Laboratoire de Physique Corpusculaire à Haute Energie - Saclay

J. Laberrigue-Frolow, O. Ouannès, M. Sené and L. Vigneron

Laboratoire Joliot-Curie, Faculté des Sciences de Paris - Orsay

N. Abbattista, S. Mongelli and A. Romano

Istituto di Fisica dell'Università - Bari

E. Benedetti, J. Litvak (**), G. Puppi, P. Waloschek and M. Whitehead (***)

Istituto di Fisica dell'Università - Bologna
Istituto Nazionale di Fisica Nucleare - Sezione di Bologna

(ricevuto il 28 Novembre 1961)

Recent theoretical studies of strong interactions at high energies in the limit of small momentum transfer [1,2] have underlined the importance of the « peripheral » interactions.

In particular D. Amati, S. Fubini, A. Stanghellini and M. Tonin have calculated π-p diffraction scattering using the « strip » approximation of Chew and Frautschi. The assumption is made that the inelastic cross-section is dominated by the one pion exchange term, and therefore the diffraction by the exchange of two pions. They give a definite prediction for the shape of the differential cross-section in the region of small momentum transfer.

(*) The work done at Bari was supported by grants from NATO and the Istituto Nazionale di Fisica Nucleare.

(**) Fellow of the Argentine « Comisión Nacional de Energía Atómica ».

(***) Senior Fulbright Research Fellow.

(1) G. F. Chew and S. C. Frautschi: *Phys. Rev. Lett.*, **5**, 580 (1960); UCRL 9510.

(2) D. Amati, S. Fubini, A. Stanghellini and M. Tonin: to be published in *Nuovo Cimento*.

We have measured the absolute differential elastic cross-section as part of our continuing study (3) of 1.6 GeV/c π^-p interactions in the Saclay 50 cm hydrogen chamber.

The events selected are those in which the recoil proton stops in the chamber and which satisfies the usual criteria for elasticity. The ranges, R, of the scattered protons are measured and the square of four-momentum transfer, Δ^2, is then determined directly from the kinetic energy T of the proton, $\Delta^2 = 2MT$. We accept events with Δ^2 between 1 and 4 square pion masses, that is, $0.94 < R < 12.5$ cm ($0.983 < \cos\theta_{\text{c.m.}} < 0.930$).

In order to avoid possible systematic losses of events, we consider only those events in which the point of interaction occurs in a well-defined volume of the chamber and we require that the angle of the plane of the scatter be greater than 30° to the optic axis.

Repeated scans show that the scan efficiency is of the order of 97%. 3361 elastic scatters with stopping protons were observed; of these, 928 appear in the final selected distribution.

According to a least-squares fit these data are best represented by a straight line:

$$\frac{d\sigma}{d\Delta^2} = [1.14 \pm 0.07 - (0.096 \pm 0.025)\Delta^2] \text{ mb per } \Delta^2 \text{ unit},$$

where Δ^2 is measured in units of the square of the charged pion mass.

If one calculates the « diffraction » scattering resulting from an imaginary gaussian potential one obtains for the cross-section

$$\frac{d\sigma}{d\Delta^2} = \left(\frac{d\sigma}{d\Delta^2}\right)_{0^\circ} \cdot \exp\left|-\frac{1}{3}\frac{a^2}{\lambda_c^2}\Delta^2\right|,$$

where a = r.m.s. radius of the potential; λ_c = pion Compton wave length.

For our values of Δ^2, this expression reduces to

$$\frac{d\sigma}{d\Delta^2} \simeq \left(\frac{d\sigma}{d\Delta^2}\right)_0 \left(1 - \frac{1}{3}\frac{a^2}{\lambda_c^2}\Delta^2\right).$$

Therefore our experiment implies an effective $a = (0.75 \pm 0.10)$ fermi.

When $\Delta^2 \to 0$, $d\sigma/d\Delta^2 \to (1.14 \pm 0.07)$ mb per Δ^2 unit. This value is in good agreement with that calculated from the optical theorem using the total cross-section of (32.1 ± 1.5) mb, measured by BRISSON *et al.* (4):

$$\left(\frac{d\sigma}{d\Delta^2}\right)_0 = (1.01 \pm 0.09) \text{ mb per } \Delta^2 \text{ unit}.$$

The straight line and experimental points are shown in Fig. 1.

(3) *Production des particules étranges par l'interaction* π^- + p à 1.6 GeV/c; Etude de l'interaction π-π cans la diffusion π^- + p à 1.6 GeV/c. Communications à la Conférence Internationale d'Aix-en-Provence sur les particules élémentaires, 14-20 Sept. 1961.

(4) J. C. BRISSON, J. L. DETOEUF, P. FALK-VAIRANT, L. VAN ROSSUM and G. VALLADAS: *Nuovo Cimento*. **19**, 210 (1961).

The theoretical distribution of AMATI *et al.*, is of the form

$$\frac{\mathrm{d}\sigma}{\mathrm{d}\Delta^2} \propto F^2\left(\frac{t}{t_0} = x^2\right) = \left| \frac{1}{x\sqrt{1+x^2}} \cdot \log\left(x + \sqrt{1+x^2}\right) \right|^2 ,$$

where $t = \Delta^2$, and t_0 is the square of the mean effective mass of the intermediate particle, responsible for the diffraction scattering. A good fit is obtained with

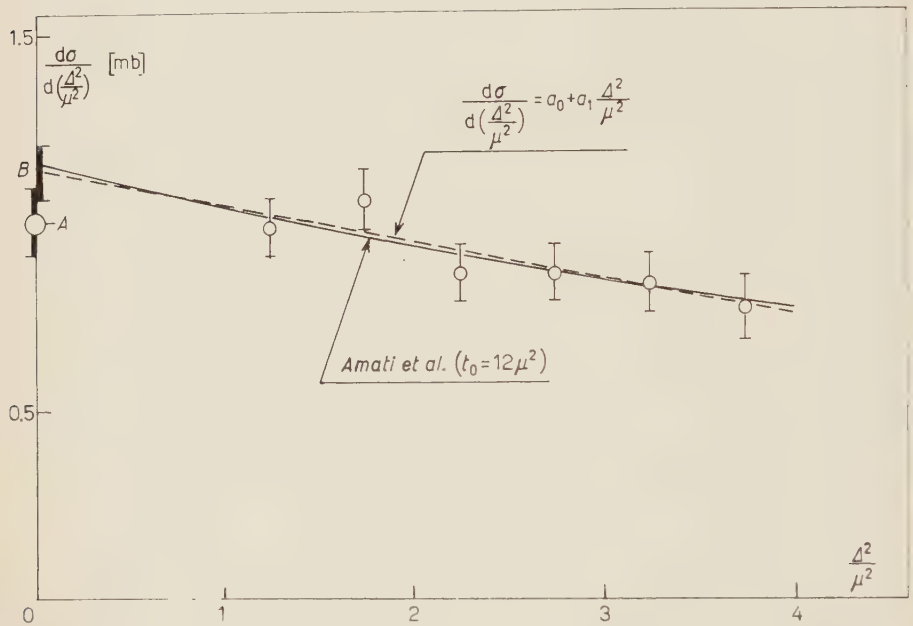

Fig. 1. – The experimental points are the open circles, shown with statistical errors. Point A is optical model prediction for $(\mathrm{d}\sigma/\mathrm{d}\Delta^2)_0$ $L = (1.01 \mp 0.09)$ mb calculated from $\sigma_{\mathrm{total}} = 32.1$ mb. Point B is the linear extrapolation to zero. (1.14 ∓ 0.07) mb.

$t_0 = 12\mu^2$, with the outer limits of 8.5 to $16\mu^2$ as is shown in Fig. 1. It can be seen that with these values of t_0 and in this region of small momentum transfer the theoretical curve is almost linear and agrees within the error with the prediction of the conventional perturbation approximation. The detailed prediction of the theory can only be verified by the determination of the final particle states of the inelastic cross-section under the same conditions.

* * *

It is a pleasure to thank A. STANGHELLINI and S. FUBINI for numerous helpful discussions and suggestions during the course of these pion experiments.

Proton Energy Spectra in the Drell Model of Double Photoproduction.

C. Gualdi

Scuola di Perfezionamento in Fisica
presso Istituto di Fisica dell'Università - Roma

(ricevuto il 6 Dicembre 1961)

The energy spectrum of the recoil proton in the double photoproduction of charged pions has been calculated at three fixed Laboratory angles. The reaction:

(1) $\gamma + p \to p + \pi^- + \pi^+$

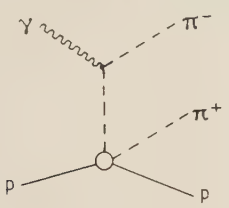

Fig. 1.

has already been studied taking into account the pion-pion interaction (2).

In this paper the Drell diagram of Fig. 1 has been considered in order to see if it predicts maxima in the proton spectra different from the ones obtained

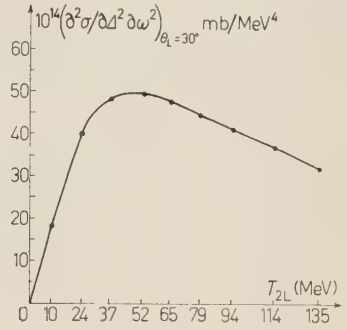

Fig. 3.

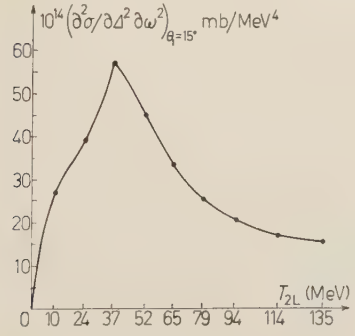

Fig. 2.

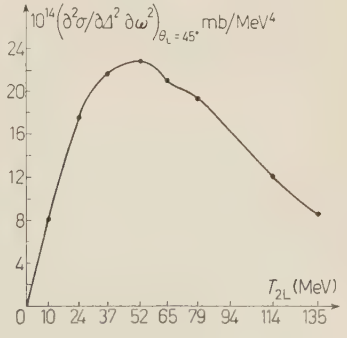

Fig. 4.

taking into account pion-pion interaction. The energy of the incident γ is fixed: 900 MeV in the laboratory system.

In Fig. 2, 3, 4 the energy spectra of the recoil proton are drawn at the laboratory angles $\theta_L = 15°$, $30°$, $45°$; T_{2L} is the proton kinetic energy in the laboratory system; $\Delta^2 = (p_2 - p_1)^2$, $\omega^2 = -(q_2 + q_3)^2$.

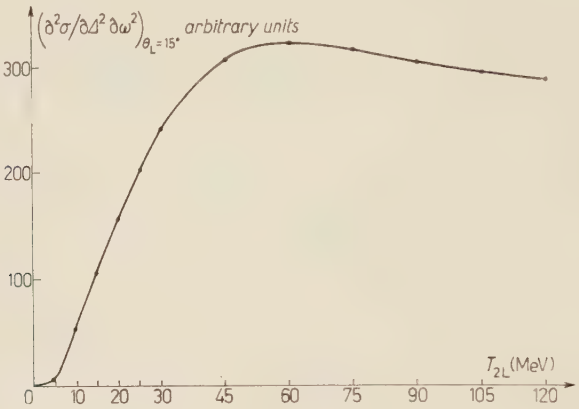

Fig. 5.

The S-matrix element is:

$$S_{fi} = (2\pi)^{-\frac{3}{2}} \left(\frac{q_{10}}{2k_0 q_{20}}\right)^{\frac{1}{2}} \cdot \frac{e \cdot \varepsilon (q_2 - q_1)}{(q_2 - k)^2 + \mu^2} \cdot S_{\pi N}\,, \tag{2}$$

Fig. 5, 6, 7 give the corrected spectra [1] obtained [2] at the same angles.

The normalization of the curves is obtained from the total cross-section given by Boccaletti and Selleri [3].

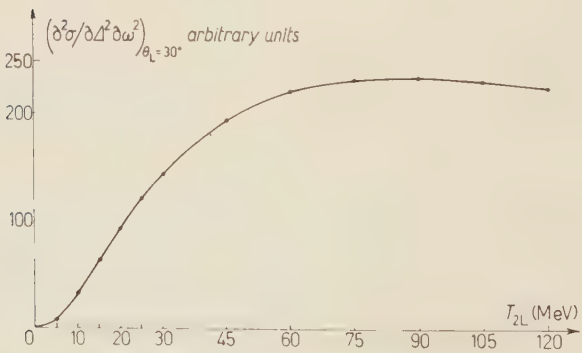

Fig. 6.

where $S_{\pi N}$ is the S-matrix for π^+p scattering and the 4-vectors are:

k for the incident γ, $p_1 p_2$ for the initial and final proton, $q_2 q_3$ for the π and π^+ respectively; q_1 is the momentum of the intermediate pion and ε the polarization vector of the proton.

(1) An error was made in the numerical computations.

(2) D. Boccaletti and C. Gualdi: *Nuovo Cimento*, **18**, 895 (1960); D. Boccaletti, G. De Franceschi and C. Gualdi: *Nuovo Cimento*, **20**, 375 (1961).

(3) D. Boccaletti and F. Selleri: *Nuovo Cimento*, **22**, 1099 (1961).

In this paper it is shown that the Drell diagram yields a total cross-section

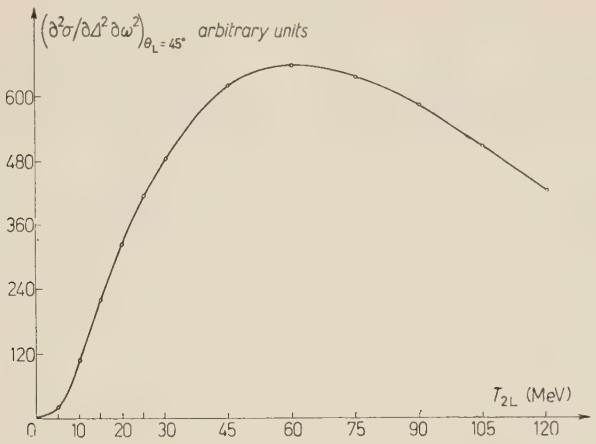

Fig. 7.

which is about 1/10 of the experimental one.

As one can see the maxima in the Drell curves are at lower energy than the corresponding maxima of Fig. 5, 6, 7.

Furthermore, the Drell effect being so small at this γ energy (900 MeV), no overlapping is possible between pion-pion interaction and the Drell effect.

Remarks on a Possible Method for Detecting the Double Compton Effect.

M. Carrassi and G. Passatore

Istituto di Fisica dell'Università - Genova
Istituto Nazionale di Fisica Nucleare - Sezione di Genova

(ricevuto il 7 Dicembre 1961)

The purpose of this paper is to suggest a method for observing the double Compton effect without the use of coincidence measurements.

All the experimental observations on the double Compton effect performed up to now are based on coincidence measurements ([1,2]). In these experiments the directions of both final photons are kept fixed and the coincidences are counted. The greatest difficulty in such experiments lies in the low value of the intensity to be measured: in fact the cross-section for the double Compton effect is already low in itself, and in such experiments one selects the pairs of photons emitted into two small solid angles around the fixed directions.

On the other hand, it is possible — though not done so far — to observe the double Compton effect without coincidence measurements: one has only to study the cross-section integrated over the direction of one of the two final photons, the direction of the other one being kept fixed. The energy spectrum of this photon is observed, and should be seen as a tail to the single Compton line, on the side of the low energies.

By using this method we gain a factor of about ten in the cross-section as an effect of the angular integration.

Let $\boldsymbol{k}_1$ and $\boldsymbol{k}_2$ be the momenta of the final photons, α_1 and α_2 their angles with the incident photon $\boldsymbol{k}_0$, β the angle between the two emission planes; the quantity to be measured is

$$\frac{\mathrm{d}\sigma_{\mathrm{d.c.}}(k_0, k_1, \alpha_1)}{\mathrm{d}k_1 \, \mathrm{d}\Omega_1} = \int_0^{2\pi} \mathrm{d}\beta \int_0^{\pi} f(k_0, k_1, \alpha_1, \alpha_2, \beta) \sin \alpha_2 \, \mathrm{d}\alpha_2 \,, \tag{1}$$

where

$$f(k_0, k_1, \alpha_1, \alpha_2, \beta) = \frac{\mathrm{d}\sigma_{\mathrm{d.c.}}(k_0, k_1, \alpha_1, \alpha_2, \beta)}{\mathrm{d}k_1 \, \mathrm{d}\Omega_1 \, \mathrm{d}\Omega_2} \,, \tag{2}$$

(k_0 and α_1 fixed).

([1]) P. E. Cavanagh: *Phys. Rev.*, **87**, 1131 (1952).
([2]) A. Bracci, C. Cocèva, L. Colli and R. Dugnani Lonati: *Nuovo Cimento*, **1**, 752 (1955).

The differential cross-section for the double Compton effect

$$\frac{\mathrm{d}\sigma_{\mathrm{d.c.}}(k_0,\, k_1,\, \alpha_1,\, \alpha_2,\, \beta)}{\mathrm{d}k_1\, \mathrm{d}\Omega_1\, \mathrm{d}\Omega_2}$$

has been given analytically in various ways ([3,4]).

Transition amplitudes for the double Compton effect between fixed polarization states of all the involved particles, and the cross-section for unpolarized particles [formula (11)] are explicitly calculated in ref. ([4]). The numerical integration of this cross section by an IBM 650 computer ([*]) has now been performed to obtain the quantity (1).

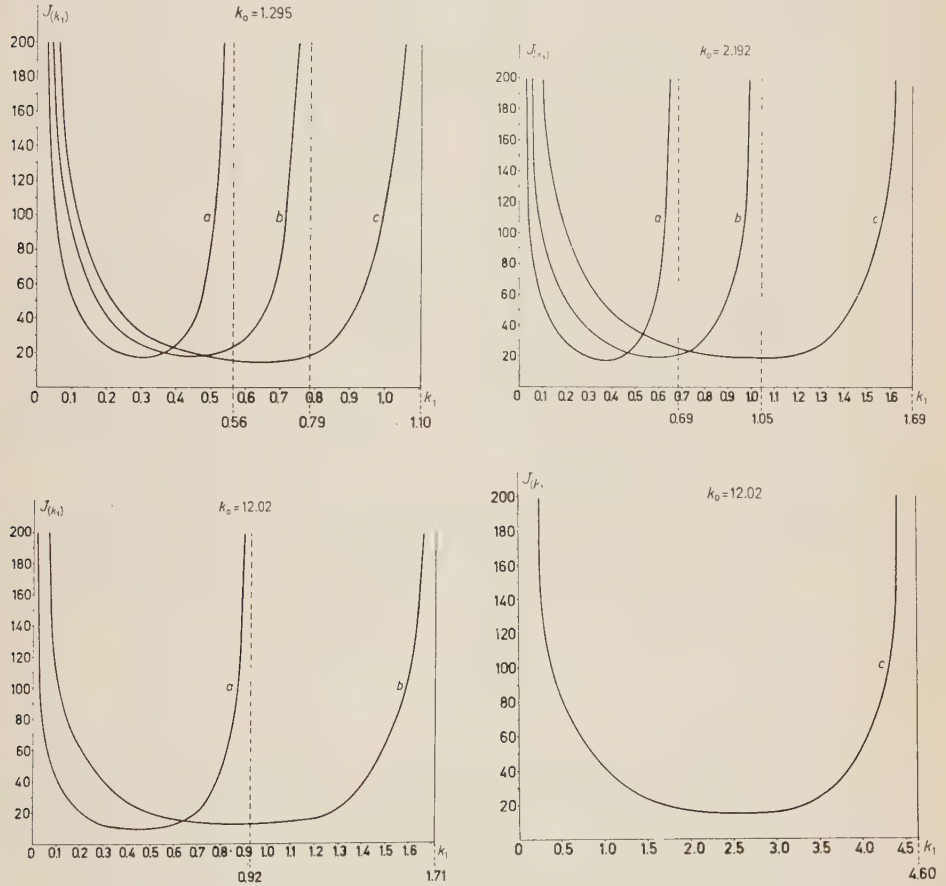

Fig. 1. – The function $J(k_0; k_1; \alpha_1)$, defined by (3), for three energy values of k_0: plotted against k_1 in electron mass units. In all graphs the curves *a*), *b*), and *c*) correspond to the angle $\alpha_1 = 90°$, $\alpha_1 = 60°$ and $\alpha_1 = 30°$, respectively.

([3]) F. Mandl and T. H. S. Skyrme: *Proc. Roy. Soc.*, A **215**, 497 (1952).
([4]) M. Carrassi and G. Passatore: *Nuovo Cimento*, **16**, 811 (1960).
([*]) At the «Centro di Calcolo Numerico dell'Università di Genova».

Figure 1 shows the values of $J(k_1)$ defined by

$$\frac{\mathrm{d}\sigma_{\mathrm{d.c.}}(k_0,\, k_1,\, \alpha_1)}{\mathrm{d}k_1\, \mathrm{d}\Omega_1} = r_0^2 A J(k_1)\,, \tag{3}$$

where

$$A = \frac{\alpha}{16\pi^2} = 0.46 \cdot 10^{-4}\,, \qquad r_0^2 = \left(\frac{e^2}{mc^2}\right)^2 = 7.94 \cdot 10^{-26}\ \mathrm{cm}^2\,, \tag{4}$$

the energy values correspond to the γ-rays of Cs (662 keV), of Zn (1.12 MeV), and from the radiative capture by ^{19}F (6.14 MeV); the emission angles are 30°, 60°, 90°.

All these energy spectra are very similar. They show a minimum around the middle of the range analogous to the one which exists for the differential cross-sections ([3,4]). These spectra go to infinity at the ends of the range, owing to the well-known infrared catastrophe.

The energy at the right-hand end is the same as that for the photon emitted in the single Compton effect for the same incident energy and angular conditions: as shown by Brown and Feynman ([5]) there is an exact cancellation in the amplitudes between the infinity arising from the double Compton and the one resulting from the third order radiative correction to the single Compton effect.

It is interesting to observe the dependence of the minima upon the incident energy and the emission angle. At low energies ($k_0 = 662$ keV) the minimum for $\alpha_1 = 90°$ is greater than the one for $\alpha_1 = 30°$. On the contrary, at higher energies the minimum decreases monotonically with increasing angle. This behaviour qualitatively corresponds to the well-known higher concentration of the emitted photons in the forward direction at higher energies.

In addition, the double Compton spectra for the incident energy of γ-rays from the radiative capture by ^{3}H (20.3 MeV) have been calculated; they do not show any qualitative difference from the spectra reported in Fig. 1 and their minima have the same order of magnitude.

In the experiment, one should observe a tail to the single Compton line just given by the central regions of the calculated spectra. The observation will be possible if this contribution of the double Compton is at least a small percentage of the response of the counters to the single Compton line in those regions. In order to make a comparison we can simulate the response by a function $R_c(k)$ defined as follows:

$$R_c(k) = R_c(k_c) \exp\left[-\alpha(k_c)\, \frac{(k - k_c)^2}{k_c^2}\right]. \tag{5}$$

where $R_c(k_c)$ is the height of the response curve when $k = k_c$ and k_c is the energy of the Compton line. With a suitable choice of $\alpha(k_c)$, (5) is a good representation of the response for all values of energy k which differ from k_c up to about 10% or 15% of the incident energy k_c itself, the exact figure depending on the particular detector.

Similarly, to obtain the response which the same detector gives to the continous spectrum of the double Compton effect, one must calculate

$$R_d(k) = \int_{k_{\min}}^{k_{\max}} R_d(k') \exp\left[-\alpha(k')\, \frac{(k - k')^2}{k'^2}\right] \mathrm{d}k', \tag{6}$$

([5]) L. M. Brown and R. P. Feynman: *Phys. Rev.*, **85**, 231 (1952).

where $R_d(k')\,dk'$ is the height of the response at the energy k' of the continuum.

In order to estimate the ratio $R_d(k)/R_c(k)$, we refer to a typical response curve of the scintillation counters. These, for all energy values which concern us, exhibit a minimum at the energy $k < k_c$ by an amount of about 10% the energy k_c itself; the height of the response curve at this minimum is, for suitable crystals, about 0.01 of the photopeak height. Hence we have calculated the ratio R_d/R_c at the energy k corresponding to this minimum assuming that the response to the Compton line gives

$$R_c(k) = R_c(k_c)\cdot 0.01 \propto I(k_c)\cdot 0.01\,, \tag{7}$$

where we have put $R_c(k_c)$ proportional to the « intensity » $I(k_c) = (1/r_0^2)(d\sigma/d\Omega)_{\text{Compton}}$; that is to say that we have neglected, at first approximation, the small variation of $R_c(k_c)$ with the energy as we are interested in the order of magnitude of the ratio R_d/R_c. In Table I we have reported some values of $I(k_c)$

TABLE I. *Values of* $I(k_c) = (1/r_0^2)(d\sigma/d\Omega)_{\text{Compton}}$.

k^0 \ α_1	30°	60°	90°
1.295	0.64	0.28	0.16
2.192	0.54	0.21	0.12
12.02	0.20	0.065	0.036
39.73	0.078	0.023	0.012

We have also valued the response to the double Compton effect by substituting the integral in (6) with a summation and making a cut in the spectrum at an energy smaller than k_c by 2 to 4% of mc^2 (the results being slightly sensitive to this cut); so we have

$$R_d(k) \propto A \sum_i J(k_i)\,\Delta k_i \exp\left[-\alpha(k_i)\,\frac{(k-k_i)^2}{k_i^2}\right], \tag{8}$$

where $AJ(k_i)$ is defined by (3). A few terms are sufficient in the summation since the contribution of all terms with $k_i \leqslant k_c/2$ is negligible on account of the exponential factor. We have also supposed $\alpha(k_i) = \text{const}$, so that the width at the half height of the gaussian is about 15% of the energy k_i. With these assumptions we hope we have underestimated $R_d(k)$ because *a*) the photopeak efficiency actually increases when the energy decreases ([6]) and *b*) the response due to the terms for which $k_i > k$ gives a contribution to the terms in which $k_i < k$; this contribution is not negligible owing to the typical continuous spectrum which the response curve exhibits on the left of the photopeak.

([6]) See, for example, W. E. MOTT and R. B. SUTTON: *Scintillation and Cerenkov counters*, in *Handb. d. Phys.*, Bd. **45**.

Considering the particular case in which $k_0 = 2.19\,mc^2$, $\alpha_1 = 90$, $k_c = 0.687\,mc^2$, $I(k_c)$ is equal to 0.12 as shown in Table I, one obtains for the ratio R_d/R_c the value 0.16. From other valuations for slightly different energies and for some angular situations one can estimate the effect as varying between 10% and 20%, and therefore it seems noticeable with the actual instrumental technique.

* * *

We wish to thank Prof. M. AGENO for his indication of the experimental interest of this calculation and Dr. S. VITALE for useful discussions.

5.2.1

Gauge Invariance of Form Factors.

P. Budini and T. Weber

Istituto di Fisica dell'Università - Trieste
Istituto Nazionale di Fisica Nucleare - Sezione di Trieste

(ricevuto il 9 Dicembre 1961)

The discussions on the limits of validity of quantum electrodynamics are usually based on the comparison of experimental results with the standard theory, into which form factors have been introduced. These form factors have only the role of introducing into the theory a comparison length, with the implicit assumption that the known defects of nonlocal theories obtained in such a way will not affect the conclusions drawn.

It has been made apparent [1] that the above assumption is not valid when the form factors destroy the gauge invariance of the theory, which occurs effectively when multiplicative form factors are introduced in the electron positron Green's function.

In this note we want to discuss this point and indicate an approach which could be taken to avoid this difficulty.

The introduction of form factors for the mentioned purpose should satisfy at least the following conditions:

a) the theory should tend continuously to the standard local theory as the introduced length tends to zero;

b) the form factors introduced for the study of different experiments should be the same;

c) the theory with form factors should not contain inconsistencies which affect the application of the theory to the experiment to be studied.

Usually [2-6] the discussions of experiments have been based on formulae obtained from the standard ones after multiplication of the photon or electron propa-

[1] See the paper of Harting *et al.* on the experiment on e^+e^- annihilation (to be published).
[2] P. Budini: *Nuovo Cimento*, **3**, 835 (1956).
[3] G. Andreassi, P. Budini and I. Reina: *Nuovo Cimento*, **12**, 488 (1959).
[4] S. D. Drell and F. Zachariasen: *Phys. Rev.*, **111**, 1727 (1958).
[5] J. D. Bjorken, S. D. Drell and S. C. Frautschi: *Phys. Rev.*, **112**, 1409 (1958).
[6] H. Salacker: *Zeits. Phys.*, **160**, 385 (1960).

gators in the matrix element by the form factor

$$\frac{\Lambda^2}{p^2+m^2+\Lambda^2}\,, \tag{1}$$

where p is the four-momentum of the virtual particle in the propagator, m its rest mass, and Λ^{-1} is the comparison length. This satisfies both *a*) and *c*) but not *b*); in fact multiplication by (1) is equivalent to the introduction into the theory of an intermediate boson field of rest mass Λ. And whereas this is allowed for transitions where a photon is exchanged, it is no longer so when the virtual particle is a spinor; in this case an intermediate boson field destroys the fermion conservation and current conservation laws, and consequently the gauge invariance of the theory. This is true not only for form factors (1) but also for any scalar form factor depending only on p^2. In fact consider the matrix element for a process which contains an electron-positron Green function in the general form:

$$\langle f|i\rangle = \left\langle \ldots \gamma_\mu \frac{f_1(q^2)i\hat{q}-f_2(q^2)m}{q^2-m^2}\gamma_\nu \ldots \right\rangle + \left\langle \ldots \gamma_\mu \frac{f_1(q'^2)i\hat{q}'-f_2(q'^2)m}{q'^2-m^2}\gamma_\nu \ldots \right\rangle . \tag{2}$$

where q' is obtained from q by exchanging the momenta of the photons appearing at the vertices. Then invariance under gauge transformation will bring about the following condition:

$$\left\langle \ldots \hat{k}\,\frac{f_1(q^2)-f_2(q^2)}{q^2-m^2}\,m\hat{k}' - \hat{k}'\,\frac{f_1(q'^2)-f_2(q'^2)}{q'^2-m^2}\,m\,\hat{k} + [f_1(q^2)-f_1(q'^2)]\,\hat{k} \ldots \right\rangle = 0\,, \tag{3}$$

which in general cannot be satisfied unless $f_1(q^2)=f_2(q^2)=f_1(q'^2)=f_2(q'^2=1)$. In other words, the electron-positron Green's function cannot be multiplied by form factors without destroying the gauge invariance of the theory.

We see two possibilities of avoiding these difficulties.

The first is to introduce the form factor in the matrix element rather than in the Green's function. This amounts to the substitution in (2), for $f_1(q^2)=f_2(q^2)$, of a function $F(q^2, q'^2)$, symmetrical in the invariants q^2, q'^2. In this case (3) is satisfied and the gauge invariance of the theory ensured.

Generally the symmetry of such a form factor with respect to the exchange of the photons allows to factorize it from the matrix element, which then maintains its original gauge invariance. It is easily seen that this is true only not when the photons emitted or absorbed are free but also more generally when one of them or both are virtual.

In order to satisfy the condition *b*) one should adopt the same method also for the modification of the photon's Green's function.

An example of such a form factor, which satisfies conditions *a*), *b*) and *c*) and identifies with (1) for $q=q'$ (in which particular case (1) preserves gauge invariance) is

$$F_e(q^2, q'^2) \cdot \frac{\Lambda^2}{\Lambda^2+(|q'^2-m^2|\,|q^2-m^2|)^{\frac{1}{2}}}\,,$$

for the electron's Green's function and

$$F_p(q^2, q'^2) = \frac{\Lambda^2}{\Lambda^2 + |q|\,|q'|},$$

for photons (obviously q and q' are the momenta of the virtual photons obtained exchanging the electrons in the vertices).

An other possibility is to alter both the positron-electron's Green's function and the neighbouring vertices. In this case we give only an example of such a form factor which can be applied when both photons and electrons at the end of the Green's function are free (Compton effect and positron-electron annihilation). One has for the modified Green's functions:

$$\left[\hat{e}' - \frac{2i}{M-m}(qe')\right]\frac{i\hat{q} - m}{q^2 - m^2}F(q^2)\left[\hat{e} + \frac{2i}{M+m}(qe)\right] +$$

$$+ \left[\hat{e} + \frac{2i}{M+m}(q'e)\right]\frac{i\hat{q}' - m}{q'^2 - m^2}F(q'^2)\left[\hat{e}' - \frac{2i}{M-m}(q'e')\right],$$

with

$$F(q^2) = \frac{M^2 - m^2}{M^2 + q^2}.$$

In this case one could easily derive the matrix element from a Lagrangian with derivatives.

More generally one could obtain non-local theories satisfying all invariance and unitarity conditions by introducing, in a rigorous way, intermediate fields and by taking into account all the virtual corrections induced by these fields at the vertices and at the Green's functions of the original fields up to a certain power of the coupling constant. Obviously, this procedure, even if more satisfying from a theoretical point of view, is very complicated for computational purposes and certainly not commensurate with the phenomenological purpose for which form factors are introduced.

The « Photon-Spurion » and Dispersion Theory.

E. Leader

CERN - Geneva

(ricevuto il 9 Dicembre 1961)

It has recently been asserted [1] that the calculation of a process $A+B \to A+B$ (see Fig. 1) in which one photon is exchanged, *by Dispersion Theory methods*, would fail to produce the correct result, *i.e.*, would not include the Coulomb interaction term. Goebel [1] has interpreted this as requiring the existence of a genuine « spurion », *i.e.*, third state of polarization of the photon, at zero energy.

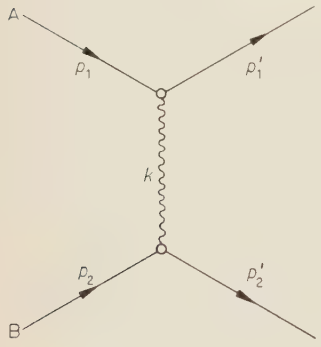

Fig. 1.

We show in the following, that this is unnecessary and that Dispersion Theory with physical, transverse photons does indeed predict the correct answer (*).

As usual define

$$t = -k^2, \qquad \text{with} \qquad k = p_1 - p_1' . \tag{1}$$

Neglecting inessential factors, unitarity in channel III ($B + \bar{B} \to A + \bar{A}$) yields

$$\text{Im} \langle p_2, \quad p_2' | T | \quad p_1, \, p_1' \rangle \sim \qquad \text{for } t \geqslant 0 ,$$

$$\sim \int \mathrm{d}^4 k \sum_{r_\perp} \langle p_2, -p_2' | T^\dagger | \gamma_k^{(r)} \rangle \langle \gamma_k^{(r)} | T | \cdots p_1, \, p_1' \rangle \delta(k^2) \delta^4(k + p_1 - p_1') , \tag{2}$$

where the polarization sum is over transverse states only.

$$\sim \int \mathrm{d}^4 k \sum_{r_\perp} J^{(B)} \cdot \varepsilon^{(r)} \cdot J^{(A)} \cdot \varepsilon^{(r)} \delta(k^2) \delta^4(k + p_1 - p_1') . \tag{3}$$

(1) C. Goebel: *An elementary particle of zero four-momentum; a genuine spurion*, University of Wisconsin, preprint (1960).

(*) *Note added in proof.* – Dr. Goebel has informed me kindly that he is aware of this formal derivation of the correct result.

Gauge invariance, $J \cdot k = 0$, together with the existence of the mass shell condition $\delta(k^2)$ allow us to write (2)

$$\sum_{r_\perp} J^{(\mathrm{B})} \cdot \varepsilon^{(r)} J^{(\mathrm{A})} \cdot \varepsilon^{(r)} \delta(k^2) = \sum_{r=1}^{4} J^{(\mathrm{B})} \cdot \varepsilon^{(r)} J^{(\mathrm{A})} \cdot \varepsilon^{(r)} \delta(k^2) = J^{(\mathrm{A})} \cdot J^{(\mathrm{B})} \delta(k^2) \,. \tag{4}$$

Carrying out the trivial integrations in (3) leaves (3)

$$\mathrm{Im} \langle p_2, -p_2' | T | -p_1, p_1' \rangle \sim J^{(\mathrm{A})} \cdot J^{(\mathrm{B})} \delta(t) \qquad t \geqslant 0). \tag{5}$$

The amplitude for the original process

$$\mathrm{A} + \mathrm{B} \to \mathrm{A} + \mathrm{B}$$

is then

$$\langle p_1', p_2' | T | p_1, p_2 \rangle \sim \frac{1}{\pi} \int_0^\infty \frac{\mathrm{Im}\, T(t')}{t' - t} \, \mathrm{d}t' \sim \frac{J^{(\mathrm{A})} \cdot J^{(\mathrm{B})}}{k^2} \,. \tag{6}$$

This agrees with formula (3) of Goebel and can be shown to contain the required Coulomb term (1).

* * *

I am grateful to Dr. D. Amati for a discussion on this matter.

(2) There is an apparent difficulty if $\boldsymbol{k} = 0$ in (4). However one can see from (3) and (6) that the point $\boldsymbol{k} = 0$ simply does not appear in the calculation. I am grateful to Dr. J. C. Taylor for pointing out this difficulty.

(3) One runs into difficulty and obtains the *incorrect* result

$$\mathrm{Im}\, T(t') \sim \boldsymbol{J}_\perp^{(\mathrm{A})} \cdot \boldsymbol{J}_\perp^{(\mathrm{B})} \delta(t') \,,$$

only if one interchanges the order of summation and integration in eq. (3) without sufficient care.

Some Remarks about the Isovector Form Factors of the Nucleons and the ρ^0 Meson.

G. Costa and A. H. Zimerman (*)

CERN - Geneva

(ricevuto il 12 Dicembre 1961)

A recent experiment on $\bar{p}$-p annihilation (1) seems to indicate that the $\rho^0 \to 2\pi$ resonance is splitted into two components ρ_1^0, ρ_2^0 with very narrow widths, of the order of 10 MeV. It seems that ρ_1^0 corresponds to a $J = 0$, $I = 0$ state, and ρ_2^0 to the neutral component of a $J=1$, $I=1$ state. In what follows we shall be interested only in the $J=1$, $I=1$ resonance, which we simply denote by ρ^0.

It is obvious that a very narrow width for the ρ^0 resonance should imply that its effect would be negligible in the pion-nucleon scattering, unless a very strong ρ^0-nucleon coupling is assumed. In fact, a narrow width implies a weak ρ^0-pion coupling.

In this note we shall examine the consequences of the hypothesis of a very narrow width for ρ^0 on the isovector electromagnetic form factors of the nucleons, and try to obtain some information about the ρ^0-nucleon coupling. It is generally believed that such resonance plays a very important role in the isovector form factors (2).

In this discussion we follow the work of Bowcock, Cottingham and Lurié (3). Their results on the isovector form factors $F_1^V(t)$, $F_2^V(t)$ are based on subtracted dispersion relations in which only the two-pion resonance contribution is taken into account explicitly, in terms of the pion electromagnetic form factor. Their results can be written in the Clementel-Villi form (2), as

$$F_1^V(t) = \frac{1}{2}\left(1 - a_V + \frac{a_V t_R}{t_R - t}\right), \tag{1}$$

$$F_2^V(t) = \mu_V\left(1 - b_V + \frac{b_V t_R}{t_R - t}\right), \tag{2}$$

(*) On leave of absence from «Istituto de Fisica Teorica», São Paulo, Brazil; Ford Foundation Fellow, CERN, Geneva.

(1) B. C. Maglić: *CERN Seminar* (Nov. 1961); J. Button, G. R. Kalbfleisch, G. Lynch, B. C. Maglić A. R. Rosenfeld and M. L. Stevenson: to be published.

(2) S. Bergia, A. Stanghellini, S. Fubini and C. Villi: *Phys. Rev. Lett.*, **6**, 367 (1961); S. Fubini: *Report at the Aix-en-Provence Conference* (Sept. 1961).

(3) J. Bowcock, W. N. Cottingham and D. Lurié: *Nuovo Cimento*, **16**, 981 (1960).

where $\mu_V = \frac{1}{2}(\mu_p - \mu_N)$, and t_R is the resonance squared energy. We quote ref. [3] for the explicit expression for a_V, b_V.

We want now simply to replace the value of the width $\Gamma \simeq 100$ MeV used in ref. [3], by the much smaller value $\Gamma \simeq 10$ MeV. The same analysis can be used *a priori*, the only difference being possibly in the ρ^0-nucleon and ρ^0-pion couplings.

To make explicit use of coupling constants, we prefer to use for a_V, b_V the expressions obtained by the « bipion » model, in which the ρ^0 resonance is considered as a « stable » particle [4]. The interactions of this particle with pions, nucleons and photons are given respectively by [4,5]

$$(3) \qquad \begin{cases} i\lambda_\pi (q_1 + q_2)_\mu \varrho_\mu^0 , \\ i\bar{u}(p_2)\left| C_1 \gamma_\mu + \dfrac{C_2}{2M} \sigma_{\mu\nu}(p_1 - p_2)_\nu \right| u(p_1)\varrho_\mu^0 , \\ \lambda_\gamma A_\mu \varrho_\mu^0 . \end{cases}$$

Then one can easily obtain

$$(4) \qquad a_V = \frac{2C_1\lambda_\gamma}{t_R} , \qquad b_V = \frac{C_2\lambda_\gamma}{\mu_V t_R} .$$

We now use the expressions of ref. [3] for the electromagnetic pion form factor which, for a small width, reduces to

$$(5) \qquad F_\pi(t) \simeq \frac{t_R}{t_R - t} ,$$

and which, in the bipion model, is written as

$$(6) \qquad F_\pi(t) = \frac{\lambda_\pi \lambda_\gamma}{t_R - t} .$$

The relations (4) can then be replaced by

$$(7) \qquad a_V = \frac{2C_1}{\lambda_\pi} , \qquad b_V = \frac{C_2}{\mu_V \lambda_\pi} .$$

Using directly the values $a_V \simeq b_V \simeq 1.62$, $t_R \simeq 25\mu^2$ obtained in a recent fit [6], we get [7]

$$(8) \qquad C_1 \simeq 0.81\lambda_\pi , \qquad C_2 \simeq 1.62\mu_V\lambda_\pi .$$

([4]) A. Stanghellini: *Nuovo Cimento*, **18**, 1258 (1960); M. Gourdin, D. Luriè and A. Martin: *Nuovo Cimento*, **18**, 933 (1960).

([5]) It si easy to show that an interaction of the form

$$(\partial_\nu \varrho_\mu - \partial_\mu \varrho_\nu)(\partial_\nu A_\mu - \partial_\mu A_\nu)$$

does not give contributions to the pion and nucleon form factors.

([6]) S. Bergia and A. Stanghellini: *Nuovo Cimento*, **19**, 155 (1961).

([7]) The parameters given in ref. ([6]) correspond to $M_\rho = 700$ MeV; we believe, however, that the values (10) will not be much changed assuming $M_\rho = 780$ MeV.

Now, the simple relation between I and λ_π^2 gives: $\lambda_\pi \simeq 5e$ (where e is the electric charge). Then it follows that the coupling between the ρ^0 and the nucleons is rather weak; in fact one gets from (8): $C_1 \simeq 4e$, $C_2 \simeq 8\mu_V e$.

This result, if taken seriously, appears to be at first sight in contrast with the fact that the ρ^0 particle is strongly produced in the $\bar{p}$-p annihilation [1].

The first argument to which one can appeal in trying to eliminate this difficulty is the following. The electromagnetic form factor of the pion given by (5), which was used by BOWCOCK *et al.*, takes into account only the effect of the ρ^0 resonance. But, if the ρ^0-pion coupling is weak, it might be reasonable to assume that such effect is not so important in comparison with the contributions coming from other intermediate virtual states.

As a first approximation, one could modify the relation (5) into a subtracted form similar to the one used for the nucleons:

$$F_\pi(t) = 1 - \alpha + \frac{\alpha t_R}{t_R - t}, \tag{9}$$

where α could be considered, in general, as energy-dependent. The relations (7) then modify into

$$a_V = \frac{2C_1}{\lambda_\pi}\alpha, \qquad b_V = \frac{C_2}{\mu_V \lambda_\pi}\alpha. \tag{10}$$

One can obtain reasonable values for C_1, C_2 in agreement with the abundant production of ρ^0, by assuming that the bipion term in (9) is small in comparison with the other term $(1-\alpha)$ coming from the other unknown contributions.

The above discussion applies to the case in which only one resonant state $J=1$, $I=1$ is taken into account in the explanation of the isovector form factors of the nucleons. It might well be that other resonances, as *e.g.* the newly discovered $I=1$ ζ-resonance ($M_\zeta \simeq 575$ MeV) [8], play an important role in this problem. The presence of two $J=1$, $I=1$ resonant states with different masses would be useful, since it should perhaps be possible in this way to explain practically all the contributions to the isovector form factors of the nucleons. This does not happen if the isovector form factors are fitted with a single (ρ^0) vector meson [9]; in fact, the values $a_V \simeq b_V \simeq 1.62$ leave a large contribution to the high-energy states. The modification of the Clementel-Villi formula with the inclusion of two-pole terms (coming *e.g.* from the ρ and ζ particles) would probably eliminate, at least in part, the difficulty pointed out above.

* * *

We acknowledge helpful discussions with members of the CERN theoretical division, and especially Prof. D. AMATI.

[8] R. BARLOUTAUD, J. HEUGHEBAERT, A. LEVEQUE, J. MEYER and R. OMNÈS: to be published on *Phys. Rev. Lett.*

[9] It might also be that both ρ_1^0 and ρ_2^0 are isovector states. In this case, one could probably fit the isovector form factors of the nucleons by assuming reasonable couplings between each of the two ρ's and the nucleons. The resulting expressions for the form factors would be still of the *CV* type, as in the case of a single resonance.

LIBRI RICEVUTI E RECENSIONI

Libri ricevuti.

L. G. Parrant: *Probability and Experimental Errors in Science*; John Wiley and Sons, New York-London, 1961; pp. ix-255; 55 s.

S. Rames: *The Wave Mechanics of Electrons in Metals*; North Holland Pub. Co., 1961; pp. xi-367. Fiorini olandesi 40.

O. J. Samoilow: *Die Struktur von Wässrigen Elektrolyt-Lösungen*; die B. G. Teubner Verlagsgesellschaft, Leipzig, 1961; pp. vi-147; D. M. 11.

Recensioni.

J. A. Richards, F. W. Sears, M. R. Wehr and M. W. Zemansky: *Modern University Physics*; Addison-Wesley Publ. Co., Reading, Mass., U.S.A. e London, Giugno 1960; pp. 993, $ 9.75.

This text is both new and old, dicono gli autori all'inizio della loro prefazione, e noi concordiamo con la loro opinione. Infatti il testo è in buona parte preso da due opere precedenti: *University Physics*, di Sears e Zemansky; *Physics of the atom*, di Wehr e Richards. L'opera è stata riscritta in alcuni capitoli (p. es. il capitolo sul lavoro e sull'energia), e vari argomenti delle due opere suddette sono stati eliminati; ma nel suo insieme il nuovo trattato è diviso piuttosto armonicamente, e questa non è una rifusione le cui cicatrici si possano scorgere a prima vista.

In molti aspetti è un libro nuovo, o almeno aggiornato. Si cerca costantemente di allineare le difficoltà di calcolo con i corsi di matematica; si introduce (nel giro di 30 pagine) la relatività speciale con un discreto commento storico, con le formule fondamentali di trasformazione, e con alcuni efficaci esempi presi dal mondo nucleare. Si dedicano 160 pagine (su un totale di 960) alla fisica delle particelle elementari, con qualche modesta apertura alla meccanica quantistica, e con una efficace presentazione della simmetria microscopica della natura. Si veda ad esempio il simpatico quadro a p. 958.

In questi anni sono attive in ogni Università le discussioni sull'ordine da seguire nell'insegnamento della fisica generale: è in aumento (o almeno io lo spero) la schiera di chi si chiede se la termodinamica non dovrebbe seguire anzichè precedere l'elettricità, per densità di concetti e per non mancare al suo compito di sintesi e di strategia nella fisica; se la meccanica relativistica non dovrebbe entrare più decisamente nei trattati della fisica generale; se la posizione dell'ottica in un trattato non andrebbe ormai profondamente revisionata. In questi riguardi il trattato di Richards e *coll.* non presenta soluzioni rivoluzionarie, ed anzi segue schemi ormai classici, con le solite conseguenze che possono apparire ad alcuni gravi e ad altri, più storicisti, coerenti ed armoniche.

La termodinamica, ad esempio, viene

prima della struttura della materia, degli atomi e delle molecole, ed il concetto principe di energia interna appare quindi al solito senza aperture, senza critica, quasi convenzionale (cfr. § 17-1).

Una domanda viene spontanea ad un docente in Italia: sarebbe adottabile per il corso biennale di fisica ai fisici?

Ebbene, in questo trattato c'è piu e c'è meno di quanto noi vogliamo normalmente dai fisici alla fine del nostro biennio: maggiore informazione e maggiore divertimento (smettiamola di fare dispense, facciamo libri, con chiari disegni, fotografie, tavole: le dispense sono tristi!); minore rigore e minore formazione matematica.

Se in generale lo consiglio? Certamente sì, anche perchè lo trovo piacevole, efficace negli esercizi, agevolmente memorizzabile.

G. Salvini

E. Fermi – *Notes on Quantum Mechanics*. The University of Chicago Press, Chicago; pp. 171, costo $ 1.50.

Questo libro riproduce i fogli manoscritti originali degli appunti per un corso di Meccanica quantistica tenuto nell'Università di Chicago da Enrico Fermi pochi mesi prima della sua morte, che egli ad ogni lezione distribuiva in anticipo ai suoi studenti. Indipendentemente dal suo valore scientifico, esso quindi rappresenta un prezioso documento personale che può permettere anche a studiosi che mai hanno conosciuto Enrico Fermi, di entrare in contatto in modo più intimo di quando lo consenta in generale la carta stampata, con alcune linee essenziali del suo pensiero fisico.

Ovviamente, in ragione della sua stessa natura e dello scopo specifico per il quale fu scritto, questo testo non può considerarsi come un trattato di meccanica quantistica vero e proprio e neppure presumibilmente come la traccia condensata di un potenziale trattato. Esso ha uno scopo essenzialmente didattico, nel senso un po' speciale di una presentazione condensata dell'argomento, destinata a marcarne quella traccia fondamentale di svolgimento logico che ogni insegnante deve avere in mente quando costruisce le sue lezioni, e che appunto nella sua scarnità ha il pregio di mettere in rilievo immediato i punti essenziali e le svolte chiave del pensiero.

Sotto tale aspetto esso potrà essere consultato con molto frutto da chiunque si accinga a svolgere un corso sugli stessi argomenti, nonchè da qualunque studioso che desideri trovare concentrati gli assiomi della meccanica quantistica.

Il corso si svolge con continuità secondo vari paragrafi che possono dividersi all'ingresso in tre parti principali distinte.

I primi sono dedicati all'esposizione della meccanica ondulatoria semi-intuitiva colle sue più immediate applicazioni; l'equazione di Schrödinger viene immediatamente dedotta dalla analogia tra l'ottica e la meccanica classica ed è seguita dalla trattazione ormai classica dei problemi semplici, come l'oscillatore armonico e le forze centrali.

Nei paragrafi successivi viene esposta la meccanica quantistica assiomatica, partendo dalle proprietà degli operatori lineari e dalla ricerca dei loro autovalori, per poi passare alla loro rappresentazione tramite matrici ed arrivare al concetto ed alle proprietà degli osservabili.

L'ultima parte, che è anche la più estesa, è dedicata ai metodi pratici di calcolo e alle applicazioni: teorie perturbative, indipendente e dipendente dal tempo, approssimazione di Born, teoria semiclassica della radiazione, teoria di Pauli dello spin, spettroscopia atomica, problema dei sistemi a due elettroni, ed infine teoria relativistica dell'elettrone.

Molti di questi argomenti sono svolti seguento trattazioni ormai del

tutto classiche, che presumibilmente Fermi nel suo ripensamento della materia, considerava come la forma più chiara e naturale di esposizione.

Altre parti invece, specie nei riguardi della meccanica operatoriale, anticipano, in modo relativamente semplice, svolgimenti e formalismi che di solito si trovano in trattazioni di livello più astratto, ciò che le rende particolarmente feconde ed istruttive.

Il libro quindi nel complesso, oltre che per il costo assai modesto, si raccomanda da sè, sia per l'interesse che offre quale avvicinamento alla visuale della meccanica quantistica di una delle maggiori personalità della fisica contemporanea, sia per l'intrinseca chiarezza che tale visuale possiede in sè e che traspare in queste brevi note, come in genere traspariva da ogni scritto di Fermi.

N. DALLAPORTA

S. S. SCHWEBER: *An Introduction to Relativistic Quantum Field Theory*. Row, Peterson and Company, 1961; pp. 905.

Questo volume monumentale è nato dall'esigenza di rivedere e aggiornare il ben noto *Mesons and Fields*, vol. 1, pubblicato sei anni fa, di cui erano autori lo stesso SCHWEBER, H. A. BETHE e F. DE HOFFMANN. Tutti coloro che hanno lavorato in questi anni con la teoria dei campi relativistici avranno certamente avuto occasione di consultare *Mesons and Fields* e probabilmente ne ricorderanno l'assoluta mancanza di sistematicità che rendeva difficile una lettura continuata. Una caratteristica evidente del nuovo libro di SCHWEBER è invece lo sforzo di presentare una visione il più completa possibile di tutti gli aspetti della teoria dei campi studiati negli ultimi dodici o tredici anni, cercando inoltre di estrarre il filo conduttore che ha portato agli sviluppi più recenti del metodo assiomatico. La struttura del vecchio volume si ritrova solo in pochi capitoli, essenzialmente in quelli riguardanti lo sviluppo perturbativo della matrice S, l'elettrodinamica quantistica e la teoria della rinormalizzazione (capitoli 13, 14, 15 e 16). Ciò si comprende facilmente non essendovi stati sviluppi recenti di questi argomenti. Vogliamo invece indicare gli argomenti che rappresentano una novità, non solo rispetto al vecchio volume *Mesons and Fields*, ma anche rispetto agli altri libri sulla teoria dei campi, oggi esistenti, nel senso che vengono per la prima volta inclusi in una esposizione sistematica. Questi argomenti possono con una certa approssimazione dividersi in due gruppi:

a) questioni trattabili nell'ambito dell'ordinario formalismo Lagrangiano;

b) problemi nati dallo sviluppo sistematico della rappresentazione di Heisenberg e che hanno portato alle recenti analisi della struttura della teoria dei campi, generalmente indicate col nome di formulazioni « assiomatiche ».

Tra gli argomenti del primo tipo nel capitolo 12 vengono trattati in dettaglio i modelli non relativistici risolubili esattamente o trattabili con metodi di approssimazione non perturbativi. In particolare vengono esposti la teoria del campo scalare, il modello di Lee e la teoria di Chew e Low. La discussione dei modelli è estremamente dettagliata, vengono eseguiti tutti i passaggi analitici importanti e se anche la trattazione ne risulta talvolta appesantita vi sono in compenso notevoli vantaggi dal punto di vista didattico. Sempre nell'ambito del formalismo Lagrangiano viene messo in rilievo il ruolo sempre maggiore avuto dai principi di simmetria nell'impostare il problema delle interazioni tra particelle elementari e il capitolo 10 viene interamente dedicato alla discussione dei possibili Lagrangiani compatibili con i principi di invarianza suggeriti dall'esperienza. È anche da ricordare il

capitolo II sulla teoria formale dei problemi d'urto.

L'ultima parte del libro dedicata alle questioni di tipo *b*), è forse la migliore e a questo proposito occorre ricordare che il lavoro di ricerca dell'autore si è svolto finora principalmente nell'ambito di questi problemi. L'interesse maggiore di questa parte sta nel fatto che rappresenta una introduzione relativamente facile agli sviluppi formali della teoria dei campi degli ultimi anni. Mentre la lettura degli articoli originali è piuttosto faticosa per il lettore che non sia particolarmente addentro nell'argomento, l'esposizione di Schweber riesce a stabilire una certa continuità tra le vecchie formulazioni della teoria e i nuovi tentativi. Particolarmente notevole la trattazione delle formulazioni di Wightmann e di Lehmann, Symanzik e Zimmermann dove l'autore mantiene efficacemente l'equilibrio tra la discussione dei dettagli matematici e delle idee generali. La dimostrazione delle relazioni di dispersione unidimensionali chiude il volume. Il contenuto di questi ultimi due capitoli costituisce oggi parte delle nozioni necessarie al fisico delle alte energie. Vi sono molte monografie sulle regole di dispersione (per lo più dispense di corsi di lezioni) che tuttavia riescono spesso di lettura non agevole poichè non si ricollegano al tipo elementare di preparazione sulla teoria dei campi ricevuto dalla maggior parte dei fisici. Il libro di Schweber ci sembra in grado di colmare questa lacuna.

È forse opportuno concludere con un breve confronto con il trattato di Bogolubov e Shirkov che rappresenta l'unica opera già pubblicata sull'argomento paragonabile a questa per la vastità della trattazione. Si può dire che le impostazioni dei due libri sono in parte complementari. Mentre nel Bogolubov e Shirkov l'interesse è notevolmente concentrato sui problemi matematici posti dalla teoria, lo Schweber ha sempre presenti i problemi applicativi. Dalla diversa impostazione segue che non vi è praticamente sovrapposizione tra i due testi e gli argomenti comuni vengono trattati con tecniche generalmente diverse. Il lettore che desideri pertanto approfondire la teoria dei campi oltre il livello elementare potrà scegliere l'uno o l'altro trattato a seconda che il suo interesse vada prevalentemente verso la matematica o le applicazioni della teoria dei campi.

G. Jona-Lasinio

Gordon Francis: *Ionization Phenomena in Gases*; London, Butterworths Scientific Publication, 1960; pp. vii-300, 60 s.

Nella prefazione del libro è detto che esso vuole essere complementare ad altri recenti libri di testo in questo campo. Si può dire subito che questo scopo è stato raggiunto, sia nella scelta degli argomenti trattati, sia nello stile con cui sono presentati. Il libro è qualche cosa di intermedio fra un testo descrittivo, in cui sono esposte le proprietà dell'arco, della scintilla e della scarica a bagliore, e un testo teorico, analogo al piccolo libro dello Spitzer, in cui, tanto per fare un esempio, non si vede mai la fotografia di una scarica.

Il primo capitolo è una breve premessa sulla struttura atomica; esso avrebbe potuto essere forse omesso in quanto un testo specializzato non può mai essere completo. Per esempio un capitolo sulle equazioni di Maxwell sarebbe stato altrettanto utile, se non di più. Il secondo capitolo è intitolato *Processi fondamentali*. La prima parte di questo capitolo consiste in una descrizione concisa degli eventi atomici, cioè urti elastici ed anelastici fra elettroni, atomi e fotoni. La seconda metà è dedicata al coefficiente α di Townsend, ai processi secondari ed ai coefficienti di mobilità

e di diffusione; sono cioè trattati fenomeni in cui entra in gioco un gran numero di particelle.

Il terzo capitolo contiene un'ottima discussione del principio di similitudine e delle sue limitazioni. Questo capitolo, breve ma chiaramente scritto, è molto utile in quanto non è del tutto chiaro dalla letteratura perchè α/p e la velocità di trascinamento v siano funzioni del rapporto X/p fra il campo elettrico e la pressione. L'autore spiega perchè e sotto quali condizioni sia valido il principio di similitudine.

Il capitolo 4 è un capitolo lungo e dettagliato su *Scariche in corrente alternata e in alta frequenza*. Questo è un argomento in cui lo stesso autore ha lavorato, e senza dubbio, molti fisici troveranno questo capitolo, con la sua vasta bibliografia, una delle parti più interessanti del libro.

Il capitolo quinto tratta brevemente l'alta atmosfera ed è seguito da un capitolo sulle scariche ad alta corrente e sulle reazioni termonucleari. Questo argomento è naturalmente di grande interesse poichè l'energia termonucleare è la ragione principale per cui negli ultimi dieci anni si è molto incrementato lo studio della fisica dei plasmi. Il capitolo in questione è una introduzione a questo argomento; sono discusse abbastanza dettagliatamente le scariche a strizione magnetica e più brevemente le macchine a specchi magnetici e gli « stellarator ». L'autore ha dato importanza ai principi fisici, evitando sia la matematica associata con la teoria delle instabilità idromagnetiche che il gergo relativo ai dispositivi sperimentali.

L'ultimo capitolo contiene una relazione sulle oscillazioni e le onde nel plasma, compreso lo smorzamento di Landau, cioè lo smorzamento che ha luogo anche in assenza di collisioni. Questa è forse la prima volta che i diversi risultati di vari autori sono raccolti in un libro di testo.

La spiegazione fisica dello smorzamento di Landau non è però molto convincente. Il meccanismo descritto è quello dell'intrappolamento delle particelle, ma non si capisce bene perchè le particelle vengano intrappolate. Ci si può infatti facilmente immaginare una onda che viaggia senza venire smorzata, sia che una data particella venga intrappolata o no. È chiaro tuttavia dalla letteratura recente che questa dispersione di energia non è ancora ben compresa.

Come in quasi tutti i libri, ci sono piccoli errori ed inesattezze; se ne citeranno qui due. La ben nota distribuzione di Druyvesteyn è data a pag. 41 ma non è detto quando essa valga. Deve esistere infatti qualche condizione per il campo elettrico, in quanto se questo è estremamente piccolo ci si aspetta una distribuzione Maxwelliana.

A pag. 232 si afferma che frequenze maggiori di quella di plasma non possono penetrare nel plasma stesso!

Io ho già raccomandato il libro ai miei studenti e colleghi. Il libro è stato scritto per laureandi e per fisici all'inizio della loro carriera, ma esso può anche costituire un'utile aggiunta alla biblioteca di chi già lavori in questo campo.

J. E. Allen

A. Goldsmith, T. E. Waterman and H. J. Hirschhorn – *Handbook of Thermophysical Properties of Solid Materials*, vol. I. Pergamon Press, Oxford, 1961; pp. 758, prezzo dei 5 volumi $ 75.

Si tratta di opera di notevole mole compilata dalla Armour Research Foundation con grande impiego di mezzi. L'opera si presenta sotto una forma tipografica eccellente e risulta di facile consultazione, ed è chiaramente il frutto di una intelligente organizzazione che ha curato in dettaglio lo studio, la valu-

tazione e poi la compilazione dei dati disponibili fino al 1960.

Le proprietà fisiche riportate sono le seguenti: punto di fusione, densità, calore latente di fusione, calore specifico, conducibilità termica, proprietà ottiche di emissione e riflessione, espansione termica, tensione di vapore e resistività elettrica.

L'opera è suddivisa in cinque volumi, per coprire gli elementi a punto di fusione superiore a 1000 °F nel primo volume, le leghe nel secondo, le ceramiche nel terzo, i polimeri ed i composti intermetallici e di altro genere nel quarto.

Certamente sarebbe desiderabile che questa pregevole raccolta di dati si trovasse nella biblioteca dei nostri istituti universitari e dei laboratori industriali, ma temiamo che il prezzo troppo elevato ne possa limitare la giusta diffusione.

G. Careri